

https://dspace.org/

The effect of low level sulfide addition and the performance of precipitated- iron Fischer-Tropsch catalysts

Bromfield, Tracy Carolyn

2016-08-31
http://hdl.handle.net/10539/20979

Downloaded from a DSpace repository. https://dspace.org/

THE EFFECT OF LOW-LEVEL SULFIDE ADDITION ON THE PERFORMANCE OF PRECIPITATED-IRON FISCHER-TROPSCH CATALYSTS

Tracy Carolyn Bromfield

A thesis submitted to the Faculty of Science, University of the Witwatersrand, Johannesburg, in fulfilment of the requirements for the degree of Doctor of Philosophy.

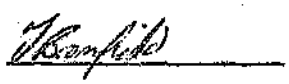
July 1997

"As a scientist, I expect statistical proof whenever possible to convince me of most things. But as I continue to mature, I've become more impressed by the frequency of statistically highly improbable events. In their very improbability, I began to see the fingerprint of God"

Scott Peck

Declaration

I hereby declare that this thesis is my own, unaided work. It is being submitted for the Degree of Doctor of Philosophy at the University of the Witwatersrand, Johannesburg. It has not been submitted for any degree or examination at any other University.



(Signature of candidate)

7 day of July 1997

Abstract

Precipitated-iron Fischer-Tropsch catalysts were sulfided in the range 500 - 20000 ppm S/Fe with an aqueous sulfide source (Na_2S, $(NH_4)_2S$, $(NH_4)_2S_5$) during the precipitation process. Sulfidation was performed at pH 10.75, 8.5 and 6.9. Sodium ions were removed by centrifugation, and atomic absorption analysis confirmed low sodium levels (0-51 ppm). Based on solution speciation models, ferrous sulfide (FeS) which formed from aqueous HS^- species, was found to influence the iron-oxyhydroxide crystallite morphology. It is proposed that, when sulfide was added at pH 10.75, FeS molecules functioned as nuclei for crystallite growth, while at pH 6.9 they assisted with the aggregation of particles. The processes of nucleation and aggregation appeared to be in competition following sulfidation at pH 8.5, resulting in a composite morphology that produced an inactive catalyst.

The bulk structure of the catalysts was elucidated using XRD, SEM and nitrogen porosimetry. All sulfided catalysts exhibited enhanced BET surface areas and total pore volumes with a maximum at 2000 ppm S (surface area = 166 m^2/g, total pore volume = 0.254 cm^3/g) compared to an unsulfided catalyst (surface area = 58 m^2/g, total pore volume = 0.184 cm^3/g). Furthermore, for any series of catalysts at the same level of sulfidation, the BET surface areas were observed to decrease as the pH of sulfide addition decreased. Increasing levels of sulfidation (to 20000 ppm) brought about an increase in crystallite size and therefore, improved crystallinity as determined by XRD measurements. Materials with larger crystallites possess smaller surface areas, and thus the crystallinity was found to increase as the pH of sulfidation decreased.

Surface characterisation by XPS after calcination at 400°C and reduction (400°C), revealed sulfate species (169.4 eV) on catalysts sulfided with 500-2000 ppm, while sulfide species (162.0 eV) emerged at higher sulfide content. No sulfates were observed on reduced catalysts following calcination at 200°C.

The effect of sulfide addition on the efficacy of iron catalysts in the Fischer-Tropsch reaction was studied using fixed bed reactors. Catalysts were calcined (200°C or 400°C, GHSV = 2000 h^{-1}), and reduced (400°C, GHSV = 500 h^{-1}), prior to commencing Fischer-Tropsch synthesis at 250°C and 8 bar pressure (GHSV = 400 h^{-1}). A specific activity of 0.35 μmolC/s/g was obtained in the absence of sulfur. Catalysts sulfided (at pH 6.9) with 500 and 2000 ppm S exhibited activities of 1.31 and 0.67 μmolC/s/g, respectively. Indeed, all catalysts sulfided in this range (500-2000 ppm S) at either pH 10.75 or 6.9, showed higher CO conversions (50-75 %) than the unsulfided catalyst (30 %). In contrast, catalysts sulfided with between 5000 and 20000 ppm S showed evidence of sulfide poisoning. For example, a catalyst sulfided with 20000 ppm S operated at 10 % CO conversion (specific activity = 0.11 μmolC/s/g).

Sulfidation at pH 8.5, in the range 2000 to 20000 ppm S, resulted in poor CO conversions (10-15%). A lack of carbide formation was observed on all low activity catalysts. This has been ascribed to a weakening of the Fe-C interaction by sulfide; the reduced CO dissociation also accounting for the high oxygenate selectivity of these catalysts. In addition to alcohols, high yields of methane and low α-values characterised the product distributions of low activity catalysts.

Low-level sulfided catalysts were less selective towards the formation of methane than the unsulfided catalyst, and gave good yields of C_7-C_{15} hydrocarbons. The olefinity of products was also enhanced and α-values in the range 0.78-0.83 were determined for low-level sulfided catalysts. In the absence of sulfur, an α-value of 0.80 was obtained.

A study of the effect of calcination temperature was made using a catalyst sulfided at pH 10.75 with 2000 ppm polysulfide. The catalyst calcined at 200°C exhibited poor activity (0.10 μmolC/s/g) compared to the catalyst calcined at 400°C (0.64 μmolC/s/g).

The source of sulfide appeared to have no effect on Fischer-Tropsch activity, and a preliminary study on a catalyst impregnated with 500 ppm sodium sulfide showed promising results (specific activity = 1.05 μmolC/s/g).

Dedication

Without nurturing, a seed may grow, but its bloom will be even more spectacular if it has been lovingly tended throughout its development.

This thesis is decidated to my family: Mom, Dad, Kim and Thanu, for all the time and effort you have sacrificed so willingly all my life. I am forever indebted to you.

Thank you for helping me become the person I am today.

To my 'soul provider', words cannot express my gratitude and appreciation. Thank you for being the best friend anyone could wish to have, and for being so much a part of who I am. Thank you for all your wonderful help and support - just when I needed it most.

I love you all

Acknowledgements

There is much that one can accomplish through hard work, dedication and perserverance. But, so much more can be achieved with the help of friends and loved ones. I would therefore like to express my sincere appreciation to the following people for all their help:

Firstly, Tens, without you there would be no thesis. Thanks, thanks, and thanks again! I would never have managed without your help and support. This one's for you!!

thanks also,

Prof Neil Coville for his guidance and enthusiasm

Dr Julian Price for helping me get so started on my project

Basil Chassoulas and the great guys at the Workshop, as well as Lyn Daniels for being so helpful

Thato Motjope and Prof Herman Pollak for their assistance with Mössbauer Spectroscopy

Stephan Coetzee and the other members of the SEM Unit

Wynand Louw and Martin van Staden of Mattek, CSIR for assistance with XPS

Vicky Curtis, Mamongae Mahlare and Claire Janisch for XRD, TPR and Porosimetry studies completed as part of Honours projects

Manuel Fernandes and Vimal Ichbaram for assistance with XRD and AAS, respectively

Prof Fabri Marsicano for his invaluable help with the modelling studies

Dr Joe Wollbrandt for teaching me all I know about DRIFTS

My mentor, Dr Leon Ferreira, as well as Dr Espinoza, Philip Gibson and other employees of Sastech for their advice

And, finally, to all the friends that I made during my studies: thanks for all the fun times we shared!

I would also like to acknowledge the financial support of Sastech R & D and the University of the Witwatersrand

Publications and Presentations

Publication

Bromfield, T.C. and Coville, N.J., Surface characterisation of sulfided precipitated-iron Fischer-Tropsch catalysts by X-ray photoelectron spectroscopy, *Appl. Surf. Sci.*, (1997) - in press

Poster Presentation

"Sulfide promotion of precipitated-iron Fischer-Tropsch catalysts" presented at Catalysis '95 held at the Wigwam Hotel, Rustenburg, South Africa (won Poretech Trophy for Best Poster)

Oral Presentations

1. "The effect of low-level sulfide on the performance of precipitated-iron Fischer-Tropsch catalysts", delivered at the SASOL Research Symposium, held at RAU University, South Africa, 1994
2. "Characterisation of sulfided precipitated-iron Fischer-Tropsch catalysts by X-ray Photoelectron Spectroscopy", delivered at Catalysis '96, held at Eskom Centre, Midrand, South Africa
3. "Promotion of precipitated-iron Fischer-Tropsch catalysts by low-level sulfide addition", delivered at the SASOL Research Symposium, held at RAU University, South Africa, 1997

Table of Contents

Declaration i
Abstract ii
Dedication iv
Acknowledgements v
Presentations and Publications vii
Contents viii
List of Figures xvi
List of Tables xxvii
List of Terms and Abbreviations xxxi

Chapter 1: Introduction

Foreward 1
1.1. Some aspects of sulfur chemistry 2
1.2. The Fischer-Tropsch Process 13
1.3. Iron Catalysts for use in the Fischer-Tropsch Reaction 18
1.4. Sulfur and the Fischer-Tropsch Reaction 23
1.5. Aims of this study 29

Chapter 2: Experimental Methods

2.1. Introduction 31
2.2. Catalyst Preparation 33
2.2.1. Co-precipitated sulfided catalysts 34
2.2.2 [illegible]regnated catalyst 36
2.3. E[illegible]al Analysis 36
2.4. Catalyst Pretreatment 36

Chapter 2: Experimental Methods (cont.)

2.5. Scanning Electron Microscopy 37

2.6. X-Ray Powder Diffraction Analysis 37

2.7. Thermogravimetric Analysis 38

2.8. Colour Evaluation 38

2.9. Porosimetry 39

2.9.1. Estimation of pore shapes 40

2.9.2. Estimation of pore neck and cavity sizes 43

2.10. X-Ray Photoelectron Spectroscopy 44

2.11. Auger Electron Spectroscopy 44

2.12. Diffuse Reflectance Infrared Spectroscopy 45

2.13. Mössbauer Spectroscopy 47

2.14. Solution Speciation Modelling 48

2.15. Temperature Programmed Reduction 49

2.16. CO Chemisorption 50

2.17. Fischer-Tropsch synthesis 52

2.17.1. Mass Balance Procedure 55

2.18. Heavy Hydrocarbon Separation 57

2.19. Wax Extraction 57

PART A:

Chapter 3: The Structural Morphology and Chemical Composition of Sulfided Catalysts

3.1. Introduction....58

3.1.1. Preparative variables affecting precipitated-iron FT catalysts....60

3.2. Results and Discussion....63

3.2.1. Effect of sulfide on the colour of precipitated-iron catalysts....65

3.2.1.1. General aspects of colour....65

3.2.1.2. Effects of sulfide on colour of iron catalysts...66

3.2.2. Chemical Composition of the precipitates....68

3.2.3. Scanning Electron Microscopy....70

3.2.4. X-Ray Powder Diffraction....81

3.2.5. Thermogravimetric Analysis....94

3.2.6. Pore Structure....96

3.3.Conclusion....105

Chapter 4: Surface Characterisation of Sulfided precipitated iron Fischer-Tropsch Catalysts by Electron Spectroscopy

4.1. Introduction....106

4.2. Experimental....108

4.3. Results and Discussion....109

4.4. Conclusion....122

Chapter 5: Surface Characterisation of sulfided iron catalysts using Diffuse Reflectance Fourier Transform Infrared Spectroscopy (DRIFTS)

5.1. Introduction....123

5.2. Experimental....126

5.3. Results and Discussion....127

5.3.1. Effect of reduction temperature on CO adsorption....127

5.3.2. Influence of sulfide content on CO adsorption....128

5.3.3. Effect of sulfidation pH on CO adsorption....132

5.3.4. Effect of sulfide source on CO adsorption....133

5.3.5. CO adsorption on a sulfide-impregnated catalyst....135

5.3.6. Pretreatment studies of sulfided iron catalysts....136

5.3.7. *In situ* Fischer-Tropsch study....145

5.4. Conclusion....159

Chapter 6: Characterisation of sulfided precipitated-iron Fischer-Tropsch catalysts by Mössbauer Spectroscopy

6.1. Introduction....160

6.2. Experimental....162

6.3. Results....163

6.4. Discussion....172

6.4.1. Effect of sulfide addition on iron particle size....172

6.4.2. Effect of sulfide content on the chemical state of iron....177

6.4.3. Analysis of spent catalysts....180

6.5. Conclusion....180

Chapter 7: Solution speciation modelling as applied to the precipitation of sulfided iron catalysts

7.1. Introduction....181

7.2. Experimental....183

7.3. Results....185

7.3.1. Effect of sulfidation level at different pH values....185

7.3.1.1. Sulfidation at pH 10.75....185

7.3.1.2. Sulfidation at pH 8.5....187

7.3.1.3. Sulfidation at pH 6.9....189

7.3.2. Effect of sulfidation pH....190

7.3.3. Effect of sulfide source....193

7.4. Discussion....196

7.5. Conclusion....201

PART B

Chapter 8: The effect of increasing sulfide content on the catalytic efficacy of iron Fischer-Tropsch catalysts

8.1. Introduction....203

8.2. Experimental....204

8.3. Results and Discussion....205

8.3.1. Reactor Study....205

8.3.2. Surface Morphology of sulfided catalysts....214

8.3.3. Influence of sulfide on catalyst reduction temperature....217

8.3.4. Bulk morphology of sulfided catalysts after FT reaction....224

8.4. Conclusion....227

Chapter 9: The effect of sulfide source on the performance of sulfided precipitated-iro.. Fischer-Tropsch catalysts

9.1. Introduction....229

9.2. Experimental....230

9.3. Results and Discussion....231

9.4. Conclusion....238

Chapter 10: The effect of sulfidation pH on the morphology and function of sulfided iron Fischer-Tropsch catalysts

10.1. Introduction....239

10.2. Experimental....242

10.3. Results....243

10.3.1. Effect of sulfidation pH on catalyst morphology....243

10.3.2. Effect of sulfidation pH on catalytic efficacy....248

10.4. Discussion....249

10.4.1. Effect of sulfidation pH on catalyst morphology....249

10.4.2. Effect of sulfidation pH on catalytic efficacy....256

10.4.3. Effect of sulfidation pH on product selectivity of sulfided catalysts....261

10.5. Conclusion....264

Chapter 11: Preliminary studies on selected sulfided precipitated-iron Fischer-Tropsch catalysts

11.1. Introduction....265

11.2. Experimental....266

11.2.1. Incipient wetness as a mode of sulfidation....266

11.2.2. Effect of calcination temperature....267

11.2.3. Same conversion study....267

Chapter 11: Preliminary studies on selected sulfided precipitated-iron Fischer-Tropsch catalysts (cont.)

11.3. Results and Discussion....268

11.3.1. Incipient Wetness as a mode of sulfidation....26

11.3.1.1. Conclusion....272

11.3.2. Effect of calcination Temperature....273

11.3.3. Is increased olefinity an artifact of high conversion?....275

11.4. Conclusion....278

Conclusion....279

References....283

Appendix 1

List of Figures

Chapter 1

Figure 1.1: Typical decomposition routes of sulfide 6

Figure 1.2: Eh-pH diagram for pyrite 8

Figure 1.3: Pentasulfide isomerism 9

Figure 1.4: Eh-pH diagrams of polysulfides at 25°C 10

Chapter 2

Figure 2.1: Precipitation apparatus for the preparation of iron catalysts 33

Figure 2.2: Shapes of adsorption isotherms 40

Figure 2.3: Type IV isotherms showing different hysteresis loops 40

Figure 2.4: Longitudinal section through the variable temperature DRIFTS reactor cell 45

Figure 2.5: Plug Flow Reactor System for Fischer -Tropsch catalyst testing 53

Chapter 3

Colour Plate I.....67

Figure 3.1a: Electron micrograph of an uncalcined, unsulfided precipitated-iron catalyst taken at 2000x magnification ...71

Figure 3.1b: Micrograph taken at 2000x magnification of a calcined, unsulfided precipitated-iron catalyst.....71

Figure 3.2a: Uncalcined catalyst sulfided with 2000 ppm $(NH_4)_2S_5$ at pH 6.9 viewed at 2000x magnification.....72

Figure 3.2b: Spent catalyst sulfided with 2000 ppm S viewed at 2000x magnification.....72

Figure 3.3a: Equiaxed crystals viewed at 2000x magnification on a catalyst sulfided with 5000 ppm S before calcination....74

Figure 3.3b: Micrograph of a catalyst sulfided with 5000 ppm S showing dendritic growth at 2000x magnification.....74

Figure 3.4a: Schematic representation of dendritic growth.....75

Figure 3.4b, c: Representation of the first stage of dendritic growth 76

Figure 3.5: Coalescent structures observed at 2000x magnification on a catalyst sulfided with 20000 ppm S.....77

Figure 3.6: Surface of a calcined catalyst sulfided with 2000 ppm S viewed at 2000x magnification.....77

Figure 3.7: Micrograph of sulfur-rich region on catalyst sulfided with 20000 ppm S at 2000x magnification.....79

Figure 3.8: Surface of a calcined catalyst sulfided with 20000 ppm S viewed at 2000x magnification, showing clusions of sulfur... 80

Figure 3.9: Diffractogram of an unsulfided catalyst....82

Figure 3.10: Diffractogram of a spent catalyst sulfided with 500 ppm Na_2S at pH 6.9 84

Figure 3.11: Diffractogram of catalyst sulfided with 2000 ppm Na_2S at pH 6.9....85

Figure 3.12: Diffractogram of a catalyst sulfided with 20000 ppm Na_2S at pH 6.9....86

Figure 3.13: Diffractogram of a catalyst sulfided with 20000 ppm $(NH_4)_2S_1$ at pH 6.9....87

Figure 3.14: Variation in the crystallinity of iron-oxide as a function of the sulfur content....88

Figure 3.15: Stack-plot of diffraction patterns obtained from catalysts sulfided with 5000 ppm Na_2S....89

Figure 3.16: a) 2-line ferrihydrite, b) 6-line ferrihydrite....90

Figure 3.17: Thermogram of a spent unsulfided catalyst recorded in an oxidising atmosphere....95

Figure 3.18: Thermogram of spent catalyst sulfided with 20000 ppm Na_2S at pH 6.9 recorded under oxygen....95

Figure 3.19: Adsorption-desorption isotherms of calcined catalysts....98

Figure 3.20: Proposed pore shapes of calcined catalysts....100

Figure 3.21: Adsorption-desorption isotherms of spent catalysts....102

Figure 3.22: Proposed pore shapes of spent catalysts....104

Chapter 4

Figure 4.1: S (2p) photopeak of catalyst sulfided with 5000 ppm Na_2S, calcined at 400°C and reduced at 300°C.....110

Figure 4.2: a) Evolution of sulfide (162 eV) and sulfate (168 eV) on a catalyst sulfided with 20000 ppm Na_2S, after calcination at 200° C and reduction at 300°C b) Fe 2p ($^3/_2$) photopeak of the same catalyst showing the presence of iron-oxide (712 eV) after hydrogen activation 111

Figure 4.3: a) S (2p) core level spectrum of catalyst sulfided as in Figure 4.2, but reduced at 400°C, showing conversion of sulfate to sulfide b) Fe (2p) photopeak typical of metallic iron, formed after reduction at 400°C.....112

Figure 4.4: Expanded view of sulfide peak at 162 eV of catalyst in Figure 4.3 a), complete with peak-fit 116

Figure 4.5: Expansion of sulfide region of polysulfided catalyst containing 20000 ppm $(NH_4)_2S_5$ 117

Figure 4.6: Auger Electron spectrum of a calcined, reduced catalyst sulfided with 20000 ppm Na_2S at pH 10.75.....120

Figure 4.7: Peak-to-peak Auger depth profile of surface of the catalyst in Figure 4.6 121

Chapter 5

Figure 5.1: a) Molecular orbital diagram of the bonding between a metal and CO b) A schematic representation of the orbital overlap in a metal-carbonyl complex 124

Figure 5.2: The effect of reduction temperature on the evolution of linear carbonyl species on 20000 ppm polysulfided iron catalysts 128

Figure 5.3: The effect of increasing levels of sulfidation on the evolution of linear carbonyl species on the surface of iron catalysts, showing correlation with extent of reduction 129

Figure 5.4: Comparison of BET surface areas and relative intensities of linear carbonyl species adsorbed on iron catalysts as a function of sulfide content 131

Figure 5.5: The effect of purging with nitrogen on the intensity of adsorbed linear carbonyl species as a function of sulfide content 132

Figure 5.6: CO adsorption on a 1000 ppm S catalyst prepared by incipient wetness 135

Figure 5.7: a) Unsulfided precipiated-iron catalyst prior to calcination b) After calcination at 400°C 137

Figure 5.8: a) Catalyst sulfided with 2000 ppm Na_2S prior to calcinaton b) Following calcination at 400°C 138

Figure 5.9: Catalyst sulfided at pH 10.75 with 2000 ppm $(NH_4)_2S$, after calcination at 400°C, showing a sharp peak near 1300 cm^{-1} 140

Figure 5.10: Sulfated TiO_2 after exchange with $H_2{}^{18}O$ at 450°C..... 140

Figure 5.11: a) Infrared spectrum of uncalcined catalyst sulfided with 20000 ppm Na_2S b) Same catalyst after calcination in air at 400°C 142

Figure 5.12: a) DRIFTS spectrum of a catalyst calcined at 200°C b) The same catalyst calcined at 400°C..... 143

Figure 5.13: Expanded view of 1700-1200 cm^{-1} region of the DRIFTS spectrum of a catalyst sulfided with 500 ppm Na_2S recorded after CO adsorption..... 144

Figure 5.14: a) Hydrocarbon formation on an unsulfided iron catalyst b) Fischer-Tropsch synthesis on a catalyst sulfided with 2000 ppm Na_2S at pH 10.75 146

Figure 5.15: a) FT synthesis on a catalyst sulfided with 500 ppm Na_2S at pH 10.75 b) A catalyst sulfided at pH 6.9 with 500 ppm Na_2S..... 148

Figure 5.16: Expanded view of FT synthesis on a catalyst sulfided with 2000 ppm Na_2S, showing 1800-1200 cm^{-1} region..153

Figure 5.17: a) FT synthesis on a catalyst reduced at 300°C 156

Figure 5.17: b) Highly active catalyst generated by reduction at 400°C..... 157

Figure 5.18: P- and R-branch band envelopes as observed on a sulfided catalyst reduced at 300°C during FT synthesis 158

Chapter 6

Figure 6.1: a) Unsulfided precipitated iron catalyst (uncalcined) b) Catalyst calcined at 400°C..... 164

Figure 6.2: a) Uncalcined catalyst sulfided with 2000 ppm Na_2S recorded at 298 K b) Mössbauer measurement at 77 K c) After calcination at 400°C, recorded at 298 K..... 167

Figure 6.3: Uncalcined sample sulfided with 20000 ppm Na_2S 168

Figure 6.4: 20000 ppm polysulfided catalyst after calcination at 400°C..... 168

Figure 6.5: Mössbauer spectrum of spent catalyst sulfided with 5000 ppm polysulfide recorded at 298 K..... 169

Figure 6.6: Mössbauer spectrum of a catalyst sulfided with 2000 ppm polysulfide, after FT synthesis, showing carbide formation (recorded at 298 K)..... 170

Figure 6.7: The effect of increasing sulfide content on particle size distribution of uncalcined catalysts sulfided in the range 2000-20000 ppm S at pH 6.9..... 175

Figure 6.8: Walker Diagram of iron species showing relationship between δ and s-electron density..... 178

Chapter 7

Figure 7.1: The effect of increasing level of sulfidation on ferric and ferrous ion solution speciation at pH 10.75.....185

Figure 7.2: Effect of sulfidation level on the equilibrium distribution of sulfide species at pH 10.75 186

Figure 7.3: Effect of increasing sulfide addition on the solution speciation at pH 8.5.....187

Figure 7.4: Distribution of sulfide species at pH 8.5, with increasing sulfide content 188

Figure 7.5: Solution speciation at pH 6.9 as a function of sulfide content.....189

Figure 7.6: Distribution of sulfide species at pH 6.9 as a function of sulfide content.....190

Figure 7.7: Effect of sulfidation pH on the system sulfided with 500 ppm S.....191

Figure 7.8: Effect of sulfidation pH on solution speciation in a system sulfided with 20000 ppm Na_2S.....192

Figure 7.9: Effect of sulfide source on the distribution of sulfide species at pH 10.16 193

Figure 7.10: Effect of sulfide source on the distribution of sulfide species at pH 6.9.....194

Figure 7.11: Effect of pH of polysulfide addition on sulfide solution speciation.....195

Chapter 8

Figure 8.1: Variation of specific activity with sulfide content 206

Figure 8.2: Activity per unit area of sulfided catalysts as a function of sulfide content 207

Figure 8.3: Olefinity of sulfided catalysts as a function of carbon number.....209

Figure 8.4: Product selectivity of catalysts sulfided in the range 500-20000 ppm S 211

Figure 8.5: Comparison of the oxygenate selectivity of sulfided catalysts.....212

Figure 8.6: Variation of surface area with sulfide content prior to calcination.....215

Figure 8.7: Temperature Programmed Reduction profiles of precipitated-iron catalysts: a) unsulfided catalyst b) Catalyst sulfided with 200 ppm S superimposed on catalyst sulfided with 20000 ppm S 218

Figure 8.8: Phase diagram of the reduction of iron oxide 219

Figure 8.9: The effect of sulfide content on the reduction peak of hematite to magnetite for precipitated-iron catalysts.....220

Chapter 9

Figure 9.1: Product selectivity of catalysts sulfided using different sulfide sources 236

Figure 9.2: Distribution of oxygenated products for various sulfided catalysts.....236

Figure 9.3: Olefinity of products obtained from catalysts sulfided using various sulfide sources.....237

Chapter 10

Figure 10.1: Pourbaix diagram for the S-H_2O system at 100°C considering only sulfur, sulfides, thiosulfates, tetrathionates and sulfites 240

Figure 10.2: Pourbaix diagram for Fe-OH system at 25°C 241

Figure 10.3: Reduction profiles of catalysts sulfided with 2000 ppm S **a)** sulfided with Na_2S **b)** Catalyst sulfided with $(NH_4)_2S$.....246

Figure 10.4: The dissociation of sulfide species as a function of pH at 25°C.....249

Figure 10.5: Effect of sulfidation pH on the solution speciation of a 2000 ppm Na_2S sulfided system 251

Figure 10.6: Variation in surface area of with pH of uncalcined catalysts sulfided with 2000 ppm S from polysulfide 255

Figure 10.7: Effect of pH of sulfidation on the specific activity of catalysts sulfided with 2000 ppm polysulfide.....256

Figure 10.8: Rate of product turnover per active site for catalysts sulfided with 2000 ppm polysulfide at the start, middle and end of precipitation 257

Figure 10.9: Schematic representation of the proposed model of the effect of sulfide addition on iron-oxyhydroxide crystallite growth.....258

Figure 10.10: Olefin selectivity of 2000 ppm polysulfided catalysts prepared by sulfidation at pH 10.75, 8.5 and 6.9.....261

Figure 10.11: Product selectivity of catalysts sulfided at various pH values with 2000 ppm polysulfide 262

Figure 10.12: Oxygenate selectivity of catalysts sulfided at various pH values 262

Chapter 11

Figure 11.1: Product selectivity of impregnated and co-precipitated catalysts....270

Figure 11.2: Olefinity of impregnated and co-precipitated catalysts....271

Figure 11.3: Effect of calcination temperature on olefin selectivity....274

Figure 11.4: Effect of calcination temperature on product selectivity....274

Figure 11.5: Olefinity of products obtained from sulfided catalysts operating at lower CO conversions....277

List of Tables

Chapter 1

Table 1.1: Physical properties of Sulfur 3

Table 1.2: Logarithms of the solubility products of some sulfides in water at 25°C 7

Table 1.3a: Estimated thermodynamics for polysulfide species 12

Table 1.3b: Equilibrium constants for polysulfide species 12

Table 1.4: Influence of H_2S on 100 Co: 18 ThO_2, Kieselguhr catalyst 27

Chapter 2

Table 2.1: Preparation of sulfided precipitated-iron catalysts 35

Table 2.2: Task description for the chemisorption of CO on iron catalysts 51

Chapter 3

Table 3.1: Colours of selected precipitated-iron catalysts 66

Table 3.2: Elemental Analysis of sulfided precipitated-iron Fischer-Tropsch catalysts by Atomic Absorption Spectroscopy 69

Table 3.3: Sulfur content of Na_2S sulfided catalysts as determined by ICP analysis 69

Table 3.4: Major Miller Indices and d-spacings of JCPDS database iron-oxide number 330664 83

Table 3.5: Crystallite sizes of iron-oxide catalysts as determined from the Scherrer equation 91

Table 3.6: Percentage weight gain for catalysts sulfided with 20000 ppm S at different pH values obtained from TGA... 96

Table 3.7: The effect of sulfidation level on the pore shapes of calcined catalysts 97

Table 3.8: Variation in pore neck size with pH and source of sulfidation 101

Table 3.9: Pore Neck and Cavity sizes of spent catalysts 103

Chapter 5:

Table 5.1: Effect of pH of sulfidation on the position of the linear carbonyl peak 133

Table 5.2: Effect of sulfide source on the position of the linear carbonyl peak 134

Table 5.3: Peak assignemnts of stretching vibrations of sulfate groups 139

Table 5.4: Catenation ability of sulfided catalysts during *in situ* Fischer-Tropsch synthesis 154

Table 5.5: The effect of sulfidation pH on hydrocarbon chain length for catalysts sulfided with 500 ppm Na_2S after 90 minutes FT synthesis 156

Chapter 6:

Table 6.1: Hyperfine parameters calculated for precipitated-iron catalysts at 298 K 165

Table 6.2: Hyperfine parameters calculated at 298 K and 77 K for the uncalcined catalyst sulfided with 2000 ppm Na_2S 166

Table 6.3: Hyperfine parameters calculated for spent catalysts..... 171

Chapter 7

Table 7.1: Effect of solution speciation on crystallite size determined using XRD 199

Chapter 8

Table 8.1: Evaluation of sulfided catalysts in the Fischer-Tropsch reaction 205

Table 8.2: Surface areas of sulfided catalysts 214

Table 8.3: Total pore volumes of sulfided catalysts 217

Chapter 9

Table 9.1: Surface areas of catalysts sulfided at pH 10.75 with 2000 ppm S 231

Table 9.2: Pore volumes of catalysts sulfided at pH 10.75 with 2000 ppm S 232

Table 9.3: Temperature Programmed Reduction of sulfided iron catalysts 232

Table 9.4: Reactor data of catalysts sulfided with 2000 ppm S from different sources 233

Chapter 10

Table 10.1: Surface areas of 2000 ppm polysulfided catalysts sulfided at different pH values 243

Table 10.2: Total pore volumes of 2000 ppm polysulfided catalysts .. 245

Table 10.3: Effect of pH of sulfide addition on the reduction of iron species 247

Table 10.4: Activity data of catalysts sulfided with 2000 ppm polysulfide at different pH values 248

Table 10.5: Activity data of catalysts sulfided with 2000 ppm Na_2S at different pH values 248

Table 10.6: The dissociation of dissolved substances as a function of pH at 75°C 250

Chapter 11

Table 11.1: Surface areas of impregnated and co-precipitated sulfided iron catalysts 269

Table 11.2: Total pore volumes of impregnated and co-precipitated sulfided catalysts 269

Table 11.3: Comparison of co-precipitated sulfided and impregnated catalysts in the FT reaction 270

Table 11.4: Reactor data of catalysts sulfided with 2000 ppm polysulfide 273

Table 11.5: CO conversions of sulfided catalysts used in olefinity study 276

List of Terms and Abbreviations

Abbreviations

AAS	Atomic Absorption Spectroscopy
BET	Brunnauer, Emmett, Teller method of surface area determination
DRIFTS	Diffuse Reflectance Fourier Transform Infrared Spectroscopy
FT	Fischer-Tropsch
ICP-MS	Inductively Coupled Plasma - Mass Spectrometry
ppm	parts per million
SEM	Scanning Electron Microscope
TON	Turnover Number
TPR	Temperature Programmed Reduction
XPS	X-Ray Photoelectron Spectroscopy
XRD	X-Ray Diffraction

Glossary of Terms

co-precipitation	sulfidation (see above) of iron catalysts during the precipitation process
impregnation	the addition of sulfide by incipient wetness to a dried precipitated-iron catalyst
sulfidation	addition of sulfide to precipitated-iron catalysts
sulfidation pH	refers to the pH at which sulfide was added during precipitation
syngas	mixture of CO and H_2 used as feedstock in the Fischer-Tropsch reaction

Part A: Characterisation studies

This section, which spans Chapters 3 to 7, deals with the effects of sulfide addition on the morphology and composition of precipitated-iron Fischer-Tropsch catalysts. Firstly, the bulk morphology is discussed with reference to XRD, SEM and porosimetry results. Then, the effect of sulfide species on the structure and composition of the catalytic surface is dealt with using XPS and DRIFTS studies. The influence of sulfide ions on the chemical environment of the iron atoms in the catalysts is further investigated using Mössbauer spectroscopy. Finally, a solution speciation model is constructed in an attempt to rationalise the observed morphology.

Chapter 1
Introduction

Foreward

This thesis deals with the addition of aqueous sulfur species to precipitated-iron Fischer-Tropsch (FT) catalysts. However, in order to place this study in perspective, a certain amount of background information is required. This chapter provides an introduction to some of the more pertinent topics.

The incorporation of sulfur into Fischer-Tropsch catalysts is expected to alter not only the morphology, but also the catalytic behaviour. It is therefore instructive to review the chemistry of sulfur and its compounds. There are certainly many aspects of sulfur chemistry which are not discussed; rather, reference has been made to the more salient topics which have bearing on the effects of sulfur on iron Fischer-Tropsch catalysts.

The current status of the Fischer-Tropsch reaction, and in particular the use of iron catalysts is then considered. Notable emphasis is placed on the development of unsupported iron catalysts. The applicability of the study of sulfur and its relation to catalysis is then demonstrated in a discussion of the effects of sulfur on the Fischer-Tropsch process.

1.1. Some aspects of sulfur chemistry

Sulfur, a name apparently derived from the Sanscrit *sulvere* and based on the Latin terms *sulphurim* and *sulphurium* [1] has found mention in texts as diverse as poetry and alchemy. In earlier vernacular it was referred to as brimstone, which symbolized the wrath of God to the inhabitants of Sodom and Gomorrah, who "witnessed brimstone and fire from the Lord out of heaven"[2]. In similar fashion, its highly inflammable nature was used by sixteenth century poets to invoke imagery of Hell's inferno [3]:

> "As when that devilish iron engine, wrought
> In deepest hell, and fram'd by furies' skill,
> With windy nitre and quick sulphur fraught,
> And ramm'd with bullet round, ordain'd to kill,
> Conceiveth fire."
>
> Edmund Spenser, 1599
>
> The Faerie Queene book 1 c VII, xiii

It was described by seventeenth century philosphers as a "mystic, inscrutable spirit" [1], and elicited much interest from alchemists who endeavoured to unravel its mystery. From the 'fixing' of mercury with sulfur to the distillation of sulfurous compounds, these early experimentalists formulated their remarkable theories which have endured for nearly fifteen centuries. The synthesis of sulfuric acid from sulfur and pyrites is perhaps the most outstanding discovery of the occidental alchemists, while the use of sulfur in gunpowder can be credited to the 12 th century Chinese phlogistans [4].

There was however, in those early days, still much debate as to the precise nature of this 'chemical enigma'. J.R. Glauber, in the mid 1600's, advocated the hypothesis that sulfuric acid and a combustible substance were the chief constituents of sulfur [1]. It was not until the 18th century that A.L. Lavoisier and other anti-phlogistans demonstrated the fallacy in such hypotheses, and proved that sulfur "does not consist of various elements, but represents one element"[4].

Atomic number 16, sulfur, is the fifteenth most abundant element in the earth's crust. It is essential for the survival of living organisms, and exists in various allotropic forms. Four of the ten reported isotopes of sulfur are stable, with a distribution of 95.1% ^{32}S, 0.74% ^{33}S, 4.2% ^{34}S and 0.016% ^{36}S [5].

The physical properties pertinent to the chemistry of this yellow, nonmetallic element are summarized in Table 1.1:

Table 1.1: Physical Properties of Sulfur

Atomic number	16
Relative atomic mass	32.06
Relative density (rhombic form)	2.07
Melting point	112.8°C
Boiling point	444.674°C
Allotropes:	
Rhombic	<95.6°C
Triclinic	>95.6°C
Molten sulfur	112.8°C - 160°C

Rapidly cooling molten sulfur results in the formation of a reddish-brown solid known as *plastic* sulfur. Flowers of sulfur, used as a plant fungicide, is obtained by subliming sulfur vapour. The latter is comprised of S_2, S_4, S_6 and S_8 molecules.

Naturally occurring compounds of sulfur are widespread, particularly sulfides and sulfates, and native sulfur deposits are found in Sicily and the USA. Equally, as a result of its abundance and reactivity, the range of synthetic products containing sulfur is impressive and encompasses both organic and inorganic compounds.

Sulfides are inorganic compounds of sulfur with the more electropositive elements. Ionic sulfides, containing the S^{2-} ion, are formed with metals, whereas organic thio-complexes are considerably covalent.

Sulfides of alkali metals with s^2p^6 configuration and low cationic charge (eg. Na^+, K^+) have large solubility products and frequently exhibit deliquiscent behaviour. This tendency is accounted for by a preferred coordination with oxygen rather than sulfur. Despite such high solubility, the crystal structures of two hydrates of sodium sulfide, namely, $Na_2S.5H_2O$ and $Na_2S.9H_2O$ have been determined. Anhydrous Na_2S assumes the antifluorite type structure, where the cations are tetrahedrally coordinated and the sulfide ions are surrounded by eight sodium neighbours forming a cube. This antifluorite structure is analogous to that formed by the corresponding oxide, selenide and telluride of sodium [5].

In contrast to the bonding between sulfide and alkali metals, the bonding in transition metal sulfides is of a more covalent nature than in the corresponding oxides, due to sulfur having a lower electronegativity than oxygen [6]. This relates to Pearson's Hard-Soft Acid-Base Theory [7], in which coulombic attraction is significant for the hard-hard interaction, while covalence is of importance in the so-called soft-soft complexes. As a consequence of their being non-ionic, metal sulfides form non-stoichiometric phases. Each phase exists over specific ranges of temperature and sulfur pressure.

For gas-phase sulfidation by H_2S, iron has a low free energy of bulk sulfide formation (ΔG_f° (600K) = -57.3 kJ/g atom). In addition, most metals used as catalysts (eg. Fe, Co) do not form stable bulk sulfides under reaction conditions, and sulfur poisoning may hence be rationalised in terms of surface sulfide thermodynamics [8].

The aqueous chemistry of sulfur is extensive and involves complex equilibria. In addition, sulfur speciation is largely dominated by kinetics, not thermodynamics. Sulfide ions are strong bases, and hydrolyse to give H_2S below pH 7, and HS^- at high pH values. Some typical decomposition routes of sulfide are shown in Figure 1.1 [9].

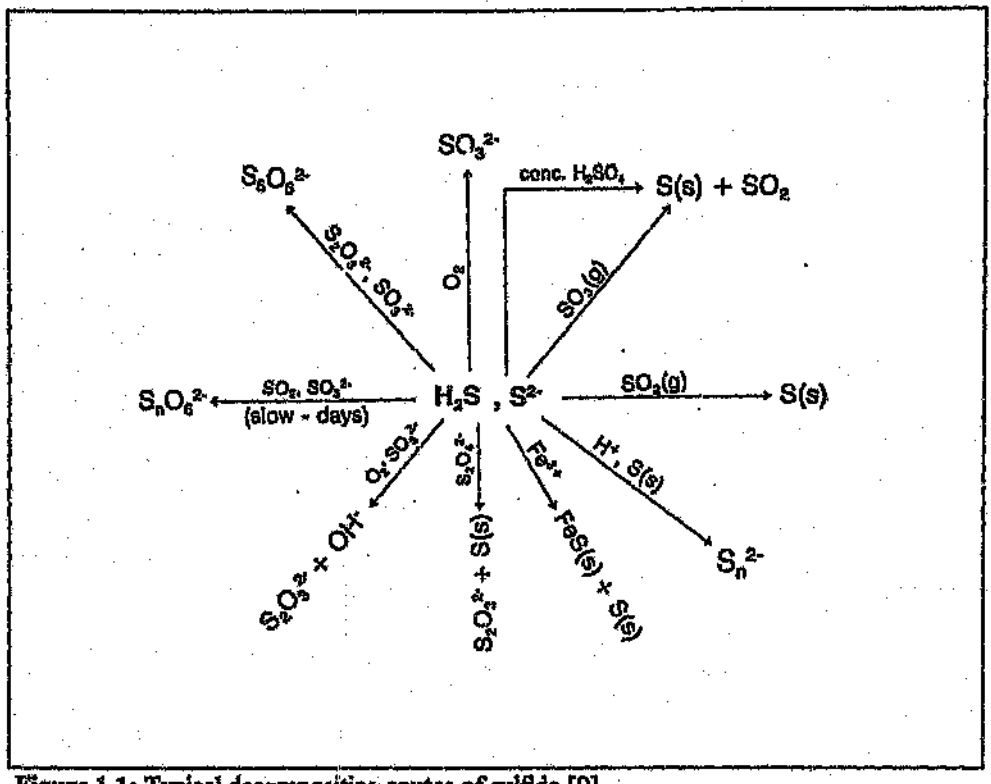


Figure 1.1: Typical decomposition routes of sulfide [9]

The S^{2-} concentration is strongly dependent on the pH of the solution and the presence of oxidising or reducing species. This in turn affects the formation of metal sulfides, the solubility product of which may be readily correlated with the electronic configuration and charge of the metal cation (Table 1.2 [5]).

Table 1.2: Logarithms of the solubility products of some sulfides in water at 25°C [5]

MS	Solubility Product K_{sp}	MS	Solubility Product K_{sp}
MnS (green)	-13	ZnS (cubic)	-24
MnS (pink)	-10	ZnS (hexag)	-22
FeS	-17	CdS	-26
CoS (α)	-20	HgS (black)	-52
CoS (β)	-25	HgS (red)	-53
NiS (α)	-19	SnS	-25
NiS (β)	-24	PbS	-27
NiS (γ)	-26	PoS	-28
CuS	-35		

The range of metal sulfides is certainly extensive and a discussion of the chemistry of each one is beyond the scope of this review. However, since the main focus in this study is on iron, the chemistry of iron sulfides is explored in more detail.

Iron sulfide obtained by precipitation from aqueous solution is of a thermodynamically unstable form. Both water held in the fresh precipitate, as well as exposure to air, converts this unstable product to FeS_2 (pyrite or marcasite form). Also incorporated are hydroxides and sulfate-containing compounds. Precipitates of Fe_2S_3 have been reported but they decompose readily [5].

The persistency-field Eh-pH diagram for pyrite is given below, showing the domain of pyrrhotite (FeS), the other thermodynamically stable sulfide phase [10].

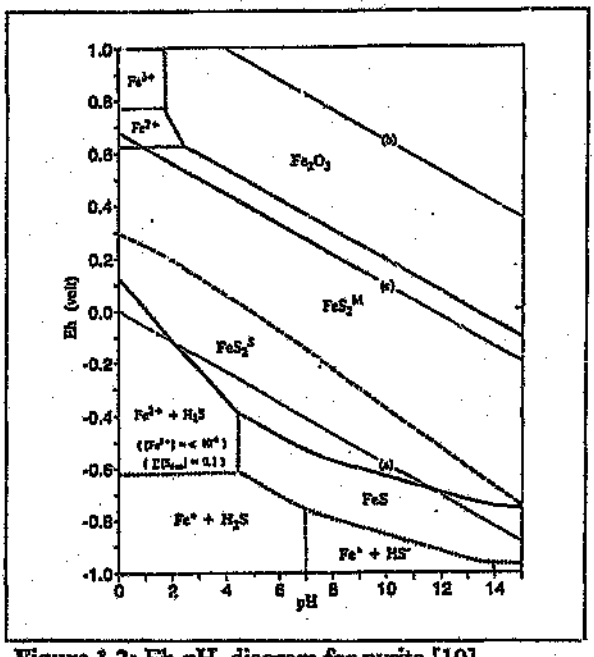


Figure 1.2: Eh-pH diagram for pyrite [10]

Polysulfides are homonuclear sulfur ligands of the form S_n^{2-} ($n \geq 2$). Owing to their high coordination number these polydentate ligands constitute a vast and rapidly expanding facet of sulfide chemistry.

Sulfur chains, S_n^{2-} with $n > 3$, exhibit stereochemistry. A dihedral angle ranging from 60° to 110° between sulfur atoms in the polysulfide chain has been found. For instance, S_5^{2-} may occur either as the cis or trans isomer, with a dihedral angle of 90° as illustrated in Figure 1.3 [6].

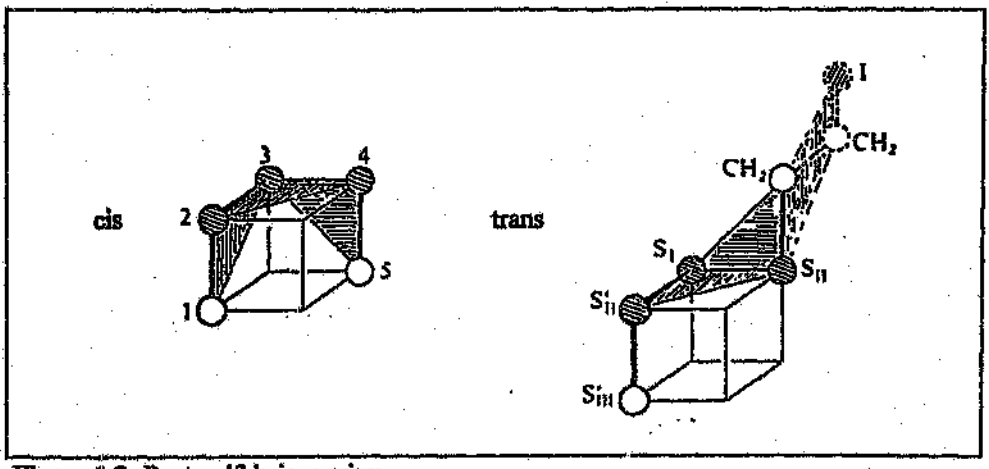


Figure 1.3: Pentasulfide isomerism

A median bond length of 2.02 - 2.06 Å has been reported for terminal S-S bonds in tetrasulfides and longer chain polysulfides, with intrachain S-S bondlengths in the range 2.05 - 2.07 Å. These bonds are all shorter than the 2.08 Å determined by Pauling on the basis of pure p-bonding character. Hence, it is inferred that p-π bonding or resonance effects assist in the distribution of negative charge evenly along the sulfur chain, and so doing reduce bondlengths [12].

Digesting sulfur with aqueous sulfide still remains one of the most widely used methods for obtaining polysulfides (mainly S_4^{2-} and S_5^{2-}) in solution. Preparations in liquid ammonia are however also common, and produce sulfur chains varying in length from S_2 to S_8 [13].

There are several routes to polysulfide complexes [11], such as the oxidative addition of elemental sulfur to a coordinatively unsaturated electron-rich metal. This method has found particular application in the synthesis of organometallic complexes such as $CpRh(PPh_3)(S_5)$. Direct substitution of other ligands by polysulfide anions is another method which has been used to good effect.

In aqueous media, polysulfides undergo hydrolysis with thermodynamic stability decreasing from pentasulfide to disulfide [9]. The polysulfide species in equilibrium with sulfate and sulfide is shown in Figure 1.4 as a function of pH and Eh.

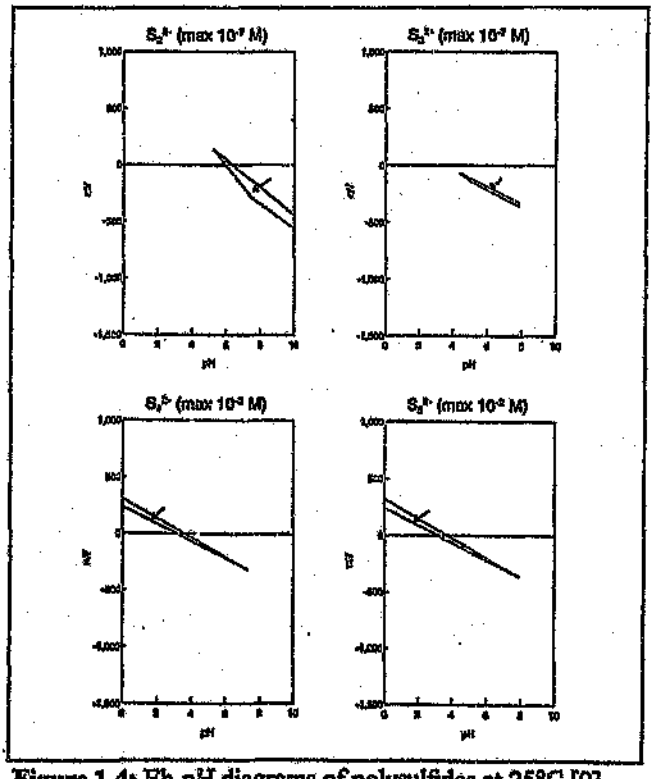


Figure 1.4: Eh-pH diagrams of polysulfides at 25°C [9]

Polysulfides are also unstable in acidic media (pH < 5), decomposing rapidly to yield elemental sulfur and H_2S [14]. This is the principal inherent in the turbidimetric determination of polysulfide in aqueous samples. In mildly acidic to alkaline solutions, polysulfides can be precipitated by a large number of metal ions.

According to Giggenbach [15], S_2^{2-} and S_3^{2-} are formed exclusively in extremely alkaline solutions, while S_5^{2-} and S_4^{2-} predominate under most conditions. These findings have been disputed by Clarke *et al* [12], who asserted that trisulfide dominated over tetra- and pentasulfide in the pH range 7.0-8.5. Furthermore, they observed the formation of polysulfides during the catenation of monosulfide to S_8 in the presence of chelated Fe (III).

Being inherently labile species, S_n^{2-} ligands are reactive and undergo both intra- and intermolecular redox reactions [16]. Novel ligands such as $S_3O_2^{2-}$ or S_3O^{2-} may be formed by oxidation of S_n^{2-} by O_2, and, via a reductive-elimination process, $Cs_2[Mo_2(S_2)_6].nH_2O$ can generate S_2.The chemistry of Cp_2TiS_5 is extensive and is of singular importance in the synthesis of polysulfur rings [17]. Owing to the oxophilicity of titanium, displacement of the pentasulfide occurs readily and this constitutes the basis of high yield syntheses of cyclo-S_6 and cyclo-S_7, via the Schmidt transfer reaction.

The decomposition of polysulfide is accelerated by increasing temperature as shown by the decreasing values of the equilibrium constants in Table 1.3a and 1.3b below [18]:

Table 1.3a: Estimated thermodynamics for polysulfide species

Reactions	ΔG° (298 K) (cal mol^{-1})	ΔS° (298 K) (cal mol^{-1} deg^{-1})
$S\ (s,l) + S^{-2}\ (aq) = S_2^{-2}(aq)$	-1500	2.7
$S\ (s,l) + S_2^{-2}\ (aq) = S_3^{-2}(aq)$	-1400	1.4
$S\ (s,l) + S_3^{-2}\ (aq) = S_4^{-2}(aq)$	-1100	1.3
$S\ (s,l) + S_4^{-2}\ (aq) = S_5^{-2}(aq)$	-800	1.3

Table 1.3b: Equilibrium constants for polysulfide species

T(°C)	pK_1^*	pK_2^*	pK_3^*	pK_4^*
25	-1.10	-1.03	-0.81	-0.59
100	-1.00	-0.88	-0.70	-0.53
200	-0.91	-0.76	-0.61	-0.48
250	-0.88	-0.72	-0.58	-0.46
300	-0.86	-0.68	-0.56	-0.44

Indeed, Giggenbach [19] is of the opinion that the presence of polysulfides in solution need not be considered above 240°C. Nonetheless, they form part of a complex equilibrium [13]:

$$S + HS^- \leftrightarrow S_n^{2-} + H_2O$$

which is affected by pH and temperature.

1.2. The Fischer-Tropsch Process

Defined as a 'hydrogenation of oxides of carbon producing higher hydrocarbons and/or alcohols, the carbon chains of the molecules being predominantly straight in the range C_4 to C_{10}' [20], the enormity of the contribution made by the Fischer-Tropsch process both economically and in the prolific amount of literature generated as a result of research, should not be underestimated.

Mechanistic studies have elucidated most, if not all, of the reaction pathways that present themselves in what is arguably the most diverse of product distributions. However, from a more fundamental perspective, the entire process when performed over iron catalysts, can be condensed into two general reactions [21]:

$$CO + 2H_2 \rightarrow -(CH_2)- + H_2O \qquad \Delta_R H_{227°C} = -165 \text{ kJ}$$

$$CO + H_2O \rightarrow H_2 + CO_2 \qquad \Delta_R H_{227°C} = -39.8 \text{ kJ}$$

$$2CO + H_2 \rightarrow -(CH_2)- + CO_2 \qquad \Delta_R H_{227°C} = -204.8 \text{ kJ}$$

The principal reactions in FT synthesis are far from equilibrium and therefore it is kinetics, and not thermodynamics, which govern the yield of products [22]. However, the maximum temperature attainable is limited by a shift in selectivity towards methane, and accelerated carbon deposition at high temperature which leads to catalyst deactivation [23].

Consequently, the relatively high exothermicity associated with FT polymerisation necessitates efficient heat transfer to avoid overheating of the catalyst and this is effectively achieved for example via fluidised bed reactors. High gas velocities permit rapid heat exchange and facilitate the introduction of fresh catalyst into the reactor without disrupting the on-line process. Despite the disadvantage of having to remove catalyst fines from product streams, fluidised bed reactors have proven cost effective alternatives to fixed-bed systems. In particular, slurry phase systems, in which catalysts are suspended in a liquid, are more isothermal than their fixed-bed counterparts and can be operated at higher temperatures [21]. Pore diffusion limitations are also minimised by the small catalyst particles.

As with any reactor system, there are disadvantages, and as far as fluidised bed reactor-design is concerned, the formation of wax constitutes a serious problem. At low temperature the wax may become too viscous and inhibit fluidisation of the catalyst, while at high temperatures hydrocracking of the wax takes place. In addition, carbon deposition on iron catalysts induces deactivation at the higher temperatures Beacuse of this, fluidised bed reactors are used selectively in the synthesis of low molecular mass olefins and oils [24].

Wax production is carried out using fixed-bed reactors of the ARGF type developed by Ruhrchemie and Lurgi in post-war Germany. Packed with iron-based catalysts, these reactors are operated at temperatures of between 225°C and 280°C, since this is the regime most selective for wax formation and low carbon deposition. Moreover, higher reaction temperatures would result in catalyst overheating owing to inefficient heat transfer. Currently, removal of heat generated by the reaction is achieved through the production of steam on the water walls of the multitubular reactor. Many advances on these stalwart reactors coupled with an increased demand for high molecular weight waxes, have ensured that they still occupy a niche in the industrial FT process. Indeed, the diversity of reactors currently in commercial use is testimony to the fact that reactor design is as crucial to a catalyst's performance as its composition and structure.

To supplement the advances made in catalyst and reactor design, efforts are being expended to reduce the unavoidable downtime that results from catalyst deactivation due to coking. The Fischer-Tropsch reaction lends itself ideally to the notion of periodic operation, since hydrogen is both a constituent of syngas and is used for catalyst regeneration. Alternately switching between two predetermined syngas compositions, one richer in hydrogen, allows the production of hydrocarbons to continue even as the catalyst is being regenerated. Forced composition cycling, as it is also known, enhances catalyst longevity and results in significant selectivity modifications. Most notably, the yield of light hydrocarbons is improved as a direct consequence of the hydrogenation of deposited carbon to yield 'CH_2' species [25].

A myriad of hydrocarbons and oxygenates feature in the extensive product spectrum. Selectivity for longer chain products is governed by the ability of a catalyst to preferentially enhance the rate of chain propagation above that of chain termination. According to the Anderson, Schultz, Flory (ASF) polymerisation kinetics model, the product distribution may be determined using an equation which incorporates the chain growth probability, α:

$$W_n \ln = (1-\alpha)^2 \alpha^{n-1}$$

A least squares regression of the logarithmic form of this equation affords α via the slope and intercept [26]. Unpromoted, unsupported iron catalysts are generally associated with low α-values indicating a propensity towards gaseous products.

However, modifications in feedstock ratio, reaction temperature and catalyst design, have procured a product distribution that is specific for higher molecular weight long-chain hydrocarbons.

In a competitive market-driven economy, optimisation of reactor design and catalyst performance is essential. This "pursuit of excellence" requires a comprehensive understanding of the elements of a catalyst and their synergistic effect. The application of principal component analysis (PCA) or ANOVA tables to a 2^k factorial formulation would promote future FT catalyst design [25]. Furthermore, the use of advanced computational techniques has proved its worth in the characterisation of heterogeneous catalysts. The approach is based on a model generated using initial data and refined with the aid of experimental results.

For FT catalysts, FTIR spectroscopy, SEM, XPS and SIMS would perhaps constitute the basis of experimental data used to qualify the proposed model It is the collaboration of a number of techniques which culminates in a comprehensive elucidation of the surface topology of an FT catalyst [27].

1.3. Iron Catalysts for use in the Fischer-Tropsch Reaction

Iron catalysts have been the mainstay of the industrial Fischer-Tropsch process since *circa* 1920 because not only are they relatively inexpensive to prepare, but give good product turnover with a broad product spectrum. Of late, much work has been done on tailoring iron-based catalysts to home in on specific products such as light olefins, oxygenates, etc. Such modifications have been brought about through the incorporation of structural and chemical promoters [28]. Indeed, extensive literature is available on impregnated catalysts, supported on a host of oxide materials that range from titania and silica to thoria.

Unsupported iron catalysts, perhaps regarded as the traditional Fischer-Tropsch catalysts, have also been modified in various ways. The Kolbel-Ralek slurry-phase system utilised pulverised catalysts prepared by precipitation or from fused iron [21]. Recent work has been based on spherical particles prepared by spray drying [29]. Ultrafine iron oxide catalysts have also found use, and exhibit high activity and oxygenate selectivity.

Precipitated iron catalysts still find application in fixed-bed reactors [28,30]. Various supports, such as silica and zinc oxide, have been added to improve the stability of these catalysts towards thermal sintering [31]. Furthermore, the rate of reduction of iron has been enhanced through the incorporation of copper.

The addition of alkali metal promoters such as sodium and potassium has been used to increase the average molecular weight and olefinity of the hydrocarbons produced, as well as promote water-gas-shift activity [26, 28]. Recent work has shown that such promotion increases CO conversion through a maximum, whereafter further addition of promoter causes a decrease in product turnover.

The presence of sodium or potassium alters the binding energy and sticking probability of reactive molecules, improving the rate of CO dissociation [32] and stabilising reactive intermediates. At high alkali content however, accessible active metal surface area is reduced, and this impacts negatively on activity and selectivity [25].

Of all the aspects of commercial Fischer-Tropsch catalysts, it is the kinetics of especially iron-based catalysts, that has received the most attention [22]. The complexity of the mechanisms and sequence of reactions has complicated kinetic studies and has promulgated many schools of thought with oftentimes conflicting opinions. Nonetheless, assuming Langmuir adsorption theory, the identity of the surface species involved in the rate-determining step is not crucial in deriving a rate equation.

Whether it be the time honoured proposal of Anderson, advocating CO dissociation giving rise to surface hydroxyl species, or the more recent formulation of hydrogenation of adsorbed CO to afford methylene groups, the rate of FT reaction over iron catalysts is given by [22]:

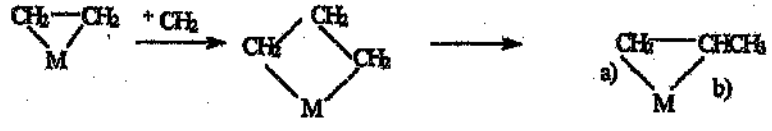
$$r = \frac{mP_{H_2}P_{CO}}{P_{CO} + \alpha P_{H_2O}}$$

where the constant, m, incorporates the rate constant as well as various experimental parameters. It may be instructive to mention that catalysts exhibiting high water-gas-shift (WGS) activity, tend to be less active toward FT reaction, as inferred by the foregoing rate e on.

The formation of liquids and high molecular weight compounds results in diffusion limitations, particularly for large particle sizes. However, Dry attests that the rates of diffusion are dependant on concentration gradients, which in turn depend on reaction rates at the surface of the catalyst. Thus the rate constant, m, incorporates a diffusion factor which varies for particle size and reaction conditions. Consequently, the aforementioned rate equation adequately describes the kinetics of all systems, from fixed-bed to slurry-phase [22].

Mechanistic studies have been complicated by the heterogeneity of the surface of the working iron catalyst. Early attempts to explain the mechanism invoked surface carbides and hydroxyl carbides [33]. The insertion of methylene into the carbon-carbon double bond of a surface vinylidene complex has also been proposed as a mechanism [34]. This vinylidene complex is supposedly formed by the reaction of a 'naked carbon atom' with surface methylene species. Current consensus among the protagonists in FT research, has shown carbene species to be involved in the chain-growth mechanism, and oxygenate activity to arise from CO insertion [24]. A detailed description of this mechanism is to be found in a review presented by Dry [22], wherein it is emphasised that the identification of a surface species does not conclusively prove its involvement and hence that this current mechanistic proposal is open to improvement.

An aspect not addressed by this mechanism is that of monomethyl branching, which is found to decrease with increasing carbon number. To this end, Dry has proposed a mechanism based on a two-point attachment to the catalyst, which proceeds via a metallacyclopropane intermediate [22]:



Owing to steric hindrance, methylene insertion at (a) is more likely than at (b) and hence this mechanism elucidates the formation of monomethyl alpha olefins or the fully hydrogenated monomethyl paraffins.

Furthermore, the symmetry of the ethylene (C_2) group allows for rapid CH_2 insertion, and this manifests itself in a lower than expected C_2 fraction in the ASF carbon number distribution.

Oxygenated products are purported to be formed via chain termination reactions or by CO insertion. Ethanol and methanol dominate at 220°C, while significant quantities of ketones and acids are produced at higher temperatures [22].

The effect of gas composition is also dependant on temperature. The ratio of hydrogen to CO correlates well with product selectivity at low temperatures (220°C), while a correlation factor is required for catalysts operating at 330°C since WGS activity is favoured at the higher temperature.

While alkali metals and light transition metal oxides (such as those derived from Mn) have been shown to ameliorate the performance of iron catalysts [35], various factors are known to accelerate their demise. Deactivation by sulfur and other electronegative contaminants has been extensively documented [36, 37, 38, 39]. In addition, fouling of catalyst pores by coke deposition reduces active surface area, as does accumulation of waxes.

Sintering is another factor resulting in loss of active surface area as crystallite growth occurs following exposure to heat [24]. For slurry phase systems, agglomeration of particles may occur, particularly when liquid waxes are produced, leading to loss of activity.

Recent research endeavours have concentrated on developing iron catalysts which exhibit a propensity towards linear paraffins, waxes and alpha olefins. Fuel production is no longer profitable owing to low crude oil prices [22], and indeed the Synthol CFB reactors - which were responsible for fuel production - have been put out of commission by Sasol [22]. The aforementioned products however, are considered to be high in value since they can be sold to other chemical concerns as feedstocks. Biodegradable detergents are produced from alpha olefins via the OXO-process, while the Aromax process requires C_6 to C_8 fractions for the synthesis of benzene, toluene and xylene (BTX's) [22]. Moreover, supported iron-manganese catalysts have been used in the production of C_2-C_4 hydrocarbons as enrichment gas for SNG (substitute natural gas) [40].

1.4. Sulfur and the Fischer-Tropsch Reaction

Owing both to its ubiquity and deleterious effects on iron Fischer-Tropsch catalysts, sulfur is among the most despised of catalyst poisons. As early as 1935, Fischer [20] cited a practical upper limit of 1 to 2 mg S/(m^3 of synthesis gas) and currently, the Rectisol process is employed to reduce the sulfur content of coal-based feedstocks to practicable levels [41].

As a consequence of the detrimental effects of sulfur on the activity and selectivity of catalysts, it has become the subject of a plethora of studies and investigations. Numerous review articles summarize the vast amount of literature that has been generated as a result [20, 31, 42].

Prior to 1960, the issue of sulfur poisoning had been little studied and the more noteworthy contributions dealt with the resistance to sulfur deactivation conferred by alkali promoters, particluarly potassium [43]. The majority of this pioneering work was done using H_2S; however, concentration gradients along the catalyst bed made interpretation of results exceedingly difficult. To circumvent this, Anderson and collegues [43] prepoisoned their alkali-promoted catalysts by immersion in a solution of a sulfur compound and heptane. Increased selectivity towards low molecular weight products was observed with increasing sulfur content.

The H_2:CO usage ratio also increased and such modifications were purported to be suggestive of sulfur having reacted with the potassium promoter. These findings are supported by the early work of Fujimura who observed similar promoter-dependant effects [42].

The selective poisoning of hydrogenation sites by sulfur has proven a convenient method for enhancing olefin selectivity [42]. Myddleton patented a Co:ThO_2:kieselguhr catalyst which, when operated in synthesis gas containing 57 mg organic S/m^3 of synthesis gas, exhibited no signs of deactivation and enhanced olefin selectivity. A similar unalkalized catalyst containing small quantities of H_2S or CS_2 showed a marked decrease in the yield of gaseous products, with a propensity towards the liquid hydrocarbon fraction [36].

There has been considerable criticism levied at (these) early poisoning studies by Bartholomew *et al*, who claimed that they were carried out under conditions of heat and mass transport effects which disguised the consequences of poisoning [37]. Furthermore, ill-defined regimes of P_{H_2S}/P_{H_2} did not provide the data necessary to predict deactivation rates during exposure to commercially applied sulfur levels. Consequently, the authors pursued deactivation studies of the effects of *in situ* low-level H_2S exposure on the activity and product distribution of cobalt and iron catalysts.

They were able to differentiate between monolayer surface sulfides formed at low H_2S concentrations (< 2ppm) at 500K, and bulk sulfide formation which was observed at higher sulfur levels and lower temperatures. For equivalent S/metal coverages, *in situ* poisoning induced greater loss of activity than presulfiding. Determination of deactivation rate constants indicated that potassium and boron conferred sulfur resistance by slowing catalyst deactivation. Their mode of operation is proposed to be either direct scavenging of sulfur or an electronic modification of iron, rendering it resistant to poisoning.

The use of an additive as a 'sulfur-sink' is also documented in a study of coprecipitated Fe/Mn catalysts sulfided with H_2S. The rapid formation of MnOS protects the iron from deactivation by sulfur [44]. The formation of manganese sulfide is thermodynamically favoured to such an extent that sulfur is removed from the gas-phase, before any detrimental effect on catalytic efficacy can be observed.

The nature of the iron surface can also determine the extent to which sulfur poisoning is allowed to proceed. In a study of the poisoning of precipitated-iron oxide copper oxide catalysts by organic compounds, Rapoport and Muzovskaya observed that partially reduced catalysts were more resitant to sulfur poisoning [43]. They alluded to the presence of iron oxides in resisting deactivation by sulfur. Carbided or nitrided catalysts used by Anderson were also more sulfur-tolerant than untreated reduced samples [20].

Intriguingly, despite the negative publicity surrounding the presence of sulfur in iron catalysts, there are reports which intimate catalyst promotion by sulfur compounds. Stenger and Satterfield [45] reported a 60% increase in the activity of a fused magnetite catalyst exposed to synthesis gas containing 1.3 mg S per gram of iron, as H_2S. Some twenty years prior to this, Anderson reported that catalysts prepoisoned with less than 3 mg CS_2/g Fe were more active than fresh catalysts. The higher activities were attributed to disintegration by excessive carbon deposition, although similar promotion of nitrided catalysts could not be accounted for [43].

Indeed, as far back as 1929, a patent was awarded to I.G. Farbenindustrie Aktiengesellschaft for a series of iron-cobalt catalysts which exhibited extended catalyst life and enhanced olefin selectivity. Sulfide, either in the form of an alkali sulfide or via syngas containing H_2S, was added in quantities of between 0.15 and 0.4 percent of catalyst weight [42] in this early study.

As shown in Table 1.4, the addition of sulfur as H_2S of 0.67 mg S per gram of a 100 Co:18ThO_2:100 Kieselguhr catalyst resulted in a marked increase in liquid hydrocarbons with a decrease in the gaseous fraction. It has been noted however, that such promotion was observed for sulfur contents of less than 0.18% by weight, and that excessive quantities of sulfur cause severe poisoning [42].

Table 1.4: Influence of H_2S on 100 Co: 18 ThO_2 ; Kieselguhr Catalyst [42]

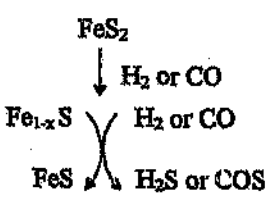
Amount of sulfur added, mg per g of catalyst	Catalyst temperature, °C	Ratio of hydrocarbon yields to corresponding yields before addition of sulfur	
		Condensed Oil	Hydrocarbons in effluent gas
0.00	183	1.0	1.0
0.67	183	2.3	1.0
3.50	183	2.1	0.8
7.94	183	-	0.5
7.94	195	2.0	1.3
13.4	195	1.5	-
33.5	207	1.2	2.1

P= atmospheric; Catalyst= 12 g in a Tubular fixed Bed Reactor

Studies on an iron-manganese bimetallic catalyst sulfated with ammonium sulfate (Fe:S 200:1) have revealed increased stability at 623K and enhanced light olefin selectivity. Both the deposition of carbon and production of methane are suppressed by this sulfation. However, the authors make mention of the fact that the amounts of sulfate added may not exceed 1 wt % S, otherwise complete deactivation occurs [46]. Unfortunately, reduced mechanical strength accompanies this promotion.

The nature of sulfur species present depends on the source and quantity of the sulfiding agent used. As mentioned previously, monolayer sulfides are formed at H_2S concentrations below 2 ppm at 500K, while bulk sulfides are formed at higher sulfur levels or lower temperatures [37].

In addition, the pretreatment and synthesis conditions to which the catalysts are exposed has a dramatic effect on the sulfur speciation. Pyrrhotite ($Fe_{1-x}S$) and pyrite (FeS_2) are converted to triolite (FeS) under reducing conditions at 400°C and 25 psig. According to the authors [47], Fischer-Tropsch reaction over synthetic pyrrhotite resulted in complete conversion to triolite based on the following scheme:



This scheme affords an explanation for the desulfurization activity of iron oxides in coal-gasification.

As a poison, the mode of action of adsorbed sulfur is principally electronic in nature although chemical effects dominate under certain conditions. For instance, the preferential formation of sulfides on sites of highest electronic density [48] serves to decrease the affinity with which the metallic catalyst attracts reactant molecules. Weakening of the CO-bond and a decrease in the binding energy of hydrogen chemisorption are consequences of the reduction in site density on metal centres. Moreover, the adsorption of olefinic compounds is enhanced under these conditions and this accounts for the lower hydrogenation activity that exists in sulfur-poisoned catalysts [48]. A competition scenario is created as the adsorption of unsaturated hydrocarbons increases the electron density at the active site, and this can function to lower the toxicity of the adsorbed sulfur.

1.5. Aims of this study

Most studies of sulfur interaction with iron catalysts have relied on the sulfur-containing compound being a gas-phase adsorbent. It is therefore the aim of this study to investigate the presence of extraneous sulfur compounds added as dissolved salts during the precipitation step of catalyst preparation. The effects of catalyst pretreatment and reaction conditions on sulfur speciation, as well as structural modifications brought about by the sulfur are to be considered as part of a detailed surface and reactor study.

The use of various characterisation techniques in the elucidation of bulk and surface morphology is to be investigated. These techniques include Mössbauer Spectroscopy, X-ray Powder Diffraction (XRD), Diffuse Reflectance Fourier Transform Infrared Spectroscopy (DRIFTS), and X-Ray Photoelectron Spectroscopy (XPS).

It is further hoped that the effect of sulfide on the aqueous precipitation system of iron catalysts, can be quantified as part of a solution speciation study.

Finally, the Fischer-Tropsch activity of catalysts co-precipitated with sulfur is to be investigated. The effect on product selectivity and rate of CO conversion are to be compared to an unsulfided catalyst.

As a footnote, a preliminary study on the effect of sulfide on impregnation is anticipated to shed some light on the influence of sodium promotion of sulfided catalysts.

Chapter 2

Experimental Methods

2.1. Introduction

It is both the chemical composition and physical structure of catalysts that provide the activity and selectivity they exhibit. Therefore, in order to fully unravel the mystery behind these essential components of industrial chemistry, a diverse assortment of experimental methodology is required.

The availability of highly specialised equipment has opened a whole field of chemistry in the form of catalyst characterisation. Modern literature abounds with methods for the elucidation of surface structure and bulk morphology. These techniques utilise the interaction of electromagnetic radiation, electrical fields, and neutral or charged particles with surfaces to characterise their geometric structure and chemical composition [49]. A comprehensive list of such techniques is given by Hirschwald [49]. Included in this are a plethora of spectroscopic techniques, as well as various forms of microscopy, and X-ray analysis. Many can be used for quantitative analysis, and some also have the facility for *in situ* characterisation. The latter feature makes these techniques applicable to the study of catalysts.

Control of synthetic procedures to ensure consistency in catalyst preparation is an important issue in catalyst synthesis. This is true for precipitated-iron catalysts where variability in temperature, concentration of reagents and pH of precipitation can result in markedly different products [31]. Since it was beyond the scope of this study to examine the effects of such preparation variables, all catalysts were prepared under conditions of controlled temperature, pH and precipitating reagent concentrations. Therefore in this investigation, catalyst differed only in the quantity of sulfur added, the source of sulfide, and the pH of sulfidation.

Numerous methods were used to assess the effect of added sulfur on the structural morphology and chemical reactivity of iron Fischer-Tropsch catalysts. Bulk characterisation via Mössbauer spectroscopy, XRD and AAS provided insight into the chemical composition and distribution of iron phases. Surface analysis was performed using XPS and DRIFTS.

Solution speciation modelling was then invoked to explain the observed morphology in terms of the metal-ligand equilibria present in aqueous precipitation systems. Furthermore, the behaviour of catalysts under Fischer-Tropsch reaction conditions was rationalised based on these model systems.

The ability of catalysts to hydrogenate carbon monoxide by the FT process was investigated using fixed-bed reactors coupled to in-line gas chromatographs. After an induction period, the activity and product selectivity was determined from a carbon mass balance under steady-state conditions.

2.2. Catalyst Preparation

Ferric nitrate ($Fe(NO_3)_3.9H_2O$) from Saarchem was used as the source of iron, and sodium carbonate (ACE chemicals) as the precipitating agent in the preparation of the precipitated-iron catalysts (Figure 2.1). In all instances, 300 ml 0.716 M $Fe(NO_3)_3.9H_2O$ at 75°C was mixed, while stirring, with 400 ml 0.7 M Na_2CO_3. Precipitation was allowed to continue until pH 6.9. Washing of the precipitate to remove sodium ions was done by successive centrifugation steps; the pellet being resuspended in deionised water between washes. Conductivity measurements of ± 200 µS of the supernatant were considered as low sodium levels. The catalyst was dried overnight at 120°C in a fan-oven and then crushed to 1180- 850 µm particles.

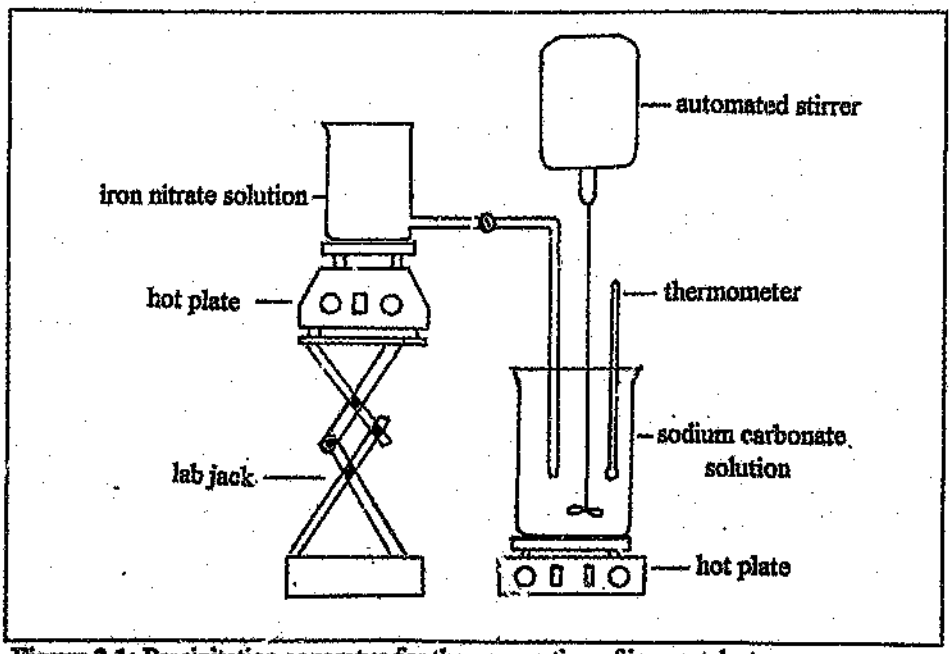


Figure 2.1: Precipitation apparatus for the preparation of iron catalysts

2.2.1. Co-precipitated sulfided catalysts

A range of co-precipitated sulfided catalysts were also prepared. The method used is analogous to that mentioned above except that sulfur was added at various pH values as shown in Table 2.1. Ammonium sulfide, $(NH_4)_2S$, was obtained as a 10% solution from Saarchem. For the polysulfided catalysts, ammonium pentasulfide $(NH_4)_2S_5$ was prepared according to the method of Krause *et al* [50], by the addition of sulfur to ammonium sulfide at room temperature, whilst stirring for 1 hour:

$$4(NH_4)_2S + S_8 \rightarrow 2(NH_4)_2S_5$$

While this procedure yields predominantly pentasulfides, minor quantities of $(NH_4)_2S_3$ and $(NH_4)_2S_9$ could also be formed [50].

Table 2.1: Preparation of sulfided precipitated-iron catalysts

CATALYST	SOURCE OF SULFUR	AMOUNT OF SULFUR[a] (parts S per million Fe)	pH OF SULFIDATION
1	Na_2S	500	10.75
2	Na_2S	500	8.5
3	Na_2S	500	6.9
4	Na_2S	2000	10.75
5	Na_2S	2000	8.5
6	Na_2S	2000	6.9
7	Na_2S	5000	10.75
8	Na_2S	5000	8.5
9	Na_2S	5000	6.9
10	Na_2S	20000	10.75
11	Na_2S	20000	8.5
12	Na_2S	20000	6.9
13	$(NH_4)_2S$	2000	10.75
14	$(NH_4)_2S$	2000	8.5
15	$(NH_4)_2S$	2000	6.9
16	$(NH_4)_2S_5$	2000	10.75
17	$(NH_4)_2S_5$	2000	8.5
18	$(NH_4)_2S_5$	2000	6.9
19	$(NH_4)_2S_5$	500	6.9
20	$(NH_4)_2S_5$	5000	6.9
21	$(NH_4)_2S_5$	20000	6.9

[a] parts per million by mass

2.2.2. Impregnated catalyst

A dried, unsulfided precipitated-iron catalyst (pore volume 0.5 ml/g) was impregnated with 500 ppm Na_2S in 2 ml deionised water using the incipient wetness procedure. Dehydration at 120°C in a fan oven afforded the sulfided catalyst.

2.3. Elemental Analysis

Atomic absorption spectroscopy (AAS) was performed on a Varian SpectrAA spectrometer equipped with Na lamp (330.2 nm, slit width 0.5) and Fe lamp (292.0 nm, slit width 0.2). Standards were prepared using $Fe(NO_3)_3.9H_2O$ (range 200-1000 ppm Fe) and NaCl (range 0- 200 ppm Na). Samples (0.1 g) were dissolved in warm *aqua regia* (2 HCl:1 HNO_3) and made up in deionised water.

Sulfur analysis was done externally on an ICP-MS apparatus with a detection limit of 0.1 % by mass.

2.4. Catalyst Pretreatment

Calcination was performed to remove nitrates and other potentially poisonous surface adsorbates prior to commencing Fischer-Tropsch synthesis. Catalysts were heated in air (GHSV = 2000 h^{-1}) at temperatures of either 200°C or 400°C for 16 hours. Where stated, calcined samples were characterised using the same techniques as freshly prepared catalysts.

2.5. Scanning Electron Microscopy

A Jeol (JSM-840) Scanning Electron Microscope (SEM) with a LINK analytical energy dispersive X-ray analysis facility (EDX) was used in the visual characterisation of the catalyst surface. Samples were mounted on aluminium stubs and carbon-coated for improved resolution. To obtain a secondary electronic image of the catalysts, beam energies of 10 or 20 keV were used. Better clarity was obtained at the higher voltage, but sample degradation occurred rapidly.

2.6. X-Ray Powder Diffraction Analysis

Catalysts were analysed both before and after calcination, and after Fischer-Tropsch synthesis. X-ray powder diffractograms were recorded on a Phillips PW1830 goniometer and optical system equipped with a Cu radiation source (CuK_{α}=1.5418 Å), operating with a generator voltage of 40 kV and current of 20 mA. A scan rate of 2 seconds per step (step size: 0.02° 2θ) was implemented in continuous scans of samples in the 10-140° 2θ range. Finely ground samples were either packed into aluminium sample holders or mounted as thin films on silicon wafers.

The database compiled by the Joint Committee on Powder Diffraction Studies (JCPDS), published by the International Centre for Diffraction Data, was used in the identification of iron phases [51].

The crystallite size of catalysts was inferred from the Scherrer equation which derives from X-ray line broadening [52]:

$$<L> = \frac{K\lambda}{\beta\cos\theta} \quad \text{.....(2.1)}$$

where <L> = particle dimension in the direction perpendicular to the reflecting plane
λ = x-ray wavelength
β = peak width {(width of broadened peak of sample)-(width of standard peak)}
θ = angle between beam and the normal on the reflecting plane (Bragg angle)
K = constant (0.9)

Owing to the relatively broad peaks observed for precipitated-iron catalysts, a certain degree of error is associated with the estimate of crystallite size.

2.7. Thermogravimetric Analysis

Spent catalyst samples were heated under oxygen atmosphere (30 ml/min) on a Du Pont 9900 TGA using a linear temperature program (10°C/min) to assess the level of carburization that took place during exposure to synthesis gas.

2.8. Colour Evaluation

A colour plate of all catalysts is included in Chapter 3 for visual assessment of the effects of sulfur on the typical dark-brown colour of hematite.

2.9. Porosimetry

Using the method of Brunnauer, Emmett and Teller (BET), the specific surface areas and total pore volumes of catalysts were measured using either an in-house built apparatus, or a Micromeritics ASAP 2010 porosimeter. Hysteresis plots of selected catalysts were generated using the latter equipment, and this information used in the estimation of pore shape.

Approximately 0.2 g of sample (uncalcined, calcined or post-reaction) was dried at 120°C prior to the adsorption of nitrogen at its liquefaction temperature. This thermal dehydration was carried out under flowing He on in-house constructed equipment, where only single-point BET values were determined. On the more sophisticated Micromeritics equipment, samples were degassed under vacuum for approximately 5 hours before multi-point BET analysis. Total pore volumes were determined at P/P_o of 0.975.

Nitrogen, at its liquefaction temperature, is one of the adsorbates most commonly used in the characterisation of surfaces by porosimetry. The quantity of gas adsorbed on a solid at constant temperature expressed as a function of the relative pressure (P_i/P_o) is termed an isotherm. The monolayer capacity (Vm) of the solid may be determined from the plateau of the adsorption isotherm. This quantity is used in the measurement of the specific surface area of the solid according to the BET equation [53].

2.9.1. Estimation of pore shapes

Following an initial proposal by Brunauer *et al*, adsorption isotherms have been classified according to the shapes they assume (Figure 2.2). These shapes are dependent on the mean pore size of the adsorbent and the intensity of the adsorbate-adsorbent interaction [54].

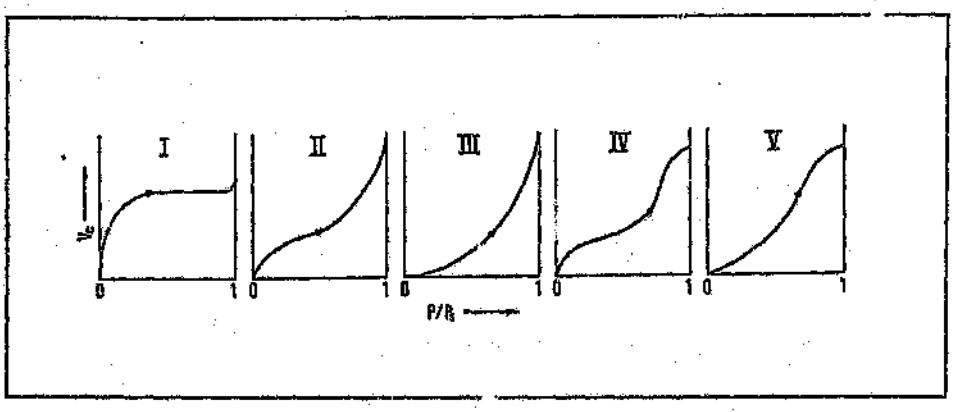


Figure 2.2: Shapes of adsorption isotherms

Type IV isotherms are typical of mesoporous solids (such as hematite) and exhibit hysteresis loops (Figure 2.3).

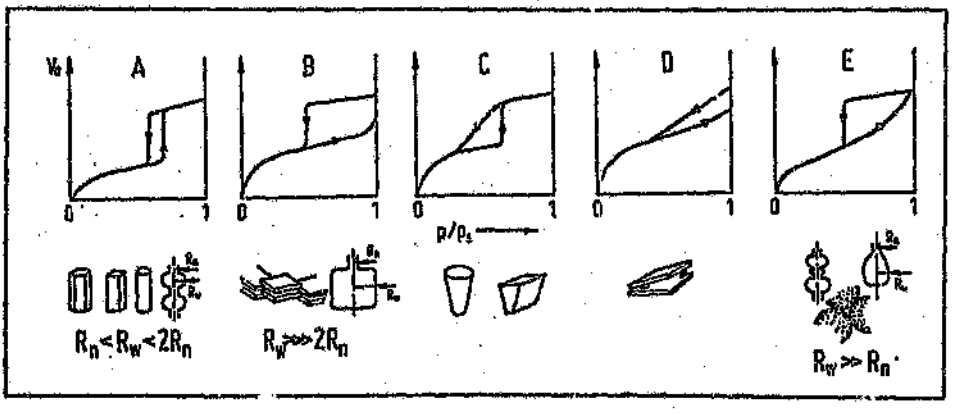


Figure 2.3: Type IV isotherms showing different hysteresis loops

These indicate the tortuosity of the pores of the adsorbent and are thought to arise from capillary condensation occurring simultaneously with multi-layer adsorption. Consequently, different radii of curvature for adsorption and desorption processes result at any given pressure within this hysteresis [55].

Associated with these hysteresis loops are various pore-shapes as proposed by de-Boer [54]. However, these were initially based on ideal solids with uniform pore-size, and since it is more common to find pore size distributions, slightly modified hysteresis loops are likely to be observed in real solids.

The Type A hysteresis loop (Figure 2.3) is associated with cylindrical pores of approximately constant cross-section. Slit-shaped pores give rise to Type B hysteresis loops, while Types C and D derive from Types A and B respectively. Seldom encountered, they indicate cone-shaped pores (Type C) and those formed by non-parallel plates (Type D). The most common hysteresis isotherm is Type E, which corresponds to pores that have constricted necks giving them the characteristic "ink-bottle" structure. Spheroidal cavities are also reported to yield Type E hysteresis loops [54].

The modified Kelvin equation (2.2) is used in the measurement of mesopore size as the adsorption/desorption isotherm becomes asymptotic at high relative pressures [56]:

$$R_k = \frac{-2\nu\cos\theta V_L}{RT} \times \frac{1}{\ln P_i / P_o} \quad \text{.....(2.2)}$$

$$t = 3.54\left[\frac{-5}{\ln P_i / P_o}\right]^{\frac{1}{3}} \quad \text{.....(2.3)}$$

$$R_p = R_k + t \quad \text{.....(2.4)}$$

where R_k = the Kelvin radius (Å)
ν = surface tension of nitrogen (8.85 ergs/cm^2)
θ = contact angle
V_L = molar volume of adsorbate (34.65 ml/g-mol)
R = gas constant
T = analysis temperature (K)
P_i/P_o = relative pressure (at least 0.99 to ensure saturation)
t = statistical thickness
R_p = pore radius (Å)

Since nitrogen is a wetting liquid, the contact angle (θ) of the meniscus it forms in a pore of Kelvin radius (R_k) is often equated to zero. Such practice has been deemed to be acceptable for desorption but is questionable for the adsorption of nitrogen [57]. Hence, desorption isotherms are regarded as a true reflection of the textural properties of a solid.

The true pore size is the sum of the Kelvin radius and the statistical thickness, t, according to equation (2.4). Determined from a de-Boer modified Halsey equation (2.3), the statistical thickness is the monolayer thickness of adsorbed nitrogen molecules on the inner wall of the pore.

In evaluating the tortuosity of mesopores, the adsorption path of the hysteresis yields cavity size, while the pore neck size may be determined from the desorption isotherm at any given relative pressure, by substitution into the Kelvin equation (2.2). Using nitrogen as adsorbate, the lower limit of the range of pore sizes for which the Kelvin equation is valid is 17.5 Å, while the upper limit is approximately 1000 Å.

2.9.2. Estimation of pore neck and cavity sizes

The method of Barrett, Joyner and Halenda (BJH), developed in 1951 was employed to determine the neck and cavity sizes of the pores [58]. Based on the Kelvin model of pore filling, and an assumption that the pores assume an approximately cylindrical shape, the BJH method relates the volume of adsorbate evaporated to the pore volume by the following equation:

$$V_{pn} = R_n\Delta V_n - R_n c \sum_{j=1}^{j=n-1} A_{pj} \quad \text{.....(2.5)}$$

where V_{pn} = mesopore incremental volume
R_n = ratio of the square of pore radius (R_p) to the square of the sum of the Kelvin radius (R_k) and the change in wall thickness (dt)
ΔV_n = volume desorbed in the nth desorption step
c = ratio of average core radius to average pore radius
A_{pj} = pore area of pores undergoing a thinning of their desorbed layers due to a desorption step. The summation of the area of these pores is over steps j =1 to j = n-1

2.10. X-Ray Photoelectron Spectroscopy

XPS spectra were recorded on a VG ESCALAB MkII spectrometer equipped with a heatable reaction cell attachment which could also be pressurised. Unmonochromatized Mg Kα X-rays at 15 kV/20 mA and an incidence angle of 45° were used to irradiate the samples. An analyzer slit width of 6 mm and pass energies , eV for wide scans and 20 eV for narrow scans were found to be optimal.

Calcined samples were reduced *in-situ* at either 300°C or 400°C under flowing hydrogen for 1 hour. The samples were then cooled to near ambient temperature before evacuation and analysis.

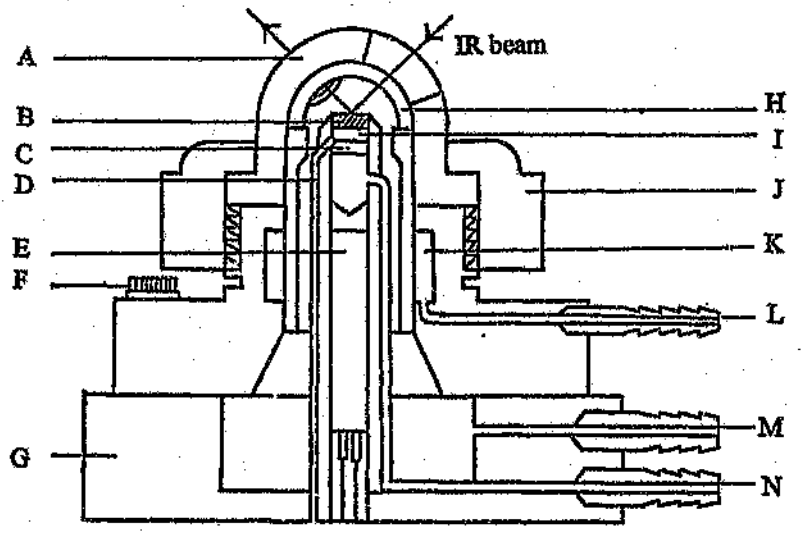
Linear background subtraction was performed prior to peak-fitting and S (2p) spectra were fitted according to the method of Termes *et al* [59], with doublets having ($^1/_2$, $^3/_2$) components and an intensity ratio of 1:2, constrained to a 20% Lorentzian, 80% Gaussian lineshape and a separation of 1.15 eV.

2.11. Auger Electron Spectroscopy

Auger electron spectroscopy was conducted on a catalyst sulfided with 20000 ppm Na_2S after it had been calcined and reduced *ex situ* at 400°C. Measurements were performed on a PHI 595 Scanning Auger Microprobe with electron beam voltage of 3 kV and current of 1 μA (stepsize 0.5 eV). Depth profiling was carried out using 3 kV Ar^+ ions at 30 μA/cm^2.

2.12. Diffuse Reflectance Infrared Spectroscopy

DRIFTS analysis was performed on a Nicolet Impact 420 spectrometer which comprised a KBr beamsplitter, DTGS detector and Ever-Glo™ mid-IR source. The sample compartment was equipped with a Harrick "Praying Mantis" DRA-2CI DRIFTS attachment. Powdered samples were contained in a variable temperature reactor cell as shown in Figure 2.4.



A: stainless steel dome
B: powdered catalyst sample
C: fritted disc
D: thermocouple
E: heating cartridge
F: screw
G: base-plate
H: ZnS hemispherical window
I: quartz powder
J: compression nut
K: water-cooled jacket
L: water outlet
M: gas inlet
N: gas outlet

Figure 2.4: Longitudinal section through the variable temperature DRIFTS reactor cell

The cell was heated via a cylindrical heating cartridge (150 W) which was inserted below the sample cup. A J-type thermocouple and RKC Rex-P90 temperature controller were used to control the temperature of the sample. The cell could be pressurized and therefore was sealed via o-ring seals. The use of a hemispherical ZnS single crystal window significantly reduced the distance that the IR beam had to traverse in air, thus improving the signal obtained from the sample. This window was held in place by a stainless steel dome.

Each measurement comprised 1024 scans in the region 4000-1200 cm^{-1}. Initial spectra were recorded using an activated carbon reference spectrum. Approximately 100 mg of each catalyst was used, and care was taken to ensure minimal differences in sample packing. Unless otherwise stated, all samples were calcined (200°C or 400°C) and reduced (300°C or 400°C) *in-situ* at the temperatures indicated. Calcination was performed in dry air (flow rate of 3 ml/min) for approximately 4 hours. Thereafter, the sample was reduced in a 1:1 H_2:He mixture (flow rate 2 ml/min) for 5 hours. Room temperature CO adsorption was performed after reduction at pressures of 2 to 8 bar using pure carbon monoxide. Fischer-Tropsch synthesis was conducted in a 2:1 CO:H_2 mixture (flow rate 2 ml/min) at 8 bar pressure, and a temperature of 250°C. Catalysts were left on-line for 5 hours, but analysed every 30 minutes. Samples were purged for 30 minutes with nitrogen gas after completion of each experiment to remove gas-phase reagents.

2.13. Mössbauer Spectroscopy

Uncalcined and calcined (400°C) catalysts sulfided with 2000-20000 ppm S from mono- and polysulfide sources (Na_2S and $(NH_4)_2S_5$) were analysed by Mössbauer spectroscopy. The effects of exposure to FT synthesis conditions on the phases of iron present in catalysts sulfided with 2000 and 5000 ppm sulfide were also investigated.

Mössbauer equipment consisted of a constant velocity drive with ancillary electronics and a $^{59}Co(Rh)$ γ-ray source. The source velocity was varied over a range of approximately 14 mm/s. Spectra were collected over 1024 channels with a dwell time of 100 μs per channel. Approximately 30 mg of sample was analysed at 298 K for room temperature measurements, and at 77 K using liquid nitrogen as a cryogen.

Initial data expressed γ-ray counts as a function of source velocity, v. Using the first order Döppler shift, this was related to γ-ray energy, E_γ [52]:

$$E\gamma = E_o\left(1+\frac{v}{c}\right) \quad \text{.....(2.6)}$$

where E_o = energy of the nuclear transition

c = speed of light

A least-squares curve fitting procedure which utilised a Lorentzian lineshape profile was employed to model the spectra as a series of quadrupole doublets and hyperfine-split sextets. Isomer shifts are quoted with reference to α-Fe (0.12 mm/s). Instrument calibration was performed using Fe foil.

2.14. Solution Speciation Modelling

The aqueous system present at pH 10.75, 8.5 and 6.9 during the precipitation of iron oxide from solutions of $Fe(NO_3)_3.9H_2O$ and Na_2CO_3 at 75°C was modelled using MINTEQA2 (Version 3.10). The input data file was created in PRODEFA2; and the parameters used are found in Appendix 1.

In order to assess the impact of aqueous sulfide species, the system was modelled following the addition of 1 ml, 60 ml, and 300 ml of 0.716 M $Fe(NO_3)_3.9H_2O$ to solutions containing sodium carbonate and the required total dissolved sulfide added from ammonium or sodium-based sources. The system was then modelled at the pH values calculated at the aforementioned additions of iron nitrate, namely pH 10.16, 8.54 and 6.88 respectively. Increasing concentrations of sulfide from any of the sources studied had no significant effect on the pH of the solution.

The carbonate concentration represented the total inorganic carbon content. The ionic strength was computed as part of the model, and activity coefficients computed using the Davies equation [60]. Mathematical details are given in Appendix 1.

An Eh value of either 100 or 280 mV was specified to allow the model to reach convergence, and the system did not appear to be sensitive to Eh inside this range. The Eh of the system was not measured experimentally; rather, the range selected was estimated from an Eh-pH diagram of water [61].

Indeed, it is noted by Brookins [61], that many problems are associated with Eh measurements since half-cell couples in water are often not in equilibrium. The Eh region selected in this study is typical of bog waters, which are said to be mildly reducing [61]. According to the Pourbaix diagram for the Fe-H_2O system, this Eh range suggests that suspended oxyhydroxides are the dominant species between pH 10.75 and 6.9 [62].

2.15. Temperature Programmed Reduction

The Gibbs free energy for the reduction of Fe_2O_3 to metallic iron is given by the expression [52]:

$$\Delta G = \Delta G^{\circ} + nRT\ln\left(\frac{p_{H_2O}}{p_{H_2}}\right) \quad \text{.....(2.7)}$$

where ΔG = change in Gibbs free energy for the reduction of hematite
ΔG° = Gibbs free energy change under standard conditions
n = stoichiometric coefficient of reaction
R = gas constant
T = temperature
p = partial pressure

Despite a positive value of ΔG° for the process, the reduction of Fe_2O_3 becomes thermodynamically feasible as the ratio of partial pressures decreases sufficiently at elevated temperatures.

The reduction behaviour of the unsulfided catalysts was investigated using in-house developed Temperature Programmed Reduction (TPR) apparatus [63]. Approximately 0.05 g of catalyst was heated to 950°C under flowing hydrogen (5% H_2/N_2 mixture) in a quartz reactor. The various reduction steps were recorded using a low temperature, dual filament thermal conductivity detector. Prior to analysis, samples were outgassed for 40 minutes at 150°C using UHP N_2.

2.16. CO Chemisorption

The use of CO chemisorption for the determination of the specific iron surface area originates from the work of Brunauer and Emmett [64]. Owing to the dissociative adsorption of CO at 300 K, low temperature chemsorption (194 K) is recommended. Unfortunately, this was not possible with the equipment used in this study, and hence CO chemisorption was performed at 300 K.

Metallic surface area was determined using CO chemisorption on an ASAP 2010 Chemi Instrument. Catalysts were reduced *in-situ* for 16 hours, whereafter CO adsorption was measured at 35°C.

The following table (Table 2.2) summarises the tasks performed by the chemisorption unit in the analysis of sulfided iron catalysts:

Table 2.2: Task description for the chemisorption of CO on iron catalysts

Task	Description	Gas	Temperature (°C)	Heating Rate (°C/min)	Time (min)
1	Flow	He	110	10.0	30
2	Flow	He	350	10.0	30
3	Flow	He	100	10.0	15
4	Evacuation	-	50	10.0	30
5	Flow	H_2	100	10.0	10
6	Flow	H_2	400	10.0	960
7	Evacuation	-	35	10.0	90
8	Evacuation	-	35	10.0	10
9	Leak Test	-	35	10.0	
10	Evacuation	-	35	10.0	20
11	Analysis	CO	35	10.0	

Samples were thoroughly dried and cleaned during the helium pretreatment to avoid erroneous results. A maximum outgas rate of 10 μmHg/min was allowed for the leak test, and the free space above the sample was computed during this procedure.

An equilibration interval of 100 seconds was found to be optimal during CO adsorption in order to achieve a tolerance of 5.000 mmHg at pressures ranging from 100 to 450 mmHg. Following unrestricted evacuation for 60 minutes, a repeat analysis was performed.

The volume of CO adsorbed per gram of sample was determined based on the assumption that Fe comprised 60% by mass, and a stoichiometry of 1:1 (CO:Fe). Since mainly linear carbonyl species were observed using DRIFTS, an adsorption stoichiometry of 1:1 CO:Fe was used. However, based on arguments of chemical bonding and steric reasons, many authors assume a 1:2 CO:Fe stoichiometry [65].

2.17. Fischer-Tropsch synthesis

Catalysts (2 g) were calcined at 200°C or 400°C as mentioned previously (section 2.4), and activated by reduction at 400°C (GHSV = 500 h^{-1}) for 16 hours. Fischer-Tropsch synthesis was performed at 250°C (GHSV = 400 h^{-1}) using syngas ($CO:H_2$:Ar; 30:60:10) at 8 bar pressure using a plug-flow reactor system described in detail elsewhere [66].

A schematic diagram of the plug flow reactor system is given in Figure 2.5, showing the location of pressure gauges and thermocouples. Separate air, hydrogen and syngas lines were fed into a manifold and directed to each of three reactors.

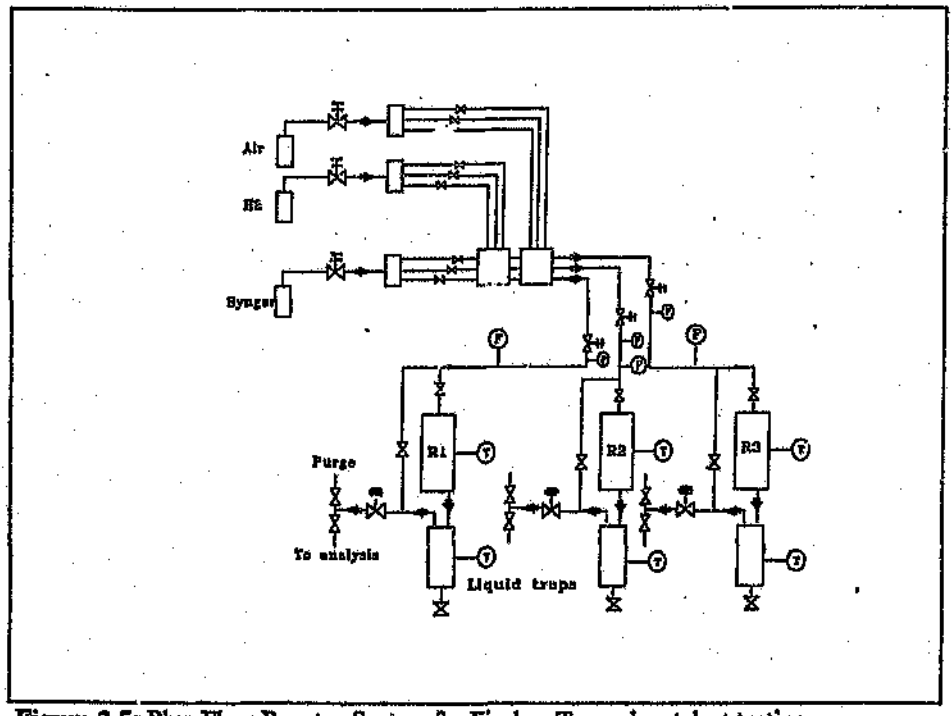


Figure 2.5: Plug Flow Reactor System for Fischer-Tropsch catalyst testing

The plug flow reactors were housed in an outer casing which was sealed via an hexagonal nut pressing against an aluminium plate inserted on a knife-edge at the top of the reactor casing. The actual reactor comprised three segments; the first being a gas preheater, and the second the catalyst bed which was lined with a wire mesh. The final section was a liquid product disengagement [66]. Reactors were heated by jacket-type solid elements (200 W). RKC Rex-P100 temperature controllers coupled to J-type thermocouples accurately monitored the temperature of the catalyst bed.

A wax trap maintained at 140°C, followed on from each of the reactors, in which high-boiling fractions were retained for off-line analysis. More volatile products exited the trap and were directed towards the on-line gas chromatograph (GC) via a series of electronically controlled solenoid selection valves maintained at 170°C. Flow rates were measured using a soap bubble-meter.

A series of sampling valves permitted automated injection of sample gas into FID and TCD sample loops contained with the GC system which was a Varian 3300 series gas chromatograph. Permanent gases, being CO, Ar and H_2, were analysed using a thermal conductivity detector (TCD), with helium as carrier gas to minimise the detection of hydrogen. Gas separation was achieved with a Carbosieve S-II (2 m, $^1/_8$", stainless steel) packed column, in conjunction with two Poropak Q columns. The column arrangement was designed to protect the carbosieve column from contamination by hydrocarbon products. Initially, the entire sample was injected into the one Poropak Q column, and once the permanent gases had eluted onto the carbosieve column, the sample valve rotated to backflush the hydrocarbons onto the second Poropak Q column.

Hydrocarbon reaction products were analysed using a flame ionisation detector (FID) with nitrogen as carrier gas. Separation of products up to C_7 was achieved with a 2.5 m, $^1/_8$", stainless steel Poropak column (PPQ); while a Megabore, 30 m wide bore (0.53 μm) fused silica capillary column with OV-5 stationary phase permitted separation of C_6 to C_{15}.

A software program written in Turbo Pascal (Borland Inc.) [66], and executed by an IBM PC equipped with an I/O card, controlled the operation of the GC system and all sampling valves. The program was written in such a way as to permit sequential sampling of reactor and syngas feed lines. Both TCD and FID were analysed in parallel and the results recorded on a Spectra-Physics 4290 integrator.

The catalysts were allowed approximately 4 days to reach steady state activity, whereafter a carbon mass balance was conducted over a period of 4 days.

2.17.1. Mass Balance Procedure

The prevailing ambient conditions of temperature and atmospheric pressure were recorded daily, as well as the reaction temperature, pressure and product flow rate. Used in conjunction with the daily average product output recorded on the integrator, this data formed the basis of a carbon mass balance.

A pre-mixed calibration standard containing CO, Ar, CO_2, CH_4, C_2H_4 and C_2H_6 was used to determine the mole percent of all products. Olefinic hydrocarbon areas were normalised to that of C_2H_4, and those of paraffinic products corrected to C_2H_6, using response factors presented by Dietz [67]. The C_6 fraction was used to standardise the areas of products separated on Poropak Q and Megabore columns. A spreadsheet was compiled from this data, together with the analysis of waxy products obtained using an off-line GC, and a carbon mass balance calculated from the moles of carbon entering the reactor to the moles of carbonaceous product formed.

The conversion of carbon monoxide to the myriad of products observed was calculated according to equation 2.8:

$$\left[\frac{CO_{in} - CO_{out}\left(\frac{Ar_{in}}{Ar_{out}}\right)}{CO_{in}}\right] \times 100 \quad \text{.....(2.8)}$$

where the (Ar_{in}/Ar_{out}) ratio is a gas contraction factor.

Using the ideal gas equation, and inlet and outlet gas flow rates, the moles of CO converted to products could be determined; and this yielded the specific activity, quoted as μmol C converted per gram of catalyst per second.

The selectivity of product i has been defined as:

$$S_i = (m_i / \sum_{out} m_n) \times 100 \quad \text{.....(2.9)}$$

where m_i = mass of component i.

The olefinity of products was defined by the olefin to paraffin ratio:

$$\left[(m_{olefin}) / (m_{olefin} + m_{paraffin})\right] \times 100 \quad \text{.....(2.10)}$$

for carbon numbers greater than two.

2.18. Heavy hydrocarbon Separation

Off-line analysis of oils and wax fractions was done on a capillary column in a Hewlett-Packard GC coupled to a Spectra-Physics 4290 Integrator.

2.19. Wax Extraction

Prior to commencing post-run analysis of catalysts, heavy hydrocarbons and waxes were removed by exhaustive extraction with refluxing xylene (16 h) in a Soxhlet apparatus. Thereafter, the xylene was removed under reflux over a 2 hour period in a 1:1 mixture of methylethylketone and benzene.

Chapter 3

The structural morphology and chemical composition of sulfided iron FT catalysts

3.1. Introduction

The laws governing the precipitation of solid substances from aqueous solutions were formulated by von Weimarn at the turn of the century [68]. These laws expressed the magnitude of the ultramicrocrystals of a precipitate in terms of the concentration of reacting solutions. Furthermore, the variables regulating the dispersoidal synthesis of such ultramicrocrystals and their aggregates, were given rigorous mathematical treatment. It was established that separate 'influences' were responsible for the dimensions of each of these particles, and that the mean dimensions of the disperse phase of a suspension were determined by a superimposition of two such 'influences'. Despite a somewhat fleeting reference to the presence of reaction by-products, no mention was made of the precise nature of these so-called 'influences'.

In more recent times, Haberman and Gordon [69], have proposed that precipitation is initiated by supersaturation, which is defined in terms of the ratio of the ion product (IP) and solubility product (K_{sp}) [69]:

$$S_{sat} = \sqrt{\frac{IP}{K_{sp}}}$$

The presence of impurities was noted to affect the critical supersaturation ratio (S_{crit}). For example Benedetti-Pichler [70], have accounted for the surprisingly small particle sizes of strontium sulfate precipitated from solutions in terms of trace amounts of impurities.

Nonetheless, when S_{crit} is exceeded, *homogeneous* nucleation occurs spontaneously [71]. In a discussion on the energetics of precipitation, Nielsen [72] described the free energy of nucleation, ΔG_n, as being governed by the supersaturation of the solution and the free energy at the interface of the newly formed embryo. The rate of nucleation, J_n, is in turn related to ΔG_n, and is hence affected by similar parameters; as S_{crit} is exceeded, J_n increases rapidly [71].

The presence of a solid phase can serve to lower ΔG_n and thus increase J_n. Such a situation could arise from the presence of minute particles of a foreign phase already precipitated, or from crystals of the phase that is crystallizing. The phenomenon of *heterogeneous* nucleation thus occurs at a lower level of supersaturation than its homogeneous analogue.

According to Dunning [73], the kinetic processes which determine the structure of a precipitate are nucleation, growth and ageing. Ageing is the term which is used to connote all irreversible or textural changes which occur in a precipitate when still in contact with an aqueous medium [73]. It is during this latter stage that changes in shape, structure and size of crystallites is most likely to occur.

However, residual water which is trapped inside the precipitate, also promotes ageing, particularly at elevated temperatures [74]. Indeed, the total porosity of precipitated catalysts is largely determined by the amount of shrinkage that accompanies drying [31].

3.1.1. Preparative variables affecting precipitated-iron FT catalysts

The impact of the variables controlling the initial precipitation, subsequent ageing and drying of Fischer-Tropsch catalysts has been detailed in a study by Davis *et al* [75]. The decrease in surface area and concomitant increase in pore size following heat treatment of the oxyhydroxide precipitate may be attributed to sintering of catalyst particles. Iron catalysts co-precipitated with 6% Al_2O_3, SiO_2 or ZrO_2 promoters exhibited improved high temperature stability under reaction conditions. Exposure to synthesis gas resulted in gradual broadening of pore size distributions and larger pores. This ageing effect is reduced in the promoted catalysts. Moreover, the addition of small quantities of potassium enhanced the surface area during reaction and hence improved conversion activity.

The initial stage of precipitation of iron catalysts requires the hydrolysis of Fe (III) salts in acidic solutions via one or more of the following reactions [71]:

$$Fe^{3+} + H_2O \rightarrow FeOH^{2+} + H^+$$
$$Fe^{3+} + 2H_2O \rightarrow Fe(OH)_2^+ + 2H^+$$
$$Fe^{3+} + 2H_2O \rightarrow FeOOH + 3H^+$$
$$2Fe^{3+} + 3H_2O \rightarrow Fe_2O_3 + 6H^+$$

Alkali-induced hydrolysis results in the formation of ferrihydrite (FeOOH), a thermodynamically unstable product. Internal dehydration and rearrangement processes transform this product into hematite. Factors assisting the aggregation of ferrihydrite particles, such as a final pH of 7-8, which is near the pzc (point of zero charge) of ferrihydrite, promotes this transformation.

It has been well established that each of the variables involved in the preparation of precipitated-iron FT catalysts has a pronounced effect on the composition and morphology of the final product. The role of pH was investigated by Diffenbach and Fauth [30], and found to influence the Cu/Fe and Na/Fe ratio in promoted catalysts. Such effects were ascribed to the charge borne by the iron species at various pH values. Above pH 6.7 (the isoelectric point), negatively charged species were formed, while in acidic media, cationic species predominated. Significant differences in surface area and pore size distribution accompanied changes in pH, with a maximum BET and total pore volume being found for the catalysts prepared between pH 5.8 and 7.6 [30]. Hence, in this study, a pH of 6.9 was selected as the end-point of precipitation when preparing sulfided catalysts.

The chemical nature of the precipitating agent also has an influence on the structure of the precipitate. Preference is usually given to precursor compounds that decompose at low temperatures to minimise sintering of the resulting iron oxide. For this reason, carbonates, hydroxides and nitrates are preferred over sulfates [76].

Indeed, the poor activity exhibited by catalysts prepared from sulfate and chloride precursors [31] may be ascribed to the presence of large quantities of these ions contaminating the surface even after calcination and reduction pretreatments.

Notwithstanding this, the oxidative hydrolysis of iron (II) sulfate has been used in the production of α-Fe_2O_3 [77]:

$$4FeSO_4 + 8NH_3 + 6H_2O + O_2 \rightarrow 4FeOOH + 4(NH_4)_2SO_4$$

$$2FeOOH + O_2 \rightarrow Fe_2O_3 + H_2O$$

The first reaction is purported to proceed via a homogeneous process catalysed by Mn^{2+} ions, followed by a heterogeneous reaction which takes place on the surface of the already formed iron (III) oxyhydroxide. The homogeneous reaction is the transition-metal catalysed oxidation of ferrous ions, and dominates at low temperatures. Increasing both the metal precursor and reaction temperature results in a propensity towards the heterogeneous enlargement and aggregation of initial particles.

Early workers determined that hydroxide precipitating agents generally resulted in the synthesis of poorer catalysts than when carbonates were used as precipitating agents [78]. It has since been established that the pH of the precipitating agent solution is instrumental in controlling the pore size distribution, with carbonates giving notably larger pores [31] than hydroxides. It is suggested that the lower pH of sodium carbonate (10.75) is conducive to the formation of porous precipitate. Moreover, significant differences in pore volume result when the sequence of addition of iron solution and precipitating agent is reversed.

From the foregoing, it is apparent that the presence of additives alter not only the chemical composition, but significantly affect the bulk morphology of precipitated-iron catalysts. To date, no studies have been reported on the influence of sulfide ions on the morphology of such systems. However, from the above overview, the co-precipitation of a sulfiding agent with a metal precursor, may be expected to modify the pore structures and crystallinities relative to the standard iron oxyhydroxide catalyst.

To obtain information on the bulk morphology of sulfided precipitated-iron catalysts Scanning Electron Microscopy, X-ray diffraction and Porosimetry were used as evaluation tools. An attempt was made to correlate morphology with the level and source of sulfide added.

3.2. Results and Discussion

The catalysts used in this study were prepared using hot solutions (75°C) of metal salt and precipitating agent. Such conditions are reported to favour the precipitation of hematite, particularly for nitrate or perchlorate-derived metal salts [79].

Thorough washing is needed to remove NO_3^-, CO_3^{2-} and Na^+ ions from the iron precipitate [71], since they constitute contaminants. Centrifugation was the method of choice owing to poor vacuum facilities in our laboratory which made filtration impossible. The small particles of ferrihydrite are known to clog filters and render this method impracticably slow [71].

Highly dispersed suspensions also present problems during centrifugation, since loss of the very small particles can occur. More importantly, as electrolytes are removed, the dispersion of the precipitate increases to compensate for the drop in the ionic strength of the supernatant. Consequently, longer centrifugation times are required to achieve sedimentation. Such phenomena were indeed observed, and on numerous occasions a solid precipiate was not obtained. Thus, conductivity measurements were applied to monitor the rate of sodium removal until the concentration of sodium ions was sufficiently low without causing dissolution of the iron hydroxide precipitate. Without doubt, the most effective method for the removal of sodium, and other undesirable contaminants, is dialysis. Unfortunately, implementation of this technique is impractical as the procedure requires 1-2 weeks to reach completion [71].

The recommended temperature at which drying should be done is 40°C, since phase modification is minimised [71]. This procedure is usually only important when metastable phases need to be retained. In the present study however, the precipitates were dried at 120°C in a fan-oven to speed up the removal of water. Crushing and screening to a particle size range of 1180-850 μm afforded the fresh catalyst.

3.2.1. Effect of sulfide on the colour of precipitated-iron catalysts

3.2.1.1. General aspects of colour

Charge transfer transitions are responsible for the colours of iron-oxides, viz:

$$Fe^{3+} - O^{2-} \xrightarrow{h\nu} Fe^{2+} - O^{\cdot}$$

Owing to the large distances traversed by the electrons, the colours are intense and range from yellow to black. For magnetite, which is obtained after reduction of hematite, the black colour is due to charge transfer from Fe^{2+} to Fe^{3+} [71].

Reflectance spectra (the complement of absorbance spectra) can be used in conjunction with Kubelka-Munk theory to assess the colour of iron oxides. This technique has found application in the estimation of the colour of hematite in soils. The Munsell system utilises a colour chart as a basis for colour specification. According to this method, the hue of hematite is defined as 5R-2.5YR where (R) denotes red and (Y) stands for yellow. The numerical value indicates the lightness of the colour, on a scale of 0 (black) to 10 (white).

A system which gives the exact numerical description of a colour, but no information regarding its actual appearance, is the CIE (International Commission on Illumination) System. Currently, new versions of this system which generate chromaticity coordinates that can be converted into the more familiar Munsell notation are being developed [71].

3.2.1.2. Effect of sulfide on colour of iron catalysts

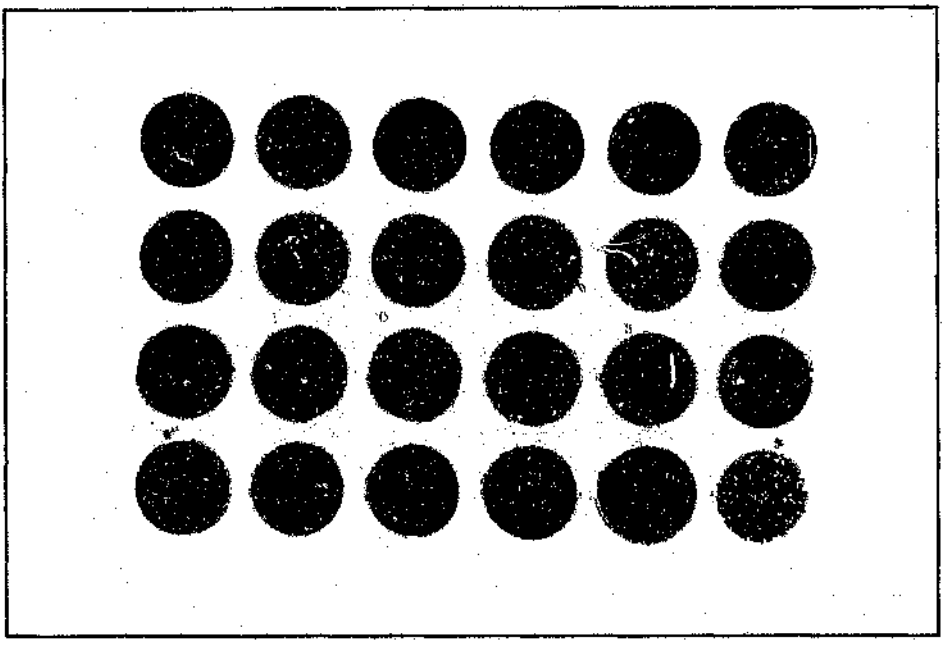
The unsulfided catalyst appeared a dark-brown colour after drying. Sulfided catalysts were lighter in colour, appearing almost yellow, when the catalysts contained 20 000 ppm sulfur (Table 3.1). Addition of dissolved sulfide to the precipitating iron-oxide resulted in localised areas which resembled iron sulfide. These were rapidly assimilated as precipitation continued and at pH 6.9, when precipitation was stopped, no evidence of iron sulfides was discernable. Generally, however, the suspension appeared lighter in colour after sulfidation when compared to the unsulfided hematite. Also, the suspension obtained after adding 20 000 ppm sulfide settled quickly, as opposed to the other precipitates which remained in suspension for a considerable time. The dried, highly sulfided catalyst was far more powdery and appeared to be lacking in mechanical strength.

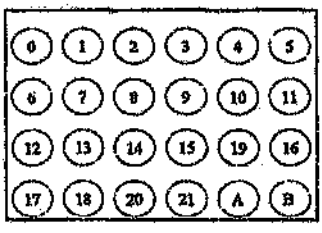
Table 3.1: Colours of selected precipitated-iron catalysts

Catalyst	Colour
unsulfided	dark red-brown
2000 ppm Na_2S	red-brown
20000 ppm Na_2S	ochreous

The colour of an iron oxide in powdered form depends mainly on its crystal structure [71]. Variation in crystal size and morphology contribute to the range of colours observed in Plate I (overleaf). Small crystals of hematite are bright red in colour, and this redness is gradually replaced by blue hues as crystallite size increases; hence larger crystals appear darker. The yellow colour of a catalyst sulfided with 20000 ppm Na_2S could be due to the presence of geothite since there is no yellow hematite.

Colour Plate I





Number	Catalyst	Number	Catalyst
0	Unsulfided	12	20000 ppm Na_2S pH 6.9
1	500 ppm Na_2S pH 10.75	13	2000 ppm $(NH_4)_2S$ pH 10.75
2	500 ppm Na_2S pH 8.5	14	2000 ppm $(NH_4)_2S$ pH 8.5
3	500 ppm Na_2S pH 6.9	15	2000 ppm $(NH_4)_2S$ pH 6.9
4	2000 ppm Na_2S pH 10.75	16	2000 ppm $(NH_4)_2S_5$ pH 10.75
5	2000 ppm Na_2S pH 8.5	17	2000 ppm $(NH_4)_2S_5$ pH 8.5
6	2000 ppm Na_2S pH 6.9	18	2000 ppm $(NH_4)_2S_5$ pH 6.9
7	5000 ppm Na_2S pH 10.75	19	500 ppm $(NH_4)_2S_5$ pH 10.75
8	5000 ppm Na_2S pH 8.5	20	5000 ppm $(NH_4)_2S_5$ pH 6.9
9	5000 ppm Na_2S pH 6.9	21	20000 ppm $(NH_4)_2S_5$ pH 6.9
10	20000 ppm Na_2S pH 10.75	A	Spent 2000 ppm $(NH_4)_2S_5$ pH 6.9
11	20000 ppm Na_2S pH 8.5	B	Spent 20000 ppm $(NH_4)_2S_5$ pH 6.9

However, the initial product of precipitation, ferrihydrite, can appear ochreous when formed by the rapid hydrolysis of Fe^{3+} salts [71], at temperatures exceeding 80°C. Inducing hydrolysis by the addition of alkali is noted to yield protoferrihydrite, a dark red-brown material.

The synthesis of all catalysts, sulfided and unsulfided, was conducted at 75°C, as previously stated. The observed differences in precipitation product can hence only be attributed to the presence of sulfur. It may be postulated that sulfide ions accelerate the hydrolysis of iron (III) nitrate, to afford the more yellow product. The effect would be more pronounced when sulfide ions are present at the start of precipitation and indeed, catalysts sulfided at pH 10.75 are observed to be lighter in colour, becoming more red in hue as the pH of sulfidation is decreased. This trend is particularly noticeable for the range of catalysts sulfided with 20000 ppm S. In addition, as is apparent from Plate I, the greater the level of sulfidation, the more ochreous the product, irrespective of the sulfide source.

3.2.2. Chemical Composition of the precipitates

Total chemical analysis using Atomic Absorption Spectroscopy (Table 3.2) confirmed the conductivity measurements made during centrifugation, and revealed that the washing procedure had effectively removed the sodium ions, which would otherwise have complicated the study of the effects of sulfur on catalyst performance. Bulk iron analysis revealed that sulfidation had not affected the iron content either.

Table 3.2: Elemental analysis of sulfided precipitated-iron Fischer-Tropsch catalysts by Atomic Absorption Spectroscopy

Catalyst*	Fe Conc (ppm)	Na conc (ppm)	Catalyst*	Fe conc (ppm)	Na conc (ppm)
unsulfided	781	19	11	773	1
1	738	37	12	822	0
2	695	51	13	777	2
3	781	0	14	821	3
4	766	0	15	784	17
5	755	1	16	623	26
6	818	7	17	742	14
7	757	12	18	726	9
8	801	0	19	741	18
9	824	0	20	827	10
10	770	2	21	816	16

* Numbers as per Table 2.1 in Chapter 2

To quantify the sulfur incorporated, bulk analysis was attempted on numerous samples by ICP, but only those to which 20000 ppm S had been added, gave results that were above the 0.1 % detection limits of the equipment (Table 3.3). Thus, a degree of speculation exists as to the precise sulfur content in the catalysts sulfided with 500-5000 ppm S.

Table 3.3: Sulfur content of Na_2S sulfided catalysts as determined by ICP analysis

Catalyst	Sulfur content (ppm)	(S: Fe) % by mass*
20 000 ppm pH 10.75	380	0.06
20 000 ppm pH 8.5	410	0.07
20 000 ppm pH 6.9	380	0.06

*The total incorporation of 20000 ppm S should give 3.3 % S: Fe

The interdependance of the elemental composition and bulk structure of solid catalysts, suggests that the addition of sulfur should have a marked effect on the morphological properties of iron-oxide. Indeed, scanning electron microscopy revealed distinct differences between sulfided and unsulfided samples in terms of local composition and structure.

3.2.3. Scanning Electron Microscopy

The scanning electron microscope (SEM) has emerged as a versatile tool for the characterisation of catalysts and metallurgical samples. It holds an advantage over the optical microscope in terms of magnification capabilities (which exceed 50 000x) and in its ability to interpret the three-dimensional relief of surfaces. The latter feature is attributable to a depth of field which is 300 times superior to that of the optical microscope [80]. This is achieved through the use of secondary electrons emitted from the sample when bombarded with an incident beam of high-energy electrons. Depending on the inclination of the various topographical features, the number of secondary electrons captured by the detector will vary accordingly and hence produce an image which reflects the surface relief of the sample.

Improved topographic contrast may be attained using backscattered electrons, particularly since the scattering coefficient increases with increasing atomic number, making this technique ideal for imaging the atomic number difference between various regions of a specimen. A complementary method which involves the use of diffusely scattered electrons in Scanning Reflection Electron Microscopy has shown promise in the elucidation of surface topography, particularly of amorphous samples [81].

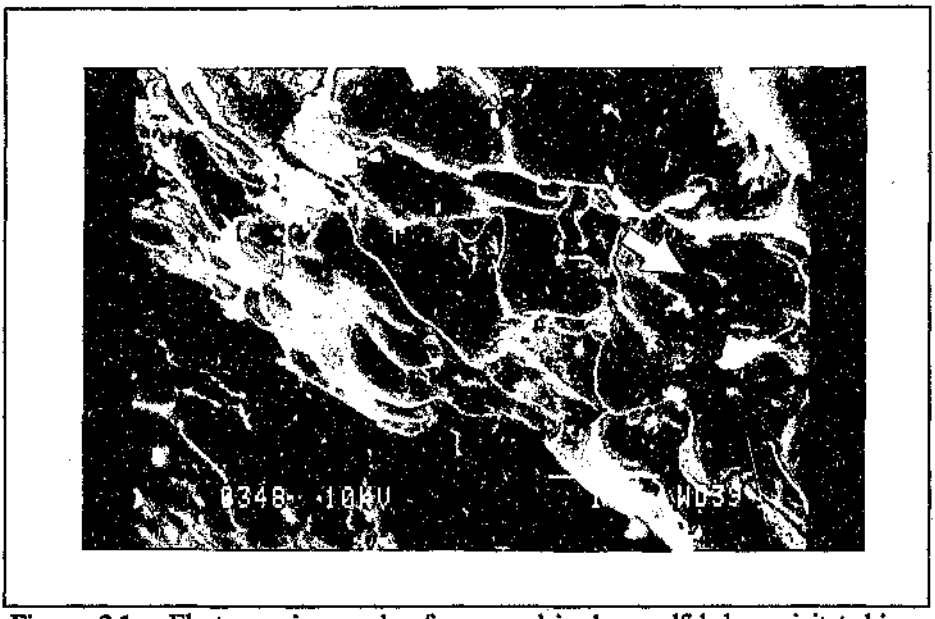


Figure 3.1a: Electron micrograph of an uncalcined, unsulfided precipitated-iron catalyst taken at 2000x magnification

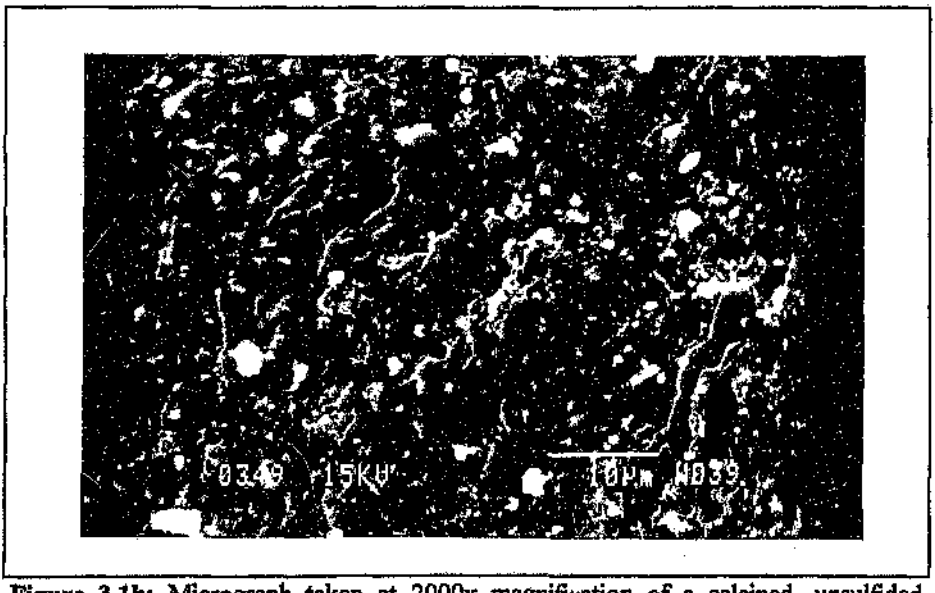


Figure 3.1b: Micrograph taken at 2000x magnification of a calcined, unsulfided precipitated-iron catalyst



Figure 3.2a: Uncalcined catalyst sulfided with 2000 ppm $(NH_4)_2S_5$ at pH 6.9 viewed at 2000x magnification

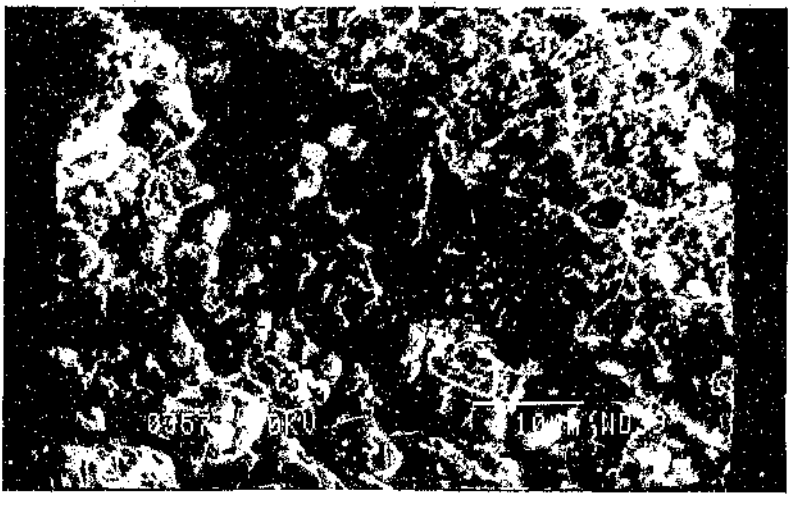


Figure 3.2b: Spent catalyst sulfided with 2000 ppm S viewed at 2000x magnification

Scanning electron microscopy of uncalcined, calcined and spent catalysts was used to provide information regarding the effects of sulfur on the nature of the precipitation process. Examination of the electron micrograph of the unsulfided catalyst prior to calcination (Figure 3.1a), revealed a surface with irregularly-shaped precipitates of iron-oxide. Pores (marked with an arrow) were observed to be scattered sporadically over the surface of the sample. For visual comparison, Figure 3.1b is included, showing the unsulfided catalyst after calcination. The effect of calcination will be discussed *vide infra*.

By comparison with other micrographs taken at 2000x magnification it can be seen that the unsulfided catalyst displays few of the textural features exhibited by the catalysts to which sulfur had been added. The surface of the catalyst sulfided with 2000 ppm S (Figure 3.2a) also appeared to be porous but exhibited a vastly different surface morphology to its unsulfided counterpart. A micrograph of a catalyst which had been exposed to syngas is also included (Figure 3.2b) for comparison with fresh and calcined samples. No sulfur species were detected on this 2000 ppm S catalyst, but modification in the surface structure is certainly evident. The randomly orientated crystals shown in Figure 3.2a are said to be equiaxed [80] since their growth in all directions is limited by neighbouring crystals nucleated at approximately identical times. According to Reed-Hill *et al* [80], heterogeneous nucleation is far more the rule than the exception when it comes to precipitation. Nuclei may form on the walls of the container or on impurity particles [82].

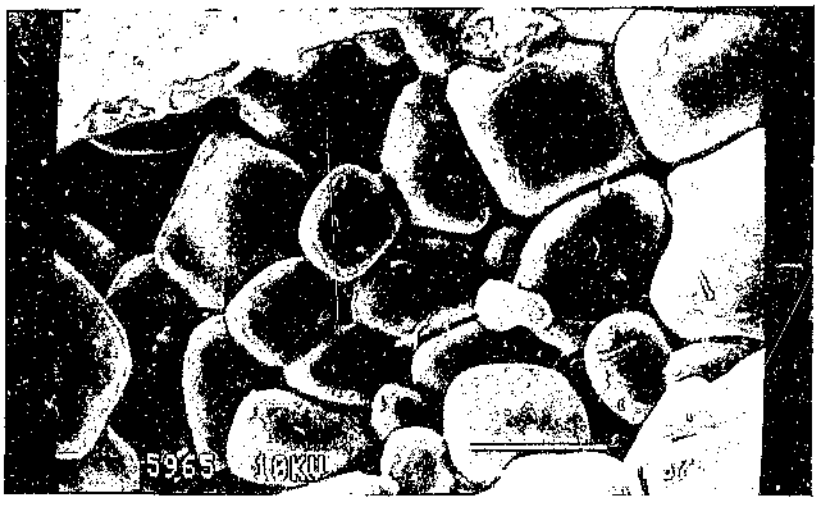


Figure 3.3a: Equiaxed crystals viewed at 2000x magnification on a catalyst sulfided with 5000 ppm S before calcination

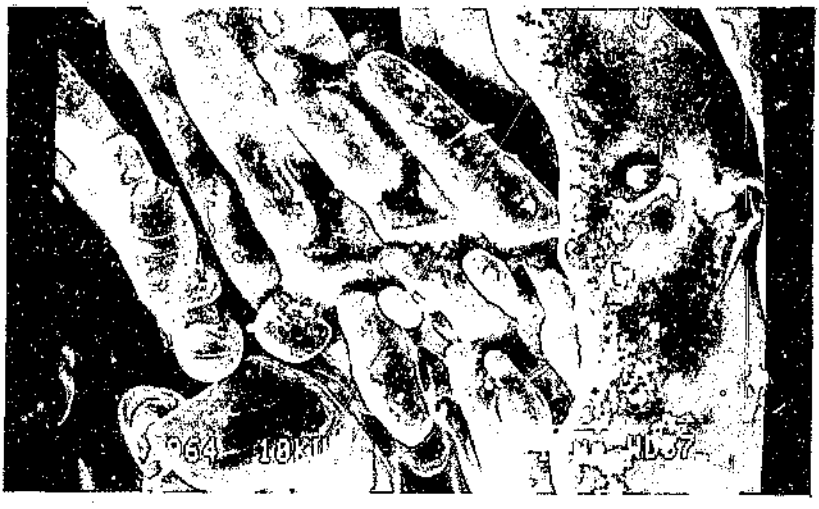


Figure 3.3b: Micrograph of a catalyst sulfided with 5000 ppm S showing dendritic growth at 2000x magnification

From the findings of Woodruff, a heterogeneous nucleant such as an impurity, is only active in forming a nucleus when certain conditions on both the crystallographic orientations of nucleant and nucleus surfaces, and their mutual orientation, are satisfied such that the degree of atomic mismatch is low [82]. Thus, the incorporation of sulfur into the growing precipitate is dependent on the formation of an iron-sulfide with the correct crystallographic orientation to the iron-oxide being precipitated.

Equiaxed crystals, produced by very rapid nucleation, were also encountered on catalysts sulfided with 5000 ppm S (Figure 3.3a). In addition to these spherical crystals however, dendrites of the type shown in Figure 3.3b were observed. The developmentel process of dendritic growth is illustrated in the schematic representation below (Figure 3.4a) [83]:

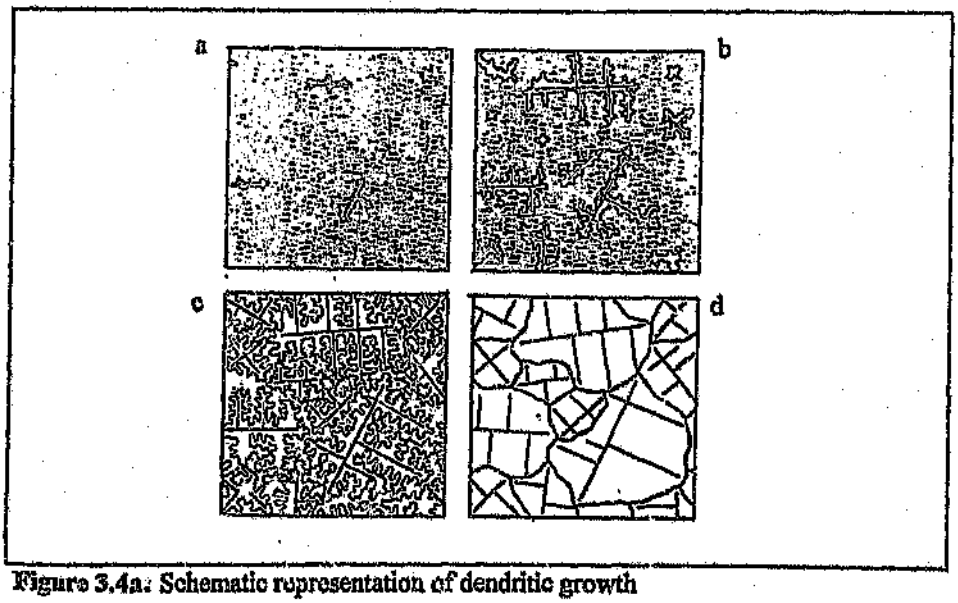


Figure 3.4a: Schematic representation of dendritic growth

During the first stage of dendrite formation a temperature inversion is thought to exist at the solid-liquid interface (Figure 3.4b) [80]. The temperature of the liquid drops in advance of the interface and this facilitates outward growth of the crystal. The direction in which these cells grow is crystallographic and is termed the dendritic growth direction.

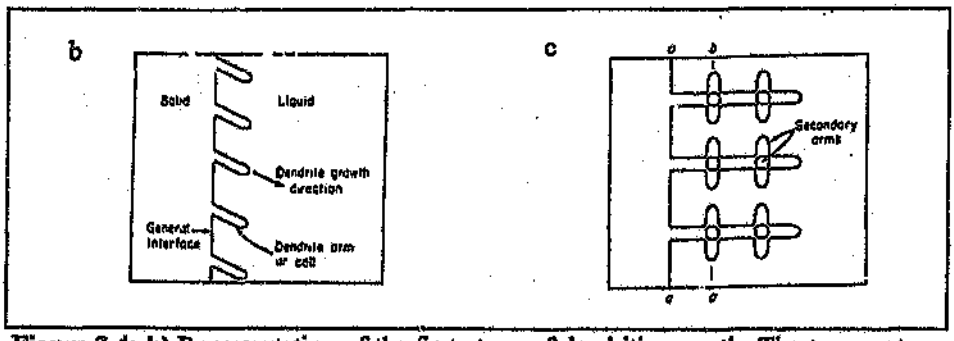


Figure 3.4: b) Representation of the first stage of dendritic growth. The temperature in the liquid drops in advance of the interface, facilitating the outward growth of the crystallites c) Secondary dendritic arms are formed when a temperature gradient exists at a point close to a primary arm and moves to a point midway from the primary arms

For ferrihydrite and hematite, both which assume hexagonal close-packed (h.c.p.) crystal structures, the dendritic growth direction is <1 0 $\bar{1}$ 0> [82]. Secondary and even tertiary branches may form in directions perpendicular to the primary dendrites (Figure 3.4c) [80]. As they increase in length, dendrite branches also increase in thickness until they eventually grow together to form a nearly homogeneous crystal [80]. It is possible that such a phenomenon is responsible for the coalescent structure visible on the surface of the catalyst containing 20000 ppm S (Figure 3.5).

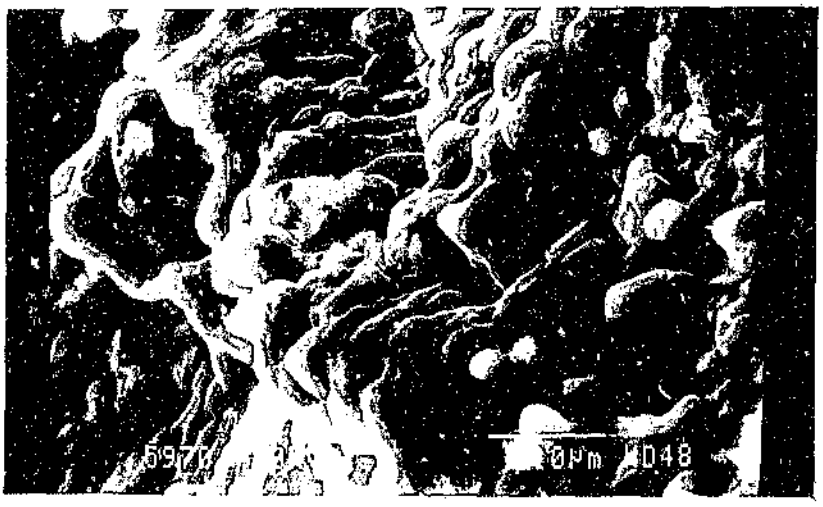


Figure 3.5: Coalescent structures observed at 2000x magnification on a catalyst sulfided with 20000 ppm S

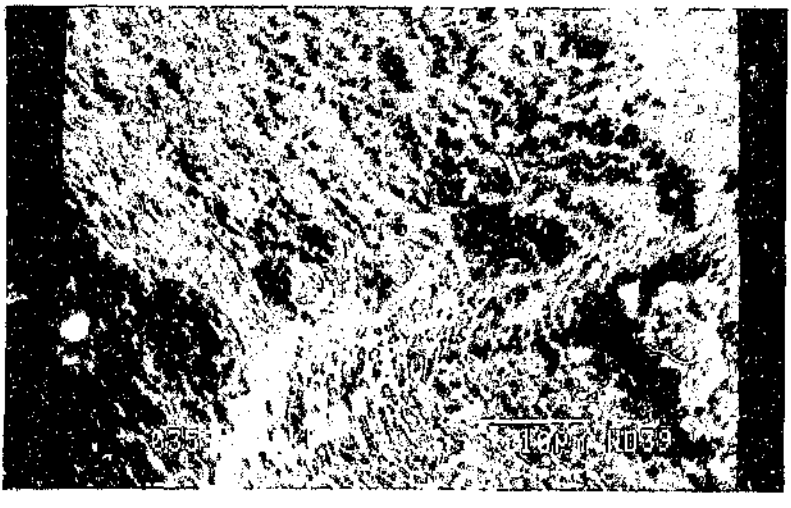


Figure 3.6: Surface of a calcined catalyst sulfided with 2000 ppm S viewed at 2000x magnification

Increasing the sulfur content of the catalysts results in a progressive increase in the crystallinity (see section 3.2.4). This improved crystallinity is also observed through the formation of dendrites at high levels of sulfidation.

Similar morphological modifications of hematite have reportedly been effected using different metal precursors, precipitating agents and ageing times [76]. The ageing time in particular, has been invoked as one of the most important preparative variables involved with controlling precipitate morphology. For instance, a few hours are required for disklike α-Fe_2O_3 structures to form, while spherical α-Fe_2O_3 particles take up to 2 weeks to form at elevated temperatures [79]. Since both the unsulfided and sulfided precipitates were aged overnight in the mother liquor prior to centrifugation, the structural modifications observed in the present study cannot be ascribed to ageing, but rather to the presence of extraneous sulfur.

The elemental composition of each catalyst was investigated using the Energy Dispersive X-Ray analysis (EDX) facility coupled to the SEM. No sulfur could be detected on catalysts sulfided with between 2000 ppm and 5000 ppm S. However, analysis of the catalyst sulfided with 20000 ppm sulfur from both polysulfide and sulfide sources revealed occlusions of sulfur on the surface. An example of such an occlusion which was found to comprise S and Fe is shown in Figure 3.7a. Elemental mapping is a feature of EDX (Figure 3.7c) and a dot-density map of this sulfur-rich region is also presented in Figure 3.7b.

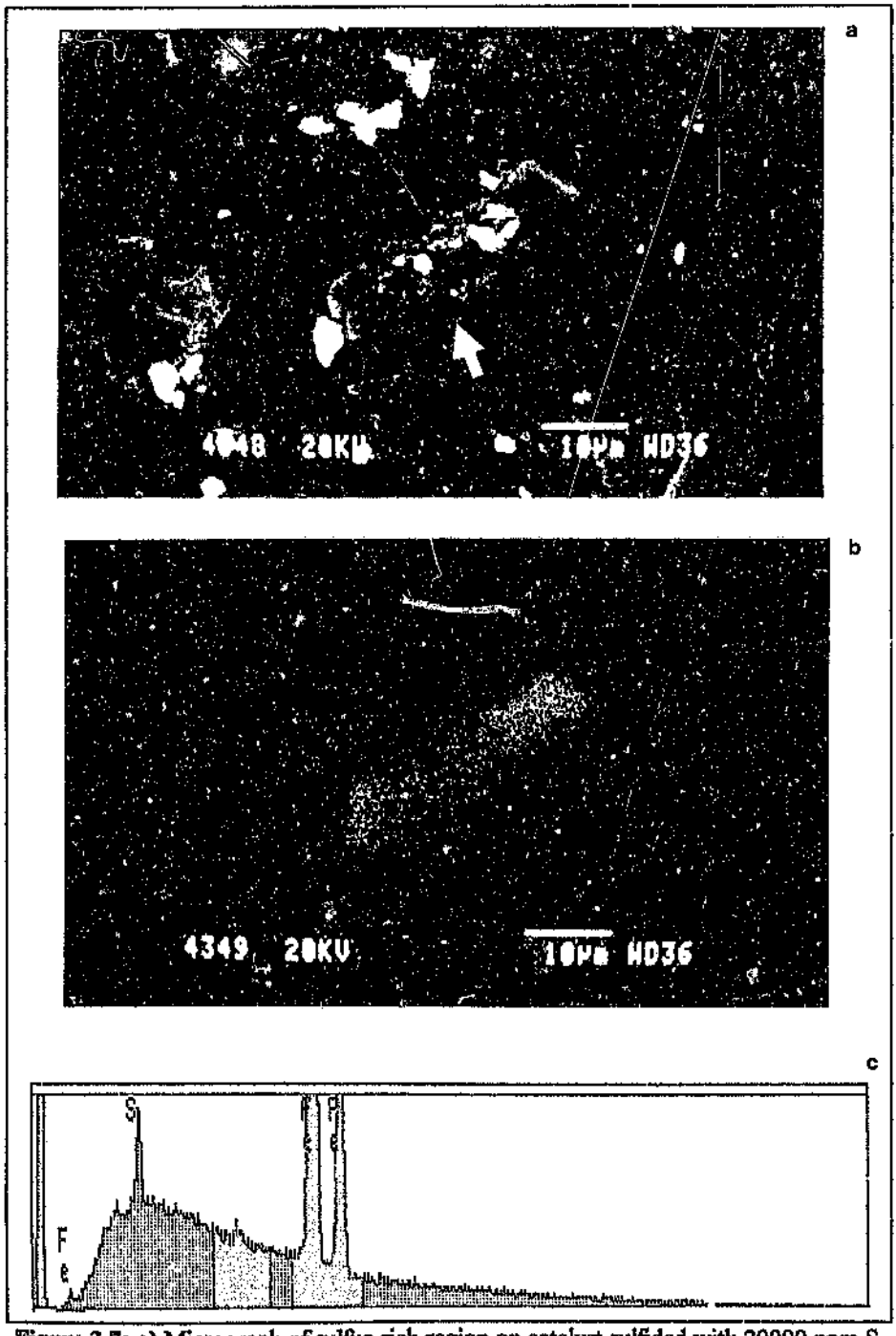
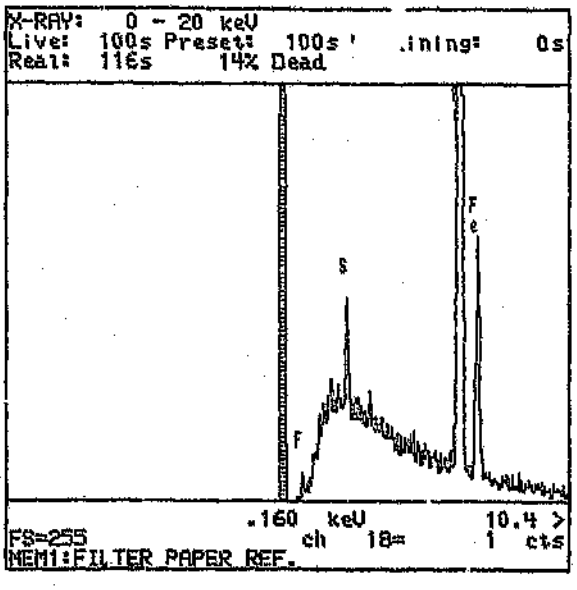


Figure 3.7: a) Micrograph of sulfur-rich region on catalyst sulfided with 20000 ppm S at 2000x magnification **b)** Dot density map of sulfur **c)** EDX analysis of sulfur rich region



a



b

Figure 3.8: a) Surface of a calcined catalyst sulfided with 20000 ppm S viewed at 2000x magnification, showing occlusions of sulfur b) EDX analysis of sulfur rich region

Catalysts which had been calcined also appeared different than before, now exhibiting a more "molten-like" texture (Figure 3.1b and Figure 3.6). Occlusions of sulfur were also more abundant on the surface of the highly sulfided catalyst after it had been calcined (Figure 3.8).

Having therefore ascertained the nature of the precipitation process, and observed the formation of dendrites which are noted to improve the crystallinity of iron oxide, the crystallographic features of the sulfided catalysts were investigated using X-ray powder diffraction (XRD). This technique permit[illegible]ification of the abovementioned phenomena.

3.2.4. X-ray Powder Diffraction

X-Ray Powder Diffraction has found application in the classification of iron oxides [71]. Valuable information regarding crystal size, structural parameters, degree of isomorphous substitution and crystallinity may be gleaned from this non-destructive technique.

X-ray diffraction is the elastic scattering of X-ray photons by atoms in a periodic lattice [52]. Using the time honoured Bragg relation, lattice d-spacings, which are characteristic of a compound, can be derived. When applied to catalyst characterisation, XRD provides information on the crystallographic phases that may be present in a catalyst. It has found particular application in the characterisation of Fischer-Tropsch catalysts [52].

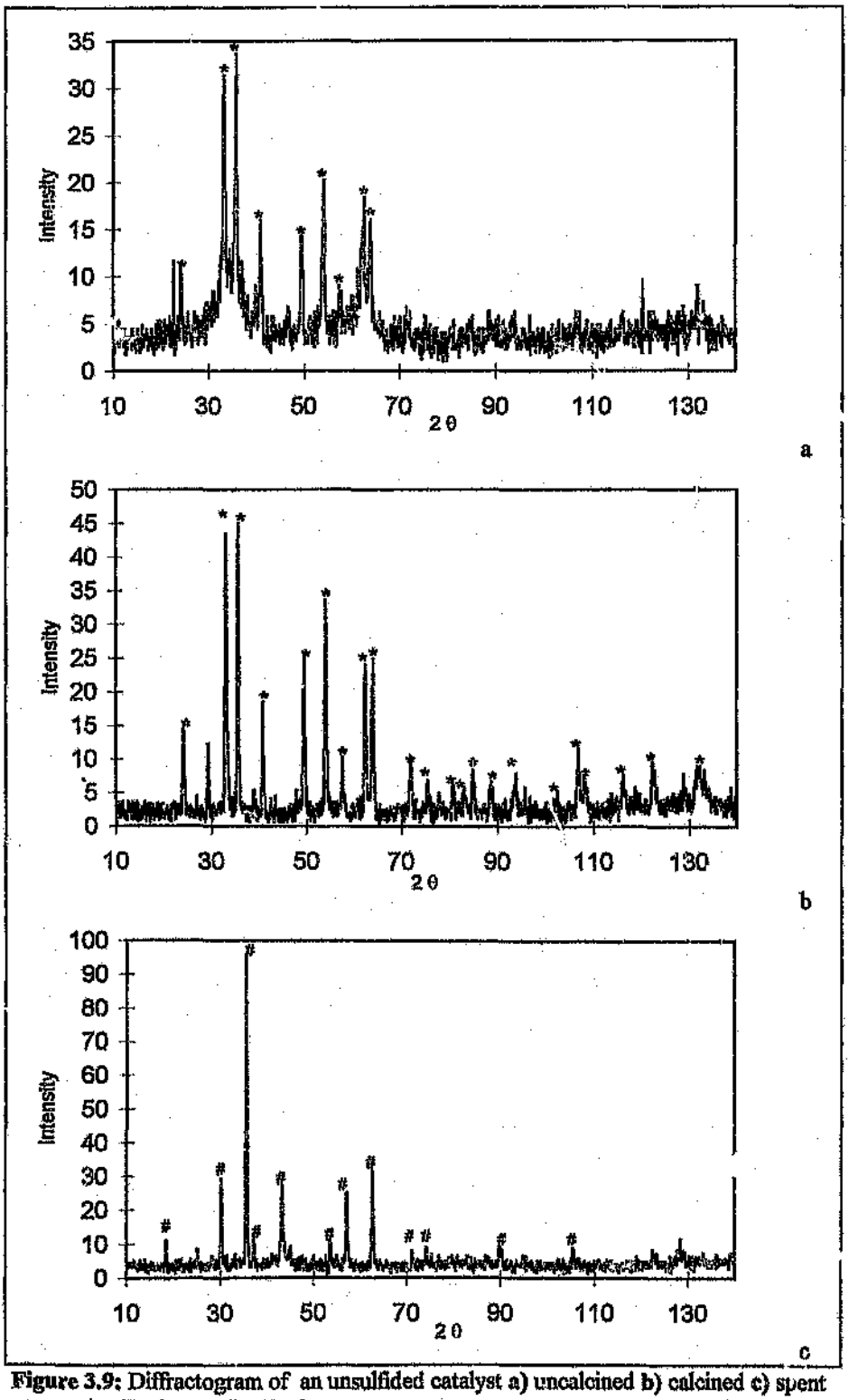


Figure 3.9: Diffractogram of an unsulfided catalyst a) uncalcined b) calcined c) spent
where * = Fe_2O_3 # = Fe_3O_4

The diffractogram of the uncalcined, unsulfided catalyst (Figure 3.9a) is typical of the initial product of precipitation of iron-oxide, that being 2-line ferrihydrite [71]. This is also referred to as protoferrihydrite, since it lacks the essential features of ferrihydrite, and is reported to be almost entirely X-ray amorphous.

The broad peaks of low intensity in Figure 3.9a are poorly resolved and bear testimony to the amorphous nature of the catalyst containing no extraneous sulfur. In addition, an XRD measurement performed between 5 and 20° 2θ revealed a high background, typical of samples of poor crystallinity [84]. According to the JCPDS mineral powder diffraction database, the phase that best corresponds to the set of d-values obtained from Figure 3.9a is 330664 Fe_2O_3 [85]. The *hkl*-indexed XRD pattern of this phase is given for comparative purposes (Table 3.4).

Table 3.4: Major Miller Indices and d-spacings of JCPDS database iron oxide number 330664

		Miller Indices		
d Å	Int	h	k	l
3.684	30	0	1	2
2.700	100	1	0	4
2.519	70	1	1	0
2.207	20	1	1	3
1.840	40	0	2	4
1.694	45	1	1	6
1.599	10	0	1	8
1.485	30	2	1	4
1.311	10	1	0	10
1.259	8	2	2	0

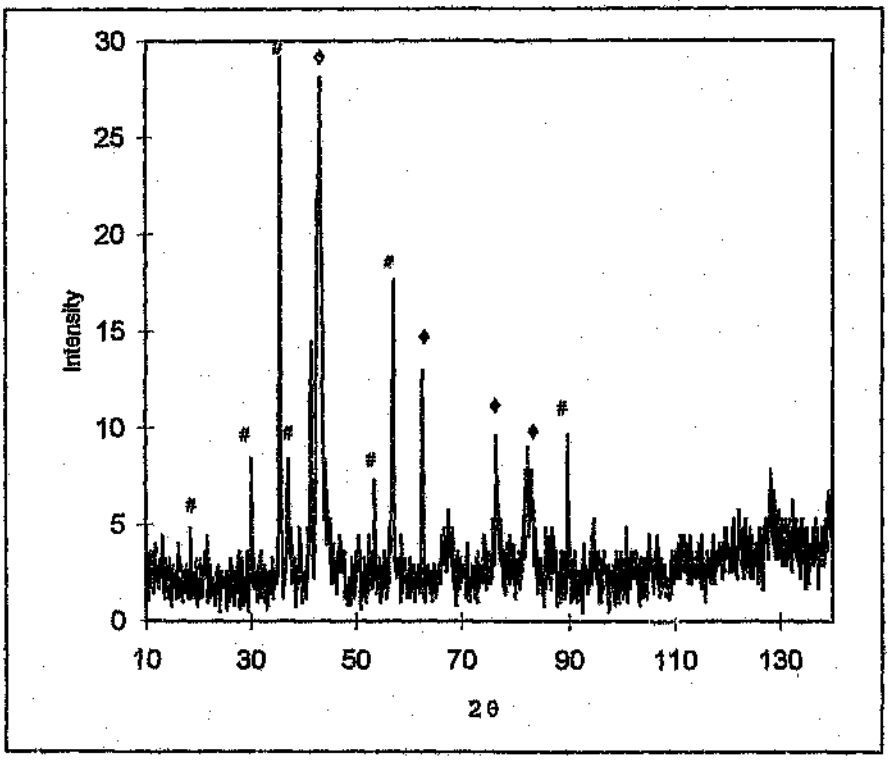


Figure 3.10: Diffractogram of a spent catalyst sulfided with 500 ppm Na_2S at pH 6.9 where # = Fe_3O_4 ♦ = ε-carbide

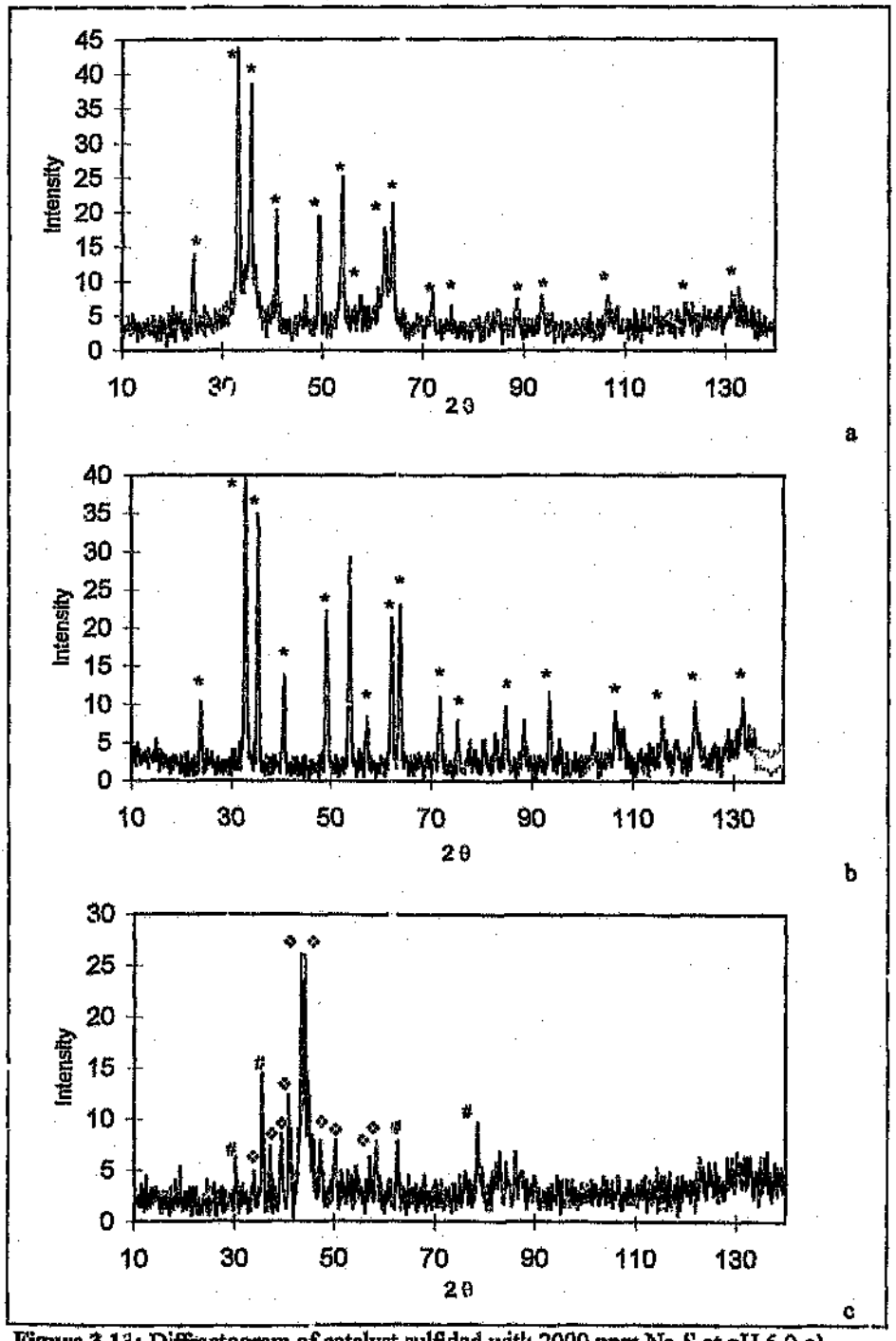


Figure 3.11: Diffractogram of catalyst sulfided with 2000 ppm Na_2S at pH 6.9 a) uncalcined b) calcined c) spent where * = Fe_2O_3 # = Fe_3O_4 ❖ = χ-carbide

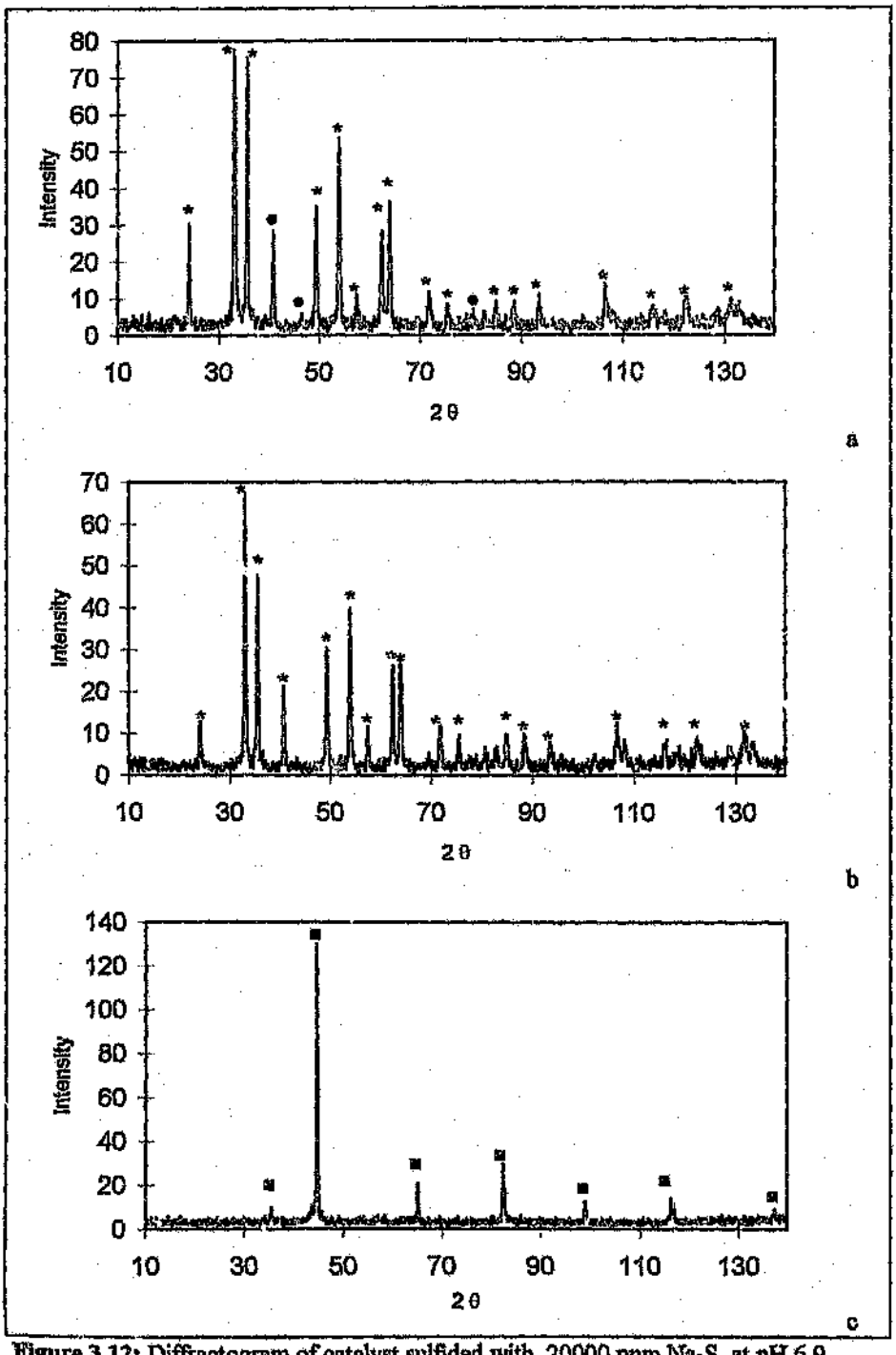


Figure 3.12: Diffractogram of catalyst sulfided with 20000 ppm Na_2S at pH 6.9
a) uncalcined b) calcined c) spent where * = Fe_2O_3 ● = FeS ■ = α-Fe

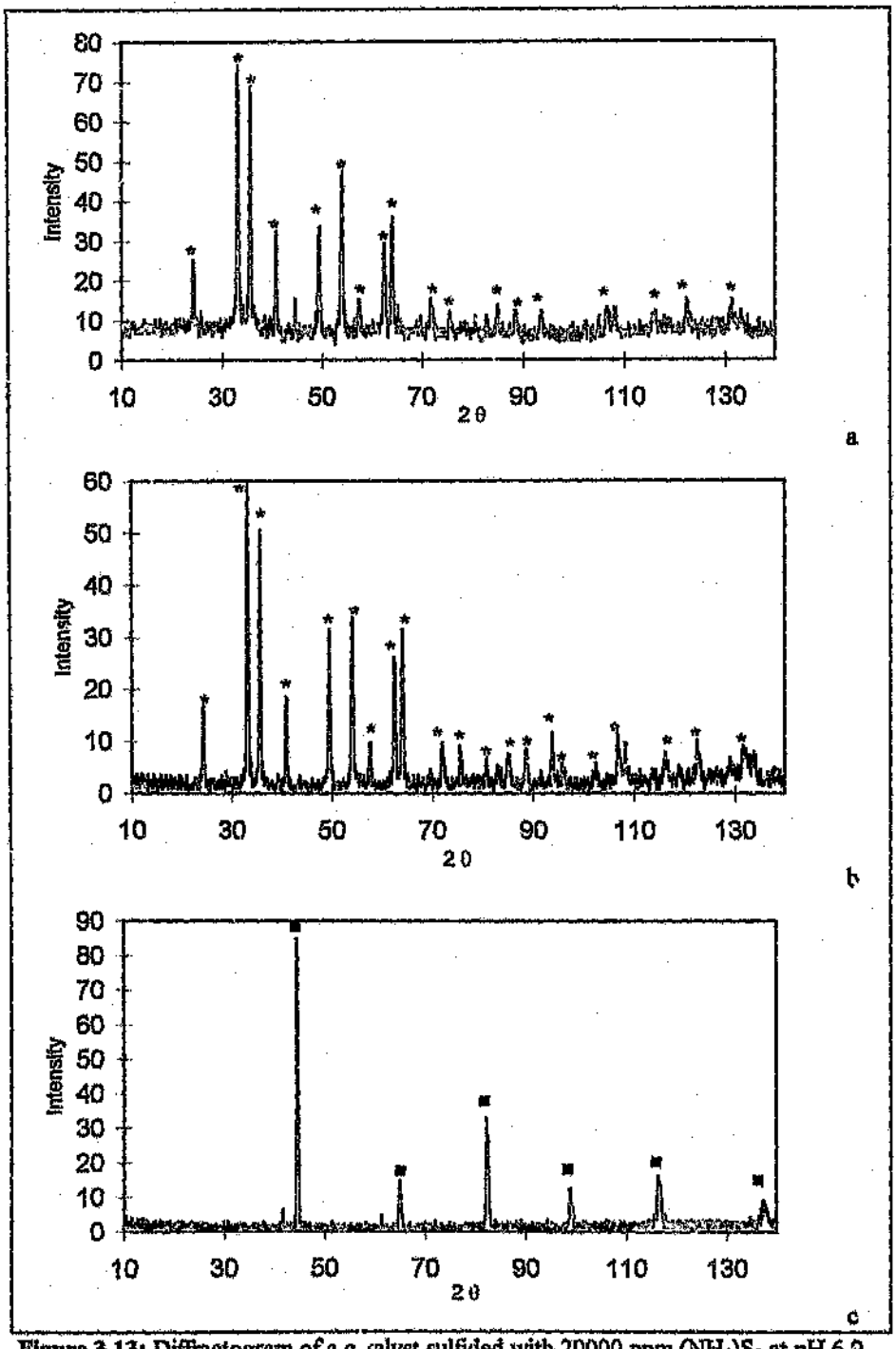
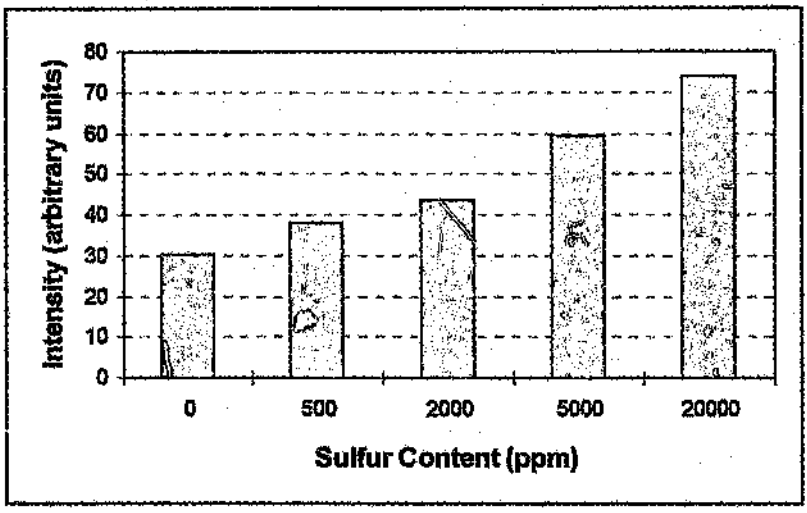


Figure 3.13: Diffractogram of a catalyst sulfided with 20000 ppm $(NH_4)S_5$ at pH 6.9
a) uncalcined b) calcined c) spent where * = Fe_2O_3 ■ = α-Fe

The addition of sulfur is observed to result in a significant increase in the crystallinity of the iron-oxide phase (Figures 3.10- 3.13). Not only were the diffractogram peaks of the sulfided catalysts more intense, but they also appeared narrower, indicating improved crystallinity as the sulfur content was increased from 500 to 20000 ppm (Figure 3.14).

Indeed, the diffractogram of the most highly sulfided catalyst, containing 20000 ppm S at pH 6.9 (Figure 3.12), showed excellent correlation with 330664 Fe_2O_3. A small amount of iron sulfide (FeS) was also discernable on the diffractogram.



*Where arbitrary units refer to the peak intensity at 33.1° 2θ, corresponding to a d-spacing of 2.700 Å

Figure 3.14: Variation in the crystallinity of iron-oxide as a function of the sulfur content

For any set of catalysts containing the same amount of sulfur, sulfidation at increasingly lower (more acidic) pH values also resulted in more crystalline iron oxide. This is evident from the stack-plot of the 35° 2θ region of the diffractograms obtained from catalysts sulfided with 5000 ppm S at the start, middle and end of precipitation (Figure 3.15).

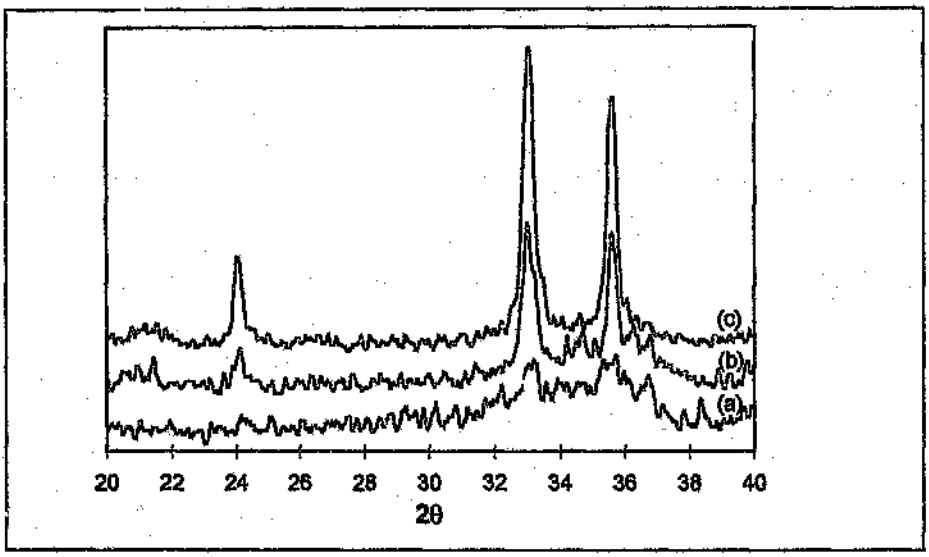


Figure 3.15: Stack-plot of diffraction patterns obtained from catalysts sulfided with 5000 ppm Na_2S a) Catalyst sulfided at pH 10.75 b) Catalyst sulfided at pH 8.5 c) Catalyst sulfided at pH 6.9

The catalyst sulfided at pH 10.75 bears strong resemblance to 2-line ferrihydrite (Figure 3.16a) while sulfidation at pH 6.9 yields a product which is similar to 6-line ferrihydrite (Figure 3.16b). According to the literature, the latter product is obtained by rapidly heating the reacting solutions to 80°C, while the less crystalline 2-line ferrihydrite is prepared by adjusting the pH to 8 with alkali [71].

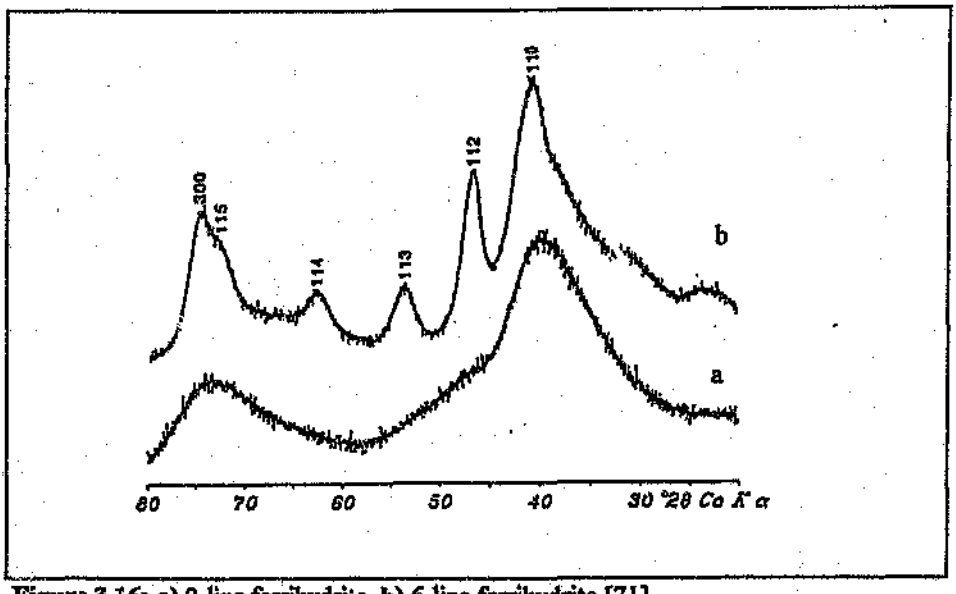


Figure 3.16: a) 2-line ferrihydrite, b) 6-line ferrihydrite [71]

It is also this difference in crystallinity which is accountable for the range of colours observed. The more crystalline 6-line ferrihydrite is ochreous, while the 2-line product appears dark-brown in colour [71], which is in accordance with the results observed for catalysts 11 and 13 in Plate I.

Calcination is performed to remove nitrates and other such impurities which may be damaging to catalytic activity. Literature reports indicate that sintering occurs following treatment in air at elevated temperatures and that crystallite size increases under these conditions [31]. Concomitantly, the crystallinity improves and this was evident from all the samples, both sulfided and unsulfided, after they had been calcined (Figures 3.9b-3.13b).

Larger crystallites give rise to more crystalline material and this is corroborated by the results shown in Table 3.5, where the Scherrer equation was used to determine crystallite size at $2\theta = 62°$.

As is evident from the data presented in Table 3.5, crystallite growth is favoured at higher levels of sulfidation and by the addition of sulfide at lower pH values. Furthermore, polysulfided catalysts generally exhibited larger crystallites than those prepared using monosulfide sources.

Table 3.5: Crystallite sizes of iron-oxide catalysts as determined from the Scherrer equation

Sulfur Content (ppm S)	pH of sulfide addition	Sulfide Source	Crystallite size (Å)[a]
0	-	-	131
2000	10.75	$(NH_4)_2S$	226
2000	8.5	$(NH_4)_2S$	262
2000	6.9	$(NH_4)_2S$	407
2000	10.75	$(NH_4)_2S_5$	245
2000	8.5	$(NH_4)_2S_5$	302
2000	6.9	$(NH_4)_2S_5$	435
500	6.9	$(NH_4)_2S_5$	356
5000	6.9	$(NH_4)_2S_5$	480
20000	6.9	$(NH_4)_2S_5$	549

[a] Obtained from XRD data using the Scherrer equation

The observed growth in crystals which occurs following the addition of sulfur, and which is more pronounced at pH 6.9, could be attributed to the process of heterogeneous nucleation. The sulfide ions act as nucleating agents and could assist with the aggregation of smaller crystallites. As discussed previously, for an impurity to function in this way, it must assume a crystallographic orientation which is nearly identical to that of the iron-oxide. The iron sulfide, pyrrhotite (FeS) (JCPDS 40832) identified in the diffractograms of the highly sulfided catalyst, assumes hexagonal close-packed geometry. This is also the crystallographic system of iron oxide so there is no mismatch between the geometries of the two precipitating systems.

The apparent increase in crystallite size accompanied by an increase in crystallinity following the addition of sulfur is in conflict with the findings of other workers who have investigated the effect of additives on precipitated Fischer-Tropsch catalysts [86]. Shao-yi Peng *et al* [86] observed that the addition of rare-earth (RE) oxides (RE:Fe = 1:100) to iron-copper coprecipitated catalysts resulted in a decrease in the intensity of the XRD patterns. It has been proposed by the authors that the role of the rare-earths is twofold: firstly, the dispersion of the iron particles is increased, and secondly the small particles are stabilised by inhibited crystal growth. The degree of reduction of iron oxide to metallic iron was also observed to decrease as a consequence of the presence of these lanthanide oxides.

Catalysts which had been exposed to syngas (see Chapter 2) were also analysed by XRD. The unsulfided catalyst comprised mainly magnetite (Fe_3O_4) with only trace amounts of carbide formation evident. The catalyst to which 500 ppm S had been added, exhibited bulk carbides as well as magnetite (Figure 3.10). The form of carbide was identified as ε-Fe_2C, in which the carbon atoms reside in octahedral interstices [87]. Another type of iron carbide, χ-$Fe_{2.5}C$, was found to be the major component of the spent catalyst that had been sulfided with 2000 ppm S (Figure 3.11c).

The formation and distribution of these bulk carbides is sensitive to the physicochemical state of the catalyst. Thomson *et al*, suggested that the type and composition of carbides formed on iron catalysts was a function of iron particle size [87]. Smaller particles were found to preferentially form ε-Fe_2C, while larger particles formed χ-$Fe_{2.5}C$.

According to the JCPDS database, the carbide identified in the 500 ppm S sulfided catalyst was ε-Fe_2C (see above). However, it is reported in the literature that it is not possible to distinguish between ε-Fe_2C and ε'-Fe_2C by XRD since they have identical diffraction patterns, and most authors follow the assignment made by Niemandtsverdriet *et al* and use the latter classification [87] when referring to either of these carbides. Notwithstanding this, the ε'-carbide is unstable and transforms to χ-$Fe_{2.5}C$ under reaction conditions [88]:

$$2.5\varepsilon' Fe_{2.2}C \rightarrow 2.2\chi Fe_{2.5}C + 0.3C$$

This transformation has been associated with the onset of FT catalyst deactivation which is associated with the buildup of nucleate carbon [87]. This inactive carbonaceous material is produced as a direct consequence of the $\varepsilon' \rightarrow \chi$ carbide transformation.

Work by Jung and Thomson [88] on an uncalcined iron catalyst under FT conditions using Dynamic XRD (DXRD), showed that magnetite indeed converted to χ-carbide via a shrinking core process. No nucleate carbon was observed and hence deactivation rates were significantly lower than have been found for catalysts exhibiting ε'-Fe_2C.

Highly sulfided catalysts however, did not appear to form any bulk carbides whatsoever and comprised essentially only α-Fe even after fourteen days of exposure to synthesis gas. The absence of carbide was common to catalysts prepared using both polysulfide and monosulfide sources. These results suggest that the sulfur assists in the reduction of hematite, so that only α-Fe is present after exposure to hydrogen at 400°C. Moreover, it must create an environment which is not conducive to carbide formation and hence precludes FT synthesis.

3.2.5. Thermogravimetric analysis

Finely divided iron-metal is known to exhibit pyrophoric behaviour [89] in oxidising atmospheres. The spent *highly sulfided* catalysts ignited spontaneously at 300°C during thermogravimetric analysis in oxygen, supporting the presence of metallic iron in this sample. A mass *increase* of 25% was measured as metallic iron was oxidised to iron-oxide (Figure 3.18).

The thermogram of the spent unsulfided catalyst showed a weight *loss* at 300°C as carbonaceous material underwent combustion in the presence of oxygen (Figure 3.17).

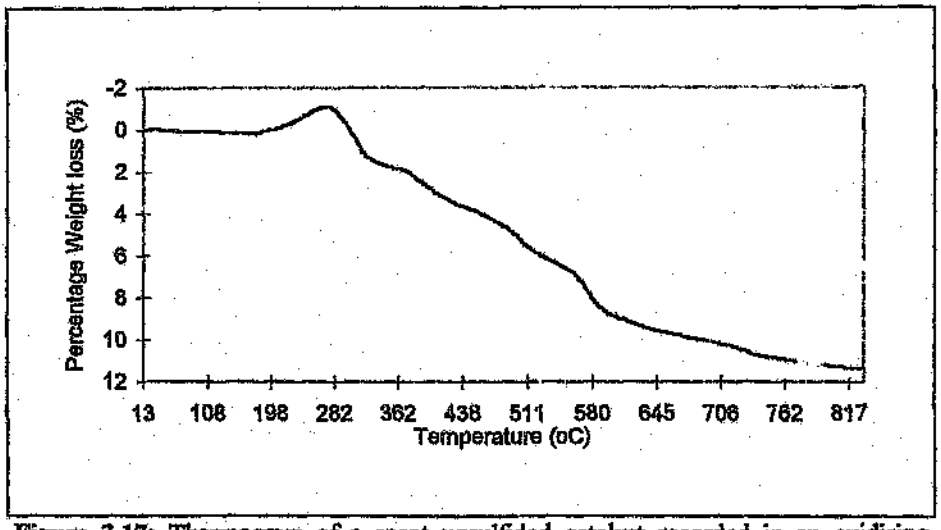


Figure 3.17: Thermogram of a spent unsulfided catalyst recorded in an oxidising atmosphere

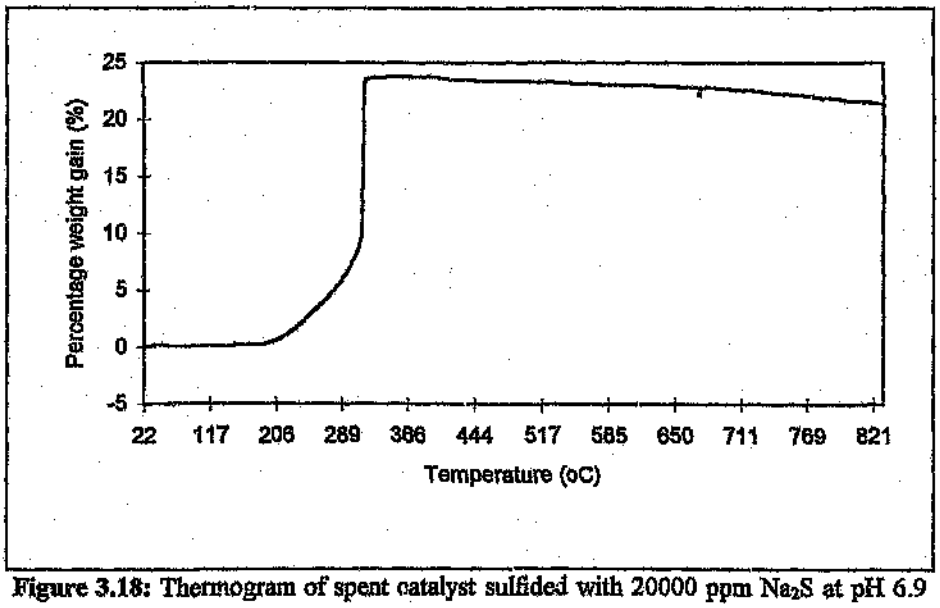


Figure 3.18: Thermogram of spent catalyst sulfided with 20000 ppm Na_2S at pH 6.9 recorded under oxygen

Similar pyrophoric tendencies were observed with other highly sulfided catalysts, prepared at different pH values. The percentage weight gain measured from the thermograms of these samples is presented in Table 3.6.

Table 3.6: Percentage weight gain for catalysts sulfided with 20000 ppm S at different pH values obtained from TGA

pH of sulfidation	% weight gain
10.75	4
8.5	8
6.9	24

3.2.6. Pore Structure

Beside the structure of a catalyst surface, the texture is also an important physical feature. According to Leclercq [54], texture is defined as geometry of the void space in catalyst particles, and encompasses pore shape and surface area measurements. The general approach to determining the porous texture of solids is based on the physical adsorption of selected adsorbates. The mechanism of physisorption depends on the nature of the solid, viz. the range of pore sizes it exhibits. For mesoporous solids, with pore diameters between 20Å and 500Å [53], a secondary adsorption mechanism based on capillary condensation is operative. This condensation is preceded by multi-layer physisorption on the walls of the pores [57].

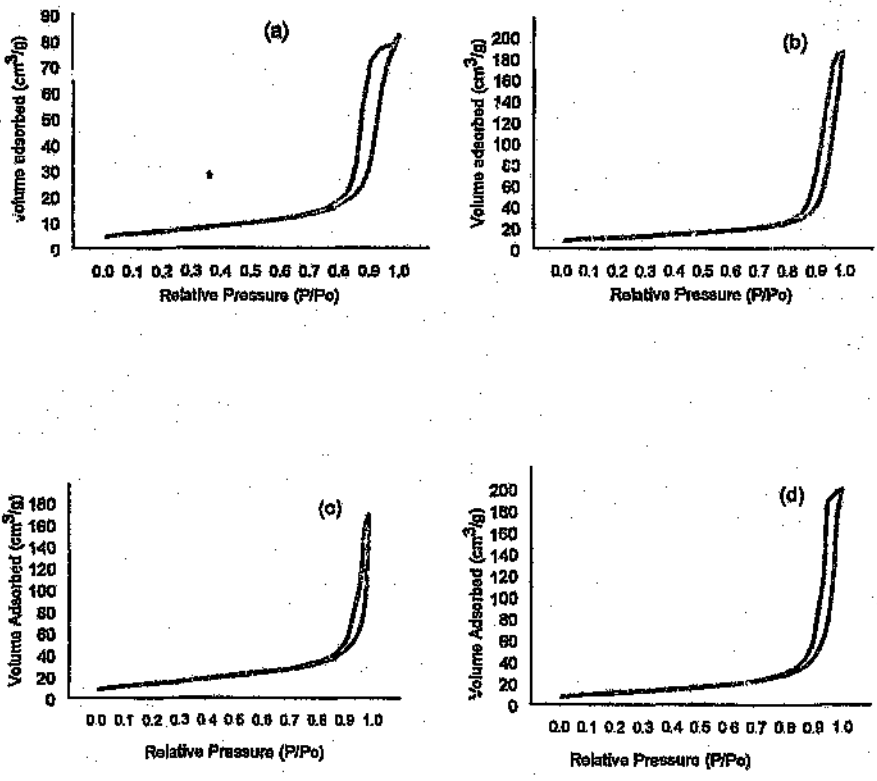
The adsorption-desorption isotherms of selected catalysts shown in Figures 3.19a-d are all typical of Type IV isotherms. The shapes of the hystereses indicate capillary condensation which is characteristic of mesoporous solids [90]. Also noteworthy in Figures 3.19a-d is the fact that the volume of gas adsorbed by the unsulfided catalyst is approximately half that adsorbed by the sulfided catalysts.

Using BJH adsorption and desorption cumulative pore volume plots, the average pore neck and cavity sizes were determined in conjunction with the pore size range (Table 3.7). For comparative purposes, the average pore diameter, determined from the BET equation, is also presented. The pore size range is extremely broad and it would appear that the average pore diameter is possibly a more accurate reflection of the maximum in the pore size distribution plots.

Table 3.7: The effect of sulfidation level on the pore shapes of calcined catalysts

Catalyst	Pore size range (Å)	Average pore cavity size (Å)	Average pore neck size (Å)	Average pore diameter (Å)*
unsulfided	150-800	310	200	208
2000 ppm S pH 10.75	180-1000	400	450	307
2000 ppm S pH 6.9	150-950	525	310	320
20000 ppm S pH 10.75	130-950	600	550	208
20000 ppm S pH 6.9	150-1000	600	350	297
2000 ppm S pH 10.75 $(NH_4)_2S$	230-1000	700	480	400

*Determined from BET measurements 4V/A where V = volume N_2 adsorbed, A = surface area



(a) Unsulfided catalyst

(b) 2000 ppm Na_2S pH 10.75

(c) 20000 ppm Na_2S pH 10.75

(d) 20000 ppm Na_2S pH 6.9

Figure 3.19 a-d: Adsorption-desorption isotherms of calcined catalysts

The data presented in Table 3.7 suggests that the presence of sulfur results in an increase in pore neck and cavity sizes. Close inspection of the hysteresis loops (Figure 3.19a-d) show them to be typical of the Type A and Type E curves in the de-Boer classification. However, according to the BJH pore distribution analysis report, the fraction of pores open at both ends is zero for the catalysts investigated. Therefore, it may be more appropriate to visualize the pores as "ink-bottle" shaped, with cylindrical rather than slit-shaped pores.

The width of the hysteresis loop also gives an indication of the pore-neck shape. The narrow hystereses of catalysts sulfided at pH 10.75 with 20000 ppm Na_2S, 2000 ppm Na_2S, and 2000 ppm polyS respectively are suggestive of wide-necked pores which facilitate ease of desorption of adsorbates from the pores. The unsulfided catalyst is noted to exhibit the broadest hysteresis implying a narrow pore-neck which would hinder the desorption of molecules (Figure 3.20). While it is conceded that a certain degree of error is associated with the BJH method of determining pore neck and cavity sizes, the trends are borne out by the shapes of the hystereses as well.

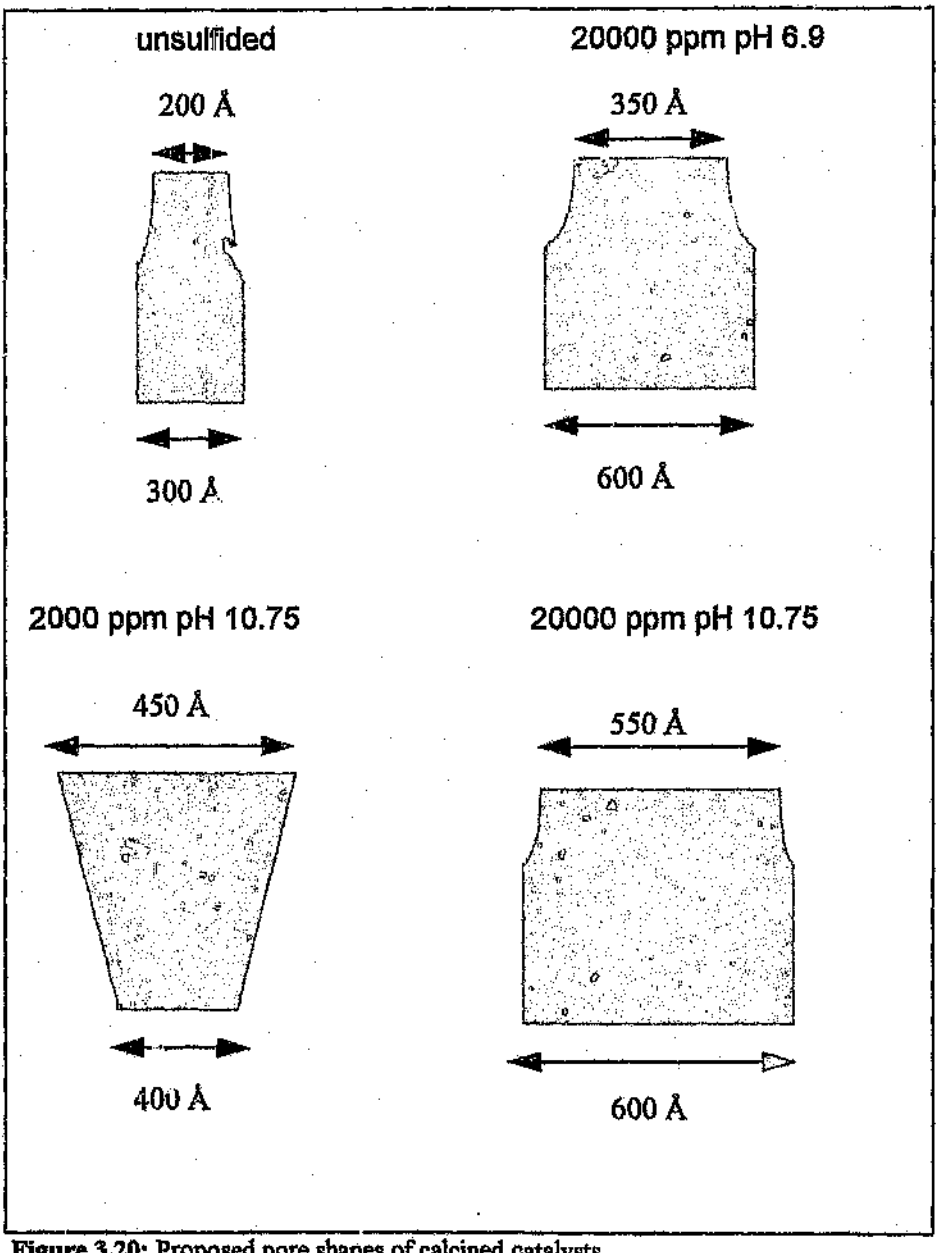


Figure 3.20: Proposed pore shapes of calcined catalysts

Catalysts sulfided at the start of precipitation were found to exhibit wider necks than those to which sulfur was added at pH 6.9, that is, the end of precipitation (Table 3.8). Such trends were observed irrespective of the amount or source of the sulfur (Figure 3.20).

Table 3.8: Variation in pore neck size with pH and source of sulfidation

Catalyst	Source	pH of sulfidation	Average pore neck size (Å)
unsulfided	-	-	200
2000 ppm S	Na_2S	10.75	450
2000 ppm S	$(NH_4)_2S_5$	6.9	310
2000 ppm S	$(NH_4)_2S$	10.75	480
20000 ppm S	Na_2S	10.75	550
20000 ppm S	Na_2S	6.9	350

It would appear that $(NH_4)_2S_5$ yield pores with narrower necks than Na_2S and $(NH_4)_2S$. At any given pH, the pore neck size is found to increase as the level of sulfidation is increased from 2000 to 20000 ppm.

Porosimetry measurements were also undertaken on catalysts after FT synthesis. Prior to analysis, exhaustive extraction of wax products was performed in a Soxhlet apparatus. The isotherms obtained after exposing the catalysts to synthesis conditions revealed significant changes to the pore structure (Figure 3.21). The shapes of the hystereses loops are typical of cylindrical pores with constant cross-sections.

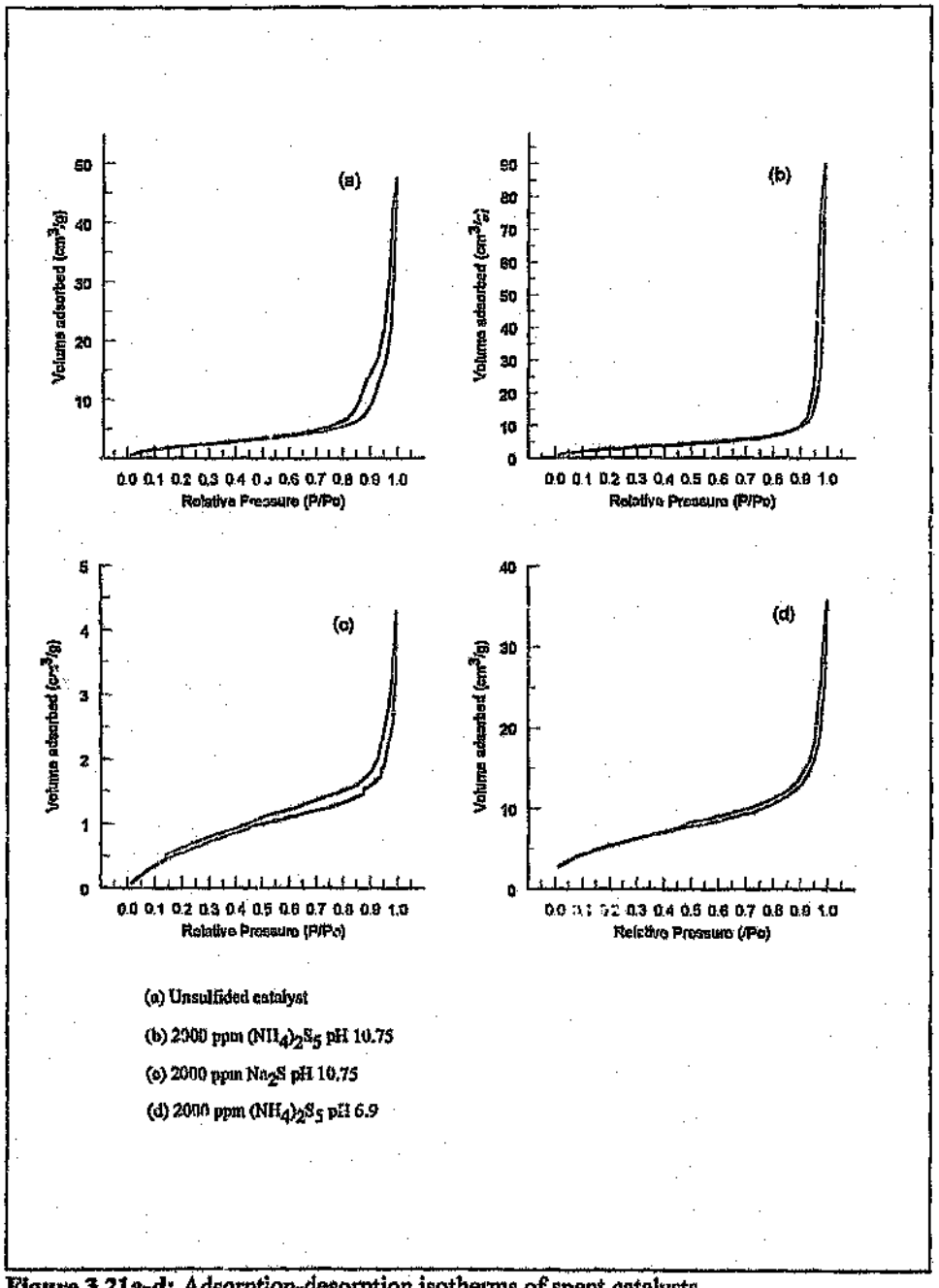


Figure 3.21a-d: Adsorption-desorption isotherms of spent catalysts

The data obtained from the BJH cumulative pore volume plots (Table 3.9) confirms that after Fischer-Tropsch synthesis the neck and cavity sizes are more alike (Figure 3.22).

Table 3.9: Pore Neck and Cavity sizes of spent catalysts

Catalyst	Pore cavity (Å)	Pore Neck (Å)	Range (Å)	Average Diameter (Å) (BET)
unsulfided	250	150	150-900	161
2000 ppm pH 10.75 Poly S	300	200	100-800	146
2000 ppm pH 6.9	150	60	40-400	53
20000 ppm pH 6.9	180	100	100-300	62
2000 ppm pH10.75	600	400	300-1000	208

For the unsulfided catalyst and the ones sulfided with 2000 ppm S, the decrease in pore volume may be due to pore blockage caused by carbon laydown. The catalyst to which 20000 ppm S had been added showed virtually no Fischer-Tropsch activity and the alterations in pore structure could be attributed directly to the presence of sulfur. As was shown by the XRD data, this catalyst was reduced to α-Fe and did not show any evidence of carbide formation. Thus, the post-reaction pore structure is that of bulk metal encapsulated by a thin layer of iron oxide due to exposure to air.

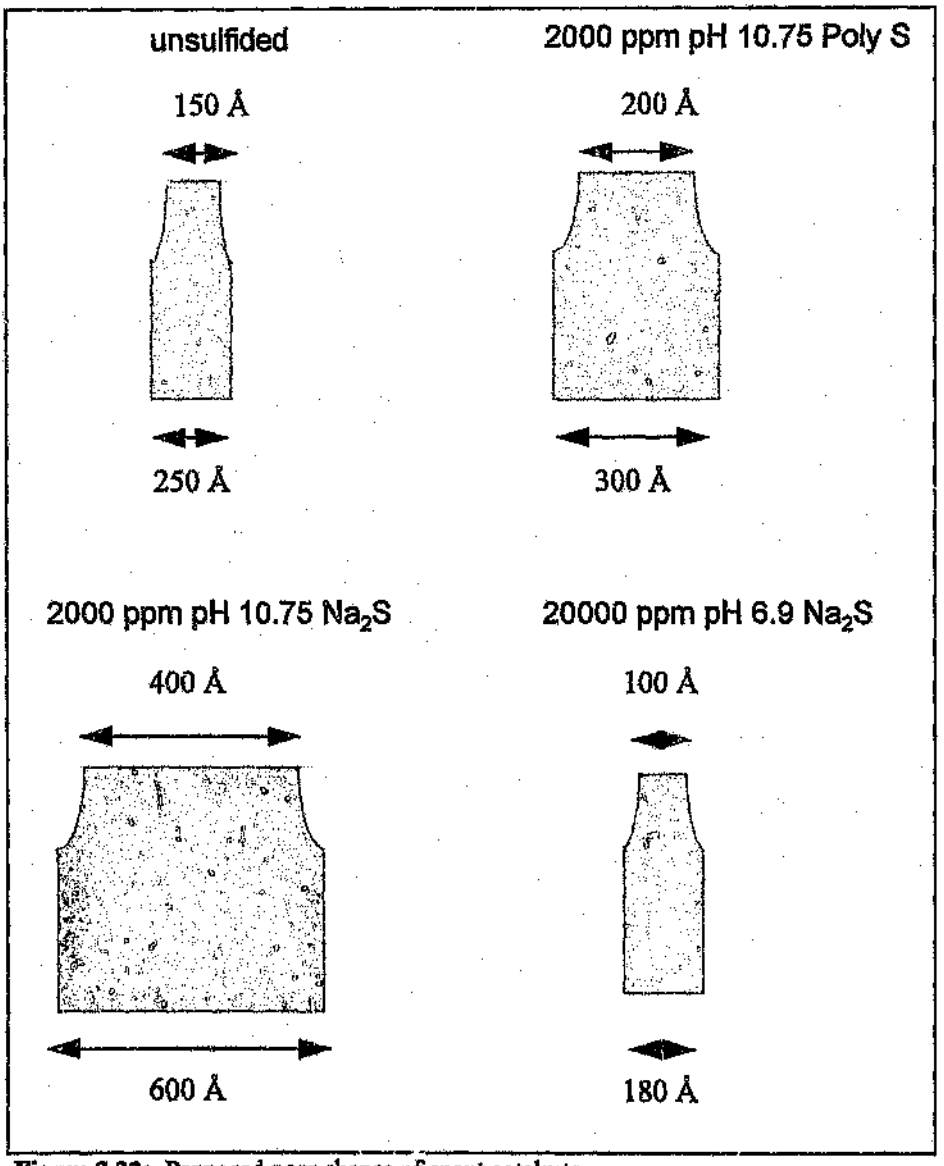


Figure 3.22: Proposed pore shapes of spent catalysts

3.4. Conclusion

Through the implementation of various characterisation techniques, the bulk morphology of sulfided precipitated-iron catalysts has been elucidated. Heterogeneous nucleation resulting in dendrite formation is observed to proceed preferentially in the presence of sulfide ions. This gives rise to a more crystalline ferrihydrite which transforms into an equally crystalline hematite as evidenced by XRD measurements. The latter material, when highly sulfided, appears ochreous compared with the dark brown colour of unsulfided hematite. Modifications in pore structure are a further consequence of precipitation in the presence of sulfide. An increase in pore volume is accompanied by the formation of pores with wider necks and cavities.

After exposure to synthesis conditions, catalysts sulfided with 2000 ppm S are converted to magnetite and exhibit bulk carbides and pore blockage due to carbon laydown. Highly sulfided catalysts show pyrophoric behaviour and comprise essentially only α-Fe.

Chapter 4

Surface characterisation of sulfided precipitated iron Fischer-Tropsch catalysts by Electron Spectroscopy[a]

The field of electron spectroscopy embraces a number of techniques including X-Ray photoelectron and Auger electron Spectroscopy, both of which have found widespread application in the study of heterogeneous catalysis [91].

4.1. Introduction

X-Ray photoelectron spectroscopy (XPS) is well entenched as a standard technique for the elucidation and characterisation of reactive surfaces. Its application in the field of heterogeneous catalysis has been known since the pioneering work of Siegbahn and has been extended to include a plethora of industrially important catalysts in use today [91].

More specifically, its usefulness in the study of Fischer-Tropsch (FT) catalysts encompasses active metals, structural and chemical promoters, and catalyst poisons [92, 93, 94, 95]. For example, in a study of promoted iron FT catalysts, Baltrus and colleagues revealed evidence of the surface re-distribution of potassium [95]. Moreover, the segregation of promoters contained within fused iron catalysts has been shown using XPS to occur with the following order of mobility: K>Ca ≅ Si > Mg ≅ Al [96]. XPS has also been used to identify reactive intermediates in the FT reaction. Thus, as part of a mechanistic study, Benziger and Madix [97] were able to identify methyl and carboxylate intermediates on Fe (100) surfaces.

[a] This work has been accepted for publication: Fromfield, T.C. and Coville, N.J. *Appl. Surf. Sci.* (in press)

Unsupported FeRu alloy catalysts have also been the subject of an intense XPS study [98, 99, 100]. Initial work focussed on the surface morphology of the fresh catalyst [98], and illustrated the surface enrichment of Fe following reduction and passivation [100]. Ensuing studies concentrated on the deposition of carbon during Fischer-Tropsch synthesis, monitored *in situ* using XPS [99].

The involvement of XPS in the study of the interaction of sulfur atoms with metal oxides has largely been restricted to H_2S adsorption on such surfaces [100]. However, isolated accounts of the detection of the segregation of sulfur species by XPS have been reported [101, 102].

Auger Electron Spectroscopy (AES) is a technique which is complementary to XPS and has also been used in FT (and related) studies. An AES study of the activation of iron Fischer-Tropsch catalysts revealed significant differences in surface morphology which is related to catalyst activity [103]. The surface composition of iron catalysts for use in ammonia synthesis also has been elucidated using AES, and an equation from which the surface concentrations of iron and promoter could be determined using Auger current has been developed [104].

Unfortunately, one of the limitations of AES is its lack of sensitivity with regard to the oxidation states of certain species, notably sulfur. A variety of sulfides have been studied by AES [105], but no correlation was found between the Auger line-shape and the presence of oxygen on the surface. Nevertheless, in a study of the interaction of sulfur with palladium surfaces, evidence was found for the migration of bulk sulfur to the surface [106]. Consequently, the major application of Auger spectroscopy is in depth profiling [91].

4.2. Experimental

Catalysts were prepared by precipitation of iron hydroxide from 0.715 M $Fe(NO_3)_3.9H_2O$ and 0.785 M Na_2CO_3 at 75°C and a pH of 6.9. Sulfidation was performed during the precipitation stage, at pH intervals of 10.75, 8.5 and 6.9. Sodium sulfide, ammonium sulfide and ammonium polysulfide [50] were used as sources of sulfur and catalysts were sulfided with between 2000 and 20000 ppm sulfur. Catalysts were calcined *ex-situ* in air (GHSV = 2000 h^{-1}) at 200°C or 400°C for 16 hours. An unsulfided precipitated-iron catalyst prepared under identical conditions to the sulfided catalysts was used as a reference to permit comparison of the effects of various calcination and reduction pretreatments.

XPS spectra were recorded on a VG ESCALAB MkII spectrometer equipped with a heatable reaction cell attachment which could also be pressurised. Unmonochromatized Mg Kα X-rays at 15kV/20mA and at incidence angle of 45° were used to irradiate the samples. An analyzer slit width of 6 mm and pass energies of 50 eV for wide scans and 20 eV for narrow scans were found to be optimal.

Calcined samples were reduced *in-situ* at either 300°C or 400°C under flowing hydrogen for 1 hour. The samples were then cooled to near ambient temperature before evacuation and analysis.

Linear background subtraction was performed prior to peak-fitting and S (2p) spectra were fitted according to the method of Termes *et al* [59], with doublets having ($^1/_2$, $^3/_2$) components and an intensity ratio of 1:2, constrained to a 20% Lorentzian, 80% Gaussian lineshape and a separation of 1.15 eV.

Auger electron spectroscopy was conducted on a catalyst sulfided with 20000 ppm Na_2S after it had been calcined and reduced *ex situ* at 400°C. Measurements were performed on a PHI 595 Scanning Auger Microprobe with electron beam voltage of 3 kV and current of 1 μA (stepsize 0.5 eV). Depth profiling was carried out using 3 kV Ar^+ ions at 30 $\mu A/cm^2$.

4.3. Results and Discussion

No sulfur species were detected by XPS on the surfaces of presulfided catalysts (2000-20000 ppm S) prior to reduction, even after calcination at 200°C and 400°C. Although hematite is intrinsically difficult to analyse by XPS owing to charging effects [52], this cannot be exclusively responsible for the inability to detect sulfur on the surface of these catalysts. Further, significant loss of sulfur from the surface, eg. as SO_2 is not expected to occur during calcination. Rather, sulfur present in the bulk is expected to be encapsulated by an oxide layer generated at the surface [107].

Notwithstanding this, the calcination temperature and sulfide concentration affected the nature of the species present after reduction. Generally, calcination of F-T catalysts is performed at low temperatures to minimise loss of surface area due to sintering. However, nitrates trapped during precipitation, could constitute catalyst poisons and are hence usually oxidatively removed at temperatures above 200°C. Thus XPS studies were performed on catalysts containing varying amounts of sulfur, after calcination at 200°C and 400°C, and reduced at either 300°C or 400°C.

For the low level sulfided catalyst (5000 ppm) calcined at 200°C, no surface sulfur species were detected after reduction at either 300°C or 400°C. However, after calcination at 400°C and reduction at 300°C, the detection of oxidised sulfur species in the form of sulfate at 169.4 eV (Figure 4.1) indicates that a sequence of redox reactions are initiated at this higher temperature.

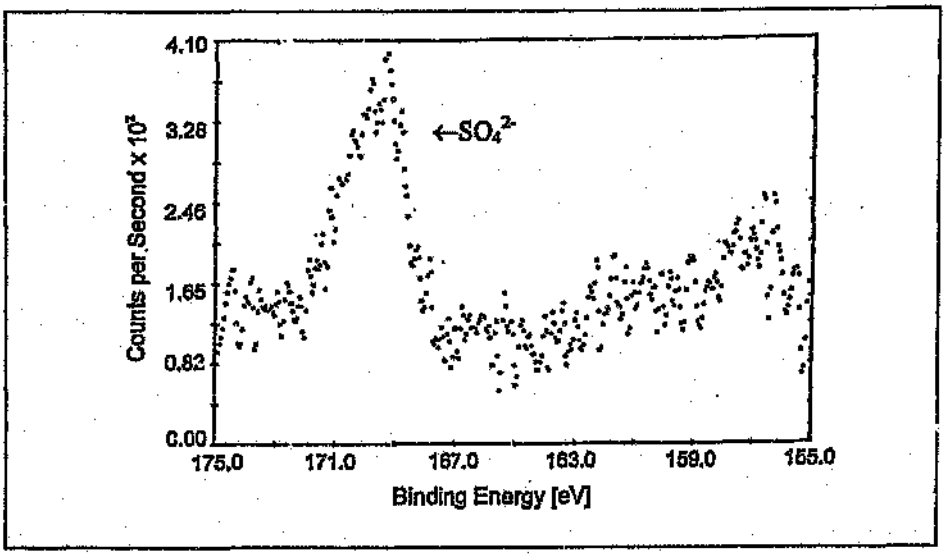


Figure 4.1: S (2p) photopeak of catalyst sulfided with 5000 ppm Na_2S, calcined at 400°C and reduced at 300°C.

The presence of sulfate is not unexpected since the major product of the oxidation of iron-sulfides is a basic iron sulfate, "$FeOHSO_4$" [108], a dimer, in which each iron atom is octahedrally coordinated with two hydroxyl and four sulfate oxygens [109]. A scheme analogous to that proposed by Kyotani [110] for the regeneration of Cu_2S to CuO which culminates in the production of a sulfate, can account for the formation of sulfate in our samples. By contrast, XPS data on highly sulfided catalysts (20000 ppm S) calcined at 200°C (and reduced at 300°C) suggest that oxidation of the added sulfide is incomplete at this temperature, as evidenced by the presence of both sulfide and sulfate species (Figure 4.2).

To establish the effect of reduction temperature on surface sulfur species, two samples of the catalyst sulfided with 20000 ppm Na_2S at pH 10.75 were calcined at 200°C. One was exposed to hydrogen at 300°C, and the other at 400°C for 1 hour.

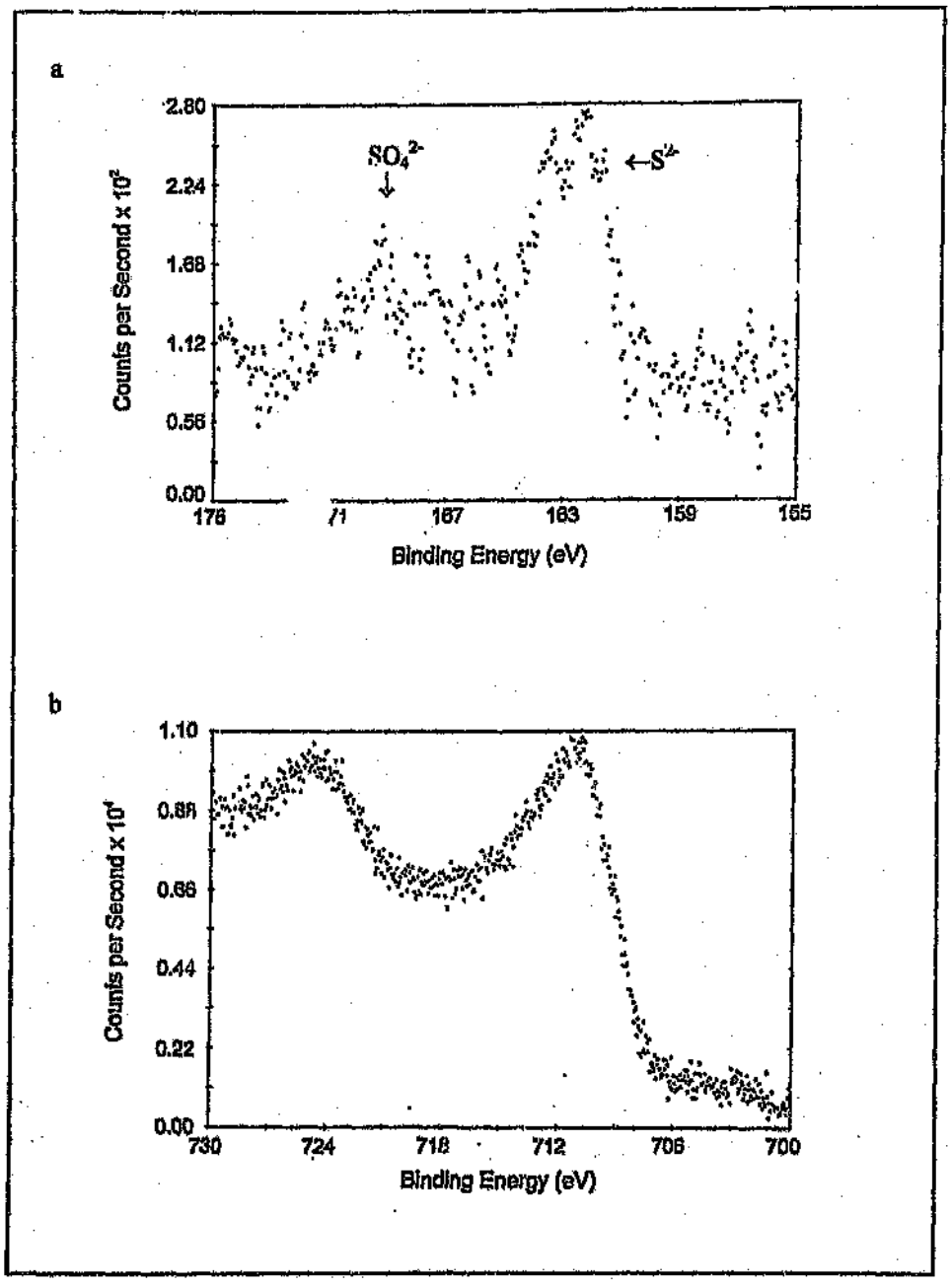


Figure 4.2:a) Evolution of sulfide (162 eV) and sulfate (168 eV) on a catalyst sulfided with 20000 ppm Na_2S, after calcination at 200°C and reduction at 300°C b) Fe 2p ($^3/_2$) photopeak of the same catalyst showing the presence of iron-oxide (712 eV) after hydrogen activation.

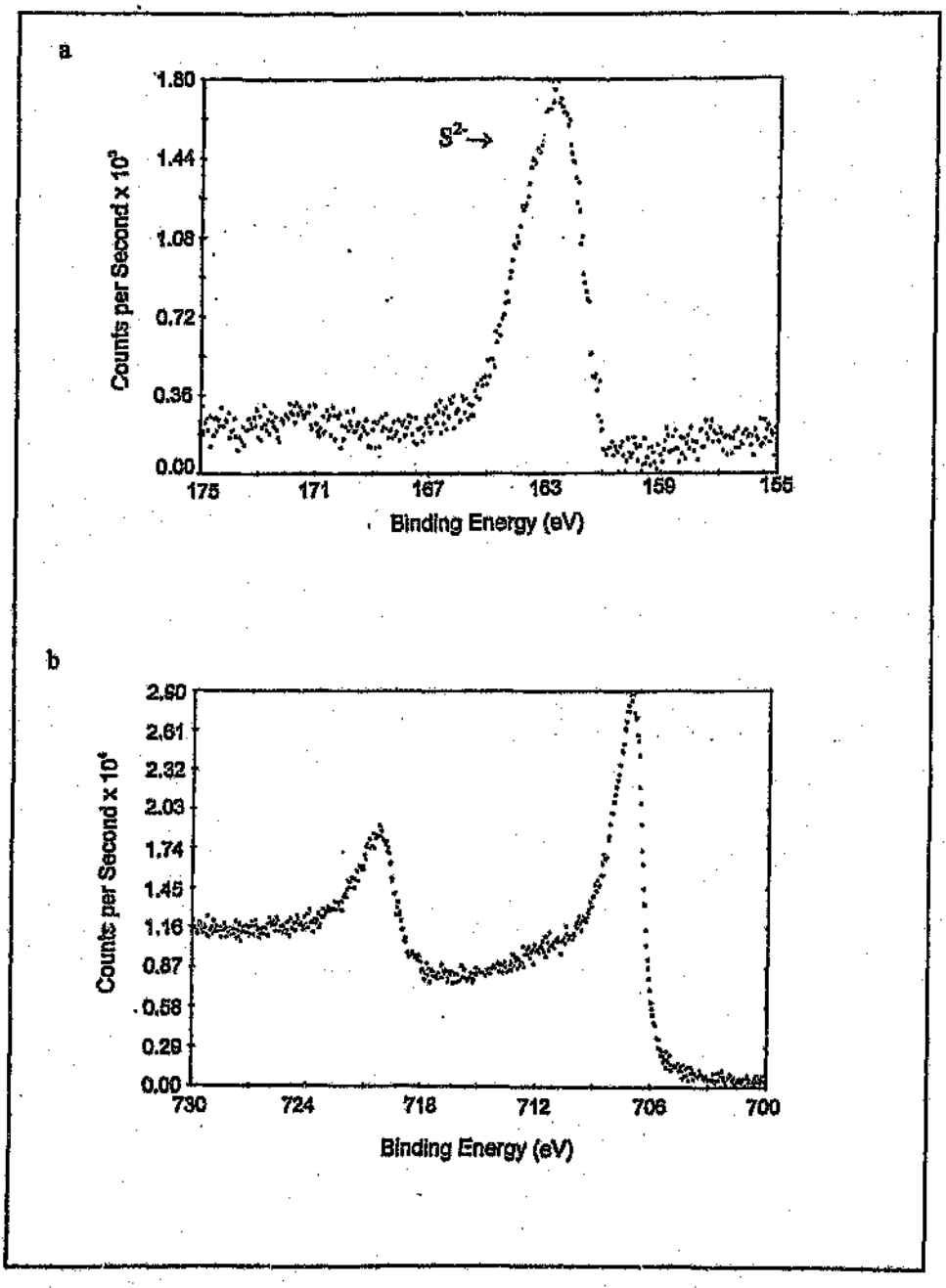


Figure 4.3: a) S (2p) co e level spectrum of catalyst sulfided as in Figure 4.2, but reduced at 400°C, showing conversion of sulfate to sulfide **b)** Fe (2p) photopeak typical of metallic iron, formed after reduction at 400°C

Examination of the S (2p) core-level spectrum (Figure 4.2a) revealed the presence of both sulfate (169.2 eV) and sulfide (162.3 eV) ions after reduction at 300°C; while only the sulfide is observed after exposure to hydrogen at 400°C (Figure 4.3a). The 162.8 eV photopeak is also enriched from 1.3 to 15.6 atomic percent, suggesting that the diffusion of sulfur species to the surface is favoured by higher reduction temperatures.

Reduction under hydrogen affects both the sulfur speciation, and the evolution of different iron species at the surface. As illustrated in Figure 3b, the Fe 2p ($^3/2$) photopeak for the catalyst reduced at 400°C is at 707.1 eV and is typical of Fe^0, unlike that of the same catalyst reduced at 300°C (Figure 4.2b), which appears at 712.0 eV, and may be assigned to Fe^{3+}/Fe^{2+} species. For both the unsulfided catalyst and those catalysts containing 2000 ppm sulfur, studied under identical conditions, the iron photopeak is typical of magnetite (Fe_3O_4) [111]. This finding is supported by Temperature Programmed Reduction studies (Chapter 8) which show that, particularly at high levels of sulfidation, the temperature of the hematite-magnetite transition is considerably lower than in the absence of extraneous sulfur.

It will become apparent in later chapters that catalysts with sulfide species at the surface show effects of poisoning, while sulfate-bearing catalysts exhibit an enhancement in activity. These results suggest that complete reduction to metallic iron in the presence of sulfur is undesirable since it is accompanied by the formation of poisonous sulfide species. Indeed, Muzovskaya and Rapoport, cited in [112], alluded to the presence of iron oxides as being necessary to prevent rapid deactivation by sulfur, since catalysts reduced predominantly to metallic iron were easily poisoned.

Examination of the S (2p) core-level spectrum (Figure 4.2a) revealed the presence of both sulfate (169.2 eV) and sulfide (162.3 eV) ions after reduction at 300°C; while only the sulfide is observed after exposure to hydrogen at 400°C (Figure 4.3a). The 162.8 eV photopeak is also enriched from 1.3 to 15.6 atomic percent, suggesting that the diffusion of sulfur species to the surface is favoured by higher reduction temperatures.

Reduction under hydrogen affects both the sulfur speciation, and the evolution of different iron species at the surface. As illustrated in Figure 3b, the Fe 2p ($^3/2$) photopeak for the catalyst reduced at 400°C is at 707.1 eV and is typical of Fe^o, unlike that of the same catalyst reduced at 300°C (Figure 4.2b), which appears at 712.0 eV, and may be assigned to Fe^{3+}/Fe^{2+} species. For both the unsulfided catalyst and those catalysts containing 2000 ppm sulfur, studied under identical conditions, the iron photopeak is typical of magnetite (Fe_3O_4) [112]. This finding is supported by Temperature Programmed Reduction studies (Chapter 8) which show that, particularly at high levels of sulfidation, the temperature of the hematite-magnetite transition is considerably lower than in the absence of extraneous sulfur.

It will become apparent in later chapters that catalysts with sulfide species at the surface show effects of poisoning, while sulfate-bearing catalysts exhibit an enhancement in activity. These results suggest that complete reduction to metallic iron in the presence of sulfur is undesirable since it is accompanied by the formation of poisonous sulfide species. Indeed, Muzovskaya and Rapoport, cited in [113], alluded

Segregation of sulfur occurs following exposure to hydrogen, with higher reduction temperatures promoting migration. Additionally, higher reduction temperatures assist in the conversion of sulfate to sulfide. In a study of metal sulfides by XPS, Lichtman [105], alluded to the presence of oxygen as having a profound effect on the evolution of a sulfate peak. The observed impoverishment in oxygen following reduction is then accompanied by a concomitant enrichment in sulfide at the surface.

The thermodynamic driving force behind surface segregation has been suggested using ASED-MO theory, to result from vacancy formation energy [113], arising from lattice vacancies created by the removal of oxygen. For sulfur migration in iron, this corresponds to a segregation energy of 1.64 eV.

Owing therefore to the migration of sulfur being favoured by oxygen depletion at the surface, the mechanism of segregation may be postulated as based on the phenomenon of site competition [114]. In this process, oxygen replacement by sulfur has been proposed to occur in two distinct regimes which depend on the amount of oxygen present on the surface. When oxygen is abundant, displacement by sulfur occurs in a 2:1 ratio, that is, the removal of two oxygen atoms is proceeded by the segregation of one atom of sulfur. This continues until the oxygen is depleted to the extent that atom-for-atom replacement occurs.

Systematically increasing the level of sulfidation from 2000 to 20000 ppm revealed that the more sulfide added, the greater the amount of segregation. For catalysts sulfided

with 2000 ppm sulfide, the S (2p) spectra exhibited only one photopeak at 169.4 eV, characteristic of a SO_x^{n-} (sulfate like) species. The evolution of this peak is independent of the sulfide source or the pH of sulfidation. These results are consistent with low-exposure H_2S studies in which only sulfate species were observed [101]. Further, it has been reported that annealing Fe_2O_3 in a gas mixture containing small quantities of sulfur resulted in the formation of a sulfate surface layer [115].

At low sulfide levels the surface species observed were independent of the sulfide source. However, sulfidation with 20000 ppm sulfide produced significant source-related differences, after calcination at 200°C. Use of both $(NH_4)_2S$ and $(NH_4)_2S_5$, resulted in the evolution of large sulfide peaks accompanied by smaller sulfate peaks.

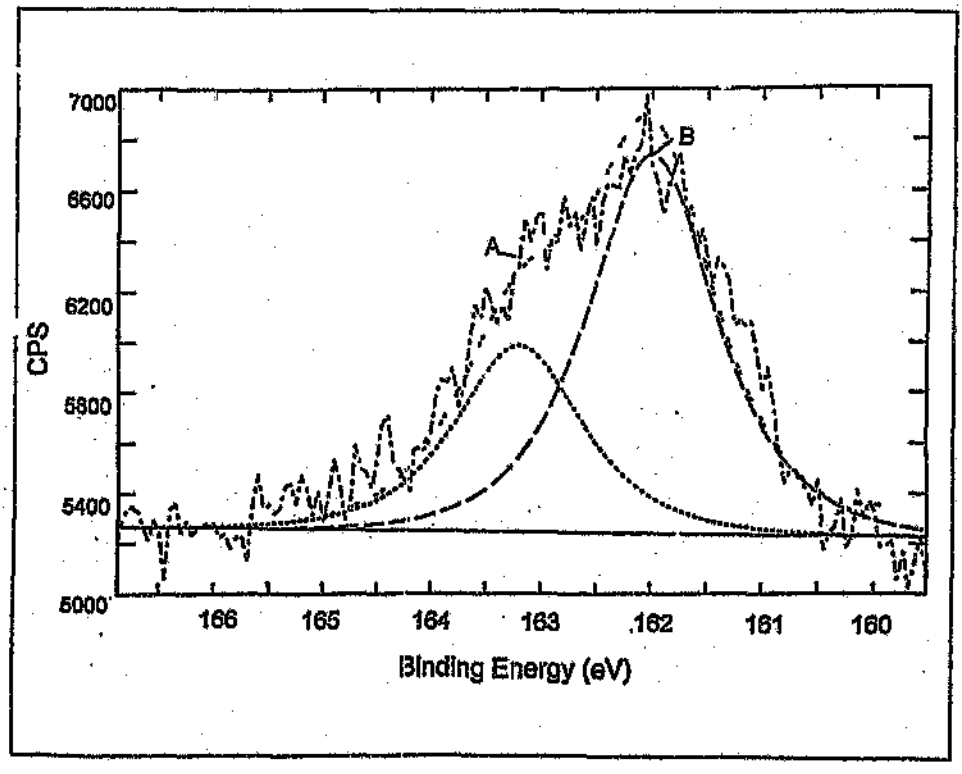


Figure 4.4: Expanded view of sulfide peak at 162 eV of catalyst in Figure 4.3a), complete with peak-fit.

It was in the deconvolution of the sulfide peak that differences became apparent. An expanded view of the sulfide region betweeen 160-166 eV for the catalyst sulfided with sodium sulfide, fitted with a ($^1/_2$, $^3/_2$) two component doublet is shown in Figure 4.4. A similar peak-fitting procedure employed for the sulfide peak of the polysulfided catalyst (Figure 4.5) necessitated the insertion of a second doublet at 163.0 eV.

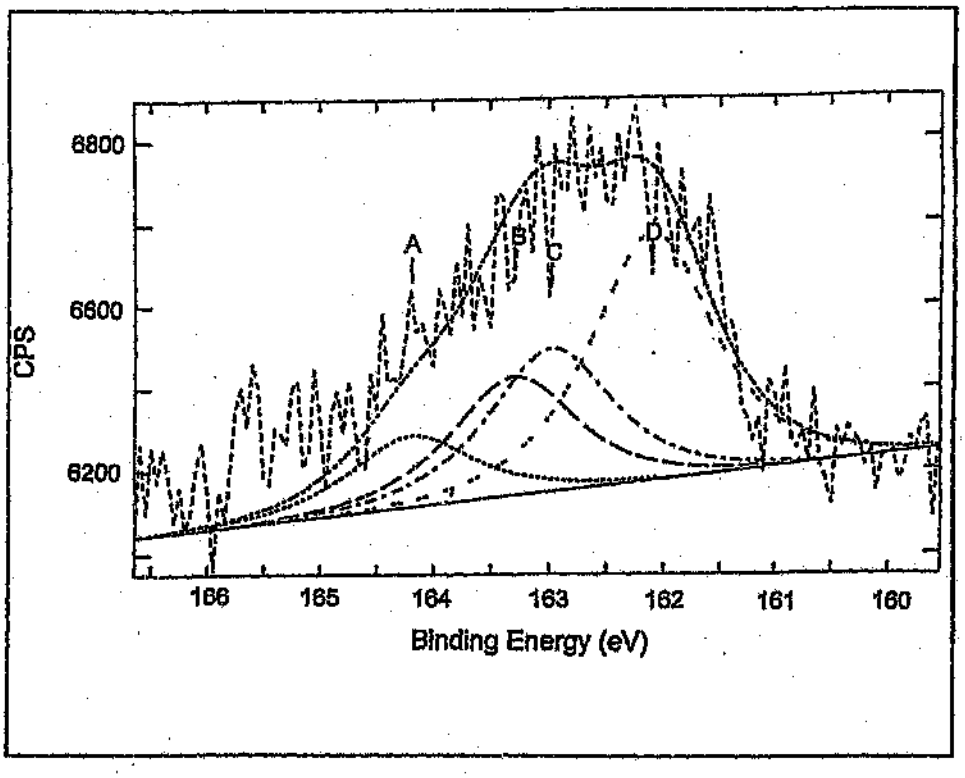


Figure 4.5: Expansion of sulfide region of polysulfided catalyst containing 20000 ppm $(NH_4)_2S_5$. Lines A and C constitute one doublet used in peak-fitting, while lines B and D make up the other doublet.

While the first doublet at 162.0 eV in Figure 4.5 corresponds to a sulfidic species attached directly to a metal atom, the position of the second is midway between that of a purely sulfidic species and elemental sulfur which has a binding energy of 164.0 eV.

These distinct sulfide species are analogous to the structurally different sulfur atoms observed in the triphenylphosphonium salt of $[Cu_3(S_4)_3]^{3-}$ [59]. This suggests that the S_5^{2-} polysulfide may have fragmented in the calcination/reduction process to give S_3^{2-} (two doublets expected) and S^{2-} (one doublet expected).

Polysulfides are thermodynamically unstable and can fragment in aqueous solvents due to their small bond energies (145 kJ/mol for S_4^{2-}) [12]. Elemental sulfur is reportedly a product of this decomposition according to this reaction:

$$S_n^{2-} \rightarrow H_2S + (n-1)S(s)$$

Although these polysulfide ligands are labile, kinetic studies indicate that their decomposition is sufficiently slow at low temperatures for them to exist for a reasonable length of time. However, at temperatures of 100 - 150°C, their decomposition is accelerated [116], and is supposedly complete below a temperature of 200°C. Moreover, it has also been postulated that the reduction of linear or cyclic polysulfides is a source of inorganic sulfide [117].

It is also possible that the S_5^{2-} did not fragment and that a cyclic Fe-polysulfide complex may have been formed. If so, there should be three distinct sulfide species identifiable by XPS [118]. The peak-fit obtained for our data (Figure 4.5) is not unique, and it may be possible to insert a small doublet at approximately 164 eV, and still obtain a reasonable data-fit.

However, this doublet appears to be outside the range of binding energies expected for sulfides, and may too closely resemble elemental sulfur. Nevertheless, it must be borne in mind that this intermediary sulfur atom is in the most 'sulfur-rich' environment of all the atoms in the ligand and may experience no effect of the metal centre whatsoever, and hence exhibit a binding energy similar to that of S_8.

Certainly, the existence of a peak between 168.8 and 169.5 eV is suggestive of polysulfide decomposition, yielding a sulfate. Unfortunately, owing to its low intensity, the position of this "sulfate" peak could not be accurately determined. However, it is in a region that is typical not only of sulfates, but also other oxidised species, such as the central sulfur atom in $S_2O_3^{2-}$ which has a binding energy of 168.6 eV [119].

In addition, the oxidation of S_n^{2-} ligands by molecular oxygen is possible and would lead to novel ligands such as $S_3O_2^{2-}$ or S_3O^{2-} [120]. Nevertheless, although partial decomposition to an oxidised species may well have occurred, it was not possible to approximate the peak at 160-166 eV with only a single sulfur species (doublet), hence confirming the existence of at least two sulfide entities.

Owing to its superior depth profiling capability [91], Auger electron spectroscopy (AES) was invoked to confirm the proposed surface segregation of bulk sulfide. The Auger electron spectrum of the calcined, reduced catalyst sulfided at pH 10.75 with 20000 ppm S is shown in Figure 4.6.

The presence of sulfur is shown by the LMM peak at 151 eV. This is in good agreement with the Auger line for FeS which occurs at 151.2 eV [105]. The large oxygen KLL peak at 508 eV, as well as the smaller KLL doublet at 470 and 485 eV indicate that oxidation of the surface has occurred during transfer of the sample from the XPS instrument. This exposure to air was unfortunate, and resulted in the emergence of a doublet at 42 and 50 eV, which has been assigned to the MVV peaks of oxidised iron [104].

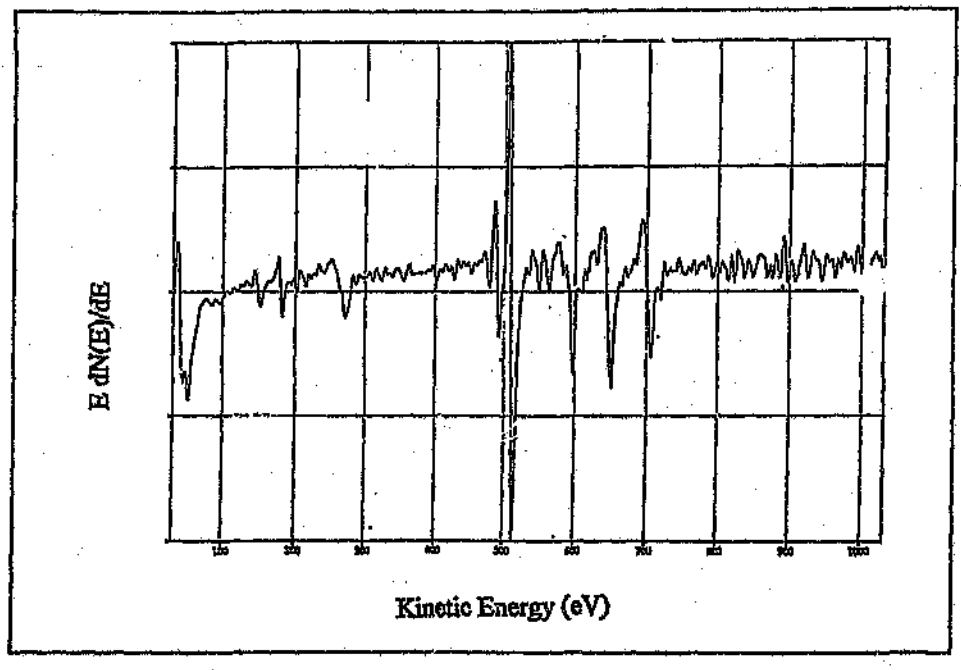


Figure 4.6: Auger electron spectrum of a calcined, reduced catalyst sulfided with 20000 ppm Na_2S at pH 10.75

The origin of the spurious carbon peak at 272 eV is unclear (Figure 4.6), although graphitic carbon was also observed at 285 eV during XPS measurements. It has been suggested that this may be due to surface contamination of the sample.

A depth profile was constructed using an argon sputter gun (Figure 4.7). The lower surface concentration of iron can be seen in the peak-to-peak spectrum, associated with the large amount of surface oxygen.

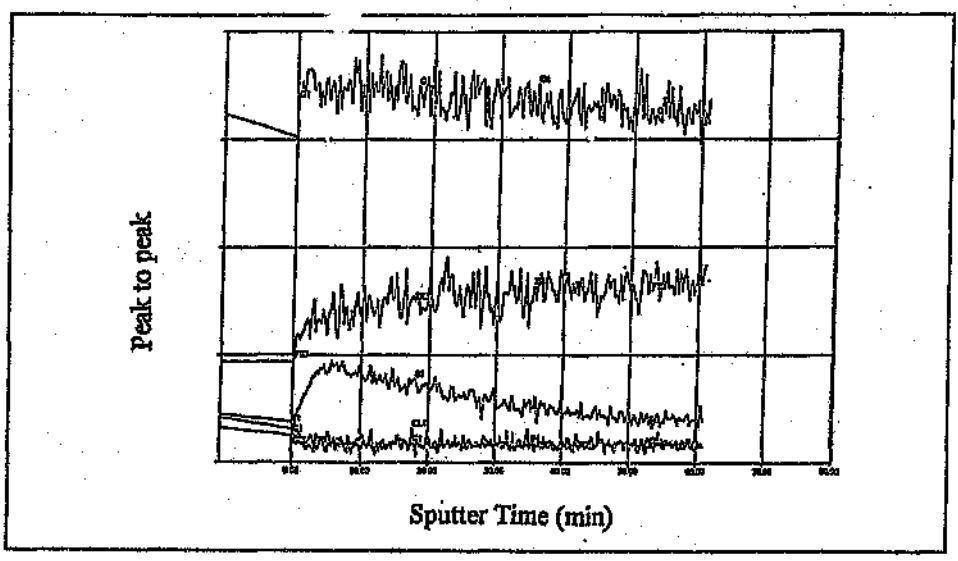


Figure 4.7: Peak-to-peak Auger depth-profile of surface of the catalyst in Figure 4.6

More important is the high concentration of sulfur close to the surface, which attests to the proposed migration phenomenon. While the presence of oxygen has a profound effect on the sulfide XPS spectrum, little or no correlation is found between Auger line structure and oxidation of the surface [105]. Hence, it is impossible to ascertain unambiguously what the effect of sulfate would be on the Auger spectrum of sulfide [105].

4.4. Conclusion

Results of the XPS analysis confirm the segregation of sulfur to the surface of sulfided precipitated-iron catalysts. This surface enrichment dramatically alters the composition and morphology of the surface-bulk interface and facilitates the formation of a low-dimensional structure of extraordinary properties. The data suggest that surface sulfates give rise to an enhancement in catalyst activity, while sulfides induce poisoning (see Chapter 8). The relative proportions of these species can be controlled by careful manipulation of both the level of sulfidation and the pretreatment conditions.

Chapter 5

Surface characterisation of sulfided iron catalysts using Diffuse Reflectance Fourier Transform Infrared Spectroscopy (DRIFTS)

5.1. Introduction

The elucidation of surface processes such as the adsorption of molecules, is imperative in the study of catalysts. Of the techniques available, vibrational spectroscopy is unsurpassed in its ability to provide information on the nature of the interaction between adsorbates and catalytic substrates [121].

Diffuse reflectance FTIR spectroscopy (DRIFTS) is a field of vibrational spectroscopy particularly well suited to heterogeneous catalysis, since species adsorbed on powdered samples can be characterised. This eliminates the energy loss at high wavenumbers caused by scattering, as encountered with pelletized samples [121]. Another significant advantage of DRIFTS over other FTIR techniques, is the facility to perform *in-situ* studies under simulated reaction conditions [122]. This provides an even more accurate assessment of the interaction between gas-phase reagents and catalytic surfaces.

Carbon monoxide is an ideal probe molecule for the characterisation of Fischer-Tropsch catalysts using DRIFTS. Its intense absorption in the 2000-2250 cm^{-1} region is uniquely sensitive to the oxidation state of the metal substrate to which it adsorbs [123].

According to a proposal by Blyholder, based on molecular orbital calculations (Figure 5.1a), the metal-CO bond comprises both σ and π dative bonds [124]. The former occurs via the filled CO σ-orbitals and unfilled metal d-orbitals [123]. Synergic bonding between filled metal dπ-orbital and vacant CO π^*-orbitals serves to further strengthen the M-CO bond, simultaneously weakening the carbon-oxygen interaction. It follows that the greater the π character of the metal-carbon bond, the weaker the C-O bond, and this shifts the frequency of the ν_{CO} stretching vibration from 2143 cm^{-1} (gas phase) to 2100-2000 cm^{-1} [123]. A scheme describing the orbital interaction of a metal with CO is shown in Figure 5.1b.

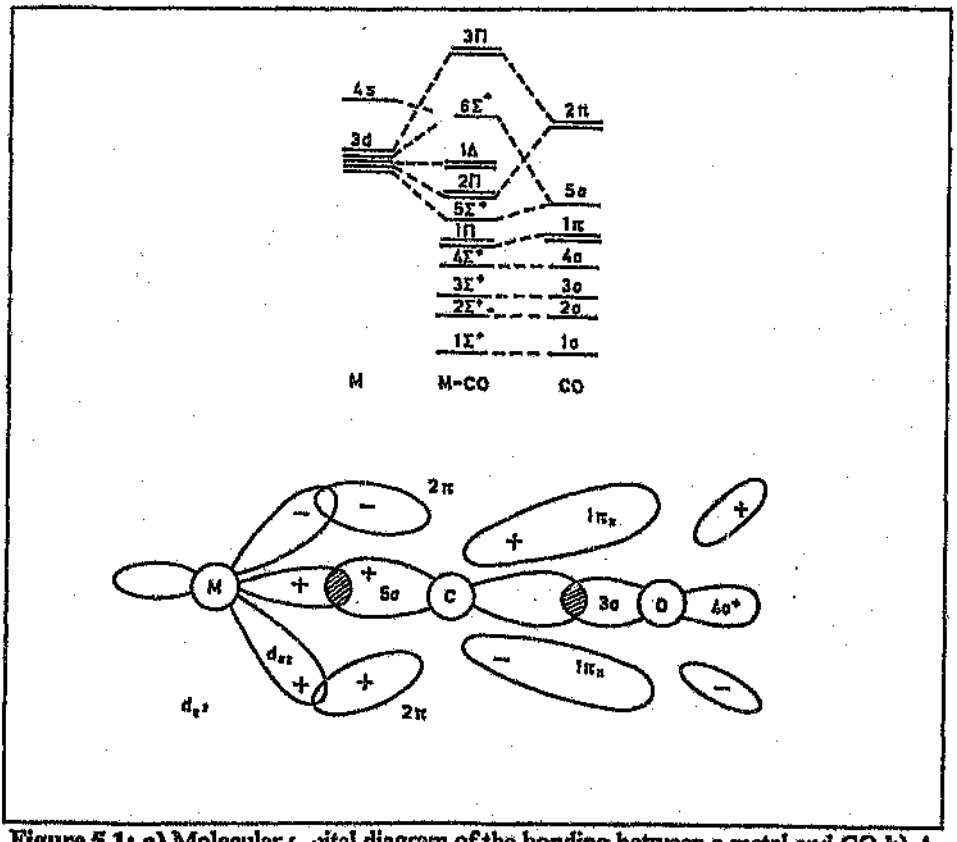


Figure 5.1: a) Molecular orbital diagram of the bonding between a metal and CO b) A schematic representation of the orbital overlap in a metal-carbonyl complex [123]

CO can also bridge two (or more) metals resulting in both single-site adsorption (δ-CO) and multi-site adsorption (β-CO), which can readily be differentiated by IR spectroscopy.

Since carbon monoxide is a constituent of syngas, the interaction between this adsorbate and metal surfaces can be used to probe mechanistic features of the Fischer-Tropsch reaction. Various factors, including the chemical environment of the metal atoms at the surface of FT catalysts, can influence their interaction with adsorbed CO molecules. Thus, through the addition of promoters or poisons, the strength of the metal-CO bond can be varied, resulting in subtle changes to the position and intensity of the ν_{CO} vibration. Indeed, CO adsorption has been employed in the study of unpromoted catalysts [125], as well as those promoted with additives such as potassium [32] and silica [125, 126, 127].

The consequences of sulfide addition on the adsorption of carbon monoxide on Ni/Al_2O_3 catalysts have been studied by Rewick and Wise [128]. It was established that the amount of single site CO adsorption (δ-CO) increased in the presence of small amounts of H_2S at the expense of β-CO (multi-site adsorption). Further exposure to H_2S resulted in a more rapid decrease of β-CO than δ-CO. Similar effects were observed by Kroeker *et al* for CO adsorption on Rh/Al model catalysts sulfided with D_2S [129]. It was found that bridged CO species converted to linear carbonyls in the presence of pre-sorbed sulfur and this resulted in an increase in the density of species with one CO molecule per Rh atom. The implication is that the bond between the metal and CO was weakened by the addition of S to the catalytic surface.

In the present study, the adsorption of CO was used to determine the oxidation state of iron in sulfided and unsulfided catalysts after reduction in hydrogen. Furthermore, the effect of added sulfide on the performance of these catalysts in the Fischer-Tropsch reaction was investigated *in-situ* under conditions that simulate those used for the reactor studies.

5.2. Experimental

Iron catalysts (prepared as described in Chapter 2) were sulfided in the range 500-20000 ppm S, using sodium and ammonium-derived sulfide sources. Sulfide was added during precipitation at pH 10.75, 8.5 and 6.9.

DRIFTS analysis was performed on a Nicolet Impact 420 spectrometer equipped with a Harrick "Praying Mantis" DRIFTS attachment. Each measurement comprised 1024 scans in the region 4000-1200 cm^{-1}. Approximately 100 mg of each catalyst was used, and care was taken to ensure minimal differences in sample packing. Unless otherwise stated, all samples were calcined (200°C or 400° C) and reduced (300°C or 400°C) *in-situ* at the temperatures indicated. Calcination was performed in dry air (flow rate of 3 ml/min) for approximately 4 hours. Thereafter, the sample was reduced in a 1:1 H_2:He mixture (flow rate 2 ml/min) for 5 hours. Room temperature CO adsorption was performed after reduction at pressures of 2 to 8 bar using pure carbon monoxide. Fischer-Tropsch synthesis was conducted in a 2:1 CO:H_2 mixture (flow rate 2 ml/min) at 8 bar pressure, and a temperature of 250°C. Catalysts were left on-line for 5 hours, but analysed every 30 minutes. Samples were purged for 30 minutes with nitrogen gas after completion of each experiment to remove gas-phase reagents.

5.3. Results and Discussion

5.3.1. Effect of reduction temperature on CO adsorption

CO adsorption studies were employed to investigate the oxidation state of iron under Fischer-Tropsch conditions. It is widely accepted that the adsorption of carbon monoxide on metallic iron occurs below 2020 cm^{-1}, and that peak maxima at higher wavenumbers correspond to CO adsorbed on ionic states of iron [130]. For the calcined, unsulfided precipitated-iron catalyst (reduced at 400°C) used in this study, a peak at 2013 cm^{-1} was assigned to linear carbonyl species adsorbed on Fe(0) at 8 bar pressure. This correlates with the position of the C=O stretching vibration of species adsorbed on the zerovalent iron species of the type $Fe(CO)_5$, at 2014 cm^{-1} [123].

The effect of reduction temperature on CO adsorption was investigated in detail using the catalyst sulfided with 20000 ppm polysulfide[1] at pH 6.9. As shown in Figure 5.2, the peak at 2013 cm^{-1} is much smaller in the catalyst reduced at 300°C compared to the peak obtained after reduction at 400°C. This confirms that the amount of linear carbonyl species generated is related to the degree of reduction, as manifested by the amount of metallic iron on the surface.

[1] It will be shown in Chapter 9 that the source of sulfide has negligible effect on the catalytic properties of sulfided precipitated iron catalysts. Hence, the use of a polysulfided catalyst in this instance can be taken to be representative of all the catalysts used in this study.

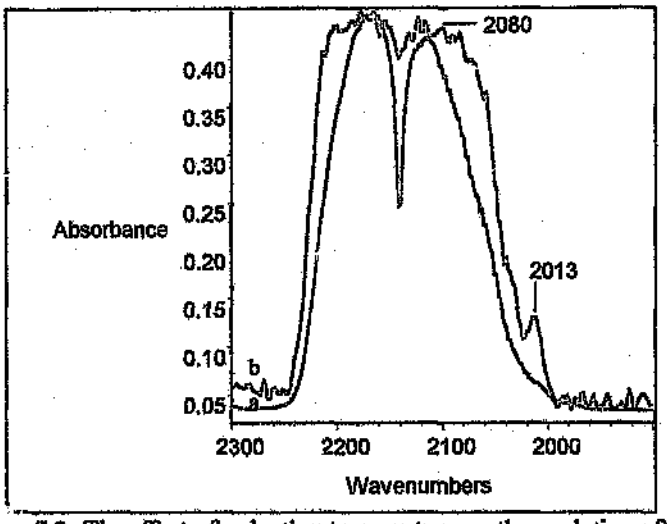


Figure 5.2: The effect of reduction temperature on the evolution of linear carbonyl species on 20000 ppm polysulfided iron catalysts a) reduced at 300°C b) reduced at 400°C

5.3.2. Influence of sulfide content on CO adsorption

In order to establish the effect of sulfidation level on CO adsorption, infrared spectra of catalysts sulfided in the range 500-20000 ppm S were recorded. The variation in the relative intensity of the peak assigned to linear carbonyl species is plotted versus sulfide content (Figure 5.3).

Superimposed on this graph is a plot showing the effect of increasing sulfidation on the temperature of the $Fe_2O_3 \rightarrow Fe_3O_4$ transition, as determined from Temperature Programmed Reduction (TPR) experiments (presented in Chapter 8).

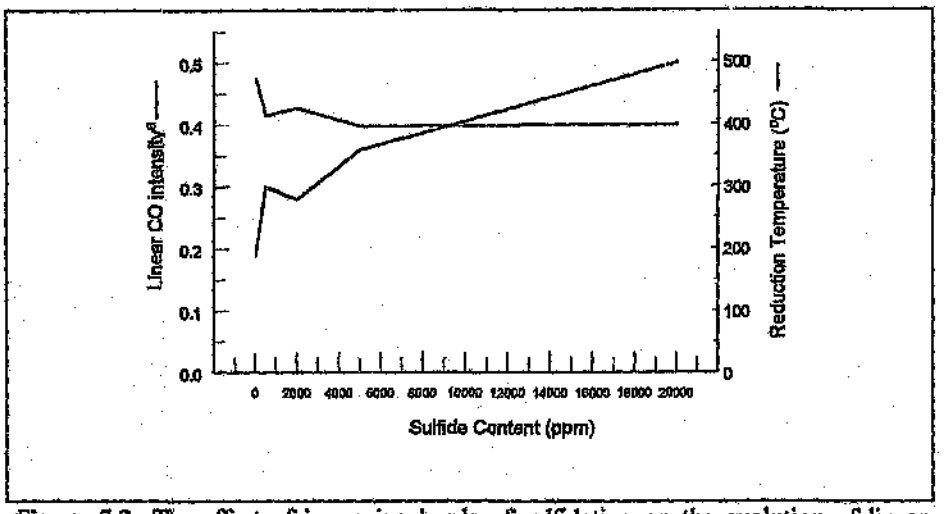


Figure 5.3: The effect of increasing levels of sulfidation on the evolution of linear carbonyl species on the surface of iron catalysts, showing correlation with extent of reduction. Catalysts were sulfided at pH 6.9 using Na_2S.

The increasing linear M-CO content with greater levels of sulfidation is clearly evident from Figure 5.3. This effect can readily be explained by the ability of sulfide to increase the amount of metallic iron after reduction at 400°C (see Chapter 8).

In the FT reaction, CO dissociates on iron to yield iron-carbide species which are believed to be active sites for chain growth [131]. In the carbide-forming reaction, a bond between carbon and Fe is formed and a concomitant weakening of the CO bond takes place. Hence, the stronger the Fe-C bond, the more rapidly carbiding occurs.

XRD analysis (Chapter 3) of the spent *highly sulfided* catalysts has shown that no carbide formation took place, although these catalysts had been reduced to Fe(0) prior to commencing FT synthesis. XPS studies (Chapter 4) revealed that these surfaces also contained sulfide species. Thus, the lack of carbide formation may be rationalised by a weak Fe-C bond caused by the presence of electron-withdrawing sulfide species [132] which retarded CO dissociation.

As shown in Figure 5.3, low level sulfided catalysts, particularly those sulfided with 500 ppm sulfur, also show enhanced intensity linear CO adsorption (compared to the unsulfided catalyst) which correlates with the lower reduction temperature calculated from TPR experiments. Only sulfate species were detected by XPS on the surface of these reduced low-level sulfided catalysts. Furthermore, carbide formation proceeded rapidly on these catalysts (as shown by XRD data) and they were highly active for Fischer-Tropsch synthesis. This suggests that the identity of the sulfide-containing species in the reduced catalyst may be important in determining whether or not carbide formation occurs under reaction conditions.

Although the addition of sulfide was found to enhance the surface areas of iron catalysts, the increase in adsorbed carbonyls cannot be ascribed to a surface area effect (as shown in Figure 5.4). The variation in surface area does not follow the same trend as the relative intensity of linear carbonyl species.

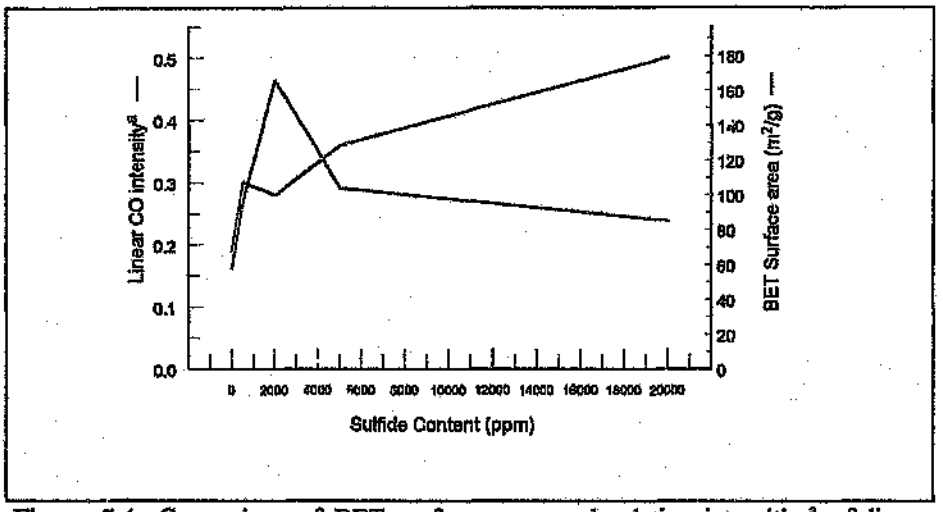


Figure 5.4: Comparison of BET surface areas and relative intensities[a] of linear carbonyl species adsorbed on iron catalysts as a function of sulfide content

[a] The intensity of the linear carbonyl peak is taken relative to that of the most intense gas phase peak at 2113 cm^{-1}

It is therefore apparent that the enhanced (non-dissociative) adsorption of CO on highly sulfided catalysts is a consequence of a larger metallic surface area effected by improved reduction, rather than due to an increase in the total (BET) surface area.

After exposing a catalyst sulfided with 20000 ppm sulfur to carbon monoxide at 8 bar pressure the system was purged. This not only removed all evidence of gas-phase CO, but also reduced the amount of linear carbonyl species (Figure 5.5). This suggests that linear Fe-CO species are not strongly bound to the surface of highly sulfided catalysts.

In contrast, the intensity of linear carbonyl species adsorbed on catalysts sulfided in the 500-2000 ppm S range, remains little changed after purging, confirming a stronger Fe-C interaction.

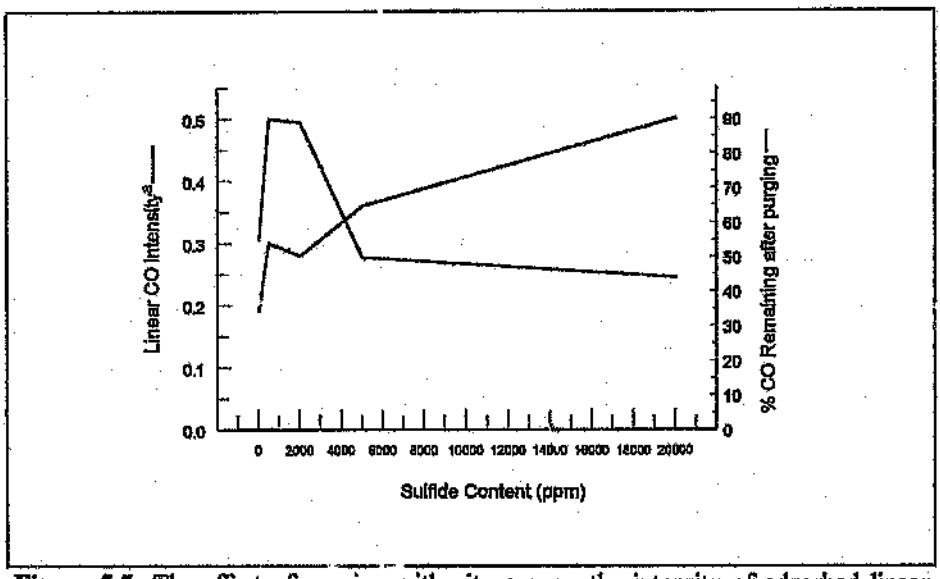


Figure 5.5: The effect of purging with nitrogen on the intensity of adsorbed linear carbonyl species as a function of sulfide content

5.3.3. Effect of sulfidation pH on CO adsorption

An effect of the pH of sulfidation on CO adsorption was also observed. Catalysts sulfided with 2000 ppm S midway through the precipitation process (pH 8.5) exhibited a greater relative concentration of linear carbonyl species (Table 5.1) than those sulfided at pH 10.75 or 6.9. This may also be attributed to the degree of reduction, since catalysts sulfided at pH 8.5 possessed a reduction peak that was at least 10°C lower in temperature than the other catalysts containing the same amount of sulfide, but added at pH 10.75 or 6.9 (Chapter 10).

Table 5.1: Effect of pH of sulfidation on the position of the linear carbonyl peak[a]

Catalyst	$\Delta\nu^b$ (cm^{-1})	Relative Intensity[b] of ν_{CO}[c]
500 ppm Na_2S pH 10.75	-0.1	0.26
pH 8.5	+1.7	0.30
pH 6.9	+0.2	0.28
2000 ppm Na_2S pH 10.75	+0.8	0.32
pH 8.5	+2.1	0.40
pH 6.9	-1.8	0.28

[a] relative to the position of linear carbonyl species adsorbed on an unsulfided catalyst (ν_{CO} = 2013 cm^{-1})
[b] the intensity of the linear carbonyl peak relative to the ν = 2116 cm^{-1} peak of gaseous CO
[c] for reference purposes, the relative intensity of ν_{CO} = 0.19 for the unsulfided catalyst

Also evident from Table 5.1 is the shift of ν_{CO} to higher wavenumbers for CO adsorbed on catalysts sulfided at pH 8.5. This implies reduced metal-carbon interaction analogous in nature to that observed on highly sulfided catalysts.

5.3.4. Effect of sulfide source on CO adsorption

The identity of the sulfiding agent may also be expected to affect the interaction between iron and adsorbed CO. The effect of mono- versus polysulfide addition, as well as the influence of the counter-ion (sodium or ammonium), on the position of linear carbonyl vibrations is presented in Table 5.2.

Table 5.2: Effect of sulfide source on the position of the linear carbonyl peak[a]

Catalyst	$\Delta\nu$ (cm^{-1})
2000 ppm pH 10.75 Na_2S	+0.8
2000 ppm pH 10.75 $(NH_4)_2S$	-1.9
2000 ppm pH 10.75 $(NH_4)_2S_5$	-1.8

[a] relative to the position of linear carbonyl species adsorbed on an unsulfided catalyst (ν_{CO} = 2013 cm^{-1})

Interestingly, Table 5.2 reveals an influence on the Fe-CO interaction for the Na_2S sulfided catalyst. However, the position of the peak maximum is observed to be shifted marginally to higher wavenumbers for this sodium sulfided catalyst, confirming the lack of alkali promotion. Indeed, it is known that the electron-donating property of alkali promoters facilitates the dissociation of carbon monoxide on catalytic surfaces [125]. For instance, it was noted by Kazansky *et al* [130] that the frequencies of CO adsorption on potassium doped iron/alumina catalysts were shifted by 10-20 cm^{-1} to lower wavenumbers relative to unpromoted catalysts. The authors report that alkali promotion results in an increase in the fraction of iron in the metallic state, brought about by a possible decrease in the amount of surface hydroxyls which would retard the reduction of Fe^{3+}.

Having established that there is essentially no effect of the counter-ion on CO adsorption, it is interesting to note that the identity of the sulfide ion itself is also not important. Catalysts sulfided with either mono- or polysulfide sources exhibit almost identical shifts in linear carbonyl peak maxima (Table 5.2).

Furthermore, it will be shown (Chapter 9) that the identity of the sulfide ion has no effect on the catalytic properties of sulfided catalysts.

5.3.5. CO adsorption on a sulfide-impregnated catalyst

A catalyst prepared by sulfide impregnation of a dried precipitate was also investigated using CO adsorption. As shown in Figure 5.6, a linear carbonyl peak for this catalyst appeared at 2013 cm^{-1}, and was considerably more intense than the corresponding peak or the unsulfided catalyst (not shown).

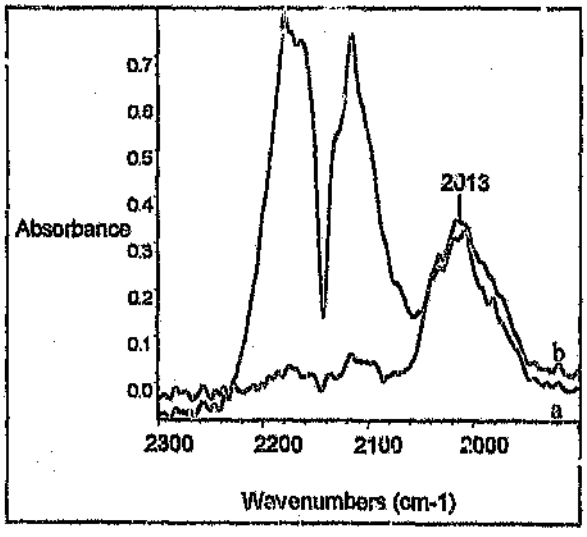


Figure 5.6: CO adsorption on a 1000 ppm S catalyst prepared by incipient wetness **a)** adsorption at 8 bar pressure **b)** nitrogen purge spectrum

Removal of gas phase CO under nitrogen had negligible effect on the intensity of the CO stretching vibration, again suggestive of a strong iron-carbon interaction. It must be borne in mind however, that the addition of 1000 ppm S^{2-} by incipient wetness from a sodium-derived source, is accompanied by the presence of twice as many sodium ions. These would remain on the catalyst surface and may exert a promotional effect on CO adsorption. However, the peak position (ν_{CO} = 2013 cm^{-1}) appeared to be unaffected by the presence of sodium or sulfide, since no shifts relative to the position of the linear carbonyl vibration on the unsulfided catalyst were observed.

5.3.6. Pretreatment studies of sulfided iron catalysts

The infrared spectrum of the unsulfided catalyst prior to calcination (Figure 5.7a) reveals the presence of surface carbonates (ν_{CO_3}= 1489.5 cm^{-1}) and nitrates (ν_{NO_3}= 1354 cm^{-1}) [133]. Adsorbed water can be identified through stretching vibrations at ν_{OH} = 3448 cm^{-1} and bending vibrations at δ_{HOH} = 1654 cm^{-1} [134].

Calcination of this catalyst at 400°C (Figure 5.7b) sees the removal of adsorbed water and the emergence of a peak at 3640 cm^{-1} which may be assigned to OH vibrations of free hydroxyl groups on hematite [135]. The 1540 cm^{-1} band which emerges when heating α-Fe_2O_3 to 400°C in oxygen is presumed to be a multi-phonon or combination band involving lower frequency lattice fundamentals [134].

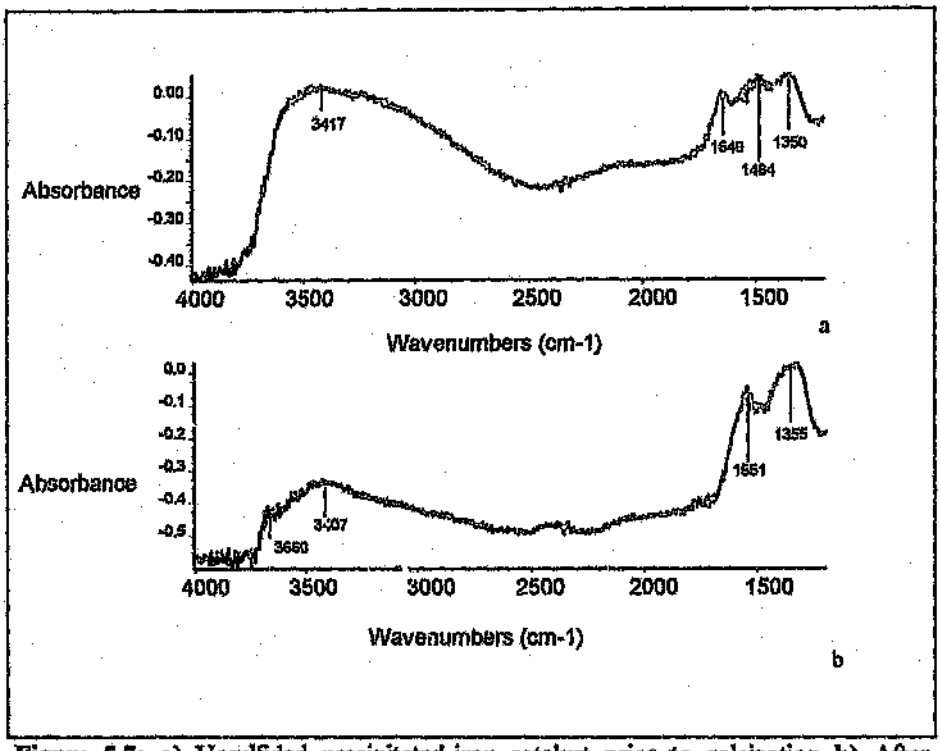


Figure 5.7: a) Unsulfided precipitated-iron catalyst prior to calcination **b)** After calcination at 400°C

The infrared spectra of sulfide [1] catalysts were also recorded, the example shown in Figure 5.8 being the catalyst sulfided with 2000 ppm Na_2S at pH 10.75. Nitrate and carbonate peaks were also exhibited on the surface of these catalysts, before and after calcination.

Moreover, combination bands are evident, although somewhat obscured by the nitrate peak. In addition to these vibrations however, is a sharp peak that emerges after calcination at 1292 cm^{-1}, and which has been assigned to a surface sulfate. Experimental data exists to show that ν(S=O) and ν(S-O) vibrations occur in the 1400-1100 cm^{-1} region [136].

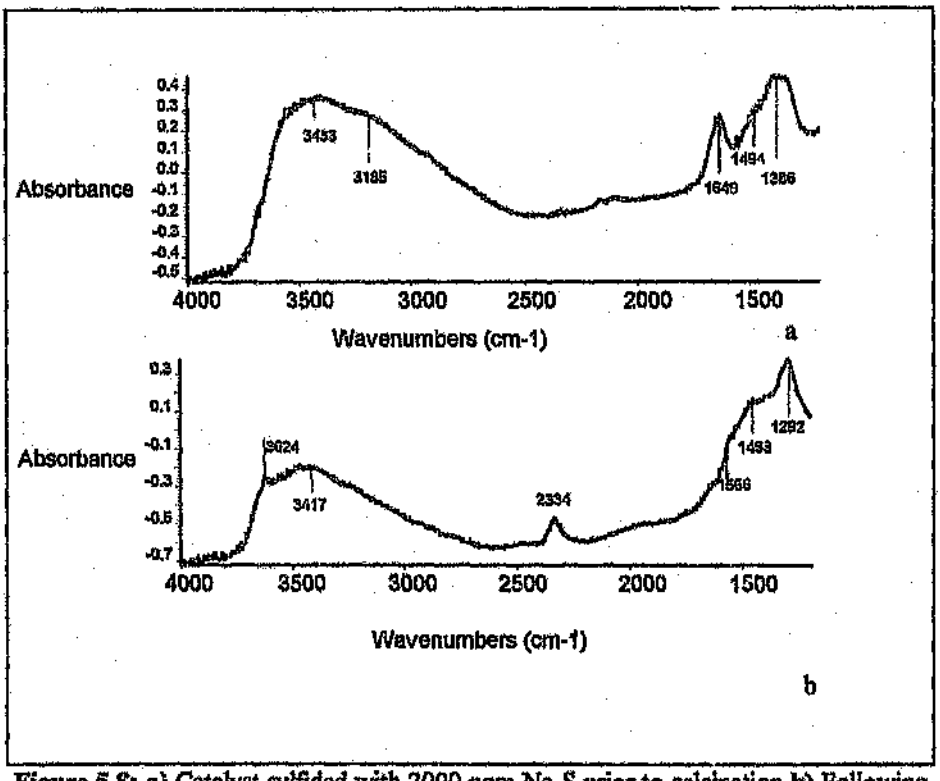


Figure 5.8: a) Catalyst sulfided with 2000 ppm Na_2S prior to calcination **b)** Following calcination at 400°C

This sharp peak near 1300 cm^{-1} was observed on numerous sulfided catalysts after they had been calcined at 400°C. Another example of a catalyst showing this peak is to be seen in Figure 5.9, which shows a catalyst sulfided with 2000 ppm $(NH_4)_2S$ at pH 10.75.

Similar peaks were observed on highly sulfided catalysts after calcination at 400°C. The uncalcined catalyst sulfided with 20000 ppm Na_2S exhibits a peak at 1226 cm^{-1} (Figure 5.11a). This falls within the 1235-1100 cm^{-1} region that characterises the $\nu_{s=o}$ vibration of metal sulfates [136]. Following thermal activation of this catalyst in air at 400°C, this peak shifts to 1287 cm^{-1} (Figure 5.11b). Once again, this may be attributed to the effect of the dehydroxylation of hematite on the $\nu_{s=o}$ vibration (as previously mentioned). According to data avaliable from the literature, the assignments of sulfate vibrations on hematite are summarized in Table 5.3.

Table 5.3: Peak Assignments of stretching vibrations of sulfate groups [138, 139]

Dehydrated Iron Oxide		Hydrated Iron Oxide	
Peak (cm^{-1})	Assignment	Peak (cm^{-1})	Assignment
1340	ν_{as}(S=O)	1271	ν_{as}(S=O)
1140	ν_s(S=O)	1090	ν_s(S=O)
1015	ν_{as}(S-O)	1015	ν_{as}(S-O)
915	ν_s(S-O)	915	ν_s(S-O)

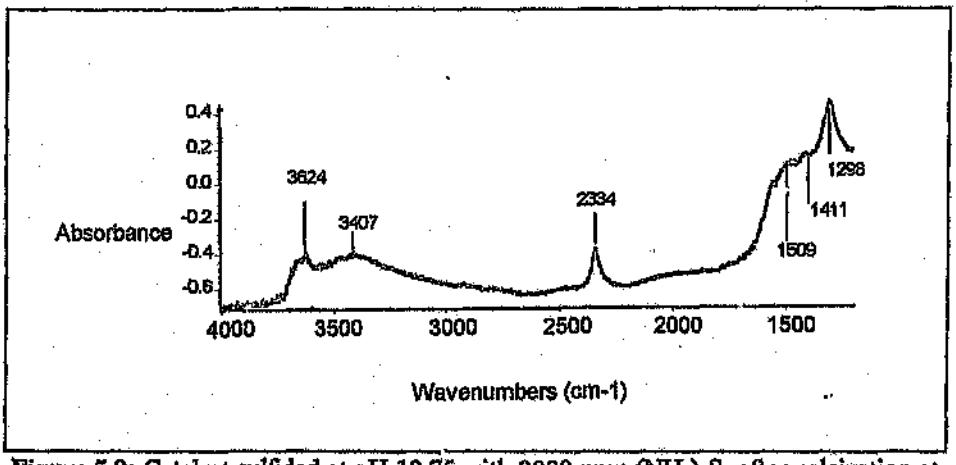


Figure 5.9: Catalyst sulfided at pH 10.75 with 2000 ppm $(NH_4)_2S$, after calcination at 400°C, showing a sharp peak near 1300 cm^{-1}

Similar oxidation reactior ... sulfide over metal supports have been reported in the literature. For example, the oxidation of H_2S in excess O_2 over Al_2O_3 or TiO_2 under anhydrous conditions yields an infrared spectrum which is characterised by an intense sharp band near 1380 cm^{-1} and a broad doublet near 1040 cm^{-1} [137]. As shown in Figure 5.10 below, the asymmetric S=O stretching vibration in the presence of $H_2{}^{18}O$ resembles the sharp peak observed near 1292 cm^{-1} on calcined sulfided catalysts.

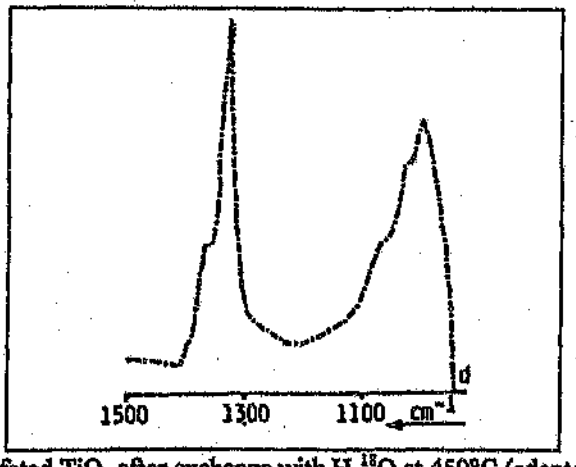
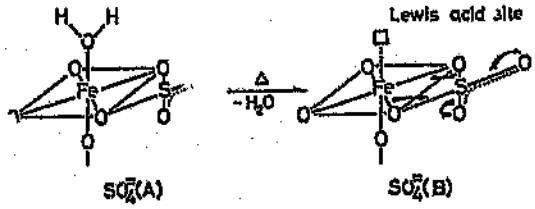


Figure 5.10: Sulfated TiO_2 after exchange with $H_2{}^{18}O$ at 450°C (adapted from [137])

According to Nakamoto [136], the spectrum in Figure 5.10 closely approximates that of a bidentate sulfate of the type proposed by Kayo *et al* [138], for a hydrated ammonium-sulfated $Fe(OH)_3$ sample. In this case, bands at 1271 [ν_{as}(S=O)], 1090 [ν_s(S=O)], 1015 [ν_{as}(S-O)] and 915 cm^{-1} [ν_s(S-O)] indicated a species of reduced C_{2v} symmetry [138]. Removal of water under vacuum at elevated temperatures resulted in a second set of adsorptions (1340, 1140, 1015 and 915 cm^{-1}) [139].

The effect of adsorbed water on the formation of sulfate on iron oxide is illustrated below [138].



The ν_{as}(S=O) peak at 1292 cm^{-1} for the catalysts sulfided with 2000 ppm Na_2S (Figure 5.8b) is slightly higher in wavenumber than the 1271 cm^{-1} (Table 5.3) reported for a fully hydrated sulfated $Fe(OH)_3$ sample discussed by Kayo *et al* [138]. However, whereas their measurements were conducted at room temperature, the spectra of calcined catalysts were recorded at 400°C and hence a shift towards higher wavenumbers is expected. A broad band in the region of 3440 cm^{-1} (Figure 5.8b) signified the presence of residual bulk or surface OH-groups at 400°C. These have been known to persist during thermal activation of Fe_2O_3 under oxygen [135]. Nevertheless, the presence of surface hydroxyls would preclude the evolution of the second set of adsorption peaks observed by other workers upon evacuation at high temperatures [139].

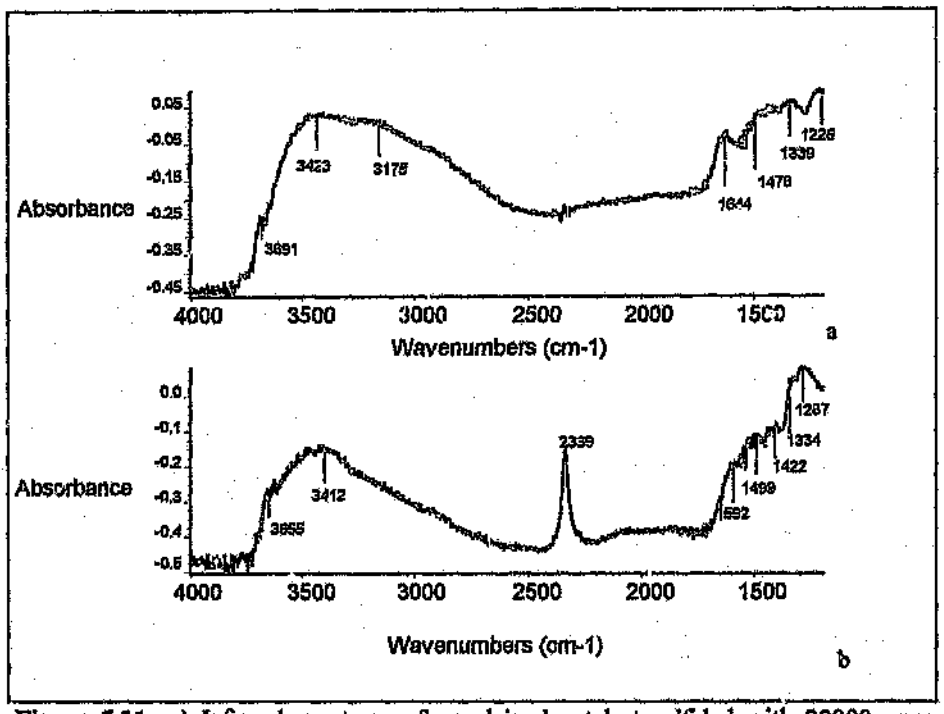


Figure 5.11: a) Infrared spectrum of uncalcined catalyst sulfided with 20000 ppm Na_2S **b)** Same catalyst after calcination in air at 400°C

As noted by Kayo *et al* [138], in the absence of water, shifts to higher wavenumbers suggest a stronger S=O bond. Hence, the removal of structural and physisorbed water promotes the formation of sulfate during calcination pretreatment. Furthermore, surface hydroxyls have been shown to retard the reduction of Fe^{3+} [130] and the thermodynamics of sulfate formation may serve to reduce the surface OH^- concentration and hence promote the reduction of iron-oxide. The temperature of calcination is also apparently important, since no sulfate peaks were discernable on the surface of catalysts calcined at 200°C (Figure 5.12).

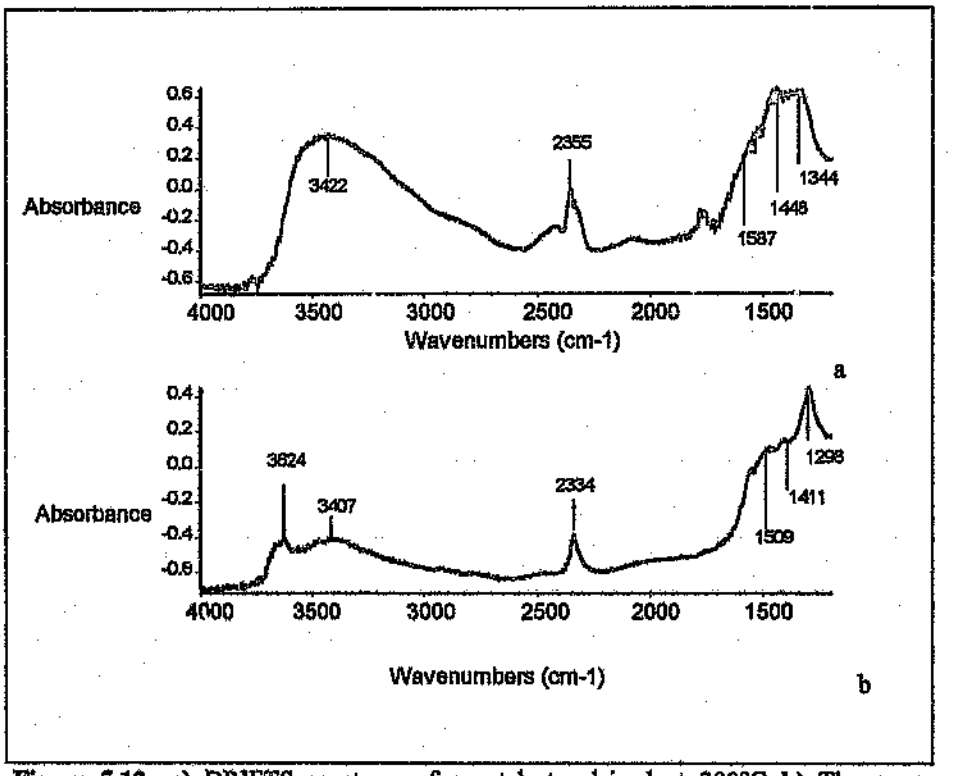


Figure 5.12: a) DRIFTS spectrum of a catalyst calcined at 200°C **b)** The same catalyst calcined at 400°C

Owing to the poor resolution of carbonate and nitrate stretching vibrations in the 1500-1300 cm^{-1} region, the existence of sulfate species could not be unequivocally confirmed prior to reduction. However, sulfate peaks were observed on calcined low-level sulfided catalysts even after reduction in H_2 at 400°C. For example, the expanded view of the 1700-1200 cm^{-1} region of a reduced catalyst sulfided with 500 ppm S at pH 10.75, recorded after CO adsorption at room temperature is shown in Figure 5.13. Two broad peaks are discernable, one typical of water at 1620 cm^{-1}, and the other at 1251 cm^{-1} which corresponds to the asymmetric stretching vibration of S=O.

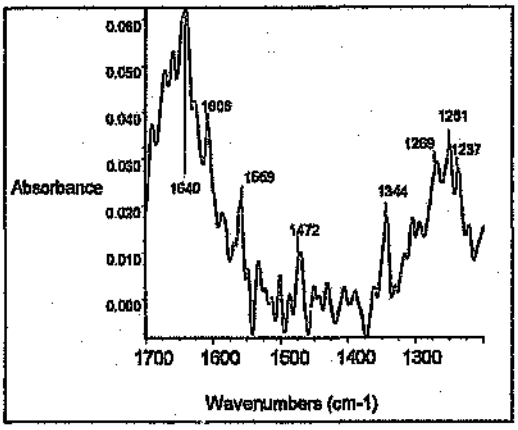


Figure 5.13: Expanded view of 1700-1200 cm^{-1} region of the DRIFTS spectrum of a catalyst sulfided with 500 ppm Na_2S recorded after CO adsorption

The origin of the water may be due to the condensation of vapour on the ZnS window at ambient temperature. At any rate, the adsorption of water induces a red shift in the asymmetric stretching frequency of S=O [140]. This frequency shift corresponds to a decrease in the bond order of the SO covalent double bond.

Indeed, the shift has been reported to be quite considerable. For example, the adsorption of water induces a red shift of $\Delta\nu = 65$ cm^{-1} of the 1380 cm^{-1} peak for SO_4^{2-} promoted $Fe/Cr/ZrO_2$ superacid catalysts [140]. In the case of the catalyst shown in Figure 5.11a, the shift is 57 cm^{-1} relative to the position of the sulfate peak observed after calcination (Figure 5.11b).

Therefore, to conclude, the presence of a band at 1251 cm^{-1} in Figure 5.13 serves to show that segregation of sulfide species does occur under conditions of calcination and reduction, and that oxidation to sulfate proceeds rapidly in the presence of oxygen. With regard to the latter reaction, it is worth stressing that complete reduction of iron oxide to metallic iron is undesirable in the presence of sulfide, since this would preclude the formation of sulfate. Residual oxygen which is present on the surface of partially reduced catalysts converts sulfide, which segregates during reduction, to sulfate species.

5.3.7. *In situ* Fischer-Tropsch study

The synthesis of hydrocarbons is initiated by the dissociative chemisorption of CO and H_2 which releases carbon and hydrogen adatoms. It is generally proposed that methyl groups result from the stepwise hydrogenation of surface carbon atoms, and act as precursors to the formation of methane and C_{2+} olefins and paraffins. The growth of hydrocarbon chains is initiated by the addition of a methylene group. Olefins and paraffins are formed by either β-hydrogen elimination from, or α-hydrogen addition to, the adsorbed alkyl intermediates [141].

Information gleaned from CO adsorption studies should thus provide valuable insight into the mechanism of the Fischer-Tropsch process at the surface of iron catalysts.

Fischer-Tropsch synthesis was conducted on both sulfided and unsulfided catalysts, and monitored *in situ* over a period of 5 hours using DRIFTS. A typical spectrum (3100-2800 cm^{-1}) observed for FT synthesis on an unsulfided catalyst is shown in Figure 5.14a. Superimposed on this spectrum, is the DRIFTS spectrum of a highly active catalyst sulfided with 2000 ppm Na_2S at pH 10.75 (Figure 5.14b

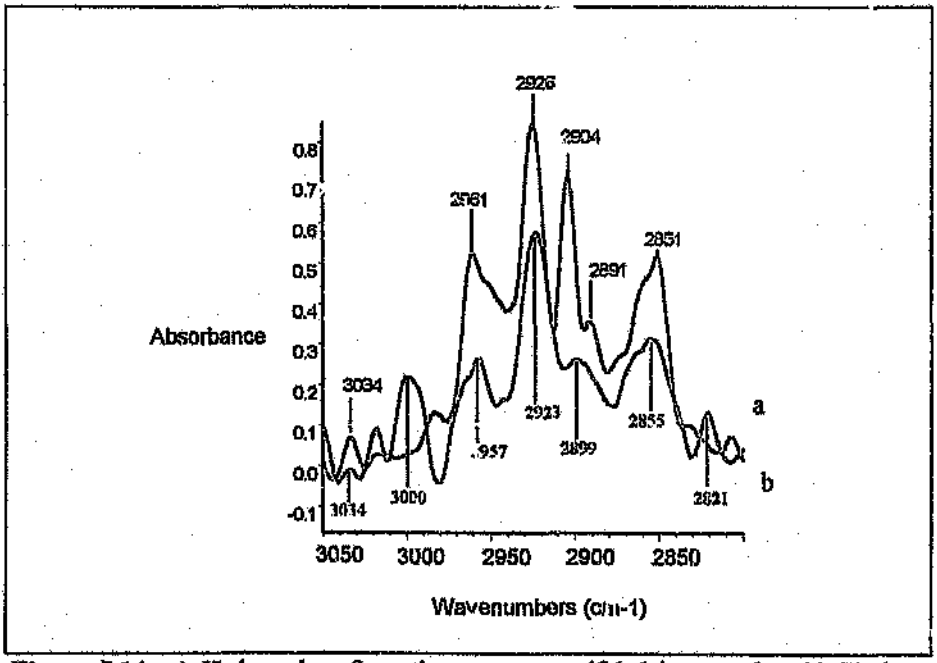
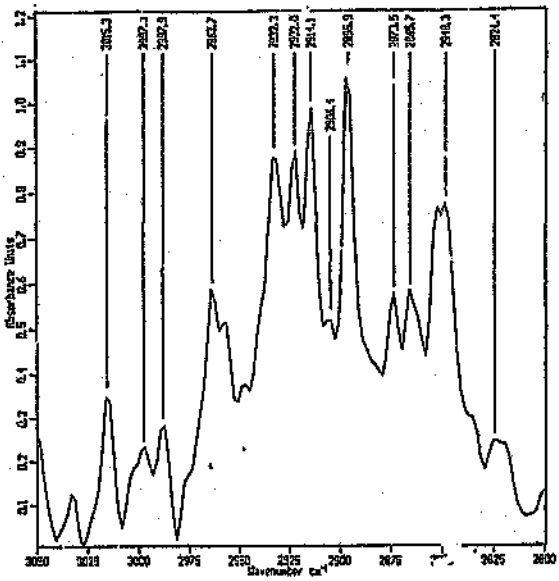


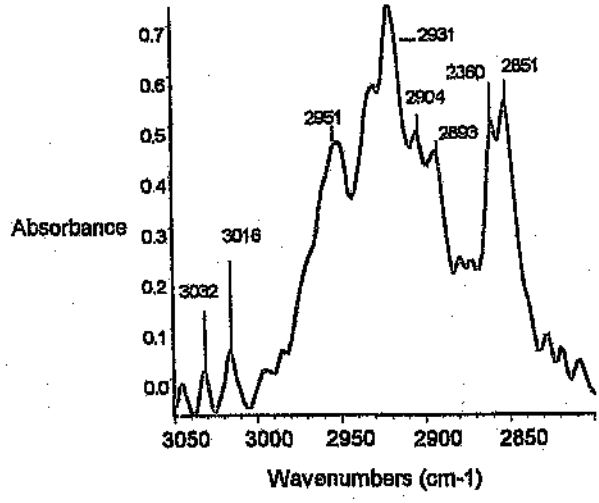
Figure 5.14: a) Hydrocarbon formation on an unsulfided iron catalyst **b)** Fischer-Tropsch synthesis on a catalyst sulfided with 2000 ppm Na_2S at pH 10.75

The evolution of peaks at 2926 and 2851 cm^{-1} herald the formation of hydrocarbon species. These correspond to CH_2 asymmetric and symmetric stretching vibrations, respectively. Following the assignment of McQuire and Rochester [142], the pair of bands at 2926 and 2851 are ascribed to CH_2 segments of alkyl chains unperturbed by the catalyst surface. The bands at 2930 and 2862 (sh) are assigned to those CH_2 fragments in direct contact with the iron surface. In addition, bending vibrations characteristic of methylene and methyl groups occur at $\delta = 1465$ cm^{-1} and $\delta = 1378$ cm^{-1} respectively. The band at 2961 cm^{-1} is characteristic of the asymmetric methyl stretching vibration ($\nu_{as}CH_3$) [142].

A comparison of hydrocarbon synthesis after 90 minutes for the unsulfided catalyst (Figure 5.14a) and the catalyst sulfided with 2000 ppm Na_2S at pH 10.75 (Figure 5.14b) reveals several significant differences. Immediately apparent is the enhanced activity of the low-level sulfided catalyst, evident from the intensity of the peak maximum at $\nu_{CH_2} = 2926$ cm^{-1} compared to that at 2961 cm^{-1}. The latter vibration is intrinsically more intense [143], and therefore the observed reversed intensity relation indicates an abundance of CH_2 groups.

Indeed, enhanced FT activity was observed for all catalysts sulfided with 500-2000 ppm S at either pH 10.75 or 6.9. Additional examples of DRIFTS spectra of highly active sulfided catalysts are shown in Figure 5.15.





b

Figure 5.15: a) FT synthesis on a catalyst sulfided with 500 ppm Na_2S at pH 10.75

b) A catalyst sulfided at pH 6.9 with 500 ppm Na_2S

The promotional effect of sulfide may be rationalised in terms of the CO species adsorbed during hydrocarbon synthesis. Linear carbonyl stretching vibrations on the unsulfided catalyst appeared at 2013 cm^{-1}. The low-level sulfided catalysts also exhibited linear carbonyl peaks at ν = 2012 cm^{-1}, showing enhanced interaction between Fe and C and this may account for the carbiding that was observed by XRD, as well as the high activity (Chapter 8). During FT synthesis, the intensity of the linear carbonyl peak at $\nu = 2013$ cm^{-1} decreased, but a peak at $\nu = 2080$ cm^{-1} remained. For all catalysts, the band at 2080 cm^{-1} may be assigned to CO adsorbed on Fe^{2+} [144], and confirms the presence of magnetite during Fischer-Tropsch synthesis.

The linear carbonyl peak for the highly sulfided catalyst (20 000 ppm S) appears at $\nu = 2018$ cm^{-1} indicating a weak interaction between the iron and carbon atoms. This implies retarded CO dissociation and hence no carbide formation since the dissociation of CO is a prerequisite for Fe_xC formation [145]. The shift in the $\nu = 2013$ cm^{-1} peak to higher wavenumbers for catalysts sulfided at pH 8.5 may be also attributed to higher levels of surface sulfide. This will be discussed in more detail in Chapter 7, which deals specifically with the effect of pH of sulfidation on catalytic activity.

During FT synthesis, all catalysts also produced varying quantities of CO_2 (2213-2393 cm^{-1}). Although a quantitative estimate of CO_2 yield was not possible, it did appear that highly active catalysts produced relatively less carbon dioxide than the unsulfided catalyst. Certainly, catalysts sulfided with 20000 ppm S produced CO_2 almost exclusively, presumably via the water-gas-shift reaction.

There are also notable differences in the types of hydrocarbon species present on the surface of each of the catalysts studied. For the unsulfided catalyst, a minor peak at 3033.9 cm^{-1} (Figure 5.14a) is characteristic of olefinic C-H stretching vibrations [146, 147]. The intensity of this peak which appears at 3032.5 cm^{-1}, is considerably enhanced in the sulfided catalysts shown in Figure 5.14b. Similar trends are evident in Figure 5.15a and 5.15b. This correlates with the high olefin selectivity observed for low-level sulfided catalysts during the reactor studies (Chapter 8).

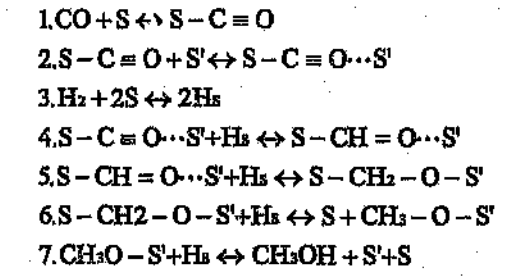
Further, an intense vibration at $\nu = 2904$ cm^{-1} is observed to occur on the surface of the sulfided catalyst (Figure 5.14b). This peak, in conjunction with the one at $\nu = 2983$ cm^{-1} has been previously assigned to the stretching vibrations typical of ethoxy groups (OEt) [142]. Indeed, all sulfided catalysts exhibited such peaks (Figures 5.14b, 5.15a, 5.15b, 5.16) and also showed a propensity toward oxygenated product formation. Moreover, alkoxy groups have been shown to function as reactive intermediates for Fischer-Tropsch synthesis on iron catalysts [148]. No evidence of oxygenate intermediates could be detected on the surface of the unsulfided catalyst, suggesting that the presence of sulfide may serve to enhance the concentration of reactive intermediates.

The phenomenon of sulfide-induced surface reconstruction has been dealt with by Somorjai [38]. It is noted that impurities such as S always occupy defect sites, irrespective of whether they are introduced onto the surface by adsorption or as a result of segregation from the bulk. The surface reconstruction that follows can lead to the appearance of new active adsorption sites or to the elimination of other sites.

In a similar vein, Jackson *et al* alluded to the reconstruction of the surface of Rh/SiO_2 catalysts as a consequence of the presence of sulfur [149], which led to a greater number of suitable sites for the adsorption of intermediates. This proposal was made in order to account for the enhanced rate of CO hydrogenation obtained with catalysts containing 10% of a monolayer of COS. Thus, in the present study, the presence of sulfide may facilitate reconstruction of the catalytic surface in such a way as to increase the number of adsorption sites for ethoxy intermediates.

The intensity of the ethoxy peak at 2983 cm^{-1} compared to the CH_2 peak at 2926 cm^{-1} is increased at high sulfide content (20000 ppm) and this is in agreement with the reactor studies which showed increasing alcohol selectivity at high levels of sulfidation. A somewhat crude estimate of the OEt:CH_2 peak intensities for this catalyst was made, and yielded a value of 1.11 (owing to the low level of FT synthesis that took place on the highly sulfided catalyst during *in situ* DRIFTS studies, the spectrum is extremely noisy and is therefore not shown). For the active catalyst sulfided with 2000 ppm S, this ratio was found to be 0.08. From a mechanistic standpoint, the presence of ethoxy groups correlates with reduced CO dissociation, as observed from the CO adsorption experiments. According to Kishi *et al* [132], the electron-withdrawing effect of sulfide on CO adsorption serves to increase methanol production.

A mechanism for the formation of methanol from syngas has been proposed by Kellner *et al* [141], where CO hydrogenation proceeds without rupture of the C-O bond. As illustrated in the scheme below, the initial stage requires the rearrangement of linearly adsorbed CO to a μ-bridge-adsorbed structure. Hydrogenation of this intermediate is postulated to occur at the carbon end of the C-O bond, and gives rise to methoxy species at the surface of the catalyst. Methanol is then formed by the process of reductive elimination which is facilitated by hydrogen adatoms. This scheme may equally apply to ethanol synthesis.



(S= metal substrate)

An alternative mechanism involves CO insertion into surface methyl groups [150]. Alkoxy intermediates have been proposed to yield not only oxygenates, but also CH_4, C_2H_4 and C_2H_6 [148]. Indeed, highly sulfided catalysts produced more methane, light hydrocarbons and alcohols than catalysts sulfided with 500-2000 ppm S.

The polymerisation capacity of sulfided catalysts was also investigated by comparing peaks at $\delta_s CH_3$ =1378 cm^{-1} with δCH_2 =1465 cm^{-1} (Figure 5.16).

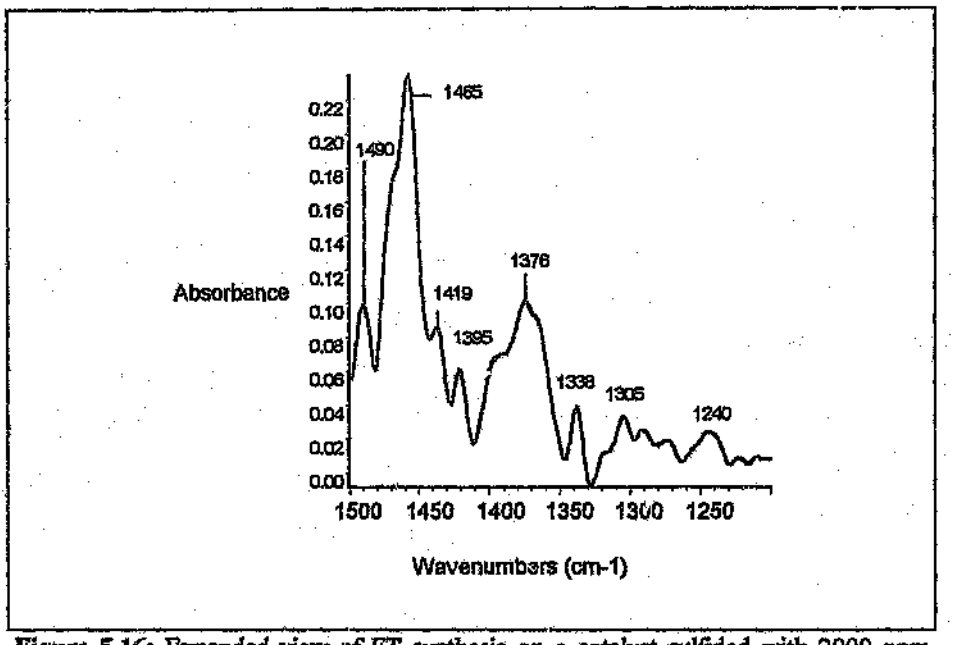


Figure 5.16: Expanded view of FT synthesis on a catalyst sulfided with 2000 ppm Na_2S, showing 1800-1200 cm^{-1} region

It is instructive to note that the symmetric CH_3 bending vibration (at 1378 cm^{-1}) is intrinsically stronger than the scissoring vibration of CH_2 groups at 1465 cm^{-1} [143]. Hence, if the intensity of the latter is greater, the presence of long hydrocarbon chains is inferred. The CH_2:CH_3 intensity ratios for selected catalysts are compared in Table 5.4.

Table 5.4: Catenation ability[2] of sulfided catalysts during *in situ* Fischer-Tropsch synthesis

Catalyst	Intensity of δCH_2 1465 cm^{-1}	Intensity of $\delta_s CH_3$ 1378 cm^{-1}	CH_2:CH_3 Ratio[a]	α- value
unsulfided	0.11	0.04	1.8	0.80
500 ppm Na_2S pH 10.75	0.27	0.09	3.0	0.81
500 ppm Na_2S pH 8.5	0.17	0.07	2.4	0.69
500 ppm Na_2S pH 6.9	0.32	0.11	3.0	0.78
2000 ppm Na_2S pH10.75	0.23	0.10	2.3	0.78
2000 ppm Na_2S pH 8.5	0.14	0.08	1.8	0.65
20000 ppm Na_2S pH 6.9	0.0026	0.0021	1.2	0.53

[a] Measurements were made after 90 minutes exposure to synthesis gas

Evident from the above table is the increased chain length of products sulfided with 500-2000 ppm S at pH 10.75 or 6.9, relative to the unsulfided catalyst. Trends correlate with α-values determined from full reactor studies (Chapters 8-10). While this method of correlating band intensities to the probability of C-C bond formation may seem crude, it is not unprecedented. M°Quire and Rochester have previously compared the ratio of the 2931 and 2857 cm^{-1} bands to the 2960 cm^{-1} band and correlated the data with hydrocarbon chain-lengths produced using various $CO:H_2$ mixtures [142].

[2] The spectra of n-alkyl compounds exhibit a series of evenly spaced bands in the 1350-1180 cm^{-1} region, which may be assigned to the wagging of methylene groups in trans conformation [143]. The number of bands is characteristic of the chain length such that: $n\text{-}CH_2$ = (bands) x 2 for *n* even; = [(bands) x 2] - 1 for n odd

Although not used in the present study, this provides an alternative method for the determination of chain length. Unfortunately, owing to the poor signal to noise ratio in the 1400-1200 cm^{-1} region of a DRIFTS spectrum, this method is not as useful as the comparison of CH_2:CH_3 vibrations.

According to Table 5.4, for low-level sulfided catalysts, the increased intensity of CH_2 vibrations signify not only more effective chain propagation, but also higher reaction rates since methylene groups constitute reactive intermediates in the Fischer-Tropsch process [151].

The use of peak intensities to gauge the average chain length of hydrocarbon species formed over iron FT catalysts has been reported elsewhere [152]. A series of empirical formulae were derived by Jones [153] for the determination of hydrocarbon chain-lengths of *n*-paraffins in solution. According to these formulae, the intensity of the CH_3 vibration at 2970 cm^{-1} is ($8n + 258$), while that of the CH_2 peak at 2925 cm^{-1} is ($77n - 18$). While their accuracy in solid-state FTIR is questionable, these equations can certainly provide an assessment of the trends that are present. This approach was used by Galuszka *et al* [152] in the estimation of the relative chain lengths of oligomeric species adsorbed on supported iron catalysts. However, it has not been used in the present study since the peak intensities of the DRIFTS spectra were not of sufficient magnitude to be applicable to the Jones formulae.

The effect of sulfidation pH on the catenation ability of catalysts sulfided with 500 ppm S was investigated and the results are shown in Table 5.5. In analogous fashion to Fischer-Tropsch activity, the chain-lengthening capability of catalysts sulfided at pH 8.5 is inferior to that of catalysts sulfided at the start and end of precipitation.

Table 5.5: The effect of sulfidation pH on hydrocarbon chain length for catalysts sulfided with 500 ppm Na_2S after 90 minutes FT synthesis

pH of sulfidation	δCH_2=1464 cm^{-1}	δCH_3=1378 cm^{-1}	CH_2:CH_3 ratio	α-value
10.75	0.38	0.12	3.0	0.81
8.5	0.14	0.08	1.8	0.69
6.9	0.32	0.11	3.0	0.78

The effect of reduction temperature on FT activity was also investigated. DRIFTS spectra obtained using a catalyst sulfided at pH 10.75 with 500 ppm Na_2S are shown in Figure 5.17. In Figure 5.17a, reduction at 300°C yields a catalyst with low activity compared to the highly active catalyst obtained after reduction at 400°C (Figure 5.17b).

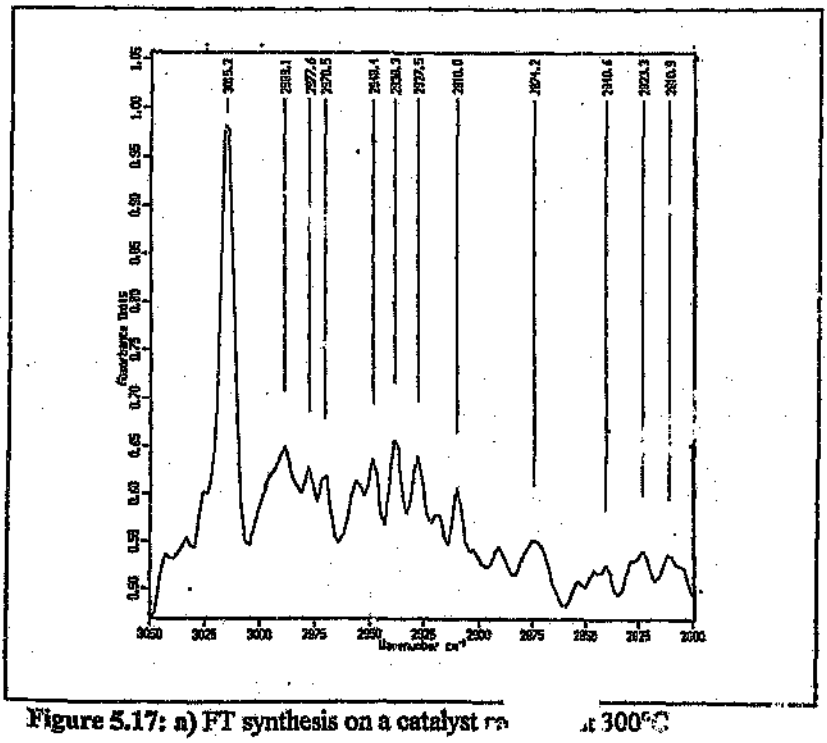


Figure 5.17: a) FT synthesis on a catalyst re[illegible] at 300°C

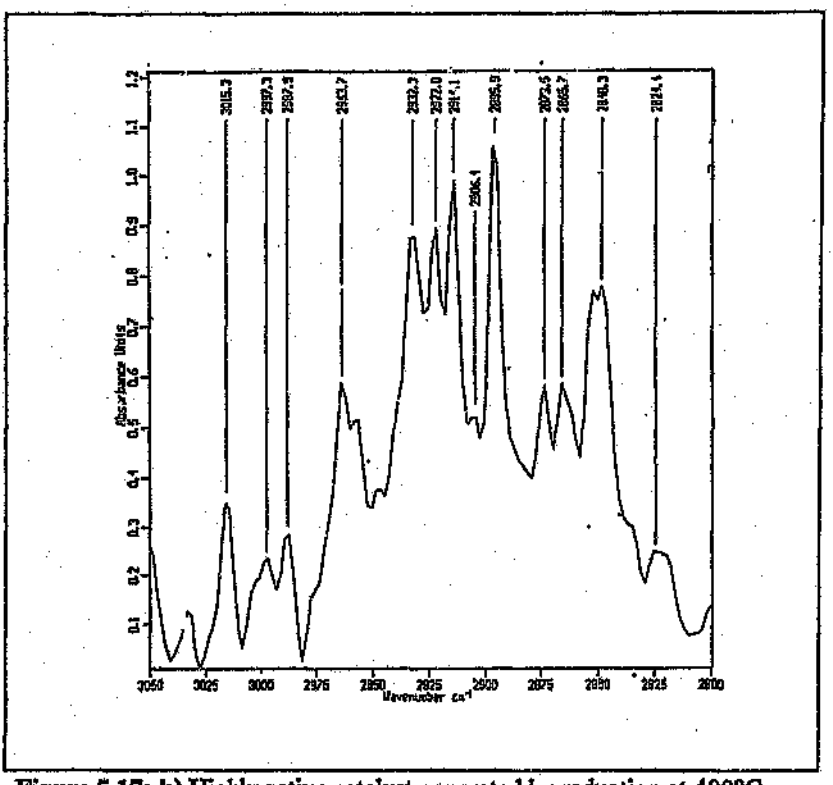


Figure 5.17: b) Highly active catalyst generated by reduction at 400°C

Notwithstanding the obvious lack of hydrocarbon synthesis on the catalyst reduced at 300°C, an intense peak at 3016 cm^{-1} is observed in Figure 5.17a which may be assigned to methane [142].

Methane formation was also observed on many other catalysts which showed poor activity. For example, a catalyst sulfided at pH 8.5 with 500 ppm S (reduced at 300°C) is shown in Figure 5.18. Both P- and R-branch band envelopes are clearly evident in this figure [142].

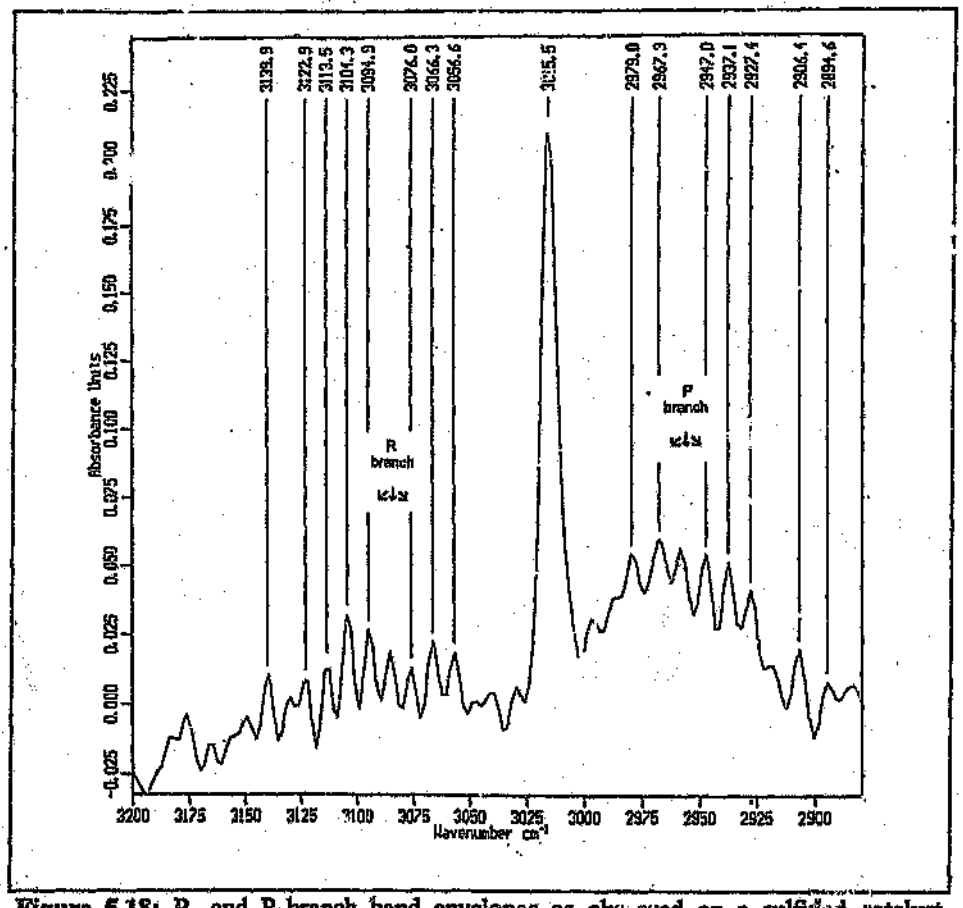


Figure 5.18: P- and R-branch band envelopes as observed on a sulfided catalyst reduced at 300°C during FT synthesis

Besides methane, catalysts reduced at 300°C produced large quantities of CO_2. Other hydrocarbon intermediates are in evidence in small amounts (Figure 5.18), such as $\nu_{OEt} = 2906\ cm^{-1}$, yet are insignificant in comparison to the intense vibrations of CH_4.

5.4. Conclusion

Using DRIFTS, Fischer-Tropsch synthesis over low-level sulfided catalysts was observed to proceed at a more rapid rate than for the unsulfided catalyst. A possible rationalisation is proposed to involve a strengthened metal-CO interaction which allows for the formation of surface carbide. Furthermore, low-level sulfidation resulted in an increased concentration of linear carbonyl and ethoxy groups which are well known intermediates in the FT reaction. It is possible that surface reconstruction in the presence of small amounts of sulfate creates a large number of sites suitable for the adsorption of reactive intermediates.

The addition of large amounts of sulfur creates an environment that is not conducive to carbide formation and hence blocks Fischer-Tropsch activity. CO adsorption studies reveal weak interaction between iron and CO on the highly sulfided catalysts, and this may account for the lack of carbide formation. A further point concerning the decreased CO dissociation relates to oxygenate selectivity. Highly sulfided catalysts have been shown to exhibit a propensity towards methanol and ethanol, at the expense of longer chain products. A similar product spectrum was observed for catalysts sulfided at pH 8.5, irrespective of sulfide source or level of sulfidation. Catalysts prepared at this pH appear to have higher concentrations of surface sulfide, which has a deleterious effect on CO adsorption and FT activity.

Chapter 6

Characterisation of sulfided precipitated-iron Fischer-Tropsch catalysts by Mössbauer spectroscopy

6.1. Introduction

For selected elements, Mössbauer spectroscopy has become a routine tool for obtaining information regarding the nature of the phases present in catalysts, particularly poorly crystalline or amorphous materials [154]. Where techniques such as XPS and DRIFTS give information exclusively on the surfaces of catalysts, Mössbauer spectroscopy is generally used as a bulk characterisation method [155].

The widespread application of Mössbauer spectroscopy for the study of Fischer-Tropsch catalysts stems from the fact that, in addition to iron, ruthenium and cobalt can be analysed using this technique [156]. For example, the influence of reduction and Fischer-Tropsch synthesis conditions on the state of iron in FeRu/TiO_2 catalysts was investigated by van der Kraan *et al* [157], and the presence of Ru was shown to enhance the reducibility of iron. In addition, Mössbauer spectra recorded after FT synthesis revealed extensive carburization of iron-rich catalysts. Hägg carbide, χ-Fe_5C_2, was identified as the phase formed from α-Fe and bcc-FeRu alloys.

The bulk oxidation state of iron that exists after various pretreatment procedures has also been elucidated using Mössbauer spectroscopy [155, 158, 159]. Furthermore, the effects of Fischer-Tropsch synthesis on phase modification can be quantified by making use of an *in situ* facility coupled to a Mössbauer spectrometer [155]. For instance, an *in situ* study of silica-supported Fe-Ru catalysts revealed increased stability and suppressed carbide formation [160].

As a bulk characterisation technique, Mössbauer spectroscopy has been used to characterise precipitated-iron FT catalysts [158]. It has been reported by Rao *et al* [158] that χ-carbide formed after CO reduction, and a correlation between FT activity and χ-carbide content was found for these catalysts.

In the present study, the effects of sulfidation during precipitation on the bulk oxidation state of iron were investigated. The observation of iron-sulfides was not expected since their concentration would be below the detection limit of this analytical method. However, it can be anticipated that the presence of sulfide might influence the distribution of iron phases in these catalysts.

Furthermore, catalysts which had been exposed to synthesis conditions for a considerable length of time were analysed to establish whether a correlation existed between XRD data on spent catalysts and the phases identified by Mössbauer spectroscopy.

6.2. Experimental

Uncalcined and calcined (400°C) catalysts sulfided with 2000-20000 ppm S from mono- and polysulfide sources (Na_2S and $(NH_4)_2S_5$), prepared as detailed in Chapter 2, were analysed by Mössbauer spectroscopy. The effects of exposure to FT synthesis conditions on the phases of iron present in catalysts sulfided with 2000 and 5000 ppm sulfide were also investigated.

Mössbauer equipment consisted of a constant velocity drive with ancillary electronics, and a $^{59}Co(Rh)$ γ-ray source. The source velocity was varied over a range of approximately 14 mm/s. Spectra were collected over 1024 channels with a dwell time of 100 μs per channel.

Approximately 30 mg of sample was required for each analysis. Room temperature measurements were recorded at 298 K, while liquid nitrogen was used as a cryogen for measurements recorded at 77 K.

Initial data expressed γ-ray counts as a function of source velocity, v. Using the first order Döppler shift, this was reluted to γ-ray energy, E_γ [52]:

$$E\gamma = E_o\left(1+\frac{v}{c}\right)$$

where E_o = energy of the nuclear transition

c = speed of light

A least-squares curve fitting procedure which utilised a Lorentzian lineshape profile was employed to model the spectra as a series of quadrupole doublets and hyperfine-split sextets. Isomer shifts are quoted with reference to α-Fe (0.12 mm/s). Instrument calibration was performed using Fe foil.

6.3. Results

The Mössbauer spectra of an unsulfided precipitated-iron catalyst are shown in Figure 6.1. A quadrupole-split doublet is the major component shown in the uncalcined spectrum (Figure 6.1a); a hyperfine-split sextet (H = 49.1 T) being the minor component.

Calcination of this sample at 400°C sees the disappearance of the doublet, compensated for by an increase in the intensity of the sextet (Figure 6.1b) compared to the uncalcined sample. Furthermore, the spectrum shown in Figure 6.1b was fitted with a second small magnetically split sextet which had a smaller hyperfine field (H = 45.4 T) than found for the major spectral component (H = 49.3 T).

The hyperfine parameters obtained for all samples at 298 K are presented in Table 6.1, which also includes an assignment of the iron species identified.

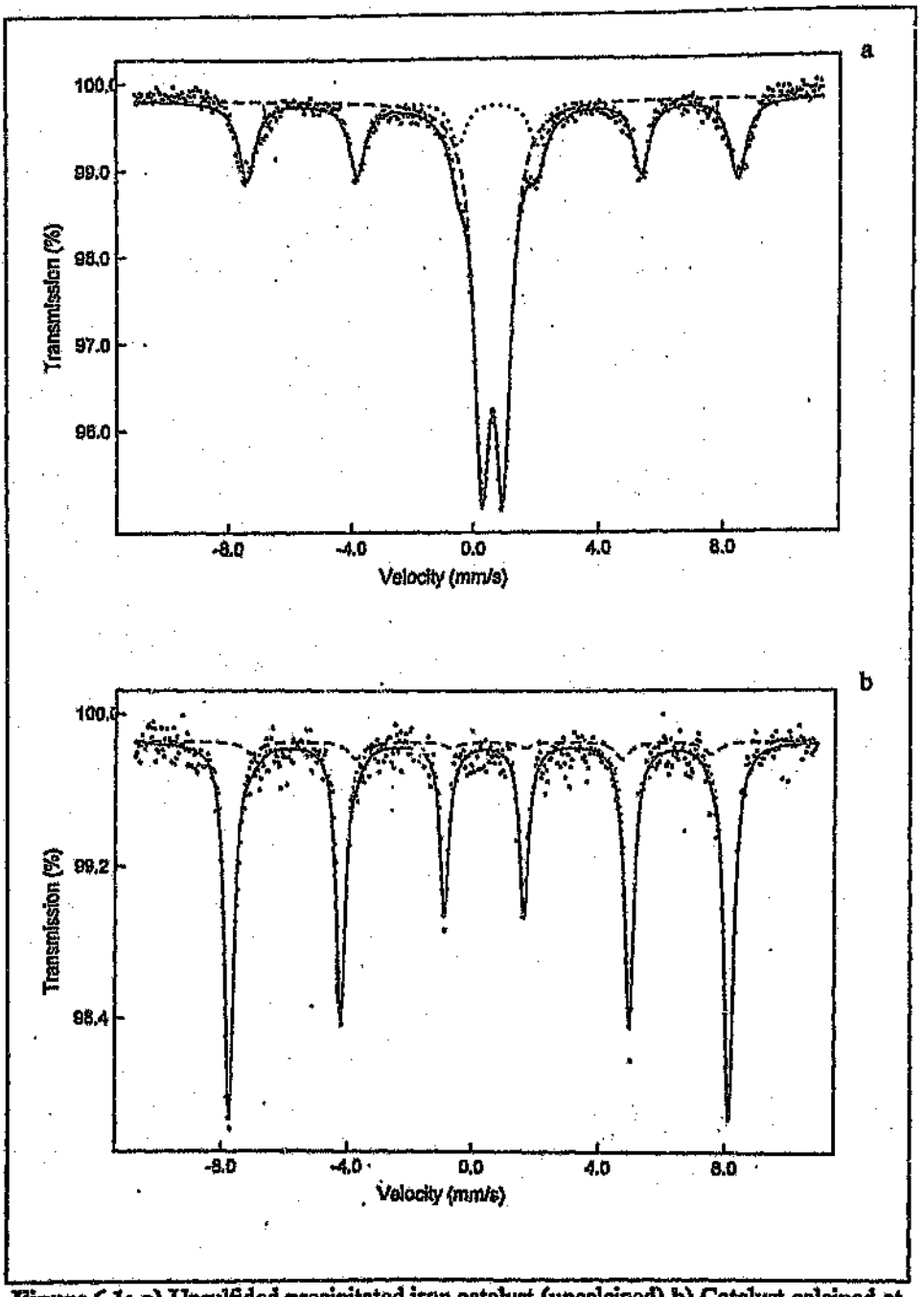


Figure 6.1: a) Unsulfided precipitated iron catalyst (uncalcined) b) Catalyst calcined at 400°C

Table 6.1: Hyperfine parameters calculated for precipitated-iron catalysts at 298 K[a]

Mössbauer Data		Catalyst			
Iron Species	Parameters	unsulfided (uncalcined) Figure 6.1a	2000 ppm Na_2S (uncalcined) Figure 6.2a	5000 ppm Poly S (uncalcined) Appendix	20000 ppm Na_2S (uncalcined) Figure 6.3
Fe^{3+}	δ (mm/s)	0.43	0.42	0.29	0.30
particle size	ΔQ (mm/s)	0.11	0.08	0.11	0.10
> 10 nm	H (T)	49.1	49.7	49.9	49.5
	RA (%)	18	31	N/A	92
Fe^{3+}	δ (mm/s)	-	-		0.34
particle size	ΔQ (mm/s)	-	-		0.06
4-10 nm	H (T)	-	-		44.1
	RA (%)	-	-		9
Fe^{3+}	δ (mm/s)	0.41	0.59		-
particle size	ΔQ (mm/s)	0.33	0.33		-
< 4 nm	RA (%)	82	69		-

Mössbauer Data		Catalyst			
Iron Species	Parameters	unsulfided (calcined) Figure 6.1b	2000 ppm Na_2S (calcined) Figure 6.2c	2000 ppm Poly S (uncalcined) Appendix	20000 ppm Poly S (calcined) Figure 6.4
Fe^{3+}	δ (mm/s)	0.39	0.35	0.44	0.19
particle size	ΔQ (mm/s)	0.10	0.11	0.11	0.11
> 10 nm	H (T)	49.3	50.2	49.7	52.1
	RA (%)	93	95	58	93
Fe^{3+}	δ (mm/s)	0.18	0.27	-	0.07
particle size	ΔQ (mm/s)	0.12	0.11	-	0.11
4-10 nm	H (T)	45.4	44.9	-	47.0
	RA (%)	7	5	-	7
Fe^{3+}	δ (mm/s)	-	-	0.42	-
particle size	ΔQ (mm/s)	-	-	0.34	-
< 4 nm	RA (%)	-	-	42	-

[a] δ = isomeric shift (±0.02) ΔQ = quadrupole splitting (±0.02) RA = relative abundance (±3) H = hyperfine field (±2)

N/A Owing to poor spectral resolution, the relative abundance of this phase could not be determined

The uncalcined catalyst sulfided with 2000 ppm Na_2S (Figure 6.2a) gave rise to a spectrum at 298 K, not unlike that of the uncalcined unsulfided catalyst except that, in the former case, the sextet is increased in intensity relative to the quadrupole split doublet. A quadrupole interaction of 0.33 mm/s determined for the doublet is typical of paramagnetic Fe^{3+}. At 77 K this doublet is partially transformed into a magnetically split sextet (H = 42.3 T) as shown in Figure 6.2b. Moreover, the quadrupole splitting of this doublet is greater at 77 K than at 298 K, suggesting a temperature-dependency (Table 6.2).

Table 6.2: Hyperfine Parameters calculated at 298 K and 77 K for the uncalcined catalyst sulfided with 2000 ppm Na_2S

Mössbauer Data		Temperature (K)	
Iron Species	Parameters	298	77[a]
Fe^{3+} particle size > 10 nm	δ (mm/s)	0.58	0.27
	ΔQ (mm/s)	0.08	0.07
	H (T)	49.7	51.2
	RA (%)	31	56
Fe^{3+} particle size 6-10 nm	δ (mm/s)	-	0.24
	ΔQ (mm/s)	-	0.2
	H (T)	-	47.0
	RA (%)	-	3
Fe^{3+} particle size 2-6 nm	δ (mm/s)	-	0.30
	ΔQ (mm/s)	-	0.06
	H (T)	-	42.3
	RA (%)	-	20
Fe^{3+} particle size < 4 nm	δ(mm/s)	0.59	0.28
	ΔQ (mm/s)	0.33	0.45
	RA (%)	69	21

[a] Spectrum not very well resolved (Figure 6.2b)

As with the calcined unsulfided catalyst, the room temperature spectrum of the low-level sulfided catalyst (Figure 6.2c) showed only the presence of two sextets with hyperfine fields of H = 50.2 T and 44.9 T (Table 6.1).

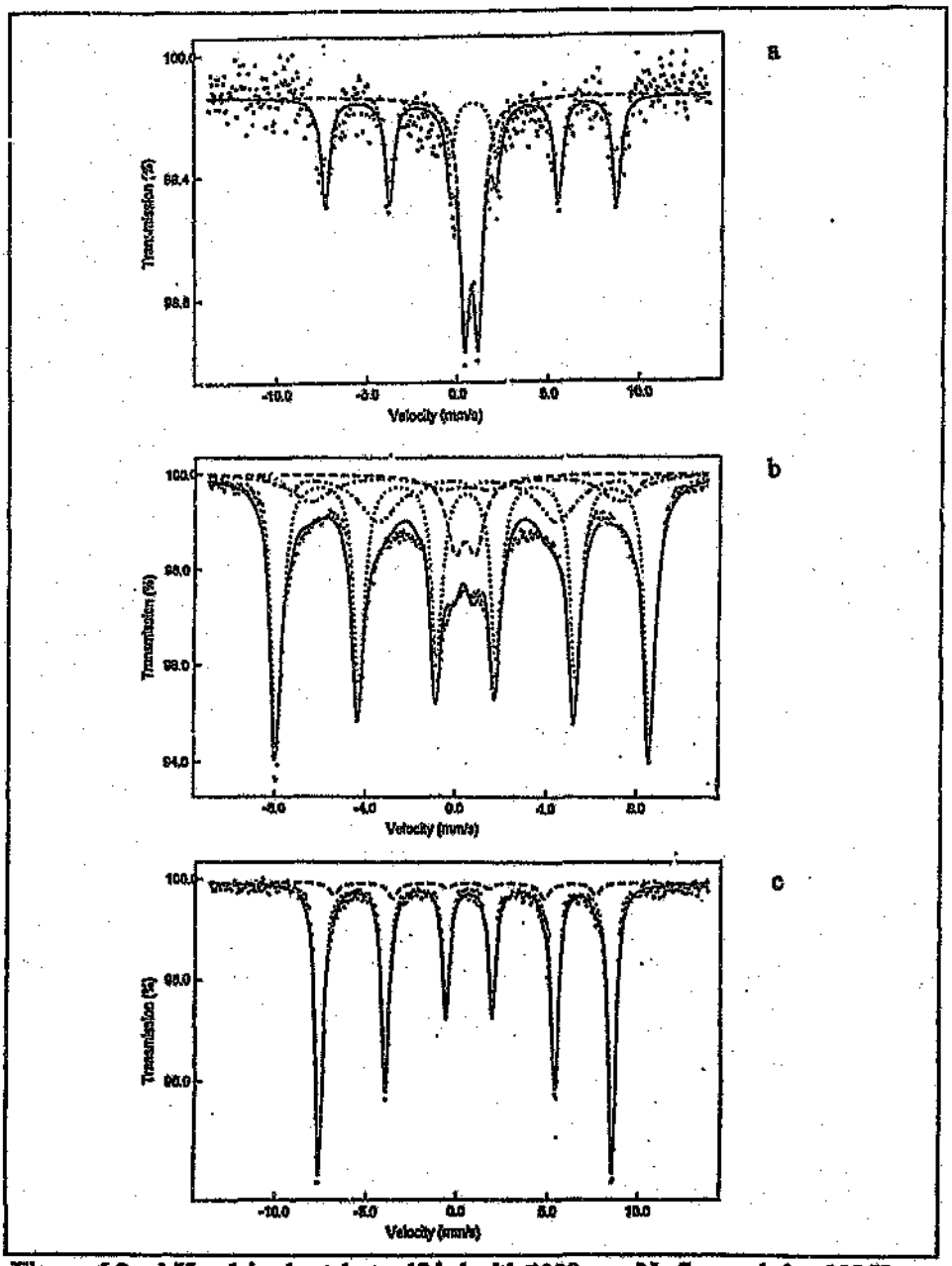


Figure 6.2: a) Uncalcined catalyst sulfided with 2000 ppm Na_2S recorded at 298 K b) Mössbauer measurement at 77 K c) After calcination at 400°C, recorded at 298 K

Increasing the sulfide content to 20000 ppm Na_2S resulted in the complete disappearance of the doublet in the uncalcined sample (Figure 6.3). The sextet with a hyperfine-splitting of H = 49.5 T dominates the spectrum.

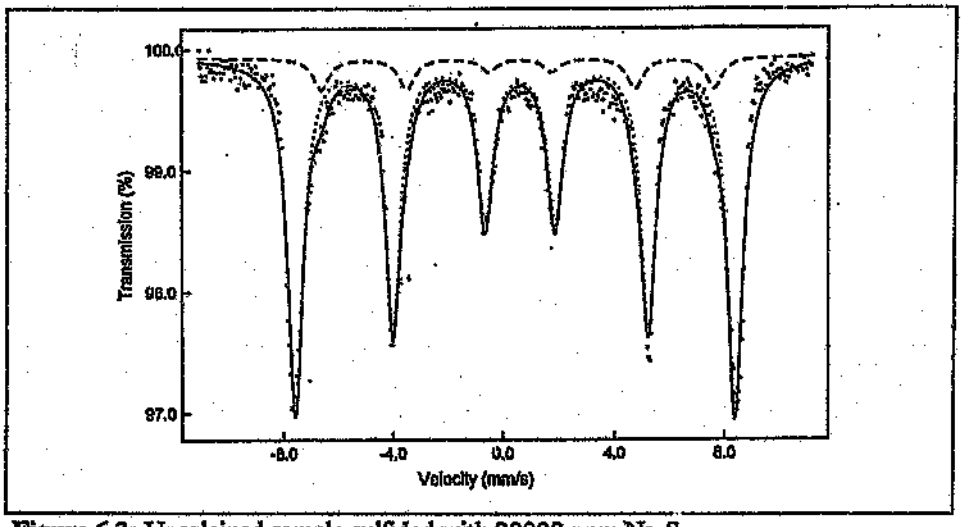


Figure 6.3: Uncalcined sample sulfided with 20000 ppm Na_2S

A 20000 ppm polysulfided catalyst that had been calcined at 400°C was also fitted with two magnetically split sextets (H = 52.1 and 47.0 T) as illustrated in Figure 6.4.

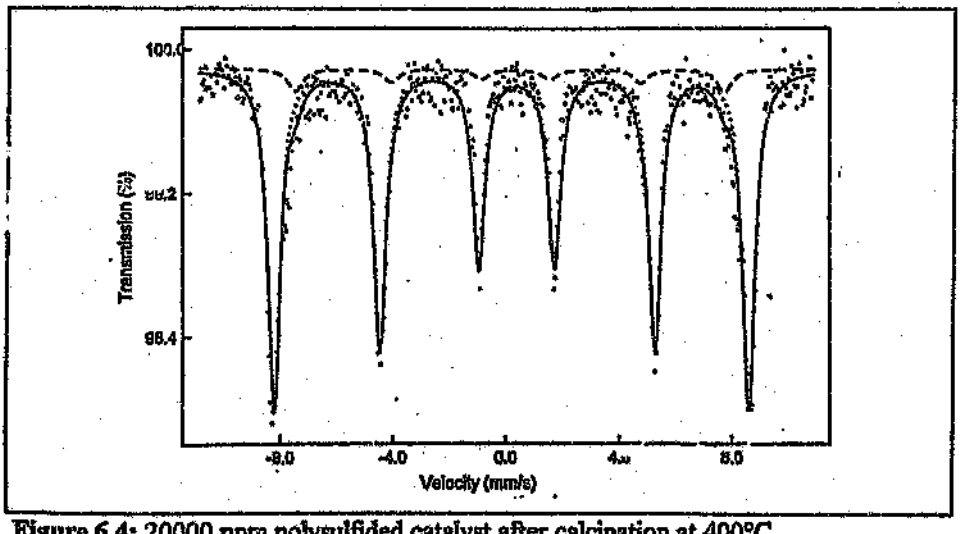


Figure 6.4: 20000 ppm polysulfided catalyst after calcination at 400°C

Several catalysts which had been calcined, reduced, and exposed to FT synthesis conditions for 14 days, were analysed to establish the effect of sulfide on bulk phase morphology (Table 6.3). The catalyst sulfided with 5000 ppm polysulfide yielded a Mössbauer spectrum typical of metallic iron (H = 33.2 T). No isomeric shift or quadrupole splitting was evident (Figure 6.5).

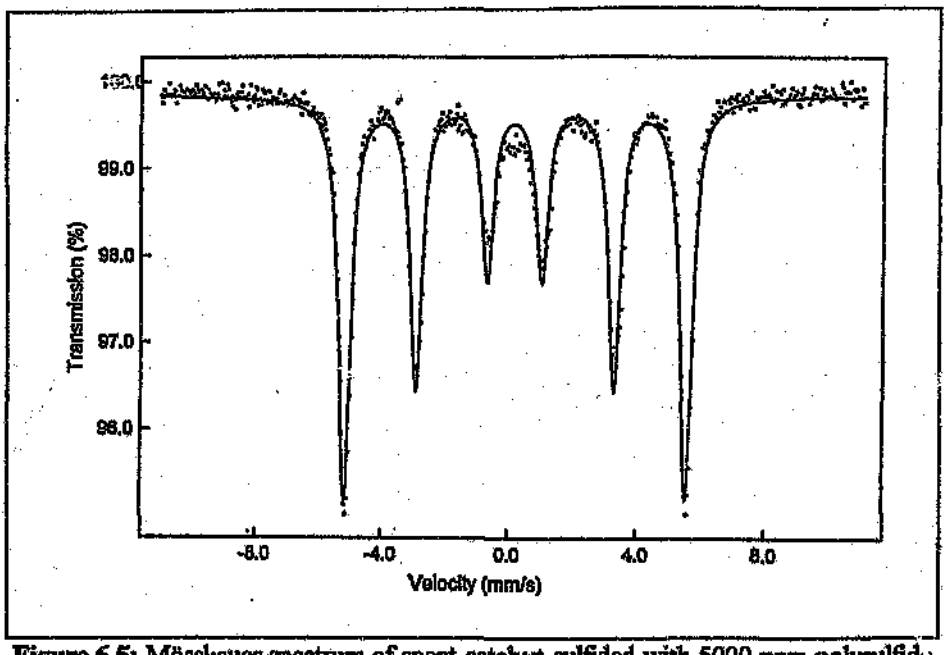


Figure 6.5: Mössbauer spectrum of spent catalyst sulfided with 5000 ppm polysulfide recorded at 298 K

In contrast, a spent catalyst sulfided with 2000 ppm polysulfide exhibited primarily Hägg carbide, and required at least 3 sextets to fit the spectrum shown in Figure 6.6. The sextets used to fit the data reprosent one of many possible combinations, since a distribution of fields was used in the fitting process. Thus the catalyst composition proposed is not unique and no doubt other hyperfine parameters could be obtained using different fitting constraints. Nonetheless, the parameters pertaining to the carbides purportedly present are given in Table 6.3.

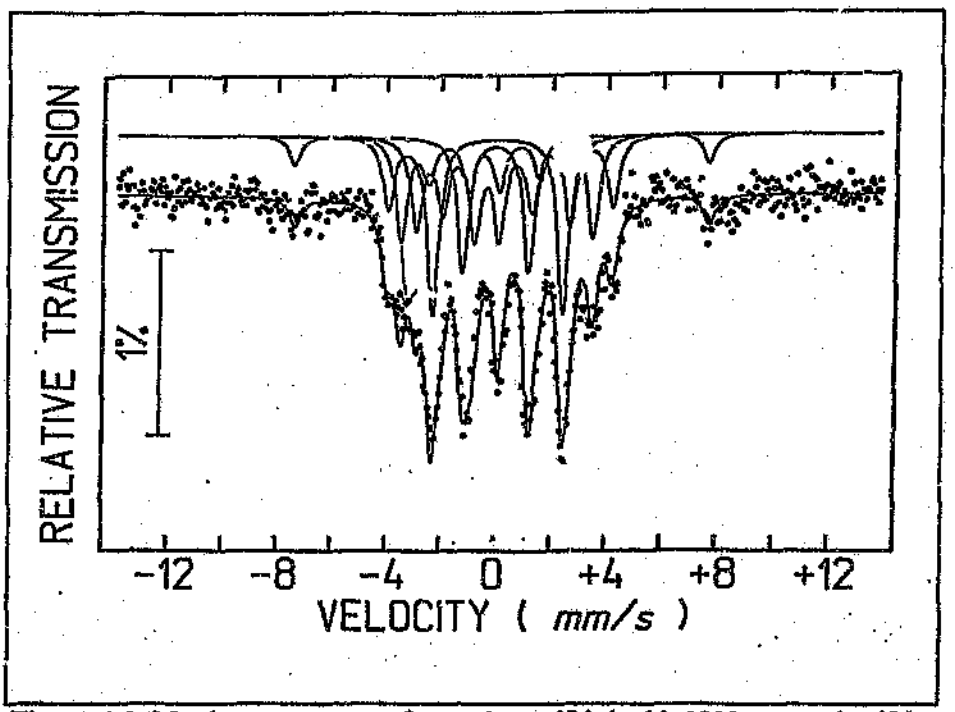


Figure 6.6: Mössbauer spectrum of a catalyst sulfided with 2000 ppm polysulfide, after FT synthesis, showing carbide formation (recorded at 298 K)

Table 6.3: Hyperfine parameters calculated for spent catalysts

Mössbauer Data		Catalyst	
Iron Species	Parameters	2000 ppm poly S	5000 ppm poly S
Fe carbide	δ (mm/s)	0.24	-
	Q (mm/s)	0.22	-
	H (T)	17.3	-
	RA (%)	29	-
Fe carbide	δ (mm/s)	0.22	-
	Q (mm/s)	0.46	-
	H (T)	21.5	-
	RA (%)	23	-
Fe carbide	δ (mm/s)	0.10	-
	Q (mm/s)	0.07	-
	H (T)	25.2	-
	RA (%)	29	-
Fe_3O_4	δ (mm/s)	0.07	-
	Q (mm/s)	0.16	-
	H (T)	46.6	-
	RA (%)	19	-
Fe^0	δ (mm/s)	-	0.00
	Q (mm/s)	-	-
	H (T)	-	33.2
	RA (%)	-	100

6.4. Discussion

6.4.1. Effect of sulfide addition on iron particle size

In Mössbauer spectroscopy, there are three parameters that characterise a chemical species or phase: isomeric shift (δ), quadrupole splitting (Δ) and magnetic hyperfine field (H) [156]. The latter is the one most easily attributed to a compound, and is therefore commonly used in the identification of chemical components. For hematite, a ferromagnetic sextet (δ = 0.40 mm/s, Δ = 0.11 mm/s, H = 51.5T) is typical [161].

In the present study, the set of experimental parameters for the unsulfided catalyst (δ = 0.43 mm/s, Δ = 0.11 mm/s and H = 49.1 T) shown in Table 6.1 and Figure 6.1a, correlate with the above data for hematite. The lower magnetic field is presumably an effect of particle size [162].

The magnetic hyperfine field is dependent on the particle size according to the relation [163]:

$$H = H_{(bulk)}(1-kT/KV)$$

with bulk = fairly large particle (greater than 50 nm)

k = Boltzmann constant

K = magnetic anisotropy constant

V = volume of the particle

Using this relation, and considering the particles as spherical, the radii can be determined.

In addition to the magnetically split sextet, the spectrum of the uncalcined unsulfided catalyst (Figure 6.1a) has also been fitted with a paramagnetic Fe^{3+} doublet. Indeed, this doublet is the major spectral component and indicates the presence of very small particles (less than 4 nm). The magnetically split sextet signifies particles greater than 10 nm in size.

As shown in Figure 6.1b calcination results in a dramatic increase in the relative intensity of the sextet corresponding to Fe_2O_3. In addition, a second sextet (H = 45.4T becomes evident and may be attributed to small particles of hematite (4-10 nm). It is well known that the field of α-Fe_2O_3 decreases with decreasing particle size due to superparamagnetic effects [162]. These particles are bigger than those which gave rise to the doublet prior to calcination, yet smaller than the major spectral component of the calcined samples.

Prior to calcination, the spectrum of the low-level sulfided catalyst (Figure 6.2a) is similar to that obtained in the absence of sulfide. The difference is that the hyperfine split sextet contributes 31 % of the total spectrum in the former case, while only 18 % in the spectrum of the unsulfided catalyst. Once again, the quadrupole doublet shown in Figure 6.2a can be attributed to the presence of hematite with very small particle size, presumably in the region of 4 nm. It is interesting to note that the paramagnetic doublet is characterised by an isomeric shift of 0.41 mm/s. This is the same value obtained for a paramagnetic doublet assigned to δFeOOH [164].

To establish whether the paramagnetic doublet (δ = 0.59 mm/s) observed in Figure 6.2a for the uncalcined low-level sulfided catalyst was due to small particles, a measurement was performed at 77 K (Table 6.2). This spectrum (Figure 6.2b) was not particularly well resolved, yet the presence of an intense sextet could be confirmed (H = 51.2 T). The partial splitting of the the doublet into a sextet (H = 42.3 T) is an indication of a wide distribution of particle sizes, in the range 2 to 6 nm. The broad line-width of the sextet also confirms the wide range of particle sizes. Furthermore, a third sextet (H= 47.0 T) giving a spectral contribution of 3% is suggestive of particles in the range of 7-10 nm. The increased quadrupole splitting of the doublet at 77 K is thus ascribed to temperature dependency [156].

Progressively increasing the sulfide content from 2000 to 20000 ppm S brings about considerable changes to the Mössbauer spectra of catalysts prior to calcination (Table 6.1). At 5000 ppm (polysulfide) the magnetically split sextet was estimated to contribute 30% of the spectrum, although the spectrum was poorly resolved. At a level of 20000 ppm S (Figure 6.3) this doublet has completely disappeared and the majority of particles are now greater than 10 nm (Table 6.1). The second sextet of low intensity (Figure 6.3) with δ= 0.34 mm/s, Δ= 0.06 mm/s and H = 44.1 T that exist for the catalyst sulfided with 20000 ppm Na_2S could also be attributed to hematite, but with reduced particle size compared to those that give rise to the main sextet. This indicates a narrow distribution of sizes for these catalysts.

It is apparent from the data presented in Table 6.1 that, for uncalcined catalysts, the effect of increasing sulfidation at pH 6.9 is to reduce the proportion of small particles. This is readily seen by plotting the spectral contributions of particles less than 4 nm and those greater than 10 nm as a function of sulfide content (Figure 6.7).

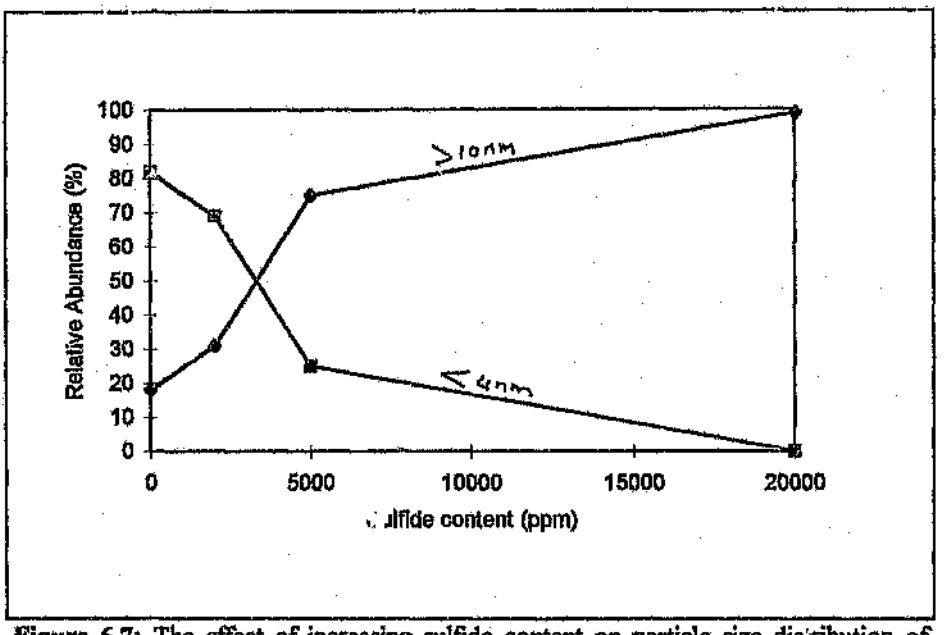


Figure 6.7: The effect of increasing sulfide content on particle size distribution of uncalcined catalysts sulfided in the range 2000-20000 ppm S at pH 6.9
[a] The 5000 ppm S sextet has been estimated to contribute 80 % of the spectrum

The trend shown in Figure 6.7 is in good agreement with estimates of crystallite size made independently using XRD data and the Scherrer equation (presented in Chapter 3). Hence, it can be concluded that increasing the level of sulfidation at pH 6.9 results in an increase in crystallite size of the precipitate. The effect of pH as a variable was not investigated using Mössbauer spectroscopy.

Therefore, as the amount of sulfide added is increased, the percentage of the paramagnetic phase deceases in the uncalcined samples. This effect seemes to be more pronounced in the case of polysulfided catalysts compared to those sulfided with Na_2S. For instance, as shown in Table 6.1, at a level of 2000 ppm S, the spectral contribution of the quadrupole doublet is greater for a monosulfided catalyst compared to that prepared using a polysulfide source.

No direct evidence could be found for the existence of bulk sulfides in any of the samples studied. This is not unexpected since the amount of iron sulfides that could have formed is expected to be below the detection limit of the Mössbauer technique. Notwithstanding this, the effect of increasing sulfidation is detected by a reduction in the fraction of small particles.

After calcination, the average particle sizes are observed to increase (since the fraction of small particles is eliminated) as shown in Table 6.1. The increase in particle size is particularly apparent from the increase in the magnetic hyperfine field. For example, H = 49.7 T for the uncalcined low-level sulfided catalyst, and after calcination H = 50.2 T. Furthermore, the trends observed prior to calcination with respect to sulfidation level are maintained in the calcined samples. The magnetic hyperfine field of 52.1 T observed for the calcined highly sulfided catalyst (Table 6.1, Figure 6.4) is typical of crystalline Fe_2O_3 [162].

6.4.2. Effect of sulfide content on the chemical state of iron

The isomeric shift arises from the coulombic interaction of the nuclear and electronic charge [156]. A significant part of this interaction is attributable to s-electron density, and therefore isomeric shifts are sensitive to the oxidation state of the iron in the absorber [52]. Moreover, within one oxidation state, the magnitude of the shift can generally be correlated with the properties of the atoms attached to the Mössbauer atom [156].

Assuming that the atomic iron nucleus is spherical, with radius R, and that the nuclear charge Ze is distributed homogeneously, the isomeric shift is related to the s-electron charge density $|\psi_s(0)|^2$ according to [156]:

$$\delta = \frac{2\pi}{5} Ze^2 \left(R_e^2 - R_g^2\right) \left\{ |\psi_a(0)|^2 - |\psi_s(0)|^2 \right\}$$

where R_g and R_e refer to the radii of atomic nuclei in ground and excited states and $|\psi_s(0)|^2$ is the s-electron density of the radiation source.

Moreover, it has been shown [156] that for iron nuclei (as absorber) an inverse proportionality exists between the isomeric shift (δ) and the value of $|\psi_a(0)|^2$. The relationship between the isomeric shift and the electronic structure of ^{57}Fe is illustrated by a Walker Diagram [156] (Figure 6.8).

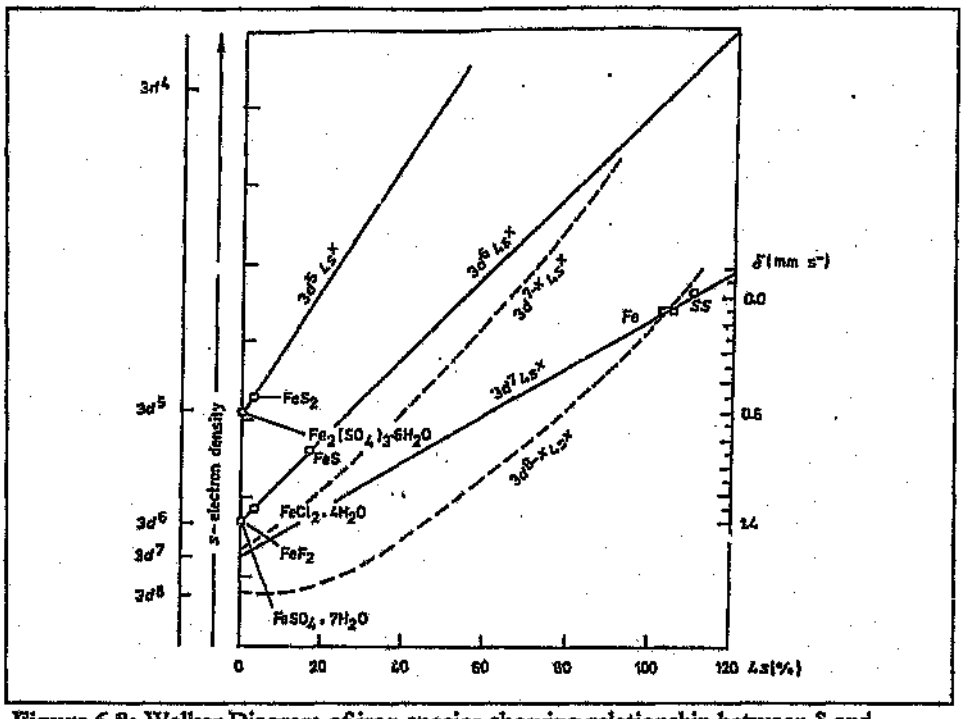


Figure 6.8: Walker Diagram of iron species showing relationship between δ and s-electron density

As shown in Figure 6.8, the electron density around an iron nucleus can be distorted by the nephelauxetic effect [156]. This relates to the degree of covalency of the metal-ligand bond. An increase in covalency is accompained by an increase in s-electron density on the iron atom, and hence a decrease in isomeric shift. Based on these findings, a nephelauxetic series of donor atoms has been established [165]:

$$F < O < N < Cl < Br < I < S < Se$$

Furthermore, it was shown by Danon [in 156], that a decreasing sequence of isomeric shifts of iron complexes correlated with this series.

For uncalcined catalysts (Table 6.1), the isomeric shifts of catalysts sulfided with (5000-20000 ppm) polysulfide or Na_2S are lower than expected for normal hematite (δ= 0.40 mm/s) and also lower than found at 2000 ppm S sulfidation. This can be tentatively attributed to the nephelauxetic effect of increasing covalency as oxygen atoms are replaced by sulfur atoms at increasing levels of sulfidation. Furthermore, these trends are maintained after calcination where the values of isomeric shifts are even lower, suggestive of an even stronger Fe-S interaction after thermal activation in air.

As mentioned previously, no bulk iron sulfides were detected in any of the samples studied. It has been calculated that, should 20000 ppm sulfide have been incorporated, a spectral contribution of 4 % due to FeS would expected. Indeed, it has been shown by ICP-MS (Chapter 3) that only a fraction of the added sulfide was in fact incorporated and this may account for the absence of any iron sulfides in the Mössbauer spectra of sulfided samples. However, the above data on the effect of sulfidation on the isomeric shift of hematite suggest that the sulfur atom may be present as part of a defect structure of the type $Fe_2S_xO_{3-x}$. In this way an effect of covalency is observed, whereas if all added S was present as an entirely new phase, no effect on the isomeric shift of hematite is expected.

6.4.3. Analysis of spent catalysts

Mössbauer studies of the spent catalyst sulfided with 2000 ppm S revealed bulk carbide formation (Table 6.3) The three sextets shown in Figure 6.6 correlate with the presence of χ-carbide. This is reportedly the main carbide observed after FT synthesis on unsupported iron catalysts [157]. A spectral contribution of 19 % due to magnetite (H = 47.0 T) was also observed. This low-level sulfided catalyst will be shown *vide infra* to be highly active for FT synthesis (see Chapter 10).

A highly sulfided catalyst that did not show any activity during Fischer-Tropsch reaction was also investigated following exposure to syngas (Figure 6.5). The hyperfine split sextet used to fit this spectrum may be assigned to metallic iron [156]. No carbide formation or oxide species are discernable.

6.5. Conclusion

Mössbauer spectroscopy has once again proved an indispensible tool in the characterisation of catalysts. The emergence of a hyperfine split sextet, indicative of larger particles, is evident at high levels of sulfidation. This is in good agreement with XRD data showing that crystallite growth is favoured by the presence of sulfide at pH 6.9. Calcination is also found to influence the growth of particles, due perhaps to pore collapse. The presence of bulk carbides in the low-level sulfided catalyst coincides with high Fischer-Tropsch activity, suggesting that these are the active phases for reaction. This conclusion is further strengthened by the absence of such carbide on the highly sulfided catalyst which was inactive during FT synthesis. The bulk structure of this catalyst was found to be α-Fe, in agreement with XRD results.

Chapter 7

Solution speciation modelling as applied to the precipitation of sulfided iron catalysts

7.1. Introduction

A comprehensive understanding of the structure of a solid catalyst requires knowledge of the chemical species in existence at the time of catalyst preparation. For supported catalysts, this entails a study of the interaction between the support and the impregnating solution. Such information may be obtained using techniques such as X-Ray powder diffraction, SEM or Mössbauer Spectroscopy which infer a description of the catalyst based on combined analysis of the active metal and its support in the solid state. However, in the case of precipitated catalysts, the metal-ligand equilibria present in *aqueous* environments are the decisive factors governing catalyst morphology and composition. Frequently, these equilibrium processes are extremely complicated and labile, and render the system inaccessible to direct analytical measurement [166]. In addition, the concentration of additives (such as sulfide in the present study) are often below the detection limits of most analytical techniques and hence their influence on the final precipitate remains undetermined.

Chemical Speciation Modelling is a procedure that enables the extent of aqueous metal-ligand interactions to be quantified as percentages of the total concentrations of any component present in a solution [166]. In this context, the term speciation is used to connote the chemical form of a given metal ion or ligand with respect to valence

state(s), concentrations of complexes and free aquated metal ions in equilibrium with solid precipitates [166].

Solution-chemistry computer simulation programs are based on the laws of Mass Action and Mass Balance, and solve complex mass balance relationships in terms of metal ion and ligand [167]. Extensive databases containing thermodynamic formation constants of possible species as well as Debye-Hückel parameters, are often coupled to these simulation programs making them applicable to a diverse range of aqueous systems. Clearly, as noted by Duffield *et al* [166], the quality of the chemical predictions is critically dependent upon the accuracy of the thermodynamic data contained within the database. An example of a well-established thermodynamic database is the compilation produced by the National Bureau of Standards [61].

Associated with the simulation of any chemical system are various sources of uncertainty. These have been categorized in terms of "modelling", "data" and "completeness" uncertainties and their bearing on solution speciation has been dealt with in detail [166]. It appears that, besides poor quality thermodynamic data, the success of a computer-based speciation analysis can be jeopardised by an imperfect understanding of the processes being modelled, as well as by an incomplete knowledge of the equilibria which are relevant to the system of interest.

An approach known as MASAD (Multivariate Approach To the Sensitivity Analysis of Data) is one of the procedures employed in the development of speciation models [168]. The aim of MASAD is to determine the sensitivity of a speciation model to

changes in the value of input parameters, notably formation constants, log β and log K_{sp}. A multivariate approach is applied to identify the so-called "pivotal" chemical species which lead to significant perturbations in modelling predictions.

In the present study, the aqueous system applicable to the precipitation of iron catalysts has been modelled using a geo-chemical equilibrium speciation modelling computational package called MINTEQA2 (Version 3.10), developed by the U.S. Environmental Protection Agency [60]. MINTEQA2 is capable of computing equilibria involving the dissolved, adsorbed, solid, and gaseous species typically present in environmental systems. The required input file is generated using an interactive program, PRODEFA2, that also allows access to the extensive database of thermodynamic data used by MINTEQA2.

7.2. Experimental

The aqueous system present at pH 10.75, 8.5 and 6.9 during the precipitation of iron oxide from solutions of $Fe(NO_3)_3.9H_2O$ and Na_2CO_3 at 75°C was modelled using MINTEQA2. The input data-file was created in PRODEFA2 and details of parameters used by MINTEQA2 may be found in Appendix 1.

In order to assess the impact of aqueous sulfide species, the above system was modelled following the addition of 1 ml, 60 ml, and 300 ml of 0.716 M $Fe(NO_3)_3.9H_2O$ to solutions containing sodium carbonate (400 ml, 0.785 M) and the required total dissolved sulfide (500 - 20000 ppm S/Fe) added from ammonium or sodium-based sources {Na_2S, $(NH_4)_2S$, $(NH_4)_2S_5$}.

The system was then modelled at the pH values calculated at the aforementioned additions of iron nitrate, namely pH 10.16, 8.54 and 6.88 respectively. An Fe^{3+}/Fe^{2+} redox couple was specified (see Appendix 1).

Increasing concentrations of sulfide from any of the sources studied had no significant effect on the pH of the solution. The carbonate concentration was reported to MINTEQA2 as the "total inorganic carbon content". The ionic strength was computed by the program, and activity coefficients estimated using the Davies equation [160] (see Appendix 1). An Eh value of either 100 or 280 mV was specified, and the system did not appear to be sensitive to values of Eh inside this range. The Eh of the system was not measured experimentally; rather, the range selected for the model was estimated from a Eh-pH diagram of water [61]. Indeed, it has been reported by Brookins [61] that many problems are associated with Eh measurements since half-cell couples in water are often not in equilibrium. The Eh region selected in this study is typical of bog waters, which are said to be mildly reducing, [61]. According to the Pourbaix diagram for the Fe-H_2O system, this Eh range suggests that suspended oxyhydroxides are the dominant species between pH 10.75 and 6.9 [62].

In the figures used in this chapter, ferric species are presented as a percentage of total added Fe^{3+}, ferrous species as a percentage of total Fe^{2+}, and sulfide species (even those containing Fe^{2+}) are given as a percentage of total added S_n^{2-} where n = 1 or 5.

7.3. Results

7.3.1. Effect of sulfidation level at different pH values

7.3.1.1. Sulfidation at pH 10.75

In the absence of sulfide, the predicted iron oxyhydroxide species at pH 10.75 is $Fe(OH)_4^-$ (Figure 7.1). Indeed 99% of all Fe^{3+} is bound as $Fe(OH)_4^-$ irrespective of sulfide content at pH 10.75. A minor component, $Fe(OH)_3$ (aq) was also identified and its concentration found to be independent of the amount of sulfide added.

The percentage of Fe^{2+} bound either as $Fe(HS)_2$ (aq) or $Fe(HS)_3^-$ is observed to increase with higher sulfide levels (Figure 7.1).

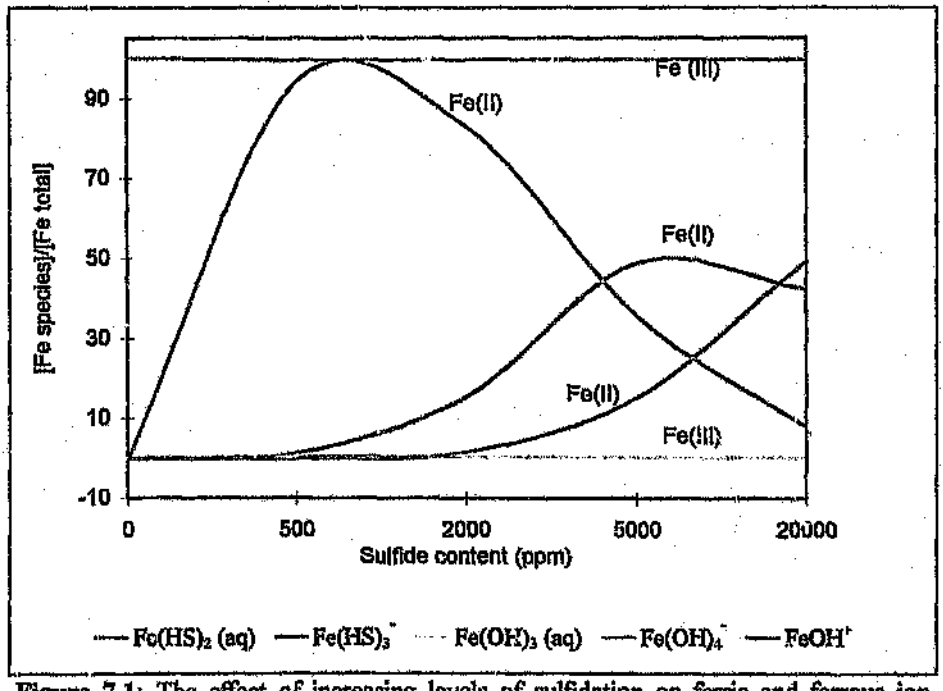


Figure 7.1: The effect of increasing levels of sulfidation on ferric and ferrous ion solution speciation[a] at pH 10.75:

[a] Aqueous ferric species are expressed as a percentage of total Fe^{3+} added, similarly, ferrous species are expressed as a percentage of total Fe^{2+} present (as determined by a Fe^{3+}/Fe^{2+} redox couple)

The aqueous $Fe(HS)_2$ species in particular, passes through a maximum at 5000 ppm sulfide addition. At low sulfide levels, the major ferrous species is $FeOH^+$ and increasing additions of sulfide shift the equilibrium toward $Fe(HS)_x^{n-}$ (x = 2 or 3) species.

Analysis of the effect of sulfide content on sulfide speciation (Figure 7.2), reveals that while 91% of added S^{2-} is HS^- at low S levels, at 20000 ppm sulfidation the proportion of HS^- in solution decreases to 84%.

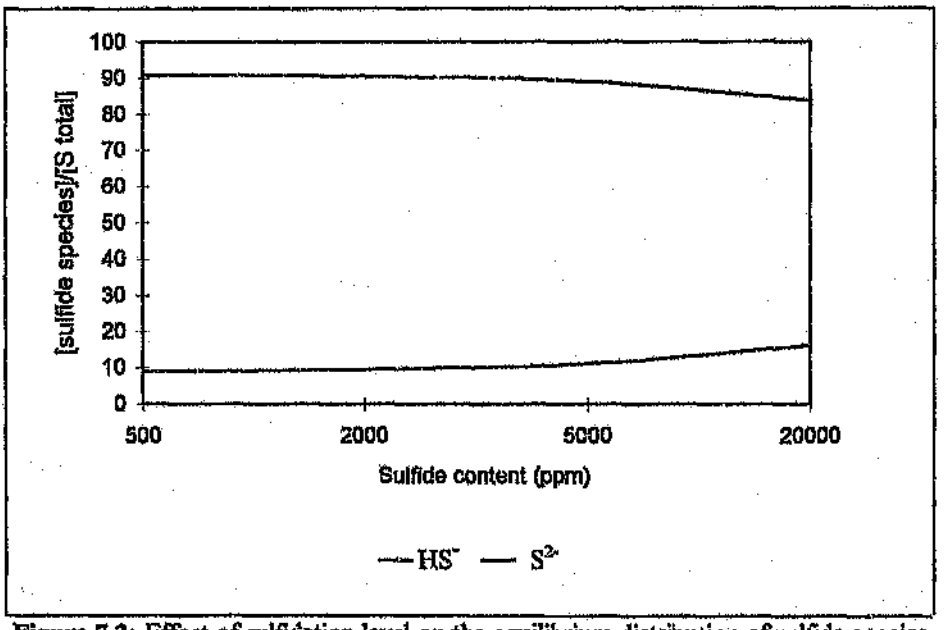


Figure 7.2: Effect of sulfidation level on the equilibrium distribution of sulfide species at pH 10.75.

Concomitantly, the percentage of S^{2-} in solution increases with increasing addition of sulfide. The dissolved H_2S concentration is observed to decrease with sulfide content. This may be ascribed to a shift in equilibrium toward the formation of $Fe(HS)_x$ species.

7.3.1.2. Sulfidation at pH 8.5

As shown in Figure 7.3, the addition of S^{2-} at pH 8.5 has an effect very similar to that observed at the more alkaline pH of 10.16. Once again, $Fe(OH)_4^-$ predominates, although the concentration of $Fe(OH)_3$ (aq) is now no longer insignificant (14% of Fe^{3+}). The emergence of $Fe(OH)_2^+$ becomes evident and as found before, the speciation is independent of sulfide content.

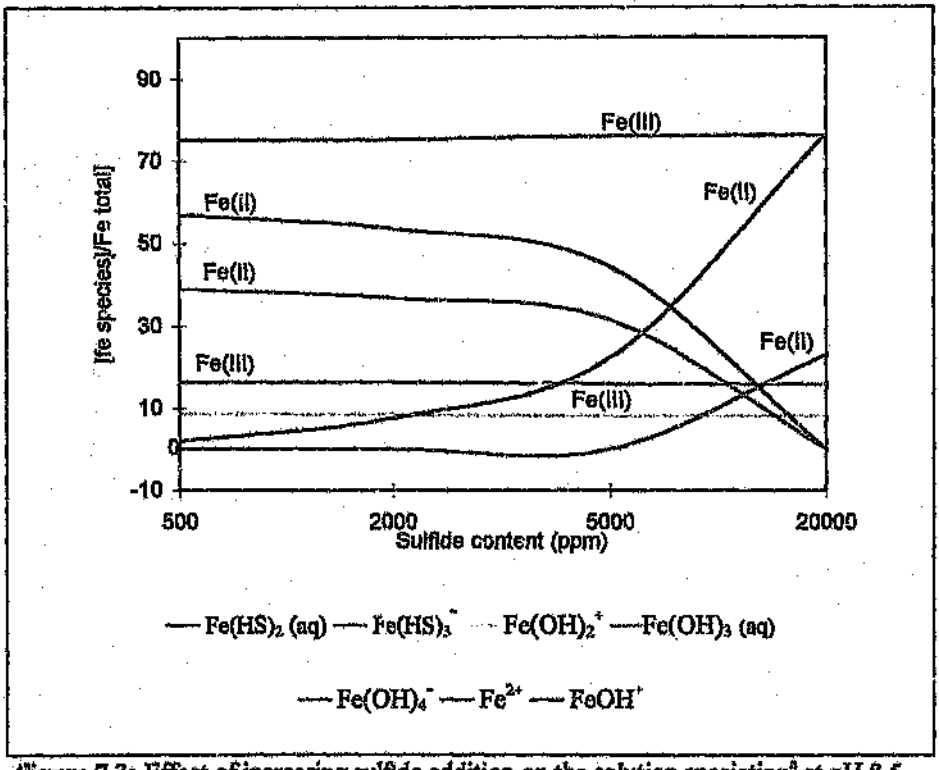


Figure 7.3: Effect of increasing sulfide addition on the solution speciation[a] at pH 8.5

[a] Aqueous ferric species are expressed as a percentage of total Fe^{3+} added, similarly, ferrous species are expressed as a percentage of total Fe^{2+} present (as determined by a Fe^{3+}/Fe^{2+} redox couple)

As expected, the distribution of ferrous species favours the formation of $Fe(HS)_x$ at this pH (Figure 7.3). At 20000 ppm S, 77% of ferrous ions are $Fe(HS)_x$ (aq) and the remainder is $Fe(HS)_3^-$. This is in stark contrast to the 52% Fe^{2+} present as uncomplexed ions in catalysts sulfided with 500 ppm S.

As far as the distribution of sulfide species is concerned, the concentration of ferrous bisulfide $Fe(HS)_x$ species reaches a maximum at 5000 ppm, whereafter it drops off significantly at high sulfidation levels (Figure 7.4). This is accompanied by an increase in the HS^- and H_2S (aq) concentration relative to the low-level sulfided systems. The decrease in aqueous $Fe(HS)_x$ species at high sulfidation levels may be ascribed to the preferred precipitation of FeS (s).

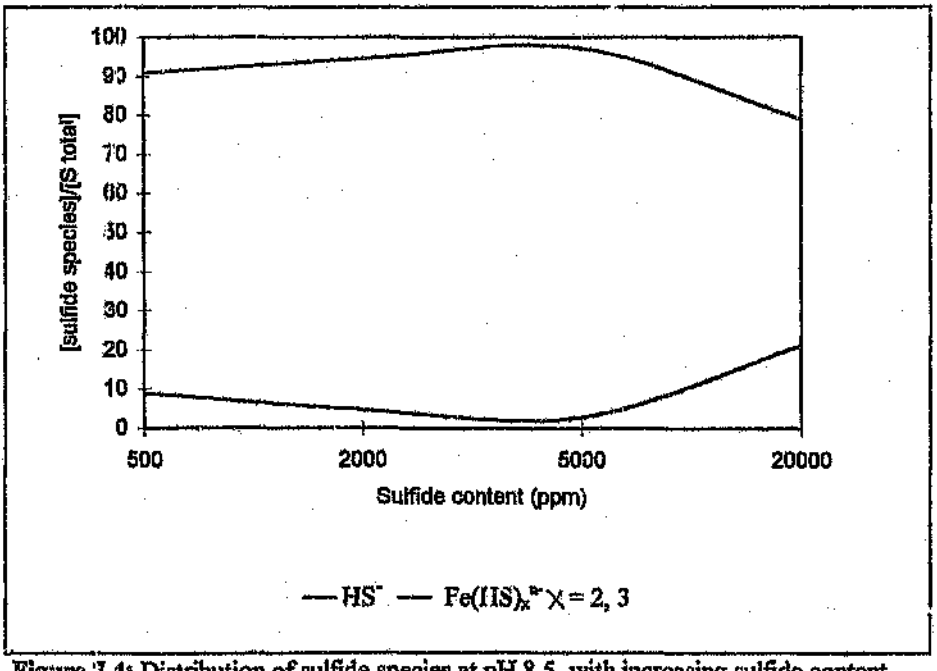


Figure 7.4: Distribution of sulfide species at pH 8.5, with increasing sulfide content

7.3.1.3. Sulfidation at pH 6.9

At pH 6.9 the situation is somewhat altered, and as shown in Figure 7.5, the distribution of most ferric oxyhydroxides is now strongly dependent on sulfide content. Up to 2000 ppm, $Fe(OH)_4^-$ still predominates and comprises 50% of dissolved Fe^{3+} species. Beyond this point an inversion occurs and the $Fe(OH)_4^-$ concentration is superceded by both $Fe(OH)_2^+$ and $Fe(OH)_3$ (aq); the latter being the only oxyhydroxide whose concentration is independent of sulfidation.

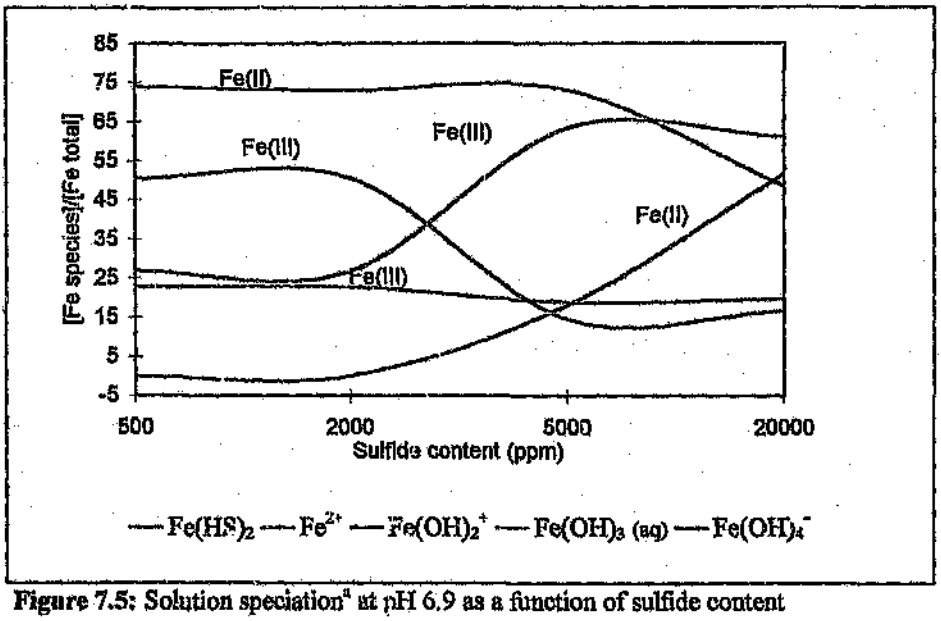


Figure 7.5: Solution speciation[a] at pH 6.9 as a function of sulfide content

[a] $Fe(HS)_x$ expressed as a percentage of total Fe^{2+} species, and $Fe(OH)_x$ species expressed as a percentage of total Fe^{3+} added.

The distribution of aqueous ferrous species in Figure 7.5 follow the same trend observed at more alkaline pH, with $Fe(HS)_x$ being favoured at high sulfide content.

With reference to sulfide speciation at this pH (Figure 7.6), notwithstanding the emergence of $Fe(HS)_3^-$ at high sulfidation levels, the $Fe(HS)_2$ (aq) and HS^- distributions are virtually independent of sulfide content. No trend in H_2S formation is immediately apparent.

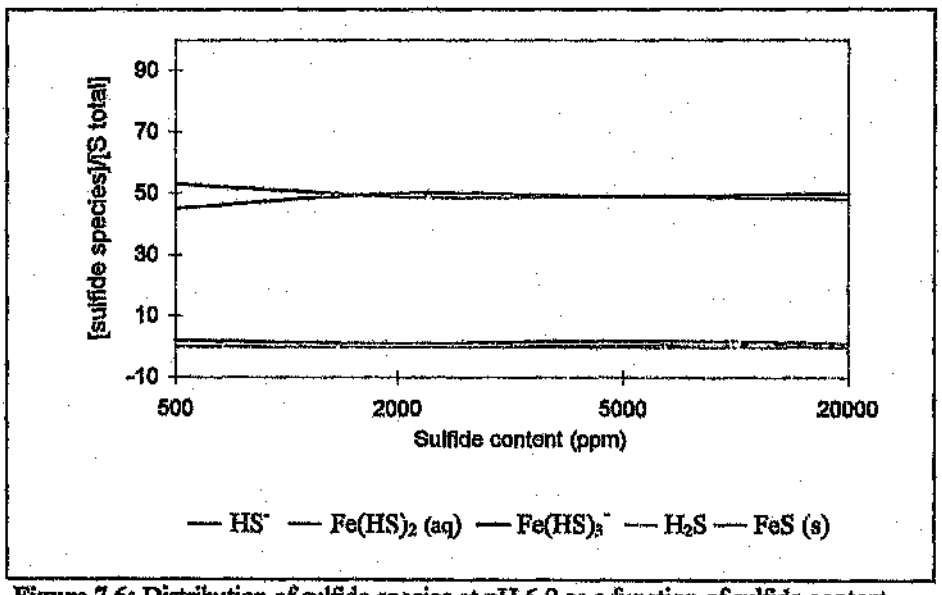


Figure 7.6: Distribution of sulfide species at pH 6.9 as a function of sulfide content

7.3.2.Effect of sulfidation pH

The effect of sulfidation pH on the system sulfided with 500 ppm S (Na_2S source) is shown in Figure 7.7. The decrease in HS^- concentration as a function of pH is accompanied by the formation of $Fe(HS)_2$ (aq), which is in turn in equilibrium with FeS(s). The decrease in S^{2-} is compensated for by an increase in the H_2S aqueous species at lower pH.

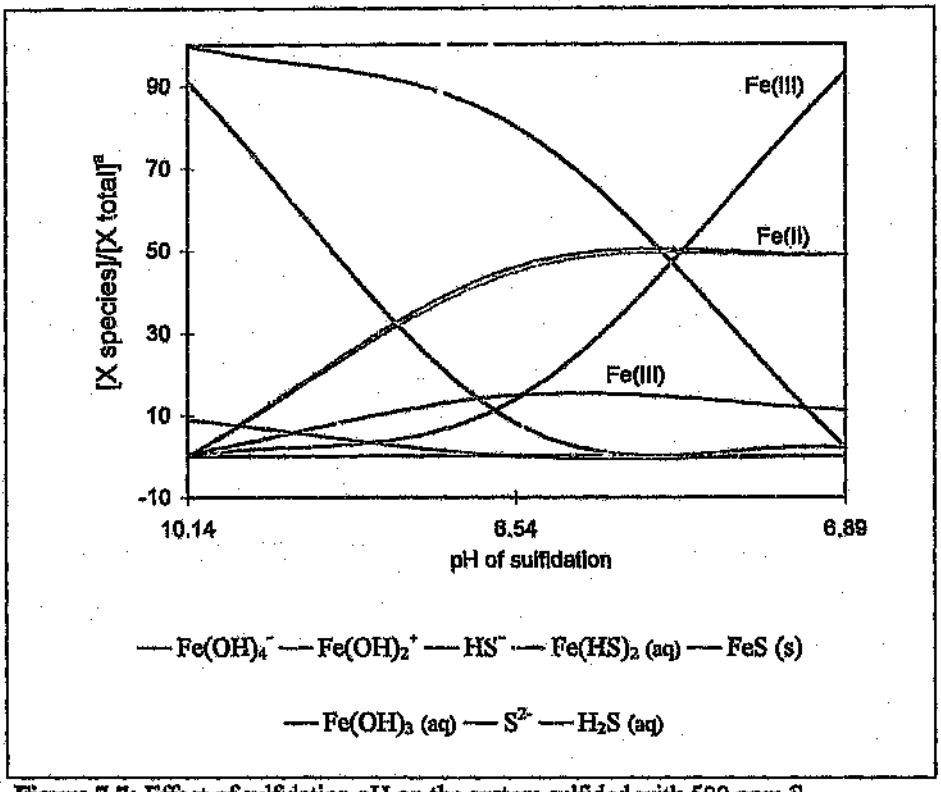


Figure 7.7: Effect of sulfidation pH on the system sulfided with 500 ppm S

* X refers to either sulfide, ferrous or ferric

At a pH slightly greater than pH 8.5, the formation of $Fe(HS)_2$ and FeS becomes significant, and the HS^- concentration drops to below 10% of the total sulfide. Furthermore, the formation of oxyhydroxides of the type $Fe(OH)_2^+$ and $Fe(OH)_3$ (aq) begins to occur at this pH.

The fraction of sulfide precipitated as FeS at pH 8.5 however, increases with sulfide content, such that 60% of the added sulfide is present as FeS(s) for the catalyst sulfided with 20000 ppm S (Figure 7.8).

This solid would act as a nucleus for the growth of iron oxide crystals. Moreover, the proportion of aqueous $Fe(OH)_3$ is at its maximum at pH 8.5.

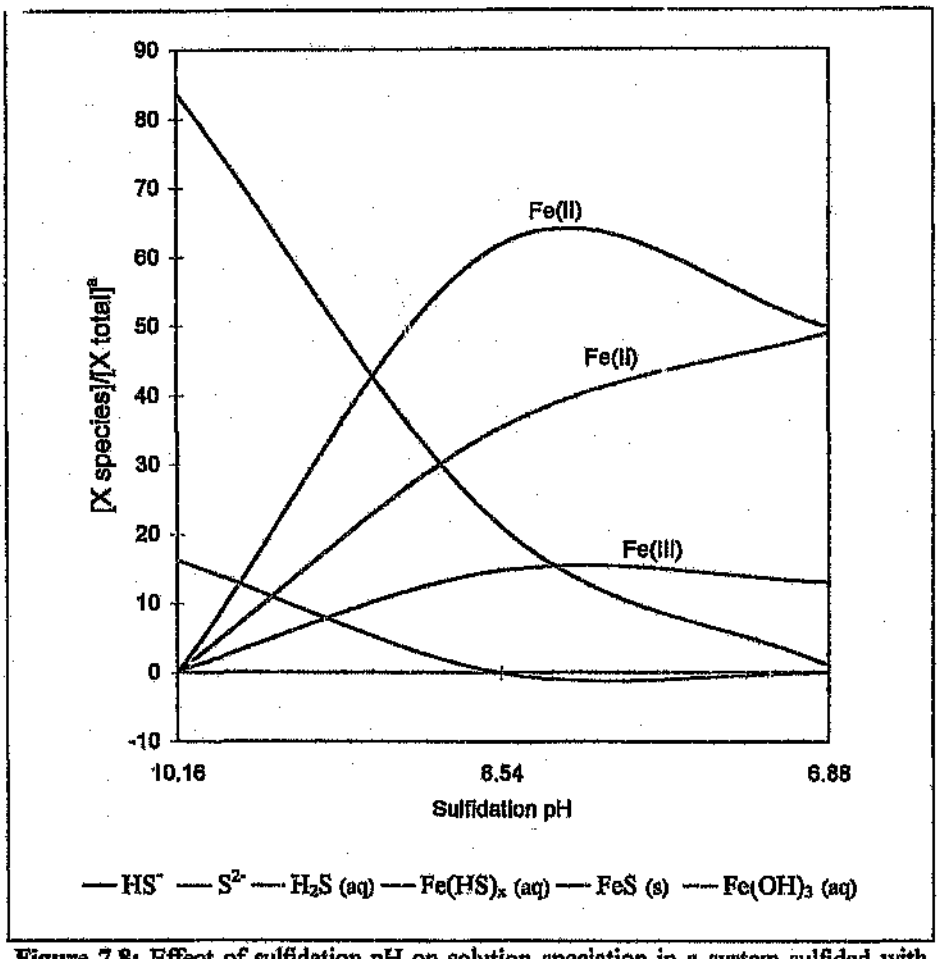


Figure 7.8: Effect of sulfidation pH on solution speciation in a system sulfided with 20000 ppm Na_2S

[a] sulfide-containing species are expressed as a percentage of total sulfide added, and $Fe(OH)_3$ species expressed as a percentage of total Fe^{3+} added. Therefore, X refers to sulfids, ferrous or ferric

7.3.3. Effect of sulfide source

The effect of sulfide source on sulfide speciation at pH 10.16 is illustrated in Figure 7.9. While 90% of monosulfide is present as HS^-, almost 98% of added polysulfide remains as S_5^{2-}.

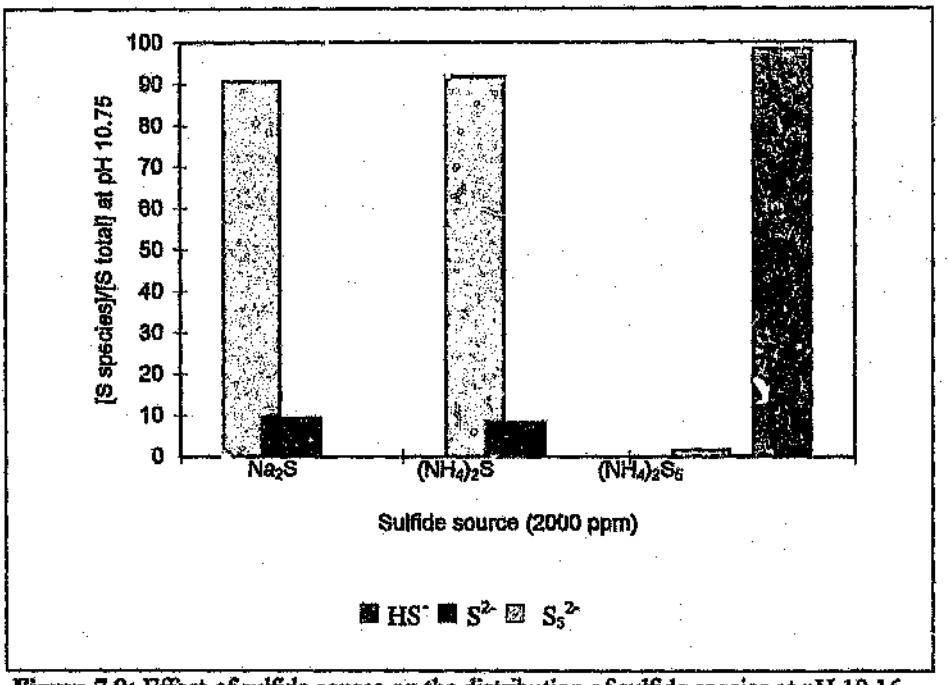


Figure 7.9: Effect of sulfide source on the distribution of sulfide species at pH 10.16

At pH 6.9, practically all added polysulfide still exists as S_5^{2-} and this remains in solution. Consequently, the $Fe(HS)_x$ species are greatly reduced in the polysulfided system, compared to those systems containing Na_2S and $(NH_4)_2S$ as shown in Figure 7.10.

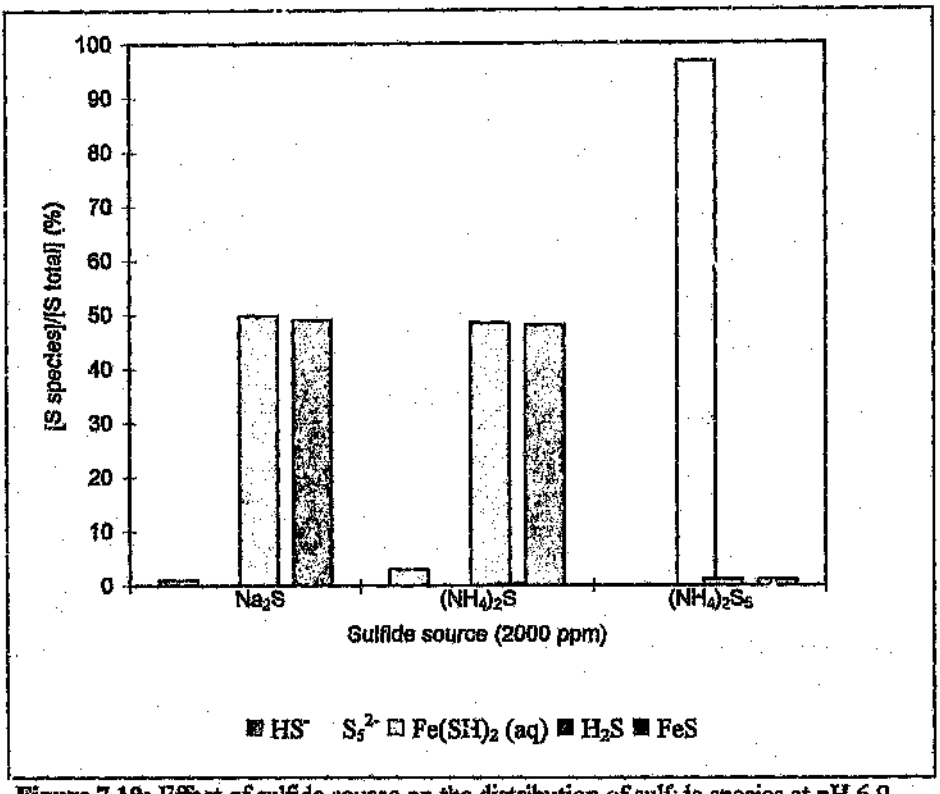


Figure 7.10: Effect of sulfide source on the distribution of sulfide species at pH 6.9

The polysulfide concentration is essentially unaffected by pH and decreases from 98 to 96% of total sulfide from pH 10.16 to 6.9. This is due to the formation of protonated species, of the type, S_4SH^- at lower pH values [19], which could then result in polysulfanes, S_5H_2. It is interesting to note that, according to Giggenbach [19], between pH 6.4 and 7.9, the optical absorption of aqueous polysulfide solutions was found to be largely due to the doubly charged species (S_nS^{2-}) and that hydropolysulfide ions were virtually absent.

Rather more interesting are the iron-sulfide species present in the polysulfided system which influence the precipitation product. The distribution of these species as a function of pH is shown in Figure 7.11.

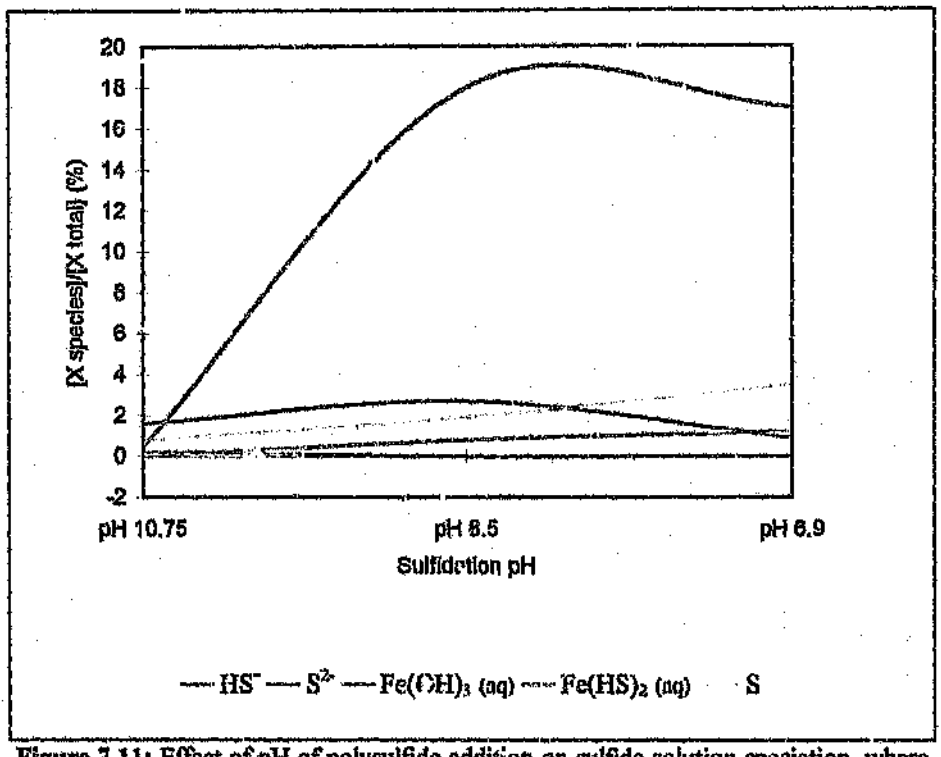


Figure 7.11: Effect of pH of polysulfide addition on sulfide solution speciation, where X refers to sulfide, or ferric

(since the polysulfide (S_5^{2-}) concentration remains unaffected by pH, it has not been included in this plot)

As a result of the preponderance of S_5^{2-}, the amount of FeS (s) is considerably less for polysulfided catalysts compared to monosulfided systems. Indeed, at pH 6.9 the FeS concentration in the system sulfided with Na_2S is 100 fold greater than when $(NH_4)_2S_5$ was employed. Less than an order of magnitude separates sodium and ammonium based FeS concentrations for monosulfided systems.

The sodium ion concentration is predicted to be negligibly affected by the sulfide source and independent of the pH of sulfide addition. Furthermore, the final dissolved concentration of ammonium ions is negligible, owing to the formation of ammonia.

7.4. Discussion

According to the speciation model used, close to the start of precipitation (pH 10.16), the addition of monosulfide results in a high concentration of aqueous HS^- species, and very little $Fe(HS)_x$. Only with further addition of ferric ions is the HS^- population reduced. When sufficient $Fe(HS)_2$ species have been formed, solid FeS begins to precipitate, viz: $Fe(HS)_2 \rightarrow FeS_{(s)} + H_2S$. Assuming this reaction occurs sufficiently quickly, these FeS species could provide nuclei for the adhesion of iron oxyhydroxides and hence allow this material to precipitate out of solution.

Increasing the sulfide content increases not only the $Fe(HS)_2$ (aq) concentration, but also the fraction of ferrous ions complexed with HS^-. Since very little solid FeS has formed at this stage, the distribution of aqueous ferric complexes is independent of sulfidation level (Figure 7.1).

These trends are maintained at pH 8.5, the only point worth noting is that the concentration of $Fe(OH)_3$ (aq) has begun to increase, and that of $Fe(OH)_4^-$ to decrease, as bulk precipitation commences (Figure 7.3).

At pH 6.9, a strong sulfide dependency is observed for ferric oxyhydroxide species (Figure 7.5). It would appear that the addition of sulfide in excess of 2000 ppm S results in the rapid precipitation of ferrihydrite, expressed in Figure 7.5 as a decrease in $Fe(OH)_4^-$ concentration. At this point, most, if not all of the added sulfide is complexed as $Fe(HS)_2$ (aq) or solid FeS. Hence high-level sulfidation (greater than 2000 ppm S) at pH 6.9 serves to precipitate iron oxide. This growth of crystallites gives rise to a more crystalline material, as shown by powder diffraction studies (Chapter 3).

Therefore, increasing levels of sulfidation at high pH (pH 10.75) implies larger surface areas due to the presence of nucleating agents. This suggests smaller particles. However, at pH 6.9, the precipitation of iron oxides at high sulfide content indicates the presence of larger crystalline particles.

The effect of sulfidation pH is best illustrated using the catalyst sulfided with 20000 ppm Na_2S. As can be seen in Figure 7.8, the concentration of FeS (s) peaks at pH 8.5, and differs considerably from that of $Fe(HS)_n$ (aq) at this pH value. At lower levels of sulfidation, the difference between these ferric sulfides is less obvious (Figure 7.7). Nonetheless, the presence of FeS signifies the possibility of many small crystallites of oxyhydroxide developing. However, saturation of the system in terms of iron oxide has already been achieved and hence some of the FeS molecules would adhere to these species. This results in larger crystallites forming than would be the case had sulfidation been performed at pH 10.75. At the start of precipitation, the $Fe(HS)_2$ (aq) generates the FeS (s) which forms the nuclei from which crystallites of FeOOH and Fe_2O_3 develop.

The concentration of FeS (s) begins to decrease at lower pH owing to the formation of solid sulfur. Hence fewer nuclei are available and crystallite size increases. Moreover, aggregation of smaller crystallites is facilitated by solid FeS. A cartoon depicting the proposed effect of sulfide addition at different pH values is given in Chapter 10.

With regard to iron oxyhydroxides, precipitation gains momentum at pH 8.5, where the concentration of aqueous $Fe(OH)_3$ reaches a maximum (Figure 7.8). This species is an intermediate in the precipitation of ferrihydrite and hence its concentration begins to decrease as solids precipitate.

The introduction of sulfide ions at pH 8.5 generates a large amount of FeS (s) at precisely the point where iron-oxide precipitates are forming. Consequently, these FeS crystals can be expected to be incorporated closer to the surface of iron crystallites, than if sulfide had been present prior to the introduction of iron. Indeed, crystallites sulfided at pH 8.5 have larger FeS content than those sulfided at pH 10.75 or pH 6.9. At pH 6.9, the addition of sulfide serves to aggregate iron-oxide crystallites, while at the start of precipitation the presence of sulfide creates a massive pool of nucleating agents. This has the effect of creating many small crystallites at pH 10.16 and hence the crystallinity of the material is lower than when aggregation occurs at pH 6.9. This proposal rationalises the XRD results which indicated increasing crystallinity (larger crystallites) with decreasing pH of sulfidation (Table 7.1).

Table 7.1. Effect of solution speciation on crystallite size determined using XRD

Sulfidation pH	Crystallite size (Å)[a]	Species in solution
10.75	226	First FeS (s), then $Fe(OH)_3$
8.5	262	Some $Fe(OH)_3$, then FeS, then more $Fe(OH)_3$
6.9	407	First $Fe(OH)_3$, then FeS

The addition of sulfide from different monosulfide sources had no effect on solution speciation (Figure 7.9). The concentrations of all species produced as a consequence of Na_2S or $(NH_4)_2S$ addition were within an order of magnitude of each other. The addition of polysulfide however greatly affected the distribution of sulfide species. Where HS^- predominated following S^{2-} addition, S_5^{2-} remains the dominant species in polysulfided systems. However, it exists as a dissolved aqueous species and hence is not expected to affect the formation of iron oxide precipitates. Rather, its incorporation may be due to occlusion rather than formal precipitation. This would account for the detection of polysulfide on the surface of highly sulfided catalysts by XPS (chapter 4).

In aqueous solution, polysulfide ions disproportionate according to the equilibrium:

$mS_nS^{2-} + H_2O \leftrightarrow nS_mS^{2-} + SH^- + OH^-$ where $n = m+1$[1] [169]. The HS^- produced as a result reaches a maximum dissolved concentration at pH 8.5, along with aqueous $Fe(OH)_3$ (Figure 7.11). Hence, the effects observed with monosulfided catalysts are mirrored by polysulfided systems in terms of HS^- speciation.

[1] the author inadvertently referred to n = m-1 [169].

As a result of the preponderance of S_5^{2-} (aq) the amount of FeS (s) produced in polysulfided systems is substantially less than that found in systems sulfided with Na_2S or $(NH_4)_2S$. Consequently, the crystallinities of polysulfided catalysts are more alike (Chapter 3), since the pool of nucleating agents is not as large as with monosulfided catalysts. It appears rather that aggregation of crystallites occurs. This means that the surface areas of polysulfided catalysts would be expected to be smaller than would be the case if many nucleating agents were present. The latter case gives rise to small crystallites which result in a large BET surface area for the catalyst.

This model describes the solution speciation as it is expected to be at 75°C, the tempe- :e at which precipitation was carried out. According to Giggenbach [19], polysulfides are stable up to 150°C, whereafter they dissociate into short-chain polysulfides, and HS^- or H_2S. Thiosulfate may also be formed and this supposedly reacts with HS^- or H_2S to form zerovalent sulfur.

A point worthy of mention is that at all pH values, for all levels of sulfidation, the H_2S (aq) contribution is insignificantly small, and can therefore be neglected. One reason for the low H_2S concentration in the presence of ferric ions is the formation of zerovalent sulfur [170]:

$$H_2S + 2Fe^{3+} \rightarrow S^o \downarrow + 2Fe^{2+} + 2H^+$$

For polysulfided systems at pH values below 7, hydropolysulfide ions (S_4SH^-) are expected to be the predominant zerovalent sulfur-containing species in solution [19]. Using equilibrium constants derived at various temperatures, Giggenbach determined

that polysulfides become thermodynamically unstable above pH 9. However, their high kinetic stability at high pH may be explained in terms of the pentasulfide ion being the main reactive polysulfide species [171], as shown by the rate expression for the disproportionation of polysulfide according to the equilibrium:

$$4S_nS^{2-} + (3n-4)OH^- \leftrightarrow nS_2O_3^{2-} + (2n+4)HS^-$$

This reaction is governed by the expression:

$$\frac{-d[S_4S^{2-}]}{dt} = k_f[S_4S^{2-}][HS^-]^{-2}[OH^-] - k_r[S_2O_3^{2-}][HS^-][OH^-]^{-2}$$

The chemical identity of the counter-ion is not predicted to influence the morphology or the final precipitate. The concentration of ammonium ions is negligible compared to aqueous NH_3, according to the speciation model. Furthermore, systems containing the same amount of sulfide, from any of the sources studied, were predicted to have the same sodium concentration.

7.5. Conclusion

The solution speciation of aqueous iron oxyhydroxides in the presence of sulfides has been successfully modelled using MINTEQA2. The species predicted to predominate at various sulfidation levels and pH values appear to rationalise the observed morphology and composition of the final precipitated catalyst.

For catalyst systems sulfided at the same level with different sources of sulfide, no counter-ion effect was observed. However, aqueous pentasulfide predominates at all pH values. This leaves a smaller base of nucleating agents than that generated by S^{2-}

addition. Consequently, polysulfide crystallites are larger, and this implies that they would exhibit smaller surface areas.

Finally, while the speciation models appear to accurately describe the aqueous processes involved in the precipitation of sulfided catalysts, they are subject to certain limitations. One important limitation of this type of solution speciation is that it supposes all processes to be at equilibrium and this may not necessarily be the case. Furthermore, no information is presented on the kinetics of reactions [61] in these speciation studies.

Part B: Reactor studies

Chapters 8 through 11 describe the influence of sulfide addition on the catalytic function of precipitated-iron Fischer-Tropsch catalyrts. Each chapter covers a separate issue, relating for instance, to the effect of sulfide source or sulfidation pH. Therefore, insofar as the aspect of sulfide addition being discussed is concerned, each chapter is unique. However, since each chapter is essentially "stand-alone", some repetition of methodology is unavoidable.

Chapter 8

The effect of increasing sulfide content on the catalytic efficacy of iron Fischer-Tropsch catalysts

8.1. Introduction

With what is arguably the most diverse of product distributions, the Fischer-Tropsch spectrum encompasses olefinic and paraffinic hydrocarbons from C_1 to C_{30+}, oxygenates, water and carbon dioxide. However, industrially, the present economic climate dictates that the yield of high-value products in the above distribution should be maximised. To this end, catalysts have been tailored to allow selective acceleration of the formation of highly sought-after regions of the wide ranging product slate.

For instance, precipitated-iron catalysts moderately promoted with manganese oxide have been found to exhibit enhanced olefin to paraffin selectivity [172]. Similarly, the use of potassium and sodium as promoters in FT catalysts is extensively documented [32, 28, 173] and results in higher α-values, lower methane selectivity and increased olefinity. The mode of action of these promoters is firstly to enhance the interaction of CO molecules with the catalytic substrate, and subsequently to facilitate a weakening of the intramolecular CO bond [52]. Extensive studies have shown however, that no matter what promoter is used, enhancement in activity and selectivity is only observed when the promoter content is low. For example, a report by Dry [31] indicated that silica supported Fe_2O_3 catalysts promoted with K_2O were increasingly active in the FT reaction up to a critical potassium content.

Potassium loadings above this level decreased catalyst activity but improved heavy hydrocarbon selectivity. Consequently, these catalysts have been used exclusively in the production of waxes and are operated at high pressures to compensate for the loss of activity incurred by high alkali content.

In this chapter, precipitated-iron catalysts sulfided with between 500 and 20000 ppm Na_2S were evaluated for their performance as Fischer-Tropsch catalysts in a fixed-bed reactor. The effect of sulfidation level on the reduction behaviour was also considered. To avoid complications arising from the sulfide source, this study of the level of sulfidation was made using catalysts prepared with sodium sulfide as sulfiding agent. The effect of sulfide source will be dealt with in a later chapter.

8.2. Experimental

The catalysts used in this study were sulfided at pH 6.9 in the 500 and 20000 ppm S range using sodium sulfide as detailed in Chapter 2. Calcination was performed at 400°C for 16 hours, whereafter the catalysts were activated by reduction under flowing hydrogen at 400°C for 24 hours. Fischer-Tropsch synthesis was then commenced at 250°C and 8 bar pressure, using a $CO:H_2$ ratio of 1:2 and a GHSV of 400 h^{-1}. All catalysts were monitored over an induction period of 4 days, followed by a four-day mass balance . Gaseous and liquid product fractions were analysed by on-line gas chromatography, while separation of the waxy products components was achieved using an off-line capillary-column gas chromatograph.

8.3. Results and Discussion

8.3.1. Reactor Study

Catalysts sulfided with increasing amounts of sulfide were evaluated for their efficacy in the FT reaction, and the results obtained are summarised in Table 8.1.

Table 8.1: Evaluation of sulfided catalysts in the Fischer-Tropsch Reaction

Catalyst[a]	% CONV	α-value	TON[b] (10^{-3} s^{-1})	Specific Activity µmol C/s/g_{cat}
unsulfided	26.5	0.80	29	0.35
500 ppm S	53.7	0.78	171	1.31
2000 ppm S	53.8	0.83	131	0.67
5000 ppm S	48.0	0.65	88	0.53
20000 ppm S	9.95	0.53	10	0.11

[a] all catalysts were sulfided at pH 6.9 using sodium sulfide
[b] TON (turnover number) refers to the number of CO molecules converted to products per exposed active site

Catalysts sulfided with between 500 and 5000 ppm S exhibited enhanced specific activity as depicted in Figure 8.1. The most highly sulfided catalyst however, showed evidence of the deleterious effects of sulfur on activity, and performed poorly under synthesis conditions.

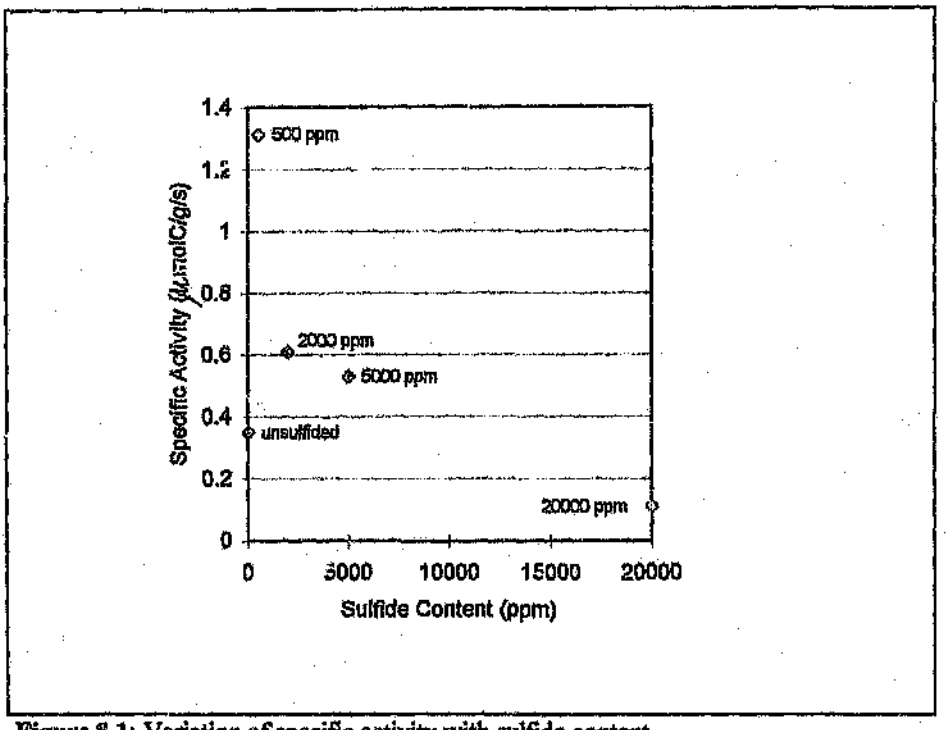


Figure 8.1: Variation of specific activity with sulfide content

The plot of specific activity versus sulfide content passes through a maximum with the addition of 500 ppm S (Figure 8.1). Owing however to the difficulties encountered with ascertaining the precise sulfur incorporation at this level, no attempt was made to prepare sulfided catalysts containing less than 500 ppm S.

The low-level sulfided catalysts which showed enhanced FT activity also exhibited surface sulfate species which were detected by XPS. Formed during high temperature calcination by the segregation of sulfide to the surface, these species affect both the structure and chemistry of the working iron catalyst. TPR evidence (section 8.3.4) shows that sulfate species withstand a reduction temperature of 400°C, and assist with the reduction of hematite to metallic iron. This appears to increase the number of active sites for reaction.

However, as shown in Table 8.1, chemical modification is also evident from the TON (Turnover Number) which refers to the number of CO molecules converted to products per exposed active site [174]. It would appear that low-level sulfidation results in the generation of metal centres with enhanced activity. That the effect is not merely one of increased activity associated with larger available surface area for reaction, is illustrated by the specific activity per unit BET surface area (Figure 8.2). A detailed discussion on the effect of sulfide content on BET surface area is presented in section 8.3.2. Nonetheless, the trend shown in Figure 8.2 is analogous to that in Figure 8.1, confirming the existence of sites with higher activity in low-level sulfided catalysts.

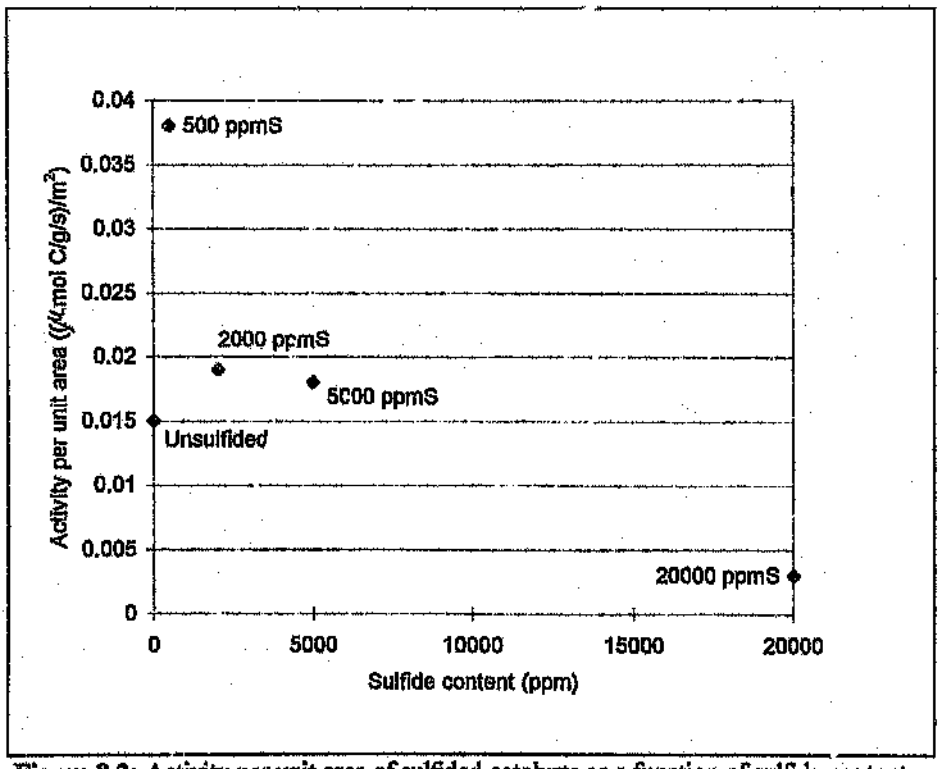


Figure 8.2: Activity per unit area of sulfided catalysts as a function of sulfide content

Improved chain-growth probability was also observed for low-level sulfided catalysts, particularly those to which 2000 ppm S had been added. A significant quantity of wax was produced as indicated by the high α-value (Table 8.1).

There is considerable debate surrounding the use of a single α-value to describe the Schultz-Flory distribution of products from a precipitated-iron catalyst. One opinion has asserted that unpromoted catalysts yield a product slate that can be adequately described using a single chain-growth probability [175]. For alkalized slurry phase catalysts however, Donnelly and Satterfield [176] proposed a double α-distribution calculated using a non-linear semi-logarithmic least squares regression of the volatile C_3 to C_{15} range of the ASF plot. The second α-value showed good correlation with the α-value calculated by linear regression of the plot of the wax sample. To add to the controversy, Davis *et al* determined one α-value for the C_1 to C_{10} fraction and a second for the C_{10}-C_{30} wax product obtained from a precipitated-iron catalyst [29]. In the present study, only one α-value was determined from the C_1-C_{14} range.

Typical α-values of iron based catalysts range from 0.75 to 0.89 and changes can be effected either by the presence of sites suitable for the production of heavier hydrocarbons, or by the re-incorporation of olefins into the growing chain [23]. The addition of alkali promoters has been shown to improve the yield of longer chain molecules, and the presence of small amounts of sulfate in the catalyst sulfided with 2000 ppm S, may achieve similar results as shown in Table 8.1.

Low-level sulfided catalysts also showed a propensity towards the production of olefins (Figure 8.3). Formed according to the following reaction [177],

$$nCO + 2nH_2 \rightarrow C_nH_{2n} + nH_2O$$

α-olefins are among the primary products formed in the FT reaction.

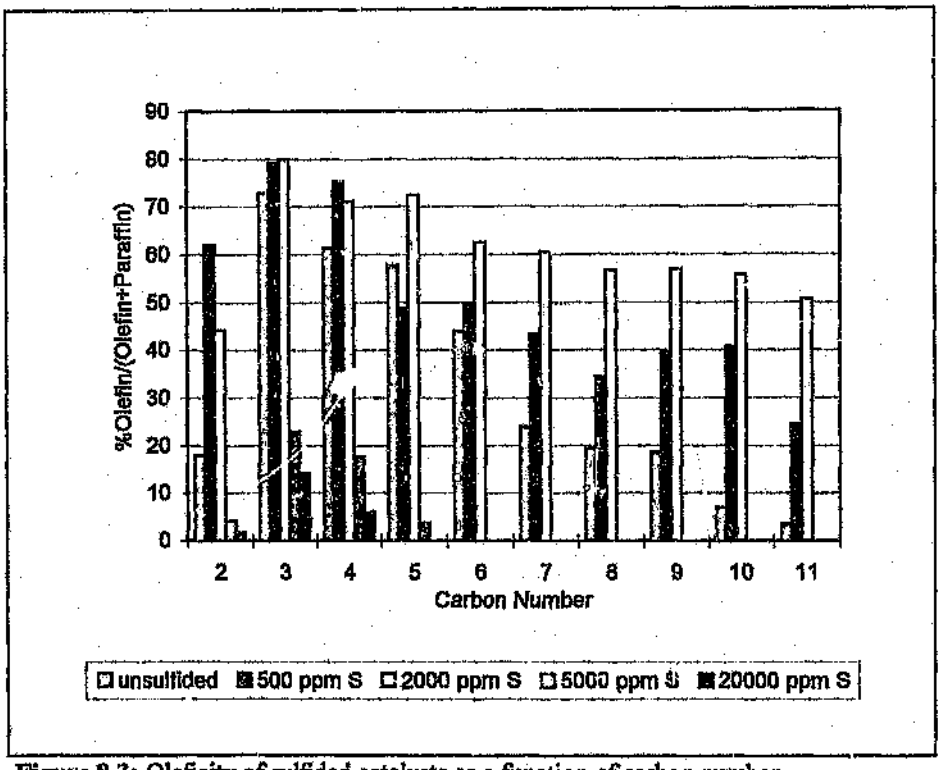


Figure 8.3: Olefinity of sulfided catalysts as a function of carbon number

This observed promotional effect has been corroborated by a study of iron-manganese oxide catalysts containing small amounts of sulfate [46]. According to the authors, the addition of sulfate below 1 wt % resulted in enhanced light olefin selectivity, and reduced methane production. However, it was found that exceeding a S:Fe ratio of 1:200 brought about complete deactivation of the catalyst.

Dictor and Bell [178] reported that alkene selectivity was greater in the presence of potassium. Potassium is known to enhance CO chemisorption at the expense of H_2 chemisorption and this retards hydrogenation activity [179, 28]. An alternative explanation given by Herzog and Graube (in [28]) sugg . . enhanced desorption of alkenes as a result of competitive CO adsorption. This is in keeping with an observation that selectivity for olefins increases with increasing CO conversion [177].

Studies by Bukur *et al* [28] on promoted precipitated-iron catalysts revealed that potassium suppresses the secondary hydrogenation of olefins, resulting in increased olefin selectivity for higher carbon numbers. It is the incorporation of olefins into longer chain molecules that lends the bell shape to the curve in Figure 8.3.

According to a group of workers cited in [180], iron oxide is thought to be an active species for light olefin production, and the addition of non-reducible oxides, such as Ti, V and Mn, is thought to retard the reduction of iron oxide to metallic iron and hence maintain high olefin selectivity. Surface sulfates may function as a source of oxygen, to maintain iron oxides as active sites for olefin production. Alternatively, their role may imitate that of potassium and involve the selective chemisorption of CO and reduced hydrogenation. Furthermore, it has been established that sulfur deactivates hydrogenation sites [48] and this may also account for the improved alkene selectivity.

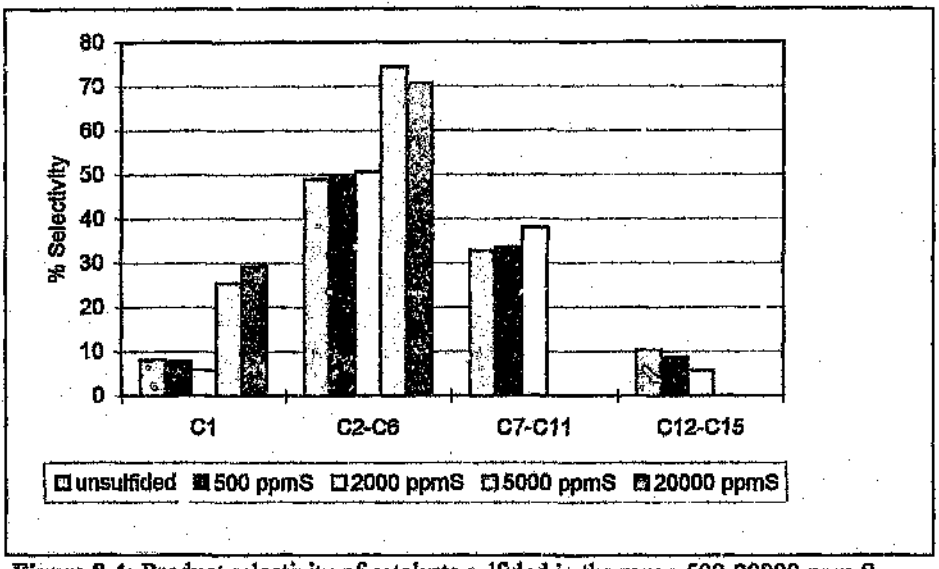


Figure 8.4: Product selectivity of catalysts sulfided in the range 500-20000 ppm S

Interestingly, catalysts containing between 5000 and 20000 ppm S exhibited poor olefin selectivity (Figure 8.3) and functioned essentially as hydrogenation catalysts. Further, a shift in product selectivity toward gaseous light hydrocarbons (Figure 8.4) was observed for these highly sulfided catalysts as evidenced by a low α-value and the absence of any wax formation. The methanation activity was also enhanced by as much as 100% compared to the unsulfided catalyst. The increased selectivity to methane and gaseous C_2-C_4 hydrocarbons is analogous to the observation made by Zhao-Tie Liu *et al* [181] of a co-precipitated Fe-Cu-K catalyst poisoned with COS. The increased methane selectivity is purported to be due to the presence of suitable hydrogenation sites [23].

The value of the TON (10×10^{-3} s^{-1}) calculated for the catalyst sulfided with 20000 ppm S (operating at 10 % CO conversion) can be compared to the 9.3×10^{-3} s^{-1} observed for supported Fe:Co (2:1) catalysts operating at 9.0 % conversion [182].

The decrease in activity of the highly sulfided catalyst may be ascribed to sulfidic species which were detected on the surface using XPS. The deleterious effect of sulfide present at the surface of catalysts is considerable since 8-10 iron atoms are poisoned for every S atom [183]. The electron-withdrawing sulfide reduces electron density on Fe and lowers CO chemisorption [184]. This has the effect of not only lowering activity, but also of producing smaller α-values since the probability of chain propagation is severely retarded.

High methane selectivity is presumed by Donnelly *et al* [176] to be due to the absence of an alkalizing agent, which improves substrate-binding by donating electrons to the active centre. According to Lox *et al* [185], the selectivity to methane is independent of the carbon monoxide conversion. Again the reduced electron density on iron, attributable to sulfide, is responsible for the high methane selectivity observed with highly sulfided catalysts.

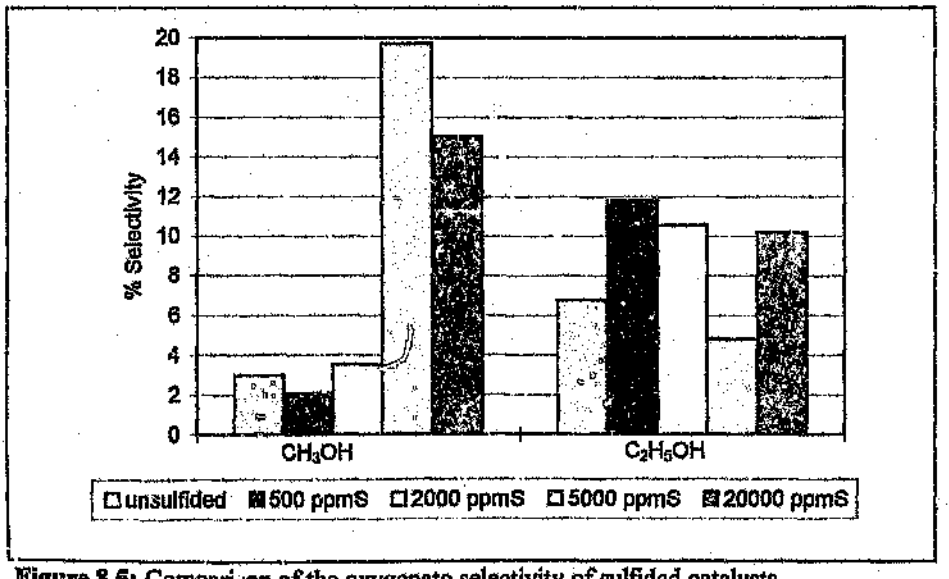


Figure 8.5: Comparison of the oxygenate selectivity of sulfided catalysts

DRIFTS studies of sulfided catalysts revealed the presence of ethoxy groups on the surface during FT reaction (Chapter 5). Hence, the observed propensity towards oxygenates particularly methanol and ethanol (Figure 8.5), is not unexpected and can be rationalised in terms of an increased concentration of reactive ethoxy intermediates. Surface reconstruction brought about through the presence of sulfur, has been known to result in a higher concentration of suitable adsorption sites for reactive intermediates [149]. Similar sentiments are echoed by Baker *et al* [186].

Stable alkoxy intermediates have been shown to form on Fe (100) surfaces during Fischer-Tropsch synthesis [148]. Furthermore, both methoxide and ethoxide species react to give CH_4 and C_2H_6 as well as alcohols. Thus higher methanol selectivity is associated with higher yields of methane, as found for highly sulfided catalysts.

Primary alcohols are incorporated into other Fischer-Tropsch products, while secondary and tertiary hydroxyls are not able to form stable intermediates due to steric constraints [148]. However, as a consequence of reduced interaction between the catalyst surface and products formed on sulfided catalysts, re-incorporation of primary alcohols is not observed.

The only oxygenate observed on an unalkalized precipitated-iron catalyst was methanol [176]; however, promotion by potassium yielded a range of higher alcohols. It has been shown by Orita *et al* [187] that C_2 oxygenate formation occurs in two stages, the first resulting in the formation of a methyl group as carbon becomes available after CO dissociation.

Based on mechanistic studies, Ponec *et al* purported that the second stage proceeded via CO insertion [150]. For the higher alcohols, a chain growth scheme proposed by Smith and Anderson [188] assumes carbon addition at the α- or β- carbon atom of the growing alcohol. Large methanol selectivities are shown to result from the rate-limiting α-addition step.

8.3.2. Surface Morphology of sulfided catalysts

BET surface area measurements (Table 8.2) were made prior to calcination, and the data revealed that increasing the level of sulfidation resulted in an increase in surface area (from 58 m^2/g to a maximum value of 166 m^2/g at 2000 ppm).

Table 8.2: Surface areas of sulfided catalysts

Catalyst	Pre-calcination Surface area (m^2/g)[a]	Post-calcination Surface area (m^2/g)[b]	Post-reaction Surface area (m^2/g)[b]
unsulfided	58	23.1	8.82
500 ppm S	97	34.8	7.88
2000 ppm S	166	37.1	3.04
5000 ppm S	104	39.0	16.09
20000 ppm S	85	40.7	20.61

[a] single point BET measurement performed on in-house equipment
[b] determined from multi-point BET measurements

Beyond this maximum at 5000 ppm S, the surface area was found to decrease, but even at a sulfidation level of 20000 ppm the BET value was 85 m^2/g, which is still higher than the unsulfided catalyst (Figure 8.6).

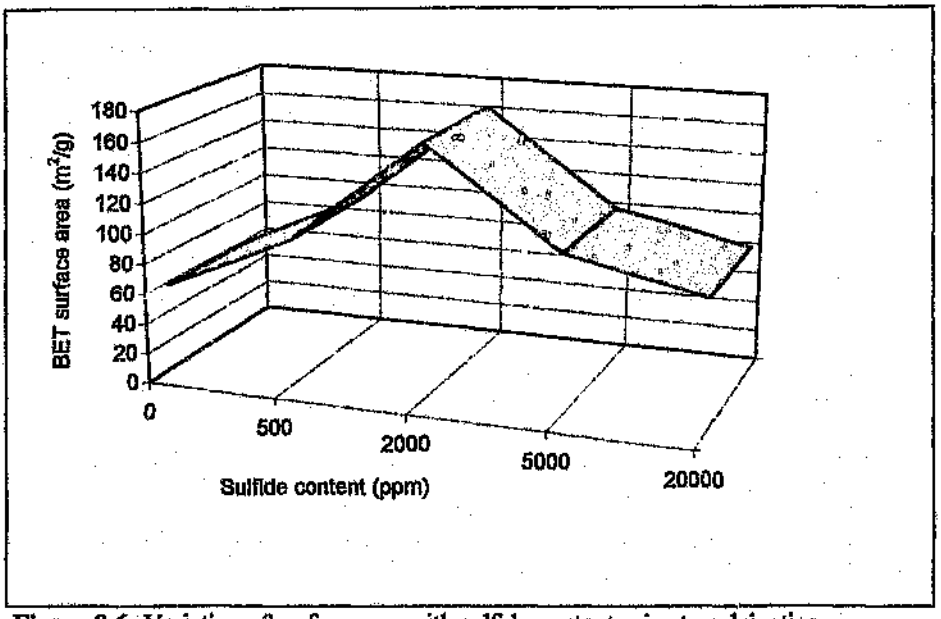


Figure 8.6: Variation of surface area with sulfide content prior to calcination.

Traditionally, mechanisms advanced to account for an increase in the surface area of catalysts have generally invoked the participation of a support of some kind. However, there are reports of the effect of additives on the surface area of unsupported catalysts [31, 75]. Furthermore, Kölbel *et al* (cited in [28]), have reported that the addition of small amounts of potassium to precipitated-iron catalysts stabilized the surface area of iron oxyhydroxides, and protected the surface against re-crystallization during calcination.

The growth of iron crystallites is presumed to involve subsequent layers being deposited on existing layers, such that the surface becomes a manifestation of the core structure. The addition of sulfide ions appears to affect the morphology of the growing precipitate in such a way as to render it more porous.

A further issue, is that while iron-sulfide may be instrumental in assisting with the epitaxial growth of crystallites *during* precipitation, reconstruction of the entire crystallite may occur as nascent sulfur is released at the end of the formal precipitation stage of catalyst preparation [12]. A possible reaction proposed by van der Kraan *et al* [189] relates to the sulfidation of hydrated Fe_2O_3:

$$Fe_2O_3.H_2O + 3H_2S \rightarrow 2FeS + 4H_2O + S$$

Therefore, vacancies created by the loss of free sulfur may account for the increase in porosity of sulfided catalysts.

After calcination to remove nitrates and other possible surface contaminants, the available surface area is observed to decrease as a result of pore collapse (Table 8.2). It was also found that the most highly sulfided catalysts, those to which 20000 ppm S had been added, appeared to be significantly resistant to pore collapse. Again, the sulfide ions may be instrumental in increasing the resistance to pore collapse by acting as a support, hence maintaining the dispersion of the iron centres.

The trend in total pore volumes (Table 8.3) is analogous to that found for surface areas, and once again reaches a maximum between 2000 and 5000 ppm S. After calcination, pore volumes decrease owing to a collapse in the bulk structure.

Table 8.3: Total Pore Volumes of Sulfided Catalysts

Catalyst	Pre-calcination Pore Volume (cm^3/g)	Post-calcination Pore Volume (cm^3/g)	Post-Reaction Pore Volume (cm^3/g)
unsulfided	0.184	0.120	0.035
500 ppm S	0.241	0.202	0.020
2000 ppm S	0.254	0.245	0.004
5000 ppm S	0.338	0.338	0.035
7000 ppm S	0.281	0.304	0.032

One explanation for loss of pore volume after reaction is that carbon deposition could cause pore blockage in the active catalysts. Since no FT activity was observed on highly sulfided catalysts, the pore volumes are unaffected by by carbon laydown and merely reflect the structure of bulk α-Fe with an oxidised surface.

8.3.3. Influence of sulfide on catalyst reduction temperature

Temperature Programmed Reduction was employed to elucidate the reduction profile of these catalysts. The reduction profile of the unsulfided catalyst (Figure 8.7a) is typical of the two-stage reduction of hematite [190]:

$$3Fe_2O_3 + H_2 \rightarrow 2Fe_3O_4 + H_2O \qquad \text{(i)}$$

$$Fe_3O_4 + 4H_2 \rightarrow 3Fe + 4H_2O \qquad \text{(ii)}$$

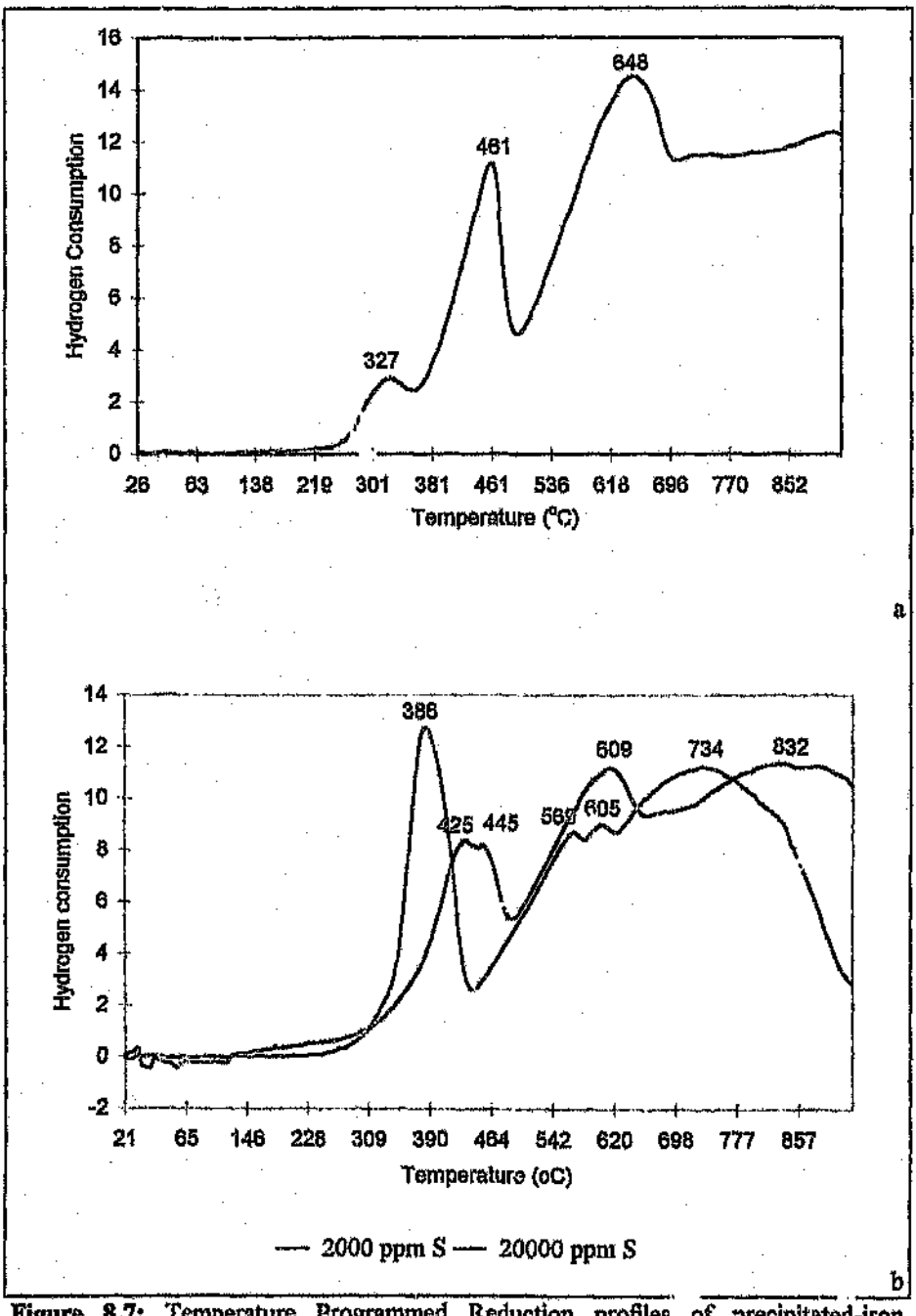


Figure 8.7: Temperature Programmed Reduction profiles of precipitated-iron catalysts: **a)** Unsulfided catalyst **b)** Catalyst sulfided with 2000 ppm S superimposed on catalyst sulfided with 20000 ppm S

A complete phase diagram for the reduction of bulk iron-oxide in mixtures of H_2 and H_2O is given in Figure 8.8:

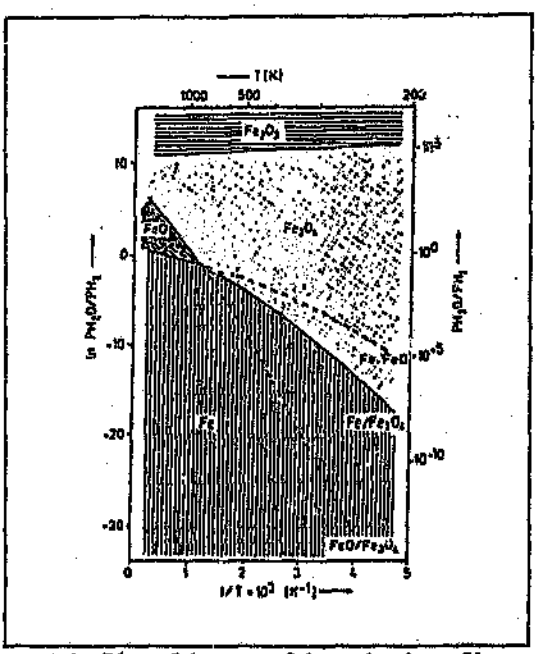


Figure 8.8: Phase Diagram of the reduction of iron oxide [52]

Physisorbed water would also increase the temperature of reduction as shown in Figure 8.8, particularly for the transition of Fe_3O_4 to Fe. Activation energies of the reduction of magnetite to metallic iron were estimated from Arrhenius plots and found to be 172 kJ/mol in wet hydrogen and 111 kJ/mol in the absence of H_2O [190].

Work by Wimmers *et al* [190] on unsupported Fe_2O_3 particles revealed that the formation of metallic iron nuclei at the surface of particles of Fe_3O_4 is the rate-limiting step for the reduction of magnetite. Based on this, a nucleation and growth model was proposed to describe the reduction of Fe_3O_4 to Fe [52]. This model applies when the initial reaction of oxide with molecular hydrogen is difficult.

As soon as metallic nuclei are formed however, the rate of reduction increases until hydrogen diffusion becomes limiting [52]. The latter scenario can be rationalised by the contracting sphere model [76]. Therefore, any agent which promotes the removal of oxygen from the iron-oxide lattice would assist with reduction.

The reduction profiles of catalysts sulfided with 2000 and 20000 ppm S are shown in Figure 8.7b. Several differences between the spectra are immediately apparent. Firstly, the temperature of the hematite-magnetite transition is lowered (425→386 °C) as the sulfur content is increased. This trend is summarised in Figure 8.9 and was found irrespective of the sulfide source used.

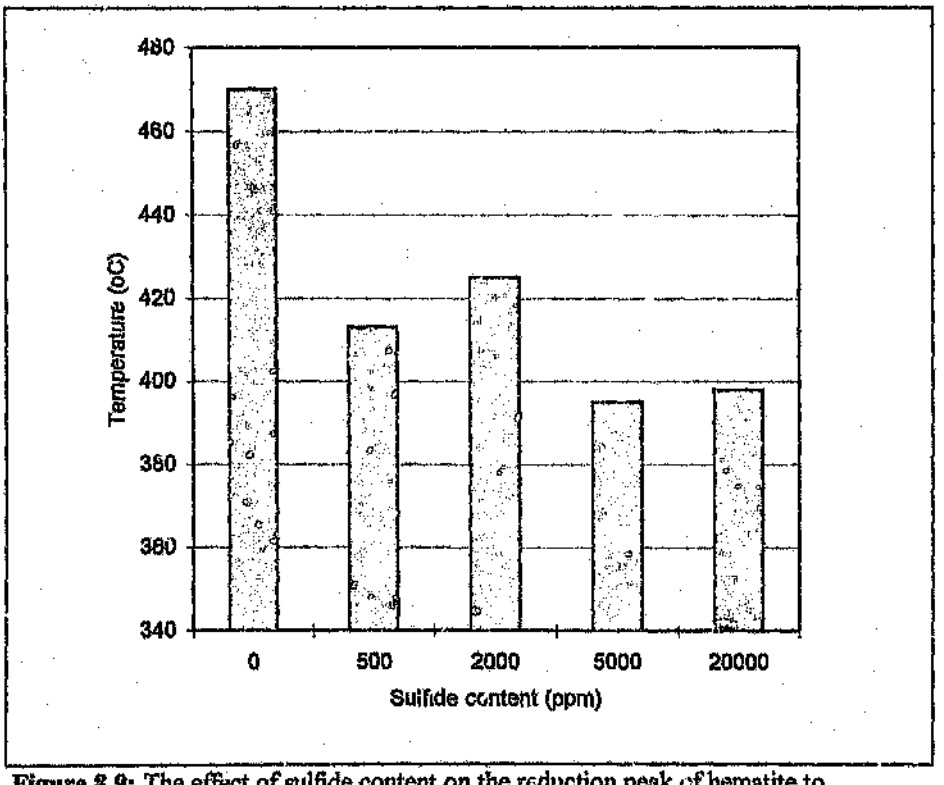


Figure 8.9: The effect of sulfide content on the reduction peak of hematite to magnetite for precipitated-iron catalysts

Independent XPS measurements (Chapter 4) revealed that the higher the level of sulfidation, the greater the amount of segregation of sulfur to the surface of catalysts under reducing conditions. Through the process of site competition [114], this surface enrichment of sulfur is accompanied by a rapid depletion of surface oxygen. The oxygen in turn, would be reactive towards molecular hydrogen and produce water. Equation 8.1 describes the effect of water on the thermodynamics of iron-oxide reduction [52].

$$\Delta G = nRT\ln\left[\left(\frac{p_{H_2O}}{p_{H_2}}\right)/\left(\frac{p_{H_2O}}{p_{H_2}}\right)_{eq}\right] \quad \ldots\ldots\ldots\ldots\ldots\ldots 8.1$$

For the reduction of Fe_2O_3 at 400°C, the equilibrium ratio of $p(H_2O)/p(H_2)$ has been found to be 0.7 [52]. Hence, to ensure that reduction is thermodynamically feasible, the experimental ratio of $p(H_2O)/p(H_2)$ must be smaller than the equilibrium value of 0.7, and consequently the efficiency with which water is removed becomes a decisive factor in determining reduction temperature [52].

Since the TPR experiments performed in this study were conducted in flowing hydrogen, the water formed *in situ* would have been efficiently removed from the system so that it did not retard the reduction process. On the contrary, the depletion of oxygen facilitated the conversion of hematite to metallic iron, because at high temperatures, the partial pressure of water would be lower for sulfided catalysts. As shown in Figure 8.8, reduction commences at a lower temperature when the ratio $p(H_2O)/p(H_2)$ is decreased.

In removing oxygen from the surface of the catalyst, sulfur also allows the formation of metallic iron nuclei. This accelerates the rate-limiting step of the reduction process, that being the transition of magnetite to metallic iron [190]. It follows then that the greater the sulfide content, the more pronounced the effect on the reduction process. As shown in Figure 8.9, the temperature of the reduction of hematite to magnetite is significantly lowered in the presence of increasing amounts of sulfide. The maximum rate of hydrogen consumption for the catalyst sulfided with 20000 ppm S is 70°C lower than in the absence of sulfur. Surface area measurements indicated that these highly sulfided catalysts were resistant to pore collapse and hence the iron centres would have remained fairly well dispersed after calcination pretreatment. This may also contribute to improved reduction behaviour.

A further difference apparent from Figure 8.7b is the additional peak at 445°C which is exhibited by low-level sulfided catalysts, and has been assigned to the reduction of sulfate to sulfide. This assignment was confirmed with a TPR experiment conducted on $Fe_2(SO_4)_3$, which yielded a bimodal reduction profile. For ferric sulfate, the first peak at 450°C is due to the reduction of sulfate to iron sulfide; and the second at 850°C to the reduction of bulk FeS to metallic iron [191]. XRD measurements by Inamura *et al* [192] revealed that triolite (FeS) is the iron sulfide phase reduced at a temperature of 850°C.

Sulfate species are associated with oxygen atoms at the surface and indicate incomplete reduction. According to the XPS measurements, sulfate species were not present on the surface of the highly sulfided catalysts following reduction at 400°C.

Consequently, there is no reduction peak at 445°C in the TPR profiles of these catalysts. However, the high temperature region clearly shows the reduction of FeS to metallic iron and H_2S. In a study of sulfided transition metal catalysts, Mangnus *et al* observed that the hydr consumption between 1000 and 1200 K far exceeded the H_2S production [191]. This suggests that a contribution from metallic iron is included in this peak. Thus the large high temperature peak observed in the TPR profile of the catalyst sulfided with 20000 ppm S is the hydrogen consumption due to the reduction of FeS, as well as a contribution from metallic iron. Nonetheless, the pyrophoric behaviour of reduced highly sulfided catalysts is testimony to the complete conversion of hematite to metallic iron which has taken place at 400°C. Compositional analysis of the surface of reduced sulfided catalysts by XPS confirmed the presence of larger quantities of iron on the surface of these catalysts by comparison with the unsulfided sample.

Since all catalysts were reduced at 400°C, and the temperature of hematite reduction is lowered as a consequence of high sulfide content, it is possible that the degree of reduction should vary considerably for the range of catalysts investigated. And, according to workers who studied the effect of reduction of a fused magnetite catalyst [178], increasing the extent of reduction resulted in substantial increases in activity, which were attributed to an increase in pore surface area. Therefore, sulfided catalysts may be expected to be more active than the catalyst containing no extraneous sulfur, purely as a result of a higher degree of reduction. However, it will be shown *vide infra* (in chapters to follow) that the effects of sulfur on activity involve more than the extent of reduction of iron brought about through the presence of sulfur.

8.3.4. Bulk morphology of sulfided catalysts after FT reaction

Carbide formation, associated with Fischer-Tropsch activity, was observed by XRD to occur to a greater extent on catalysts sulfided with between 500 and 2000 ppm S (Figures 3.11 and 3.12c) than on the unsulfided catalyst. Iron carbides are widely regarded as the active sites for hydrocarbon synthesis [177]. Also evident from the diffractograms of the low-level sulfided catalysts is that magnetite constitutes the iron-phase present after reaction. The existence of an oxide phase indicates that sulfate species are likely to remain on the surface even after exposure to synthesis conditions. Indeed, Tof-SIMS analysis of the spent catalyst sulfided with 2000 ppm S confirmed the presence of surface sulfate species [193].

What phase is active for Fischer-Tropsch synthesis?

The working iron catalyst is composed of many phases, including α-Fe, Fe_3O_4 and Fe_xC. However, there is much controversy as to which of these is catalytically active for FT synthesis. In 1982, Reymond *et al* [194] observed that active carbon species were formed more abundantly on Fe_3O_4 than α-Fe. This led to the supposition that magnetite constituted the active phase. Later, this was disproved by Shroff *et al* [195] who observed no initial FT activity on a catalyst composed only of magnetite; only that small amounts of CO_2 were formed. Similarly, other researchers found poor results when attempting FT synthesis on magnetite [196].

It has also been contended that metallic iron is the phase that is active for the Fischer-Tropsch reaction. For instance, in a study of iron-manganese catalysts, metallic iron was found to be responsible for initial activity [197]. However, it has been argued that

complete reduction to metallic iron is undesirable since it leads to an inactive catalyst [195]. Once again this is the opinion of Shroff *et al* (amongst others) and follows an observation that only after carbiding had occurred did a catalyst develop FT activity. The catalyst that had been completely reduced to metallic iron did not carbide easily and this was the reason given by the authors for the poor activity. In contrast, a catalyst containing some residual magnetite, ie., partially reduced, was rapidly carbided and hence exhibited high CO conversion [195]. According to Shashkin *et al* [196], high catalytic activity is linked to the presence of χ-iron carbide and non-stoichiometric magnetite, the latter being about 30 % deficient in Fe^{3+} and O^{2-}. These defects are purported to facilitate diffusion through the cationic and anionic sub-lattices. It has also been suggested that the carbide phase consists of discrete porous aggregates as well as intercalating inclusions in the magnetite [196].

This has promulgated the theory that iron carbide is a prerequisite for active FT catalysts. However, while many authors concur that carbides are vital, there is considerable speculation as to the precise nature of their involvement. It has been asserted by Matsumoto [198] and other workers [199] that carburization of iron catalysts plays an important role in the formation of active surfaces. A second school of thought shares the opinion that carbidic carbon is the reactive intermediate in hydrocarbon synthesis. This relates to the "carbide mechanism" first proposed by Fischer and Tropsch [33]. Evidence against the latter was presented by Matsumoto, who observed that hydrogenation of carbidic carbon took place at temperatures as high as 400°C, while hydrocarbon synthesis (such as that found in the FT reaction)

proceeded at 250°C. Hence it was deduced that carburization contributed not to the formation of reactive intermediates, but to the creation of active surfaces [198].

The term *carburization* has been used by Jensen *et al* [172] to describe 'the surface and bulk property changes that occur to many Fischer-Tropsch catalysts'. These so-called changes refer to the diffusion of carbon atoms from the surface of the catalyst to the bulk during the start-up period of FT synthesis. According to the competition model proposed by Niemantsverdriet *et al* [200], this induction period is associated with low activity as bulk carbiding takes place. As soon as this process is complete, the formation of hydrocarbons is initiated. Hence, the overwhelming tendency for CO to dissociate on reduced Fe can be considered to be due (at least partially) to a thermodynamic driving force for bulk carburization [131]. Therefore, although metallic iron itself showed little catalyst activity, carburization resulted in a dramatic increase in the rate of FT synthesis [198]. Metallic iron is neccesary for carbiding to occur, hence the need for reduction pretreatment. However, the presence of magnetite in conjunction with the carbide phase creates an active catalyst.

From the foregoing arguments, it is apparent that while there is still some heated debate over what constitutes the "active phase " in FT catalysts, the evidence for iron-carbides is overwhelming. Certainly in the present study, highly active catalysts appeared to exhibit a greater degree of carburization than the unsulfided catalyst. Hägg carbide was identified as the major carbide phase using Mössbauer spectroscopy (Chapter 6) and X-Ray powder diffraction (Chapter 3). In addition, magnetite was also shown to be a component of highly active catalysts.

X-Ray diffraction studies and Mössbauer spectroscopy of spent catalysts sulfided with 20000 ppm S did not reveal the presence of any bulk carbide. These catalysts were shown by TPR studies to be completely reduced to α-Fe during hydrogen activation at 400°C. Furthermore, highly sulfided catalysts gave low CO conversions and only metallic iron was identified by post-reaction XRD and Mössbauer spectroscopy. It is also interesting to note that, at low conversions, syngas is reducing in nature, and the oxidising properties of the reactant gas mixture increase with increasing conversion due to the formation of water [201]. This ensures that magnetite is maintained as a phase in the active catalysts.

This finding supports the hypothesis that carbide formation is a requirement for active FT catalysts. It also suggests that complete reduction to metallic iron in the presence of sulfur creates an environment that is not conducive to carburization. These sentiments were echoed by Rapoport and Muzovskaya who proposed that iron oxides were necessary to avoid complete deactivation by sulfur [43].

4. Conclusion

The addition of sufficiently small quantities of sulfide is observed to result in modifications of iron oxyhydroxide morphology in terms of enhanced surface area and porosity. These features are a manifestation of a precipitation process involving epitaxial growth of crystallites which have incorporated iron-sulfide into their structure. Similarity in crystallographic orientation between the iron sulfide and hematite gives rise to an iron-oxide phase with improved crystallinity.

Through the phenomenon of site competition, sulfur segregates under conditions of calcination and reduction pretreatment. The forced removal of oxygen from the surface assists with the reduction of hematite to metallic iron.

Low-level sulfided catalysts exhibited sulfate species on their surfaces which improved Fischer-Tropsch activity. These sulfate groups are also associated with higher olefinity and oxygenate selectivity. A higher concentration of reactive alkoxy intermediates are purported to be responsible for oxygenate selectivity. The presence of sulfate species confirms that only partial reduction has taken place after exposure to hydrogen at 400°C, and this may also account for the observed sulfur resistance of these catalysts. The importance of iron-oxides in resisting poisoning by sulfur has been alluded to in previous studies [43].

Highly sulfided catalysts on the other hand, are reduced to metallic iron rapidly by exposure to hydrogen and hence exhibit a high surface concentration of sulfide. Each sulfide atom has been shown to poison 8-10 atoms of iron [183] and this may account for the poor FT activity of these catalysts. A propensity towards methane and light hydrocarbons clearly reflects sulfur poisoning.

The identity of the phase active for FT synthesis has long been a bone of contention amongst research groups. In the present study, the poor FT activity associated with α-Fe surfaces which have high sulfide levels suggests that iron carbide is the active phase for Fischer-Tropsch synthesis. The formation of Hägg carbide is enhanced on the highly active low-level sulfided catalysts, while no carbiding is observed on highly sulfided catalysts which were reduced to α-Fe.

Chapter 9

The effect of sulfide source on the performance of sulfided precipitated-iron Fischer-Tropsch catalysts

9.1. Introduction

The sulfidation of iron catalysts does not only involve the addition of sulfide ions to a hematite matrix. To maintain electrical neutrality, cationic species are necessarily associated with the sulfide ions. Since there is no reason why these counterions should not be occluded by the growing precipitate, it follows that the source of sulfide could impact upon the activity of precipitated-iron catalysts. To this end, a study was undertaken involving the addition of three different sulfides, namely Na_2S, $(NH_4)_2S$ and $(NH_4)_2S_5$, to iron catalysts in an attempt to quantify the effect of sulfide source on FT activity.

Sodium ions are commonplace promoters of iron Fischer-Tropsch catalysts and assist with improved olefin activity and suppressed methane selectivity [173]. Their mode of action is based on inductive electron donation to iron which weakens the C-O bond of adsorbed carbon monoxide, and hence facilitates carbide formation. Ammonium is another common counter-ion associated with sulfide species. During calcination it decomposes to ammonia which is lost from the surface [202] and hence should not impact on catalytic behaviour.

Finally, the identity of the sulfide ion is important to consider, since longer chain polysulfides might be expected to confer different catalytic properties to monosulfides.

To better understand the effects of the sources of sulfide on the morphology and function of precipitated-iron catalysts, a study was undertaken using catalysts sulfided at pH 10.75 with 2000 ppm sulfide.

9.2. Experimental

In order to assess the possible effect of the source of sulfide, all catalysts were sulfided with 2000 ppm S at pH 10.75. Sodium sulfide (Na_2S), ammonium sulfide ($(NH_4)_2S$) and ammonium polysulfide ($(NH_4)_2S_5$) were used as sulfide sources.

Sulfided catalysts were calcined and reduced at 400°C prior to commencing Fischer-Tropsch synthesis at 250°C and 8 bar pressure (GHSV = 400 h^{-1}). Gaseous and light liquid hydrocarbon fractions were analysed by on-line gas chromatography; while the separation of long-chain waxes was achieved using an off-line gas chromatograph equipped with a capillary column.

9.3. Results and Discussion

The surface areas of pre-calcined catalysts, sulfided using various sources, are substantially different (Table 9.1). Indeed, all sodium sulfide catalysts possessed larger surface areas than catalysts sulfided using ammonium-derived sources. Furthermore, polysulfided catalysts generally yielded smaller areas than their monosulfided analogues.

Table 9.1: Surface Areas of catalysts sulfided at pH 10.75 with 2000 ppm S

Sulfide source	Pre-calcination surface area (m^2/g)	Post-calcination surface area (m^2/g)	Post-reaction surface area (m^2/g)	Crystallite size (Å) (un calcined)
Na_2S	269	36.8	9.95	180
$(NH_4)_2S$	130	24.2	5.70	226
$(NH_4)_2S_5$	60	25.2	3.20	245

After calcination, the areas are more alike, yet the catalyst sulfided with sodium sulfide still has the largest surface area. It is also more porous than the other catalysts studied (Table 9.2). As discussed in Chapter 3, catalysts sulfided with small quantities of sulfide (50 -2000 ppm) exhibit cylindrical pores which permit easy access to active sites.

Table 9.2: Pore volumes of catalysts sulfided at pH 10.75 with 2000 ppm S

Sulfide source	Pre-calcination pore volume (cm^3/g)	Post-calcination pore volume (cm^3/g)	Post-reaction pore volume (cm^3/g)	Average pore diameter (Å) (calcined)
Na_2S	0.298	0.283	0.05	307
$(NH_4)_2S$	0.245	0.243	0.013	400
$(NH_4)_2S_5$	0.206	0.198	0.02	350

Temperature programmed reduction studies revealed that the reduction of Fe_2O_3 occurs at a marginally lower temperature when sodium sulfide is used Furthermore, the reduction peaks for the ammonium based catalysts are nearly identical to each other (Table 9.3). As previously stated, ammonium ions readily convert to ammonia during heating, and thus this counter-ion escapes from the surface.

Table 9.3: Temperature Programmed Reduction of sulfided iron catalysts

Sulfide source	$Fe_2O_3 \rightarrow Fe_3O_4$ (°C)[a]	$SO_4 \rightarrow S^{2-}$ (°C)	$Fe_3O_4 \rightarrow Fe$ (°C)	$FeS \rightarrow Fe$ (°C)
Na_2S	411	460	629	853
$(NH_4)_2S$	417	452	605	854
$(NH_4)_2S_5$	418	485	612	850

[a] Unsulfided catalyst, reduction temperature = 461°C

No particular trends are evident for the reduction of sulfate to sulfide, or the formation of metallic iron from magnetite (Table 9.3); and the reduction of FeS appears unaffected by sulfide source. Alkali promotion is purported to lower the temperatures of reduction by accelerating the removal of hydroxyl groups from the surface.

Table 9.4: Reactor Data of catalysts sulfided with 2000 ppm S from different sources

Sulfide source	% CO conversion	α-value	Specific Activity (μmolC/s/g)	Activity/ unit area	Sodium content (ppm)
Na_2S	56	0.78	0.70	0.019	0
$(NH_4)_2S$	66	0.81	0.71	0.029	2
$(NH_4)_2S_5$	57	0.80	0.64	0.025	26

All catalysts investigated exhibited higher activity than the unsulfided catalyst (specific activity = 0.35 μmolC/g/s as shown in Chapter 8). Moreover, the promotional effect appears to be independent of the sulfide source. It is the slightly larger surface area of the sodium sulfided catalyst which may account for the higher activity shown in Table 9.4, especially since the activity per unit area is not as high as found for the other catalysts. This finding, in conjunction with the sodium content of the catalyst sulfided with Na_2S, confirms that the abovementioned effect is sulfidic in origin and not sodium-based.

According to the speciation model generated using different sulfide sources (Chapter 7), the choice of cation has no effect on the solution species. The addition of Na_2S does not appreciably increase the total dissolved sodium concentration. Furthermore, in the case of ammonium sulfided systems, the predicted NH_4^+ (aq) concentration is extremely low owing to the $NH_4^+ \leftrightarrow NH_3$ (aq) equilibrium lying very far towards the right.

Polysulfided systems, by contrast, appear very different to their monosulfided analogues. At each of the sulfidation pH values, the distribution of aqueous sulfide species favours S_5^{2-} to the extent that it contributes more than 95% of the dissolved sulfide concentration. However, this species is not expected to precipitate, and remains in solution possibly as a polysulfane, S_4SH_2 [19]. Consequently, as with monosulfides, the "pivotal" chemical species in these systems are not polysulfides, but $Fe(HS)_x$ and FeS. And it is for this reason that very minor differences exist between mono- and polysulfided catalysts.

The existence of HS^- in polysulfided systems comes as a result of disproportionation: $S_5^{2-} \leftrightarrow HS^- + S_4^{2-}$ [19]. This hydrosulfide ion (HS^-) is then responsible for the formation of aqueous ferrous sulfides, which precipitate as FeS, in analogous fashion to monosulfided systems. Only in the latter case, is the complexation of added S^{2-} as ferrous sulfide at pH 6.9 almost quantitative, while the proportion of added polysulfide that precipitates as FeS is extremely small. The implication for polysulfided catalyst morphology is that larger crystallites are formed, and this explains the smaller total surface areas exhibited by these catalysts (Table 9.1). Indeed, XRD analysis of minor crystalline phases, revealed that polysulfided catalysts contained less FeS than catalysts sulfided from other sources. Moreover, the speciation model (Chapter 7) predicted that the FeS concentration in monosulfided systems should be 100 fold that found in polysulfided precipitates.

The prediction that all S_5^{2-} would remain as aqueous species does not preclude the incorporation of these entities by the process of occlusion. The larger size of the pentasulfide ion would disrupt the crystallinity of the precipitate and result in it being forced to the surface of the iron-oxide particles. As a result, just as nitrate and carbonate ions decorate the surface of dried precipitates, so too might polysulfide species. This would rationalise the observation made using XPS, showing the presence of at least a trisulfide on the surface of a reduced polysulfided catalyst. As discussed in Chapter 4, which deals with the XPS study, the polysulfide was only detected on the surface of the catalyst sulfided with 20000 ppm $(NH_4)_2S_5$. No source-related effects were found for low-level sulfided catalysts, where only sulfate species were observed following reduction and calcination.

Alkali promoters improve the chain-lengthening capacity of FT catalysts, and hence give a product distribution characterised by higher α-values [32]. No such effect is seen for the catalyst sulfided with Na_2S, and indeed there is little variation between the α-values obtained using any of the sulfiding agents (Table 9.4). Furthermore, the product selectivity is essentially identical (Figure 9.1), since the variation between catalysts is within 10 % for each of the product fractions.

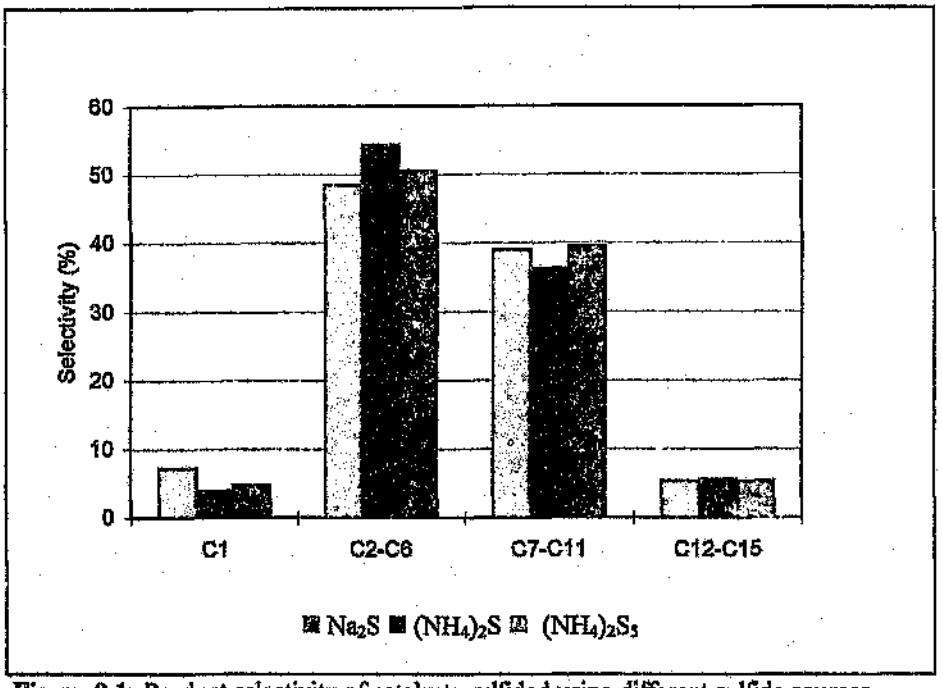


Figure 9.1: Product selectivity of catalysts sulfided using different sulfide sources

Oxygenate selectivities were also very similar (Figure 9.2), and only the sodium sulfided catalyst exhibited a marginally higher yield of ethanol. This was accompanied by a greater propensity towards methane production than the other catalysts.

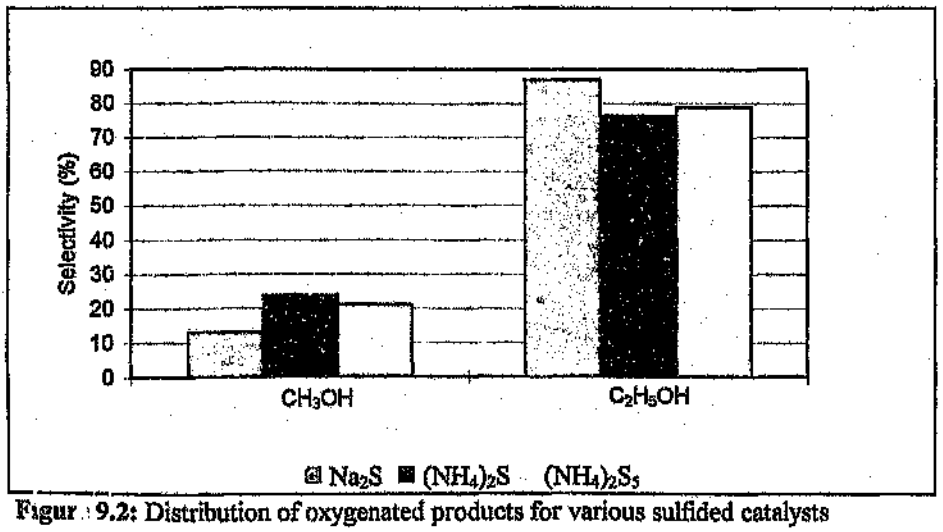


Figure 9.2: Distribution of oxygenated products for various sulfided catalysts

Little variation in the olefinity of hydrocarbons of these three catalysts is to be found, except that the polysulfided catalysts appeared to produce slightly less olefinic products than the monosulfided catalysts (Figure 9.3).

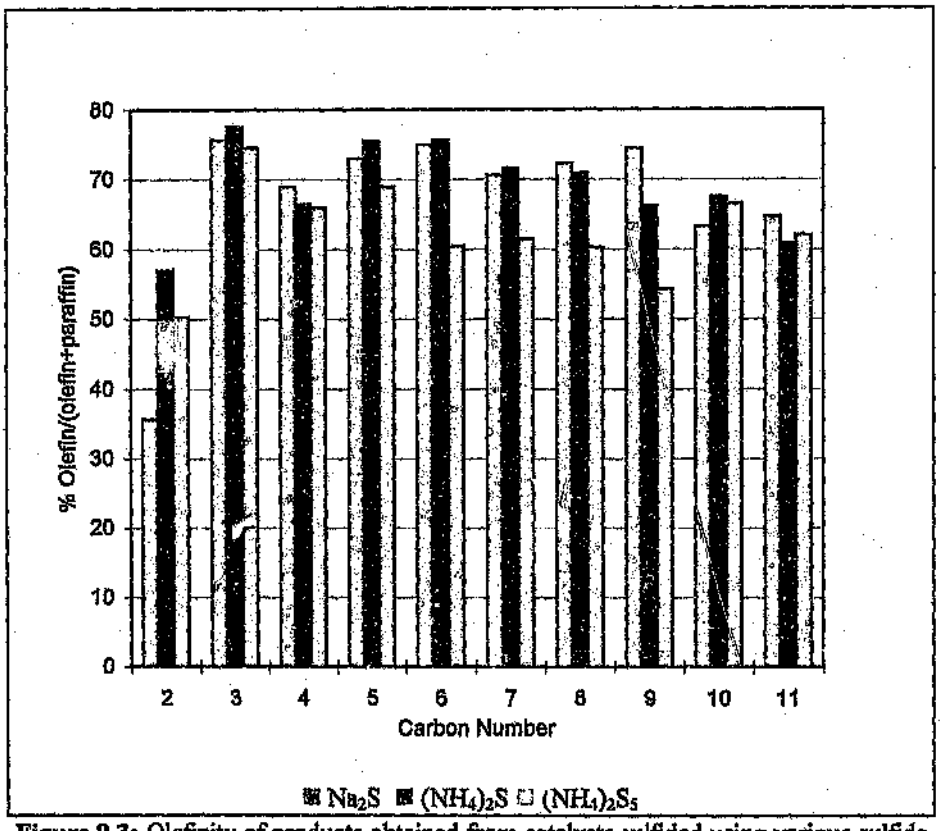


Figure 9.3: Olefinity of products obtained from catalysts sulfided using various sulfide sources

9.4. Conclusion

The addition of sulfide from different sources does not significantly affect the distribution of products. This stems from the finding that HS^- ions are the critical species in determining catalyst morphology. In monosulfided systems, all added sulfide is protonated to yield hydrosulfide, while less than 10 % of polysulfide added is hydrolysed to HS^-. Consequently, the monosulfided catalysts exhibit similar morphologies in terms of crystallite size and surface area. The reduced FeS concentration in polysulfided catalysts results in larger crystallites with low surface areas.

Aqueous S_3^{2-} ions may become occluded by the growing precipitate and hence form part of the precipitate. These species are fairly large, and their incorporation into an iron oxide crystallite may disrupt the crystallinity of the material. During catalyst pretreatment, decomposition of the pentasulfide is expected, although the detection of at least a trisulfide suggests this decomposition to be kinetically unfavourable.

Chapter 10

The effect of sulfidation pH on the morphology and function of sulfided iron Fischer-Tropsch catalysts

10.1. Introduction

The Fischer-Tropsch process is propos[illegible] a small ensemble reaction, involving clusters of atoms that constitute active sites [203]. As a result, FT synthesis is sensitive to the structure and composition of the catalysts used.

Generally, the morphology of a catalyst can be inferred from measurements of surface area, pore volume, reduction behaviour, and so on. With specific reference to precipitated catalysts however, a knowledge of the solution chemistry pertaining to the aqueous precipitation system is also essential in the elucidation of bulk structure.

The species that determine the composition and structure of a precipitate are those which are the most stable under the various conditions of pH, temperature and concentration. It follows that there are many synthetic variables that can be manipulated to achieve the precipitation of materials with ranging morphology. The effects of sulfide source and content on the s[illegible]ture of sulfided precipitated-iron catalysts have been dealt with in previous chapters (see Chapters 8-10). Herein, the pH of sulfide addition as a synthetic variable is discussed in terms of catalyst morphology, and the consequences for FT activity.

Equilibria involving sulfur-containing species are important for understanding the chemistry of sulfidation of catalysts at selected pH values. Pourbaix diagrams, constructed from electrode potential data and acid dissociation constants, describe the conditions of Eh (electrochemical potential) and pH for which various species are stable [18]. Equilibrium diagrams for the S-H_2O system are available at temperatures ranging from 0° to 150° C [204], thus permitting assessment of the equilibria at play under a variety of experimental conditions.

Although, in this study, the precipitation of iron catalysts was done at 75°C, no Eh-pH diagram was available for this temperature. Instead, the Pourbaix diagram for the S-H_2O system at 100°C is shown below (Figure 10.1) [adapted from 204]:

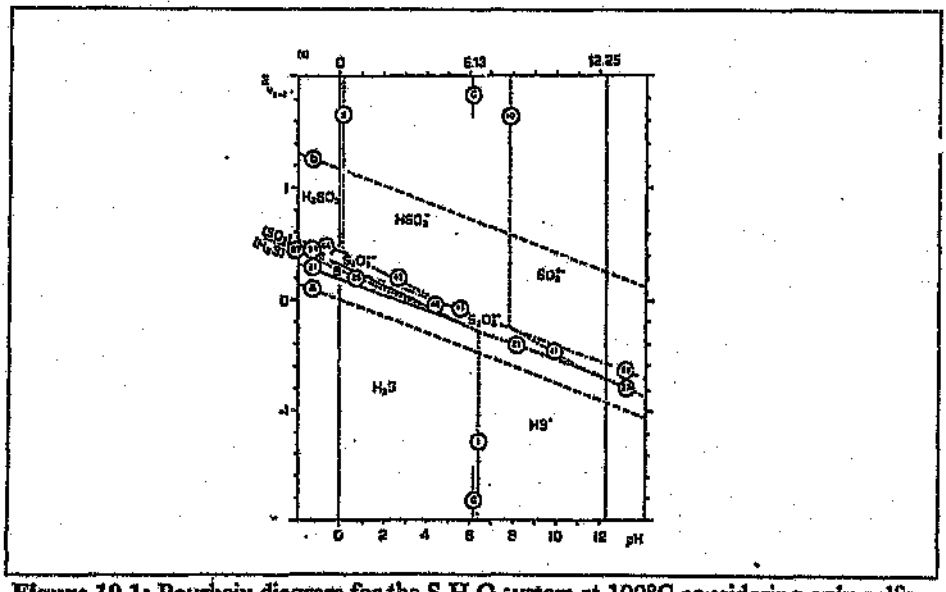


Figure 10.1: Pourbaix diagram for the S-H_2O system at 100°C considering only sulfur, sulfides, thiosulfates, tetrathionates and sulfites (log c = 0)

where a, b, c, d refer to reactions of the solvent, viz:

a: reduction of H_2O in gaseous H_2
b: oxidation of H_2O in gaseous O_2
c. dissociation of liquid water
d: vaporization of liquid water

The Eh-pH diagram for various iron species at 25°C is shown in Figure 10.2, where $Fe(OH)_3$ denotes the general stable phase for a generic Fe(III) precipitate which comprises many Fe(III) aqueous species [61]. While these diagrams are for studies carried out at temperatures different from that used in this case (75°C), major differences are not expected.

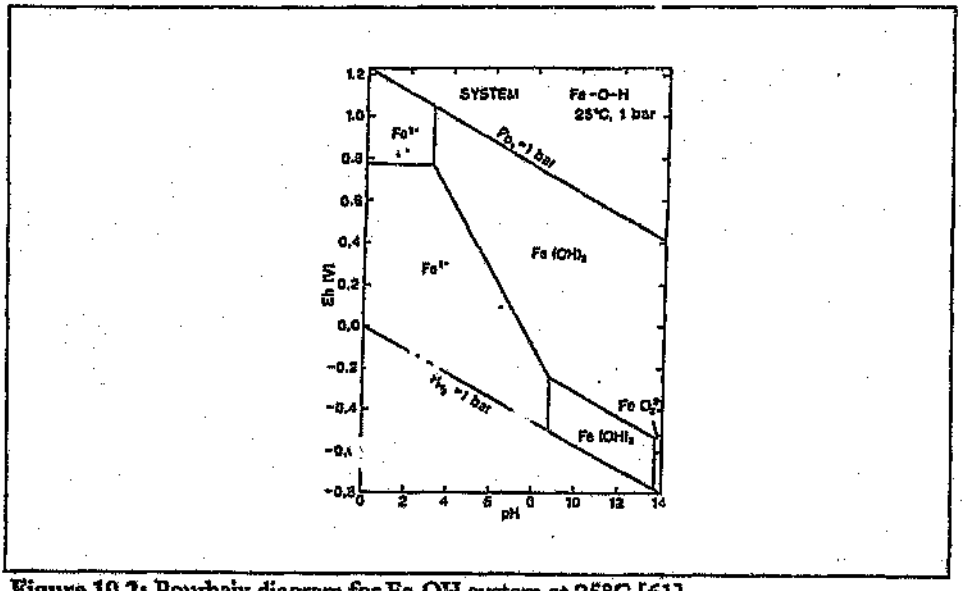


Figure 10.2: Pourbaix diagram for Fe-OH system at 25°C [61].

In this study, the morphology of iron catalysts prepared by sulfidation at pH values of 10.75, 8.5 and 6.9 is discussed. Figures 10.1 and 10.2 have been used in conjunction with the solution speciation model presented in Chapter 7, to predict which species are most likely to exist under the conditions of pH and concentration used in this study. This information was then correlated with the results obtained using a variety of standard catalyst characterisation techniques. Finally, having thus described the influence of sulfidation pH on morphology, the implications for Fischer-Tropsch synthesis have been described.

10.2. Experimental

Iron catalysts were sulfided with 2000 ppm polysulfide at various pH values (10.75, 8.5 and 6.9) during precipitation. Finely graduated pH paper was used to determine the pH of sulfide addition, since attempts to use a glass electrode gave inconsistent results.

Information regarding the morphology of the sulfided catalysts was obtained using various techniques, including XRD, TPR, BET surface area and pore volume measurements, as detailed in Chapter 2.

Before the assessment of FT activity, catalysts were calcined at 400°C for 16 hours, and activated by reduction under flowing hydrogen at 400°C for 24 hours. Fischer-Tropsch synthesis was then commenced at 250°C and 8 bar pressure, using a $CO:H_2$ ratio of 1:2 and a GHSV of 400 h^{-1} (see Chapter 2). All catalysts were monitored over an induction period of 4 days, followed by a four-day mass balance. Gaseous and liquid product fractions were analysed by on-line gas chromatography, while separation of the components of waxy products was achieved using an offline capillary-column gas chromatograph.

10.3. Results

10.3.1. Effect of sulfidation pH on catalyst morphology

In Chapter 9, it was shown that the use of mono- or polysulfides as sulfiding agents in precipitated-iron catalysts yielded similar results. Thus, in this study, the influence of sulfidation pH on polysulfided catalysts is taken to be representative of catalysts sulfided using either Na_2S, $(NH_4)_2S$ or $(NH_4)_2S_5$. To substantiate this assumption, selected results obtained using catalysts sulfided with monosulfide sources (Na_2S or $(NH_4)_2S$) will be presented where appropriate.

The effect of sulfidation pH on the surface areas of catalysts sulfided with 2000 ppm polysulfide is summarised in Table 10.1. Catalysts sulfided at pH 10.75, that is at the start of precipitation, yielded the highest surface areas, and those to which sulfide was added at the end of precipitation gave the lowest surface areas.

Table 10.1: Surface areas of 2000 ppm polysulfided catalysts sulfided at different pH values

pH of sulfidation	Crystallite size (Å)[a]	Pre-calcination surface area (m^2/g)	Post-calcination[b] surface area (m^2/g)	Post-reaction[c] surface area (m^2/g)
10.75	245	60	25.2	3.20
8.5	302	56	23.5	2.47
6.9	435	48	20.3	3.05

[a] crystallite size was determined from XRD data using the Scherrer formula
[b] Catalysts were calcined at 400°C for 16 h prior to measurement
[c] BET measurement made after FT synthesis and exhaustive wax extraction

This trend of decreasing surface area with decreasing sulfidation pH was observed irrespective of the sulfide source or level of sulfidation. For instance, the pre-calcinatic BET surface areas of a series of catalysts sulfided with 500 ppm Na_2S at pH 10.75, 8.5 and 6.9, were found to be 170, 124 and 97 m^2/g respectively.

After calcination, the surface areas of all catalysts decreased considerably due to pore collapse (see below, Table 10.2), yet still generally maintained the same trend of decreasing surface area with pH (Table 10.1).

The effect of sulfidation pH on crystallite size is also shown in Table 10.1, where larger crystals possessed lower surface areas. A decrease in surface area implies an increase in crystallite size, and hence improved crystallinity. The variation in crystallinity follows a trend analogous to that shown previously in Figure 3.16 (Chapter 3), in which a decrease in pH of sulfidation gave an increase in the intensity of Fe_2O_3 diffraction peaks at $2\theta = 35°$ for catalysts sulfided with 5000 ppm Na_2S. This increased intensity is accompanied by a narrowing of the peaks, a phenomenon that is indicative of higher crystallinity.

Improved porosity is another feature that has been detected after early sulfidation (Table 10.2). Trends similar to those observed for BET surface areas are found for pore volumes, and these trends are maintained after calcination pretreatment. The small value obtained after reaction for the catalyst sulfided at pH 6.9 may be due to pore blockage by residual wax products.

Table 10.2: Total pore volumes of 2000 ppm polysulfided catalysts

pH of sulfidation	Pre-calcination pore volume (cm^3/g)	Post-calcination pore volume (cm^3/g)	Post-reaction pore volume (cm^3/g)
10.75	0.206	0.198	0.020
8.5	0.170	0.164	0.020
6.9	0.161	0.163	0.004

An effect of sulfidation pH on pore shape was previously alluded to in Chapter 3. It appears that the addition of sulfide at pH 10.75 results in pores with broader necks than those obtained after sulfidation at pH 6.9. An example of this is given using catalysts sulfided with 20000 ppm Na_2S in Figure 3.21.

The reduction behaviour of the above catalysts was investigated using Temperature Programmed Reduction (TPR). As an example, the reduction profiles of the catalysts sulfided with 2000 ppm S using Na_2S and polysulfide are shown in Figure 10.3.

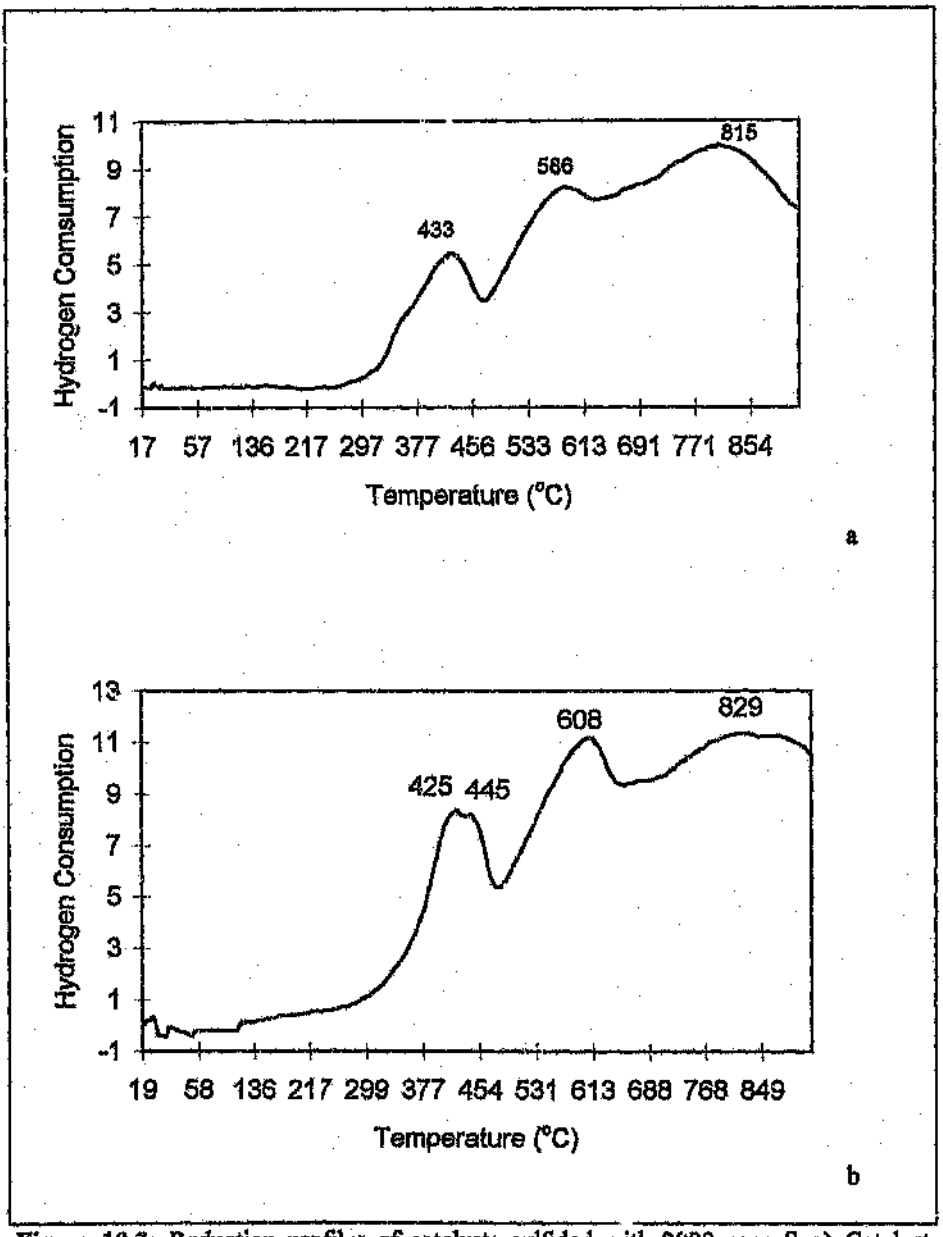


Figure 10.3: Reduction profiles of catalysts sulfided with 2000 ppm S **a)** Catalyst sulfided with Na_2S **b)** Catalyst sulfided with $(NH_4)_2S$

TPR studies confirmed that the hematite-magnetite transition took place at a lower temperature in the presence of sulfide (Table 10.3). Catalysts sulfided at the beginning and end of precipitation exhibited reduction peaks marginally higher in temperature than the catalyst sulfided at pH 8.5.

Table 10.3: Effect of pH of sulfide addition[a] on the reduction of iron species

pH of sulfidation	$Fe_2O_3 \rightarrow Fe_3O_4$ (°C)[b]	$Fe_2(SO_4)_3 \rightarrow FeS$ (°C)	$Fe_3O_4 \rightarrow Fe$ (°C)	$FeS \rightarrow Fe$ (°C)
10.75	418	485	612	850
8.5	410	477	618	849
6.9	430	484	622	859

[a] Catalysts sulfided with 2000 ppm $(NH_4)_2S_5$
[b] For the unsulfided catalyst, the Fe_2O_3-Fe_3O_4 transition occurred at 461°C

According to Table 10.3, the reduction of magnetite to iron is observed to occur at higher temperatures with decreasing pH of sulfidation. Furthermore, while the reduction of bulk FeS is unaffected by pH, the reduction of sulfate species is observed to proceed at a lower temperature for the catalyst sulfided midway through precipitation.

10.3.2. Effect of sulfidation pH on catalytic efficacy

Fischer-Tropsch synthesis was performed using catalysts sulfided with 2000 ppm polysulfide at pH 10.75, 8.5 and 6.9. Data relating to the activity of these catalysts is presented in Table 10.4.

Table 10.4: Activity data of catalysts sulfided with 2000 ppm polysulfide at different pH values

pH of sulfidation	% conversion	α-value	TON[a] ($\times 10^{-3}$ s^{-1})	Specific Activity (μmol C/s/g_{cat})
10.75	57	0.80	128	0.64
8.5	12	0.73	28	0.13
6.9	73	0.82	75	0.75

[a] TON refers to the number of carbon atoms converted to product per exposed active site

To confirm that the trends in Table 10.4 were reproducible, and that source effects were absent, the activity data relating to catalysts sulfided with 2000 ppm Na_2S at pH 10.75, 8.5 and 6.9 are also presented (Table 10.5):

Table 10.5: Activity data of catalysts sulfided with 2000 ppm Na_2S at different pH values

pH of sulfidation	% conversion	α-value	Specific Activity (μmol C/s/g_{cat})
10.75	56	0.78	0.70
8.5	15	0.68	0.10
6.9	54	0.83	0.67

The data presented in Tables 10.4 and 10.5 serve to illustrate that catalysts sulfided at pH 8.5 are inferior for the Fischer-Tropsch reaction compared to those sulfided at pH 10.75 and 6.9. The effect of sulfidation pH on the distribution of products is dealt with *vide infra* as part of the Discussion.

10.4. Discussion

10.4.1. Effect of sulfidation pH on catalyst morphology

The data presented in the Results section clearly show that the catalyst sulfided at pH 8.5 is dissimilar to those sulfided at pH 10.75 and 6.9. This suggests that two different factors are responsible for morphology and activity observed for the latter two catalysts. Furthermore, it appears that these two phenomena are in competition at pH 8.5.

Since all catalysts in this study were sulfided with 2000 ppm polysulfide, the observed differences in catalyst morphology, and hence Fischer-Tropsch activity, are expected to correlate with the species present in solution that dominate at each of the pH values at which sulfide was added.

The influence of pH on the dissociation of dissolved sulfide species at 25°C is illustrated in Figure 10.4 [204].

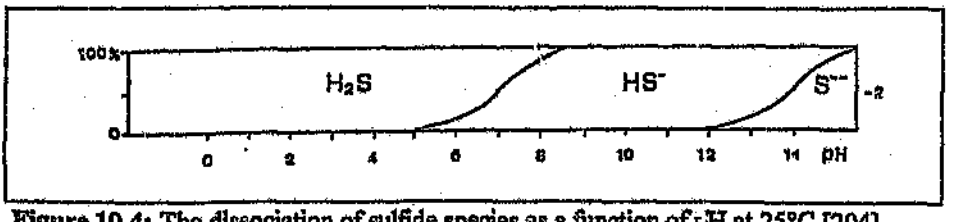


Figure 10.4: The dissociation of sulfide species as a function of pH at 25°C [204]

As mentioned previously, the preparation of sulfided catalysts was performed at 75°C. The equilibrium conditions that apply at this temperature may be represented by the expression [204]:

$$\log\left(\frac{HS^-}{H_2S}\right) = -6.699 + pH$$

Hence, the relative proportions of HS^- and H_2S at the pH values used for sulfidation can be determined (Table 10.6).

Table 10.6: The dissociation of dissolved substances as a function of pH at 75°C

pH of sulfidation	$((HS^-)/(H_2S))$
10.75	11246
8.5	63
6.9	1.59

In alkaline solutions, at the start of precipitation, essentially all added sulfide exists in the semi-protonated bisulfide form (HS^-). A solution of sodium carbonate has a pH of approximately 10.75, which is not high enough for the stabilization of S^{2-} species (Figure 10.4). The bisulfide ions still predominate at pH 8.5, and to a far lesser extent at pH 6.9, the end-point of precipitation.

Solution speciation modelling was applied to the $Fe(NO_3)_3$-Na_2CO_3 system which had been sulfided with 2000 ppm Na_2S. The species present in solution as a function of pH are shown in Figure 10.5.

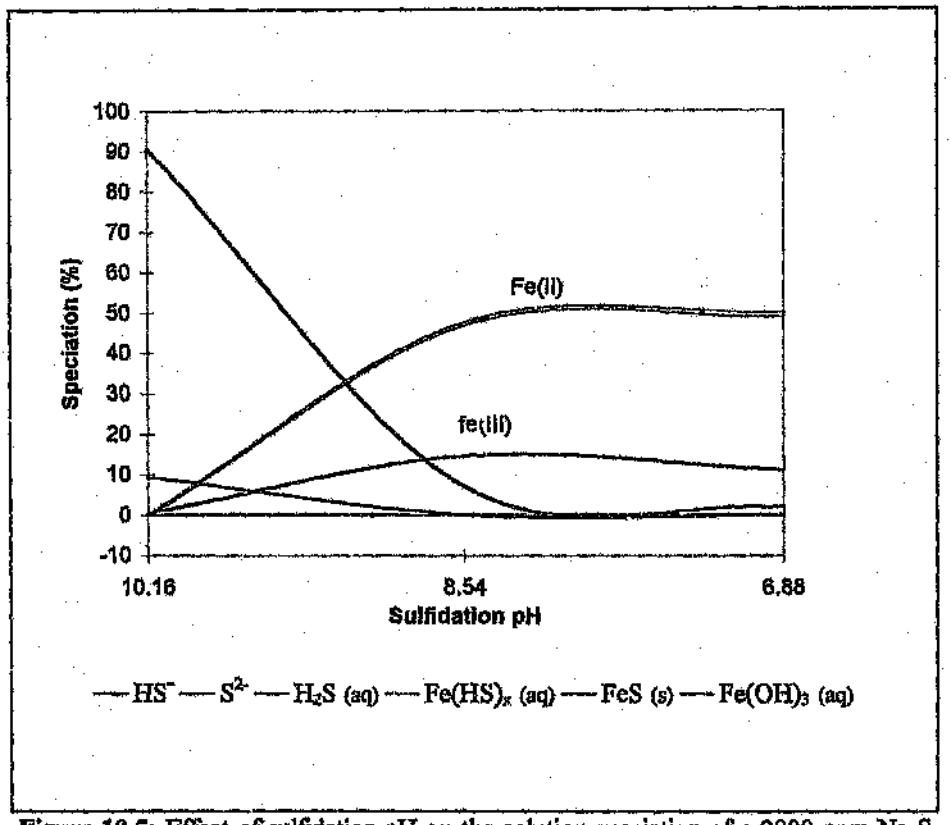


Figure 10.5: Effect of sulfidation pH on the solution speciation of a 2000 ppm Na_2S sulfided system, where sulfide species are presented as a percentage of total sulfide, and ferrous species as a percentage of total Fe^{2+}

It is evident from Figure 10.5 that at pH 10.75 virtually all Fe^{3+} is found as $Fe(OH)_4^-$, and S^{2-} as HS^-. As the pH becomes less alkaline, ferric ions are reduced to ferrous ions and this is accompanied by the formation of iron-sulfide species.

The formation of ferrous species in a suspension of iron oxide can proceed according to the reaction [10]:

$Fe_2O_3 + 6H^+ + 2e^- \Leftrightarrow 2Fe^{2+} + 3H_2O$ $\quad Eh = 0.719\text{-}0.1773pH\text{-}0.0591 \log [Fe^{2+}]$

This reaction is strongly pH dependent, and the yield of Fe^{2+} would therefore be maximised under increasingly acidic conditions.

The first precipitate formed through the reaction between Fe(II) species and dissolved sulfide at ambient temperatures and pH < 9 is $Fe(HS)_2$ [205]. The estimated solubility of this phase is variable, but is purported to be one to two orders of magnitudes greater than amorphous FeS. This material is black in colour, and hence it is possible that it is the initial product formed following sulfidation of the iron catalysts during precipitation, since swirls of black were observed in the stirred suspension the instant the sulfide was added.

The precipitation process can be represented by the following reaction scheme [205]:

$$Fe^{2+} + HS^- \rightarrow (FeSH)^+_{(aq)}$$
$$(FeHS)^+ + HS^- \rightarrow Fe(SH)_{2\,(s)}$$
$$Fe(SH)_2 \rightarrow FeS + H_2S$$

According to Rickard, the second step is rate-determining, while the first step occurs rapidly. The third reaction represents a phase transformation to release hydrogen sulfide, and marks the beginning of ordering of the precipitate; essentially crystal growth [205].

The concentration of $Fe(HS)_2$ and FeS species reach a maximum at pH 8.5 (Figure 10.5). At this pH value, the concentration of $Fe(OH)_{3\ (aq)}$ also reaches a maximum indicating that precipitation of iron oxyhydroxides is highly favoured thermodynamically.

It is hence proposed that the effect of sulfide addition is to create FeS molecules which act as nuclei for the proliferation of iron-oxide crystallites. When added at the start of precipitation (pH 10.75) the FeS molecules supplement the pool of nucleating agents. Together with $Fe(OH)_3$ embryos, the iron-sulfide provides a large number of nuclei, giving rise to many small crystallites of iron oxyhydroxide when precipitation is complete (pH 6.9).

The addition of sulfide at pH 8.5 introduces nucleating agents at a point where the formation of $Fe(OH)_{3\ (aq)}$ is most favourable, that is, precipitatic . of iron oxyhydroxides has commenced in earnest. As a result, the FeS molecules become incorporated into the growing iron oxide crystallite, acting as sites of adhesion for precipitating material. Furthermore, as shown in Figure 10.5, the formation of FeS is most favoured at this pH, and thus the system has additional nucleating agents following sulfide addition at pH 8.5. Thus the final morphology of this precipitate is characterised by crystallites that are generally larger than those obtained after sulfidation at pH 10.75. Moreover, the sulfide is situated closer to the surface of the crystallite when added at pH 8.5.

Sulfidation at the end of precipitation (pH 6.9), introduces FeS species after most of the formal iron oxyhydroxide precipitation is complete. Therefore, while some residual nucleation may still take place, the majority of iron-sulfide functions as aggregating agents and promotes the growth of iron-oxide crystallites.

The growth of crystallites is accompanied by an increase in bulk crystallinity as detected by XRD measurements. Indeed, an increase in crystallite size with decreasing pH is shown in Table 10.1. This trend is reflected in improved crystallinity as a function of decreasing pH (Figure 3.16). The crystallite sizes of sulfided catalysts (Table 10.1) were found to be greater than that obtained for the unsulfided catalyst (131Å). Therefore, sulfidation at pH 10.75 provides a source of aggregating agents as well as nuclei for crystal growth, giving rise to a more crystalline precipitate than in the absence of sulfur. However, the proportion of FeS that function as aggregating agents is small at pH 10.75 compared to pH 8.5 and 6.9.

Materials composed of small crystallites generally exhibit large BET surface areas and total pore volumes, and this is illustrated in Table 10.1 and 10.2. Certainly, for all series of catalysts containing the same amount of sulfide, added at different pH values, the surface areas are observed to follow the trend shown in Figure 10.6.

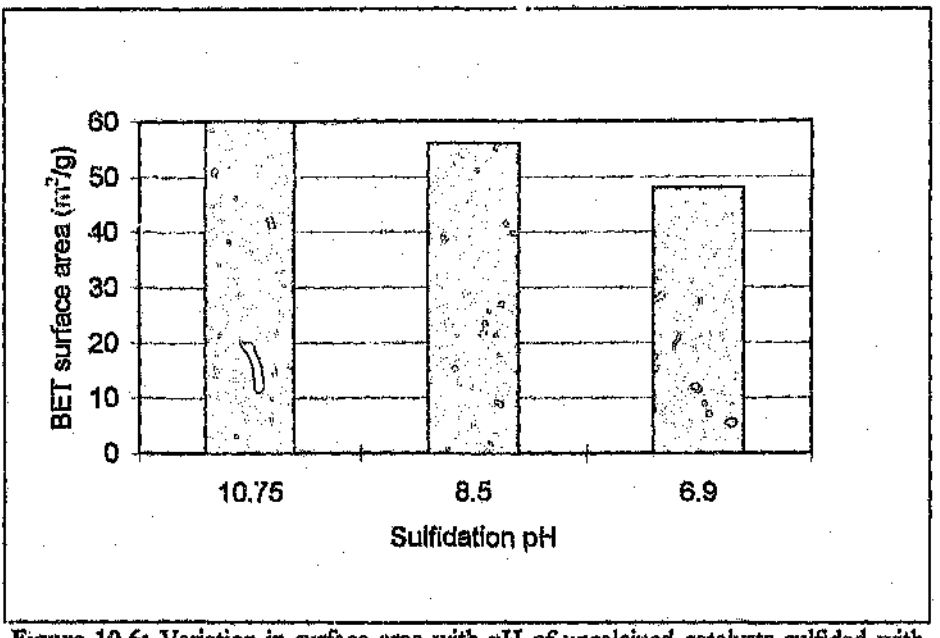


Figure 10.6: Variation in surface area with pH of uncalcined catalysts sulfided with 2000 ppm S from polysulfide

Thus, sulfidation at the end of precipitation promotes the growth of iron crystallites, possibly by a process of aggregation of smaller particles. Low-temperature sulfidation of noble metal catalysts is reported to yield larger particles, and the formation of a 'compound bridge' between smaller particles has been proposed [206]. In order to maintain crystallinity however, the phase of iron sulfide that becomes incorporated must closely approximate the phase of iron oxide being precipitated. Pyrrhotite (FeS) was identified by XRD as the sulfide phase present in uncalcined highly sulfided catalysts (Chapter 3), and this indeed has the same hexagonal close-packed geometry as hematite.

10.4.2. Effect of sulfidation pH on catalytic efficacy

According to Figure 10.7, which pictorially represents the data presented in Table 10.4, catalysts sulfided at the start and end of precipitation exhibit enhanced activity (relative to the unsulfided catalyst - which has a specific activity = 0.35 μmol C/s/g), while the rate of product turnover for the catalyst sulfided at pH 8.5 is poor.

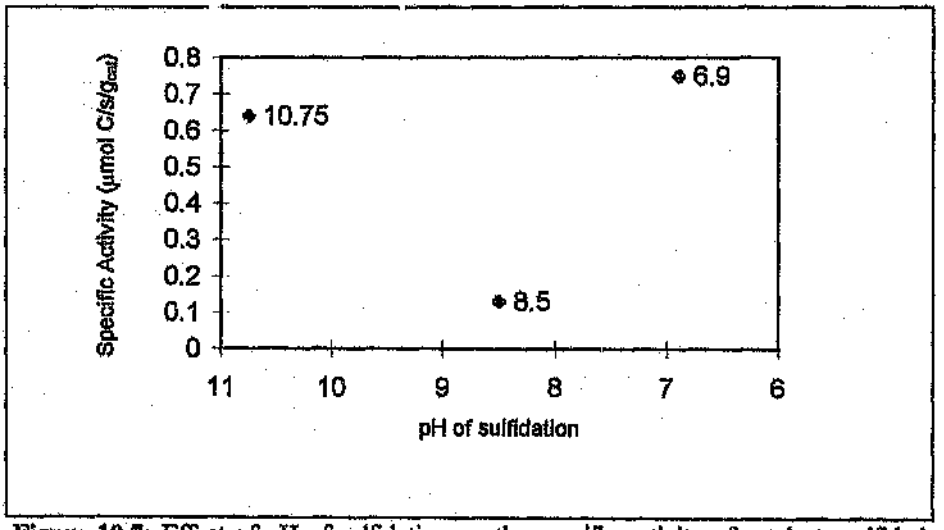


Figure 10.7: Effect of pH of sulfidation on the specific activity of catalysts sulfided with 2000 ppm polysulfide

The higher TON's calculated for catalysts sulfided with 2000 ppm polysulfide, at pH 10.75 and 6.9, are reflected in the enhanced activity per unit area (Figure 10.8). Highly active sites are generated by sulfidation at the start and end of precipitation; while poisoning appears to take place following the addition of sulfide at pH 8.5.

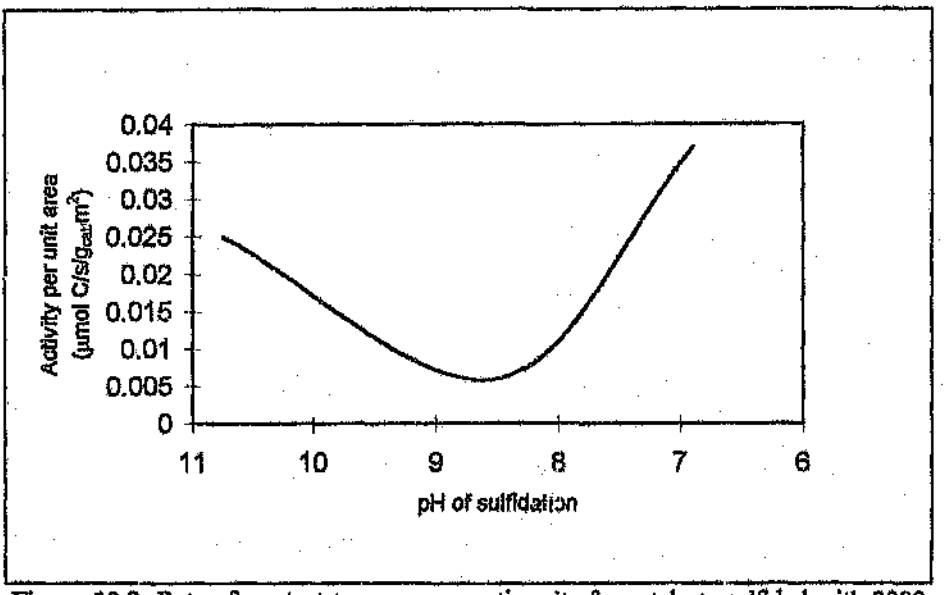


Figure 10.8: Rate of product turnover per active site for catalysts sulfided with 2000 ppm polysulfide at the start, middle and end of precipitation

The shape of the activity-pH plot (Figure 10.7) suggests that more than one factor is responsible for the effects observed. Solution speciation modelling has once again been invoked to assist with an understanding of the results.

The morphology of sulfided catalysts appears to be determined by the stage at which sulfide is added to the growing crystallites. During catalyst pretreatment however, the segregation of sulfide to the surface has been shown to occur (Chapter 4).

Therefore, the variation in depth of the sulfide within the crystallite of iron oxide appears to influence the degree of sulfide segregation in these catalysts.

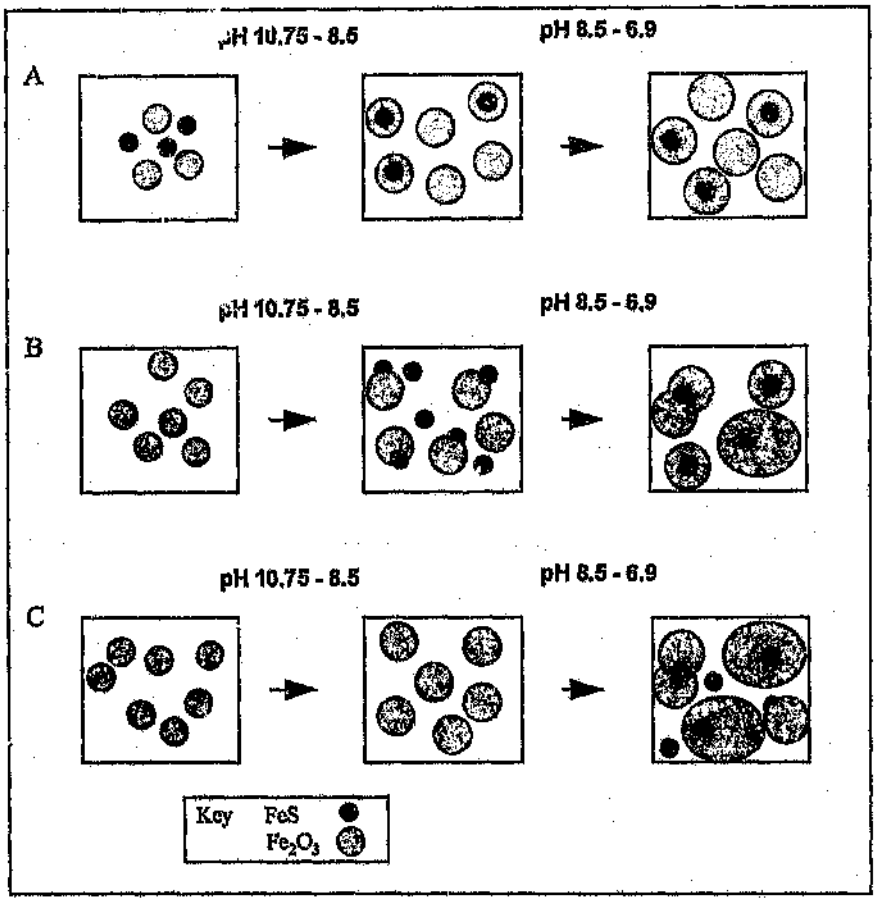


Figure 10.9: Schematic representation of the proposed model of the effect of sulfide addition on iron-oxyhydroxide crystallite growth

According to the proposed crystallite growth model illustrated in Figure 10.9, the addition of sulfide at high pH provides a source of nuclei through the formation of FeS molecules. These form the core of iron-oxyhydroxide crystallites and hence are situated far from the surface. As a result, very little sulfide segregates to the surface during pretreatment. Similarly, sulfidation at the end of precipitation produces FeS molecules once crystallite growth is essentially complete; or at least, large crystallites

are already present. Rather than acting as nuclei, FeS molecules now act as points of adhesion for the aggregation of crystallites. Once again, this suggests that the added sulfide is buried deep within the iron-oxide matrix, and therfore only a small porcentage segregates to the surface during calcination or reduction.

At pH 8.5, the processes of nucleation and aggregation appear to occur simultaneously. As shown in Figure 10.5, the formation of FeS (s) and $Fe(OH)_3$ (aq) are most favoured at this point. Hence, iron-oxyhydroxide crystallite growth has already commenced before the introduction of sulfide, so a considerable amount of aggregation occurs following sulfidation at pH 8.5. However, the thermodynamic equilibrium favours the formation of FeS above all other sulfide species at this pH, resulting in additional nuclei for crystallite growth.

The competing processes of nucleation and aggregation appear to create a catalyst that exhibits the effects of sulfide poisoning, such as observed with highly sulfided catalysts (Chapter 8). This leads one to suppose that the FeS molecules may be closer to the surface of the crystallites than when sulfidation was performed at pH 10.75 or 6.9.

An alternative explanation suggests that individual crystallites sulfided at pH 8.5 contain more FeS (due to the competing processes for nucleation and aggregation) than those sulfided at pH 10.75 or 6.9. At each of the latter two pH values, only one of the processes is occurring. This would then create a situation resembling that found at high levels of sulfidation (at all pH values). Unfortunately, owing to the fact that the sulfur content of catalysts could not be accurately determined, this proposal cannot be confirmed. It is interesting to note, however, that the results of the ICP analysis of sulfur incorporation (Chapter 3), did show that the catalyst sulfided at pH 8.5

contained marginally more sulfur than the catalysts sulfided at the other pH values. While these ICP results are suggestive, they must be treated with due caution. The difference in S content between the catalyst sulfided at pH 8.5, and those at pH 10.75 and 6.9 was found to be only 30 ppm, and this may actually lie within the margins of experimental error.

Nonetheless, for this hypothesis to hold, the reduction behaviour and FT product distribution of the catalyst sulfided with 2000 ppm S at pH 8.5, should approximate that of the more highly sulfided catalysts. Analysis of TPR data (Table 10.3) shows that the temperature of reduction of iron sulfate to iron sulfide is lower for the catalyst sulfided at pH 8.5, compared to the other two catalysts studied.

During calcination and reduction pretreatment, sulfide has been shown to migrate towards the surface of catalysts [91]. The larger the quantity of sulfide present on the surface as a result of segregation, the less well distributed it is likely to be. Hence, while this sulfide may be converted to sulfate during calcination, the likelihood of reduction to sulfide is also enhanced. This effect is then identical to that observed with high-level sulfidation, but occurs irrespective of the amount of S added at pH 8.5. This effect is less noticeable for 500 ppm sulfidation, but becomes significant for catalysts sulfided with between 2000 and 20000 ppm S. Indeed, a sulfate reduction peak was absent from the reduction profiles of higly sulfided catalysts.

Furthermore, Mössbauer spectroscopy and XRD analysis of highly sulfided spent catalysts revealed predominantly metallic iron, and the absence of carbide formation. The diffractogram of the spent catalyst sulfided with 2000 ppm polysulfide at pH 8.5 shows evidence of FeS (troilite) species. No carbide formation is discernible and some

metallic iron can be seen. By contrast, the catalyst sulfided at pH 6.9 comprised mainly Hägg carbide and magnetite.

The lack of carbide formation is therfore in line with results obtained for highly sulfided catalysts and correlates with reduced interaction between Fe and CO as detected by DRIFTS, for catalysts sulfided at this pH (Chapter 5). This weakened Fe-C bond also implies a stronger C = O bond and hence the absence of carbide formation.

10.4.3. Effect of sulfidation pH on product selectivity of sulfided catalysts

All low-level sulfided catalysts exhibited high olefinity, but the catalyst sulfided at pH 8.5 showed a propensity to form unsaturated hydrocarbons (Figure 10.10), and higher methane selectivity as illustrated in Figure 10.11.

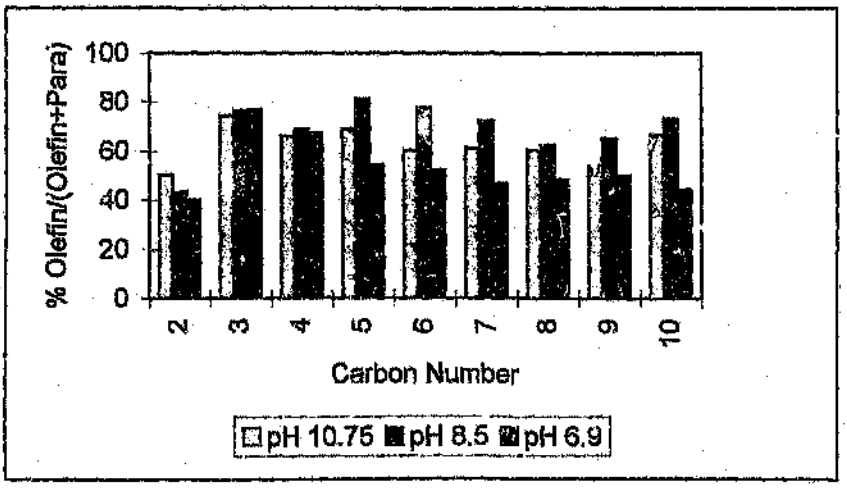


Figure 10.10: Olefin selectivity of 2000 ppm polysulfided catalysts prepared by sulfidation at pH 10.75, 8.5 and 6.9

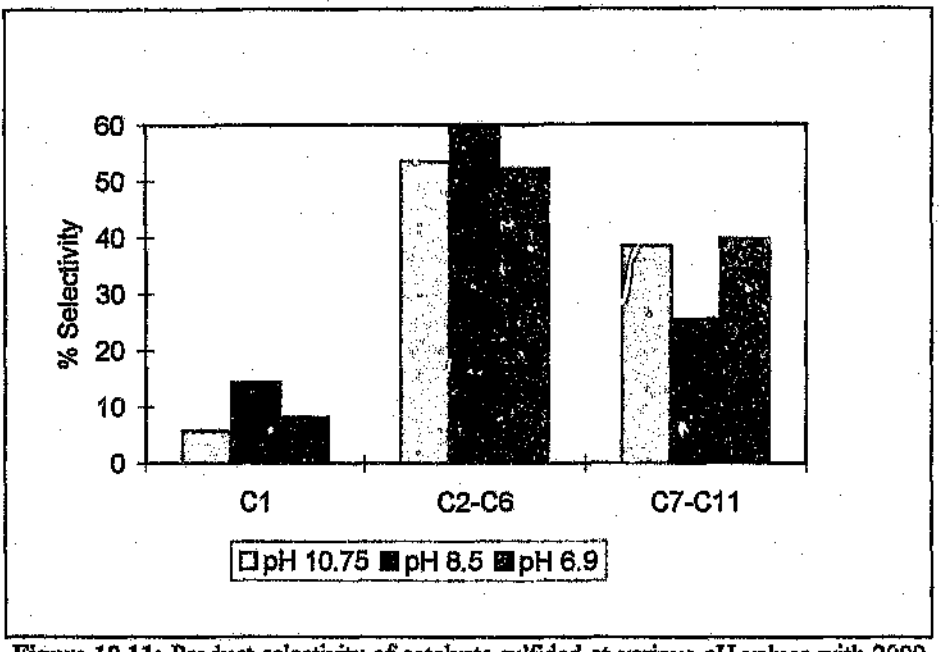


Figure 10.11: Product selectivity of catalysts sulfided at various pH values with 2000 ppm polysulfide

The oxygenate selectivity (Figure 10.12) of catalysts sulfided at pH 8.5 is higher than for those catalysts sulfided at the start and end of precipitation.

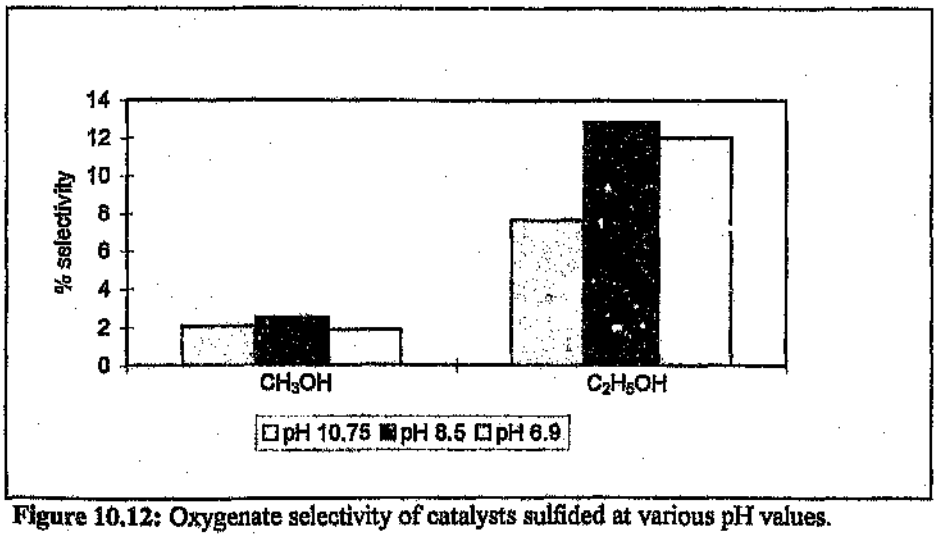


Figure 10.12: Oxygenate selectivity of catalysts sulfided at various pH values.

While the product selectivity of catalysts sulfided at the start and end of precipitation is very similar, that of the catalysts sulfided at pH 8.5 is noticeably different. The high oxygenate and methane selectivity, coupled with lower olefinity are synonymous with high levels of sulfidation (Chapter 8).

This confirms that the presence of sulfide species (as opposed to sulfate species) on the surface deleteriously affects FT activity. Moreover, it indicates that the morphology of catalysts sulfided at pH 8.5 is affected by the competing processes of nucleation and aggregation to the extent that it results in greater quantities of sulfide segregating to the surface during pretreatment.

10.5 Conclusion

The key factor involved with the effect of pH of sulfidation is proposed to relate to the epitaxial growth of iron oxide crystallites. At high pH, the FeS forms the nucleus from which a precipitate develops, thus becoming trapped deep inside the crystallite. At pH 6.9, the FeS acts as points of aggregation of crystallites. These two processes are in competition when sulfide is introduced at pH 8.5, resulting in an inactive catalyst. The poor activity, and high oxygenate and methane selectivity correlate with sulfide poisoning.

The overall surface area is enhanced by the addition of sulfide, yet this is not as important in promoting catalyst activity as the surface speciation that arises from segregation phenomena.

Chapter 11

Preliminary studies on selected sulfided precipitated-iron Fischer-Tropsch catalysts

11.1. Introduction

The ability of a catalyst to actively and selectively convert reactants to products depends on its chemical composition and morphology. The addition of promoters can markedly affect the rate of product turnover as well as the appearance of the product slate.

Promotion of precipitated-iron catalysts is generally achieved by the impregnation of the washed and dried precipitate with potassium waterglass [31]. It has been found that the greatest promotion results when the alkali content is low, hence the precipitate is washed thoroughly to remove the large amount of sodium or potassium present as counterions during precipitation, prior to impregnation with a known quantity of alkali.

The effect of low-level sulfidation during precipitation has already been discussed, and the logical progression would be to consider the impregnation of a dried precipitate with an alkali-sulfide. In this instance, the influence of sodium as a promoter is under consideration. Its role as a chemical additive in FT catalysts has already been demonstrated by other workers [173].